# Adaptation et réduction de modèle dans les couplages local-global non-intrusifs : application à la conception robuste

Alexandre Verwée

université PARIS-SACLAY

# Adaptive and reduced order modeling in non-intrusive local-global couplings: application to robust design

-

## *Adaptation et réduction de modèle dans les couplages local-global non-intrusifs : application la conception robuste*

**Thèse de doctorat de l'Université Paris-Saclay**

Ecole doctorale n°579 Sciences mécaniques et énergétiques, matériaux et géosciences (SMEMAG)
Spécialité de doctorat: Solides, structures et matériaux

Graduate School : Sciences de l'Ingénierie et des Systèmes, Référent : ENS Paris-Saclay

Thèse préparée au LMT - Laboratoire de Mécanique et Technologie (Université Paris-Saclay, ENS Paris-Saclay, CNRS), sous la direction de Ludovic Chamoin, Professeur des Universités

**Thèse présentée et soutenue à Gif-sur-Yvette, le 24 mars 2022, par**

**ALEXANDRE VERWÉE**

**Composition du Jury** :

| | |
|---|---|
| **Hachmi Ben Dhia**<br>Professeur des Universités, CentraleSupélec | Président du jury |
| **Alexei Lozinski**<br>Professeur des Universités, Université de Franche-Comté | Rapporteur |
| **Eric Florentin**<br>Professeur des Universités, INSA Val-de-Loire | Rapporteur |
| **Basile Marchand**<br>Ingénieur de Recherche, Mines ParisTech | Examinateur |
| **Valentine Rey**<br>Maîtresse de Conférences, Université de Nantes | Examinatrice |
| **Ludovic Chamoin**<br>Professeur des Universités, ENS Paris-Saclay | Directeur de thèse |

THESE DE DOCTORAT
NNT : 2022UPAST022

# Remerciements

Après plus de trois années de travail passionantes au LMT, je souhaite remercier les personnes qui ont rendues cette thèse possible.

Mes premiers remerciements vont à Ludovic Chamoin. Merci pour tous ces échanges et ton encadrement plein de sagesse, de patience et de savoir scientifique qui m'ont beaucoup apportés et qui m'a permis de mener à terme ce doctorat. Merci pour avoir toujours été disponnible, de m'avoir incité et appuyé dans mes recherches.

Je souhaite aussi remercier les membres du jury pour le grand honneur qu'ils ont fait en acceptant de juger ce travail. À Alexei Lozinski et à Éric Florentin pour avoir acceptés de relire cette thèse et d'en être rapporteurs. Vos remarques et nos échanges ont été très précieux et enrichissants. À Hachmi Ben Dhia pour avoir présidé mon jury. Et enfin je tiens à remercier Valentine Rey et Basile Marchand d'avoir acceptés d'assister à la présentation de ces travaux de thèse.

Je remercie toute l'équipe du LMT pour les moments de convivialité au sein du laboratoire, pour tout ces échanges enrichissants au cours des séminaires mais aussi au quotidien. Je tiens aussi à remercier le Département de Génie Mécanique pour m'avoir accordé la chance d'enseigner, ce qui fut une expérience très enrichissante, malgré les difficultés lié à l'enseignement à distance.

Je tiens à remercier tous les doctorants du laboratoire pour la bonne ambiance de travail mais également les bons moments passés ensemble. À échanger à la fois sur nos sujets mais aussi à sortir la tête de nos recherches le temps d'un café . Une pensée particulière pour Ariane, Camille, Pascale, Aya, Livio, Raphaël ainsi que toute l'équipe structure.

Enfin je souhaite remercier tous mes proches et ma famille pour leur soutien indéfectible. Pour m'avoir soutenu tout au long de ces trois années et avoir cru en moi. Un grand merci à Sandrine, Francis, Quentin, Lu, Mathieu, et Camille.

# Contents

# List of Figures

# List of Tables

# Introduction & motivations

*"Essentially, all models are wrong, but some are still useful"* (G.E. Box)

In the context of structural mechanics and computational engineering, physical systems are nowadays commonly analyzed by means of modeling and simulation tools. These constitute a fundamental pillar in science and engineering activities, reducing design time and cost. They are usually based on physics-based models, described by PDEs, that provide an idealized mathematical abstraction of the underlying physical system. They permit to virtually represent the mechanical behavior and make predictions for understanding and decision-making. Nevertheless, and out of the validation of numerically predicted outputs (by comparison with experimental data), a recurring issue is related to the computational effort generated by numerical simulations. One the one hand, the fine analysis of localized complex (multiscale, multiphysics) phenomena has always been of major interest in simulation-based structural mechanics engineering. A typical case is aerospace engineering, in which local phenomena associated with nonlinearities, heterogeneities, or geometric details are frequently studied over structures exhibiting various scales (from micrometer-sized composite fibers up to meter-sized aircraft components, see Figure 1). This requires the use of high-fidelity and computationally intensive physics-based models, which are now available and mature. On the other hand, despite considerable advances in computing capabilities, such models often remain intractable or hardly manageable in practical applications, in particular those associated with multi-query procedures. In order to circumvent this difficulty, model reduction techniques have been the object of many research works and developments during the last two decades. They aim at reducing the numerical complexity, and therefore the computational cost, in order to make simulations affordable in the industrial context.

A first and natural approach for model reduction consists in using multi-fidelity models, in which the initial high-fidelity model is replaced (totally or partially) by computationally cheaper surrogate models. These latter models may be obtained from homogenization or considering the linear range of the material behavior, for instance. In this context, a wide variety of numerical methods, dedicated to multiscale and/or multi-model computations, have emerged. In the present work, we deal with model coupling in which a high-fidelity model is kept in local spatial zones (e.g. in the vicinity of regions of interest) alone, while it is replaced with a surrogate model in the remainder of the mechanical structure (i.e. at a more global scale). This leads to a local analysis method in which data transfer

between models is performed across a coupling interface (Figure 1). The PhD work focuses on a specific and advanced model coupling method referred to as *non-intrusive local-global coupling*. Initially developed in [Gendre et al., 2009, Gendre et al., 2011], it performs a strong coupling between models compared to traditional sub-modeling (with one-way weak coupling) which is still a standard in industry [Jara-Almonte and Knight, 1988, Voleti et al., 1996, Cormier et al., 1999]. An attractive aspect is its non-intrusive feature that facilitates the management of several models coming from different software and used within parallel computations. For that, a substitution approach with iterative solver is implemented, which enables local modifications of an existing finite element model (in terms of mesh refinement, introduction of local features related to the geometry or material behavior, ...) while keeping the corresponding initial numerical operators unchanged at the global level. A coarse global numerical model is thus defined over the whole physical domain, in which geometry, connectivity and operators are fixed (the initial factorized global matrix is thus conserved along the iterative coupling procedure), while local modeling evolutions are performed through a separate numerical model defined over local zones denoted *patches*. Besides the increased flexibility with no global remeshing, this non-intrusive technique involving independent local-global solvers permits an easy merging of commercial software with any other specific simulation code dedicated to the modeling of complex phenomena of interest. The non-intrusive local-global coupling method has been the topic of several research advances during the last decade, and has been applied in many engineering situations exhibiting complex local phenomena e.g. [Chevreuil et al., 2013, Bettinotti et al., 2014, Guguin et al., 2014, Guguin et al., 2016, Bouclier and Passieux, 2018, Blanchard et al., 2019], and in association with commercial codes such as Abaqus or Code-Aster. An overview on the capabilities of the non-intrusive local-global coupling method is given in [Duval et al., 2016].

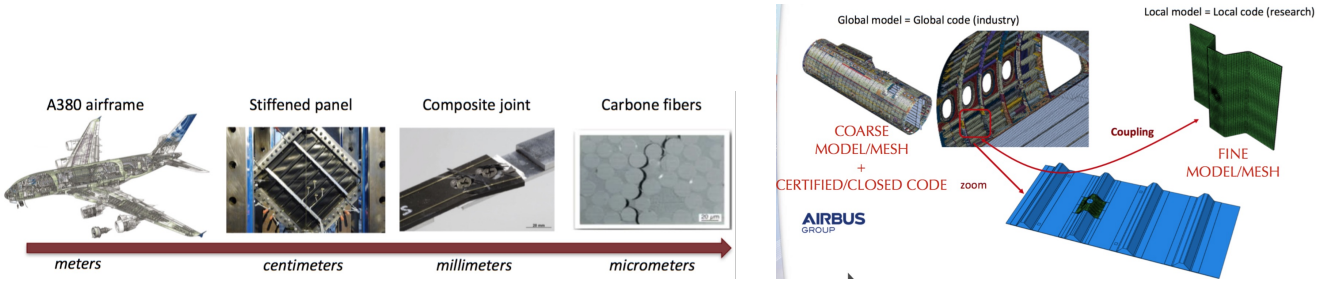


Figure 1: Typical multiscale application in the aeronautics industry (left), and local-global coupling philosophy on large and complex parts (right). [Courtesy of Airbus Group]

Another strategy for model reduction has been a hot research topic from the late 2000's, with the objective to reach simulation times which are compatible with engineering requirements for multi-query analyses with parametrized problems (e.g. uncertainty quantification, inverse analysis, or parametric optimization). Instead of decreasing the complexity of the initial high-fidelity physics-based model, it rather aims at decreasing the complexity of the solution scheme by exhibiting features of the parametric solution to enhance the computational efficiency. The general idea is to construct, in an offline phase and with a computationally intensive procedure, a convenient reduced basis for the effective approximation of the parametrized solution. In the online phase, this parameterized

solution is then recovered in a fast and cheap manner. Here, we deal with the Proper Generalized Decomposition (PGD) technique [Chinesta et al., 2014] with modal decomposition (see Figure 2), and we use it in association with model coupling for two objectives: (i) to accelerate the coupling algorithm by parametrizing boundary conditions of the local model; (ii) to facilitate local parametric design and structural shape optimization [Samareh, 2001, Haslinger and Makinen, 2003] from a parametrized description of the geometry, inside regions of interest, involving design variables. In this framework, the local-global analysis is performed with a global solution raised from FEM and a local solution evaluated online from a virtual chart constructed offline, from PGD reduced order modeling. Such a virtual chart integrates as variables (i.e. extra-parameters) some features of the local model such as boundary conditions, geometry, or material behavior. Complementing the non-intrusive global-local coupling with local ROM leads to a more flexible exchange between interface quantities, and higher performance in terms of computational efficiency, particularly in the multi-query context. This is one contribution of the PhD.

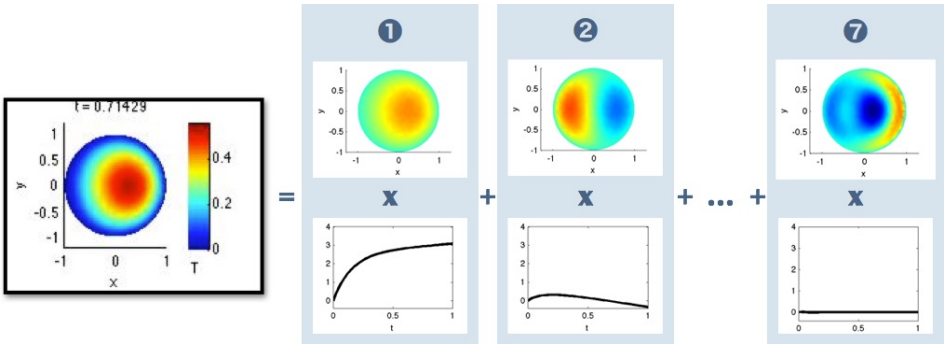


Figure 2: Example of a PGD decomposition for a space-time problem.

In the previously mentioned multi-fidelity framework with model coupling, the mathematical representation of a given system may be picked in a hierarchical list of possible models, with increasing complexity. The chosen mathematical model is then further numerically processed by means of discretization schemes (such as the finite element method (FEM)) and specific algorithms, leading to a numerical model used as a virtual twin and delivering an approximate solution. Insights of computational approaches depend on the numerical model at hand being a faithful abstraction of the real world, but all models are wrong to some extent. In the framework of computational mechanics based on FE analyses, there are various error sources along the modeling and simulation chain. In the present context, taking the high-fidelity model as the reference, errors may come from (i) bias in the reduced model, related to the size of the local zone chosen to represent fine-scale effects in the model coupling (and potentially to the PGD representation when it is employed); (ii) numerical approximation in terms of discretization (mesh size) or algebraic errors associated with iterative computational solution schemes. The selection of model and numerical parameters is traditionally performed from *a priori* knowledge on the system (e.g. *a priori* placement of the coupling interface and definition of local/global meshes, crude criterion for stopping iterations...). However, for the sake of quantitative numerical information, reliable prediction, and safe decision-making, there is a practical need for

certification of the computed outputs. This is the matter of model verification, which is part of the larger Verification and Validation (V&V) concept (Figure 3). V&V has been an active research topic for more than 30 years [Roache, 1998, Oberkampf et al., 2003]; it has been listed as one of the most important challenges in simulation-based engineering sciences (SBES) [Oden et al., 2006a].

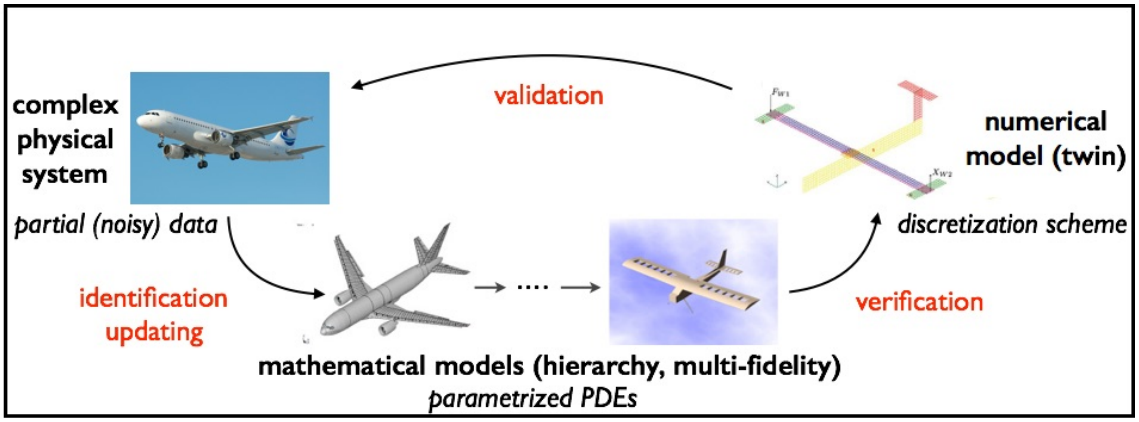


Figure 3: General overview of V&V activities.

Out of certifying the outputs of the numerical model, an objective of model verification is also to provide computational efficiency, with fast simulation and predictions. This is in perfect line with industrial constraints to accommodate engineering times and accurate simulations, and it is becoming a major requirement for *online* real-time control of systems from simulation tools and assimilation of in-situ measurements, in the framework of Dynamic Data-Driven Application Systems [Darema, 2004, Darema, 2015]. In modern computational engineering, the goal is thus to compute right at the right cost, with appropriate physics and smart management of computing resources (trade-off between reliability and computational cost) depending on the objective. This resorts to model adaptivity in terms of an appropriate selection of a computational model and associated numerical parameters, in order to address complex problems with both fast and credible numerical strategies.

The PhD work falls into this verification framework. Its objective is to master calculations, in terms of modeling and numerical simulation, in the context of structural computations performed by means of non-intrusive local-global coupling (with possible additional PGD reduction applied on the local fine-scale model). We wish to control, in a robust manner, the accuracy of the approximate solution by developing reliable and efficient numerical techniques. There is currently no equivalent tool, and more generally the issue of certification and optimal driving of non-intrusive local-global coupling methods has been addressed in very few works until now. A recent work on the topic is [Tirvaudey et al., 2020a] where only linear models where considered and error estimation was performed using a residual-based approach. Here, we rather rely on the Constitutive Relation Error (CRE) concept which is a general verification tool for FEM computations [Ladevèze and Pelle, 2005, Ladevèze and Chamoin, 2015, Chamoin and Díez, 2016]. Based on dual analysis with strong enforcement of mechanical equilibrium, it was first developed

in [Ladevèze and Leguillon, 1983] then successfully used as a robust *a posteriori* error estimate to drive adaptive algorithms in many applications involving a large scope of structural mechanics problems (elasto-plasticity, damage, dynamics...). In the context of non-intrusive local-global couplings, we show that the CRE concept also constitutes an effective tool that permits to optimally control the accuracy of the computed solution, both globally and on specific quantities of interest. It defines fully computable and guaranteed error bounds, and provides indicators on the three error sources: modeling error coming from the use of a coarse global model, error of the local model in terms of FE discretization or PGD reduction, error in the iterative coupling algorithm. The last indicators are obtained by weakening the concept of admissibility associated with CRE. A dedicated adaptive algorithm, based on these error indicators, is then derived to compute right at right cost depending on the objective, with an automatic adaptive procedure to select optimal computation parameters (e.g. optimal size of the local zone in the coupling, or number of iterations), and thus avoiding unnecessary computing efforts while satisfying accuracy up to a preset tolerance. The obtained computation is thus both reliable and manageable, permitting certification for action.

We also show that the adaptive strategy can be implemented within a reduction strategy that couples non-intrusive local-global coupling and PGD model reduction, in order to effectively conduct sensitivity analysis and optimization associated with localized phenomena (structural details, defects). In this context, parameterizations of geometry of the local domain (external and internal) and boundary conditions on the local model are here investigated. Eventually, the verification strategy is used in the context of tolerance analysis, taking into account local design uncertainties (which are unavoidable when manufacturing mechanical products) while guaranteeing that quality requirements are met. We thus illustrate the interest of the approach, in terms of numerical speed-up and guaranteed margins, for optimal or robust design in which many similar simulations need to be performed over the design parametric space to propagate uncertainties [Zang et al., 2005, Guedri et al., 2012].

Throughout the work, we assume that the continuous fine-scale model is free of error, that boundary conditions on the model problem are perfectly known (no variability or uncertainty in their definition), and that error sources coming from round-off of loading/geometry representation are negligible.

The manuscript is organized as follows:

- In Chapter 1, we perform a bibliographic study on two main points of the PhD work: (i) model couplings, with a focus on non-intrusive coupling; (ii) modeling error estimation, with specific application to such a coupling strategy;

- In Chapter 2, we develop the new strategy based on CRE to control the accuracy of non-intrusive couplings involving linear or nonlinear models in statics. We thus derive error estimator and indicators, as well as an associated adaptive algorithm that optimally drives the coupling algorithm in order to optimally meet a preset tolerance;

- In Chapter 3, the proposed strategy is tailored to goal-oriented control that is control on specific quantities of interest. A main ingredient for this purpose is the introduction and approximate solution of an adjoint problem associated with the chosen quantity of interest;
- In Chapter 4, we extend the approach to non-intrusive local-global couplings in which local PGD model reduction is additionally used. The framework merging model coupling and PGD is developed, before addressing again error control and adaptivity issues;
- in Chapter 5, the overall strategy is applied for tolerance analysis, in which illustrations of optimal or robust designs are shown;
- eventually, conclusions of the work are drawn and some research prospects are indicated, with first ideas and preliminary results for the extension of the proposed tools to advection-diffusion problems resulting for instance from applications with moving sources.

# Chapter 1

# Bibliographic review

In this first chapter, we start with a state-of-the-art on the methodology implemented for non-intrusive model couplings, focusing on specific features as well as on recent developments. We then address modeling error estimation when employing surrogate models, first presenting the general strategy then applying it to non-intrusive coupling. In the whole chapter, and for the sake of simplicity and clarity, the theoretical and subsequent numerical developments are conducted for static linear models and local material heterogeneities.

## 1.1 Non-intrusive coupling between concurrent models

### 1.1.1 Context and placement with respect to alternative approaches

A wide variety of numerical methods, dedicated to multiscale and/or multi-model computing, have emerged along the three last decades for a high-fidelity analysis of local phenomena. They can roughly be categorized in two main classes. The first class, particularly devoted to multiscale analysis, consists in local model enrichment by means of augmented approximation spaces (using finer meshes or specific enrichment functions) and superposition of micro/macro solutions. We may cite in this class:

- methods with enrichment based on a partition of unity (PUM) [Melenk and Babuska, 1996] such as the Generalized Finite Element Method (GFEM) [Strouboulis et al., 2000a, Babuska et al., 2003, Duarte and Kim, 2008] or the eXtended Finite Element Method (XFEM) [Moës and andT. Belytschko, 1999];
- other methods, such as adaptive localized Multiscale FEM (MsFEM) [Hou and Wu, 1997, Efendiev and Hou, 2009, Chamoin and Legoll, 2018], in which specific basis functions encode fine-scale details of the solution;
- methods with local correction, as performed in the Variational MultiScale method (VMS) [Hughes et al., 1998], the hierarchical modeling method [Oden et al., 1999], multigrid methods involving prolongation and restriction

operators [Parsons and Hall, 1990, Rannou et al., 2009], the bridging scale method [Wagner and Liu, 2003], the Chimera method [Brezzi et al., 2001], numerical homogenization [W.E et al., 2003, Feyel, 2003], or structural zooming with FE patches [Glowinski et al., 2005, Picasso et al., 2008, Lozinski and Pironneau, 2011].

Nevertheless, a major drawback of these model enrichment methods is that they may hardly be used in practical multiscale engineering activities due to their level of intrusiveness in existing commercial software. The implementation of such methods in a legacy code is not straightforward mainly because the creation of the coupling operators requires complex integration operations.

A second class of numerical methods, on which we particularly focus in this work, refers to model coupling methods with interface data transfers. These have received much interest with the emergence of new simulation trends in which several models, potentially coming from different software or physics, are used into parallel computations that are run on modern computing facilities (clusters). Among the wide list of coupling methods, and out of traditional sub-modeling (with one-way weak coupling) which is still a standard in industry [Jara-Almonte and Knight, 1988, Voleti et al., 1996, Cormier et al., 1999], we may refer to several advanced methods with strong coupling:

- improved iterative sub-modeling methods with global correction (taking into account the influence of local phenomena) or static condensation [Hirai et al., 1984, Mao and Sun, 1991, Cresta et al., 2007];
- the mortar method [Belgacem, 1999, Bernardi et al., 2005, Brivadis et al., 2015] enforcing weak equalities at the coupling interface by means of Lagrange multipliers;
- the Nitsche method [Hansbo and Hansbo, 2002, Ruess et al., 2014];
- energy averaging methods with volume interface such as the Arlequin method [Ben Dhia, 1998, Ben Dhia and Rateau, 2005, Prudhomme et al., 2012], the bridging domain method [Xiao and Belytschko, 2004], or the MAAD method for atomic-to-continuum couplings [Broughton et al., 1999].

Domain decomposition methods, such as well-known FETI [Farhat and Roux, 1991], BDD [Mandel, 1993], FETI-DP [Farhat et al., 2001], or mixed LATIN [Ladevèze, 1999, Ladevèze et al., 2001, Daghia and Ladevèze, 2012], are also coupling methods based on Schwarz algorithms [Lions, 1987] and are widely used in structural engineering [Le Tallec, 1994, Gosselet and Rey, 2006]. Furthermore, nonlinear localization algorithms are available to effectively apply such domain decomposition methods to nonlinear problems [Cai and Keyes, 2002, Cresta et al., 2007, Klawonn et al., 2014]. Here again, all these model coupling approaches are intrusive as such, in the sense that they require quite deep modifications of FE solvers and software, and sometimes time-consuming meshing procedures at the global scale, which is not always feasible in an industrial context. Nevertheless, it is fruitful to indicate the attempts made to decrease the intrusiveness level in some of the former methods, as in [Ruyssen, 2021] for the Arlequin method.

About ten years ago, a new and attractive class of model coupling methods referred to as *non-intrusive local-global coupling* has emerged [Gendre et al., 2009, Gendre et al., 2011], following pioneering ideas developed in [Whitcomb, 1991]. It consists in a substitution approach, with iterative solver, that enables local modifications of an existing finite element model (in terms of mesh refinement, introduction of local features related to the geometry or material behavior, ...) while keeping the corresponding initial numerical operators unchanged at the global level. It defines a coarse global numerical model over the whole physical domain, in which geometry, connectivity, operator and solver are fixed (the initial factorized global matrix is thus conserved along the iterative coupling procedure), while local modeling evolutions are performed through a separate numerical model defined over local zones or patches (see Figure 1.1). Interface data are then iteratively exchanged between these two models, with lower convergence performance compared to intrusive coupling; this is the price to pay for non-intrusiveness. Besides the increased flexibility with no global remeshing, the non-intrusive coupling technique involving independent local-global solvers permits an easy merging of commercial software with any other specific simulation code dedicated to the modeling of complex phenomena of interest. Indeed, no modification of the commercial software is required and standard input/output specifications of such software can be fulfilled.

Over the last decade, the non-intrusive local-global coupling method has been extensively applied and analyzed in many engineering situations exhibiting complex local phenomena (buckling, plasticity, cracking, contact...). It was in particular implemented for problems with local plasticity [Gendre et al., 2009] or visco-plasticity [Blanchard et al., 2019], for crack propagation problems [Gupta et al., 2012, Passieux et al., 2013, Gerasimov et al., 2018], for the analysis of local uncertainties from a global deterministic operator [Chevreuil et al., 2013, Nouy and Pled, 2018], for 2D/3D couplings in thin composite panels with local stress concentration and debonding [Guguin et al., 2014, Guguin et al., 2016, Guinard et al., 2018], for problems involving a NURBS definition of the domain shape and including local geometric details, fracture, or mesh refinement [Bouclier et al., 2016, Bouclier and Passieux, 2018], or for transient dynamics problems [Bettinotti et al., 2014, Chantrait et al., 2014, Bettinotti et al., 2017]. It was also used in conjunction with domain decomposition techniques [Duval et al., 2016, Oumaziz et al., 2017, Gosselet et al., 2018]. A global overview of the current capabilities of the non-intrusive local-global coupling method is available in [Duval et al., 2016]. Alternative proposals exist, based on volume coupling, using for instance a non-intrusive version of the Partition of Unity method [Plews et al., 2012]. Here, we restrict to surface coupling.

### 1.1.2 Basic implementation

#### Reference high-fidelity model

We consider a structural mechanics problem defined over a body occupying the closure of an open bounded domain $\Omega \subset \mathbb{R}^d$ ($d = 1$, 2 or 3 being the space dimension), with regular Lipschitz boundary $\partial\Omega$ (Figure 1.2). We assume that a given displacement field $\mathbf{u}_d$ is prescribed on a non-zero measured part $\partial_u\Omega \subset \partial\Omega$, while given traction forces

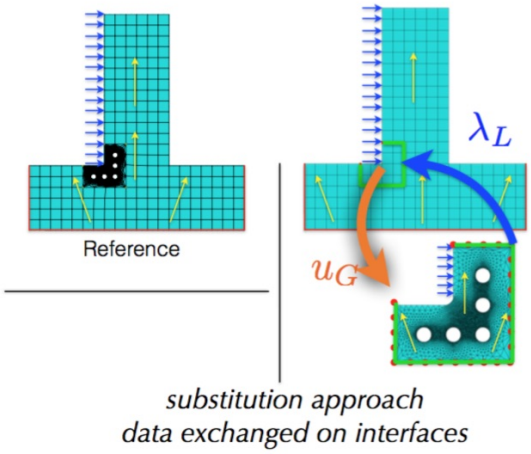


Figure 1.1: Schematic representation of non-intrusive local-global coupling (from [Blanchard et al., 2019]).

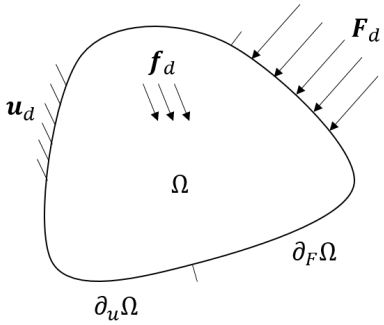


Figure 1.2: The reference problem and its environment.

$\mathbf{F}_d$ are prescribed on the complementary part $\partial_F\Omega \subset \partial\Omega$, such that $\partial_u\Omega \cap \partial_F\Omega = \emptyset$ and $\overline{\partial_u\Omega \cup \partial_F\Omega} = \partial\Omega$. A given body force field $\mathbf{f}_d$ may also be active in $\Omega$. In the following, and without loss of generality, we choose $\mathbf{u}_d = \mathbf{0}$ (homogeneous Dirichlet boundary conditions). Furthermore, we consider a quasi-static isothermal evolution with small perturbations regime. The material behavior is supposed to be described by a heterogeneous linear elasticity model, with possible fast variations of the material parameters.

The mechanical problem then consists in finding the displacement-stress pair $(\mathbf{u}, \sigma)$ verifying:

$$
\begin{aligned}
&\mathbf{u} = \mathbf{0} \quad \text{on } \partial_u\Omega \quad \text{(kinematic constraints)} \\
&\begin{cases} \mathbf{div}\, \sigma + \mathbf{f}_d = \mathbf{0} & \text{in } \Omega \\ \sigma\mathbf{n} = \mathbf{F}_d & \text{on } \partial_F\Omega \end{cases} \quad \text{or equivalently} \quad \int_\Omega \sigma : \varepsilon(\mathbf{v}) = \int_\Omega \mathbf{f}_d \cdot \mathbf{v} + \int_{\partial_F\Omega} \mathbf{F}_d \cdot \mathbf{v} \quad \forall \mathbf{v} \in \boldsymbol{\mathcal{V}} \quad \text{(balance equations)} \\
&\sigma = \mathbf{K}\varepsilon(\mathbf{u}) \quad \text{in } \Omega \quad \text{(constitutive relation)}
\end{aligned}
\tag{1.1}
$$

where $\mathbf{n}$ is the outward unit normal vector, $\mathbb{e}(\mathbf{u}) = \frac{1}{2}\left(\mathbb{G}\mathrm{rad}(\mathbf{u}) + \mathbb{G}\mathrm{rad}^T(\mathbf{u})\right)$ is the linearized strain tensor, and $\mathbf{K}$ is the heterogeneous linear Hooke operator. The weak form of this problem reads:

$$\text{Find } \mathbf{u} \in \boldsymbol{\mathcal{V}} \text{ such that } \int_\Omega \mathbf{K}\mathbb{e}(\mathbf{u}) : \mathbb{e}(\mathbf{v}) = \int_\Omega \mathbf{f}_d \cdot \mathbf{v} + \int_{\partial_F \Omega} \mathbf{F}_d \cdot \mathbf{v} \quad \forall \mathbf{v} \in \boldsymbol{\mathcal{V}} \tag{1.2}$$

where $\boldsymbol{\mathcal{V}} = \{\mathbf{v} \in [H^1(\Omega)]^d; \mathbf{v} = \mathbf{0} \text{ on } \partial_u \Omega\}$ is the appropriate functional space.

**Surrogate model and intrusive iterative coupling strategy**

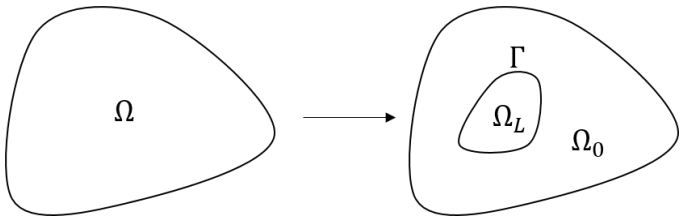


Figure 1.3: Sub-structuring of the physical domain.

We assume that in the previously considered model problem (1.2), phenomena of interest are localized in space. Consequently, a natural approach to reduce computational efforts consists in performing sub-structuring and restrict the use of a high-fidelity model to localized zones inside $\Omega$, switching to a simpler model (in terms of material behavior, but also later in terms of mesh size) in the complementary part. We thus partition the physical domain $\Omega$ in two non-overlapping zones (see Figure 1.3):

- a local zone $\Omega_L \subset \Omega$, also denoted patch, that should encompass the support of the phenomena of interest to be analyzed. For the sake of simplicity, the zone $\Omega_L$ is assumed here to be located strictly inside $\Omega$. In this zone, the initial high-fidelity model (based on the heterogeneous constitutive operator $\mathbf{K}$) is preserved;
- the complementary zone $\Omega_0 = \Omega \backslash \overline{\Omega}_L$ in which a coarser concurrent model is implemented. It is defined by substituting the initial material behavior with an homogenized linear elastic behavior with Hooke's operator $\mathbf{K}_0$.

*Remark. In the remainder of the section, we assume that the initial position of the patch $\Omega_L$ is a priori set from the support of phenomena of interest. An alternative, in the case where these phenomena are not identified, would consist in using a coarse model over the whole domain $\Omega$ and determine critical zones (by means of standard error estimates) from which the initial location of $\Omega_L$ should be defined [Picasso et al., 2008].*

The coupling problem is here formulated in a weak form using the Lagrange multipliers method. Introducing the interface $\Gamma$ between zones $\Omega_L$ and $\Omega_0$, the continuous coupling problem then consists in finding a global displacement field $\mathbf{u}_G$ defined in $\Omega_0$, a local displacement field $\mathbf{u}_L$ defined in $\Omega_L$, and a Lagrange multiplier field $\boldsymbol{\lambda} \in \boldsymbol{\mathcal{M}}$ (representing reaction forces on $\Gamma$), verifying:

- a global problem over $\Omega_0$:

$$\text{Find } \mathbf{u}_G \in \boldsymbol{\mathcal{V}}_0 \text{ such that } \int_{\Omega_0} \mathbf{K}_0 \mathbb{e}(\mathbf{u}_G) : \mathbb{e}(\mathbf{v}_G) = \int_{\Omega_0} \mathbf{f}_d \cdot \mathbf{v}_G + \int_{\partial_F \Omega} \mathbf{F}_d \cdot \mathbf{v}_G - \int_\Gamma \boldsymbol{\lambda} \cdot \mathbf{v}_G \quad \forall \mathbf{v}_G \in \boldsymbol{\mathcal{V}}_0 \tag{1.3}$$

  with $\boldsymbol{\mathcal{V}}_0 = \{\mathbf{v} \in [H^1(\Omega_0)]^d ; \mathbf{v} = \mathbf{0} \text{ on } \partial_u \Omega\}$. The associated stress field is $\mathbb{\sigma}_G = \mathbf{K}_0 \mathbb{e}(\mathbf{u}_G)$;

- a local problem over $\Omega_L$:

$$\text{Find } \mathbf{u}_L \in \boldsymbol{\mathcal{V}}_L \text{ such that } \int_{\Omega_L} \mathbf{K} \mathbb{e}(\mathbf{u}_L) : \mathbb{e}(\mathbf{v}_L) = \int_{\Omega_L} \mathbf{f}_d \cdot \mathbf{v}_L + \int_\Gamma \boldsymbol{\lambda} \cdot \mathbf{v}_L \quad \forall \mathbf{v}_L \in \boldsymbol{\mathcal{V}}_L \tag{1.4}$$

  with $\boldsymbol{\mathcal{V}}_L = \{\mathbf{v} \in [H^1(\Omega_L)]^d\}$. The associated stress field is $\mathbb{\sigma}_L = \mathbf{K} \mathbb{e}(\mathbf{u}_L)$;

- a continuity condition on $\Gamma$:

$$\int_\Gamma (\mathbf{u}_L - \mathbf{u}_G) \cdot \boldsymbol{\mu} = 0 \quad \forall \boldsymbol{\mu} \in \boldsymbol{\mathcal{M}} \tag{1.5}$$

This formulation naturally ensures the kinematic compatibility between global and local displacements and the balance of tractions on the interface $\Gamma$ [Hansbo et al., 2005].

Using a discretization method with FE spaces $\boldsymbol{\mathcal{V}}_0^H \subset \boldsymbol{\mathcal{V}}_0$ (defined from a coarse partition $\tau^H$ of $\Omega_0$), $\boldsymbol{\mathcal{V}}_L^h \subset \boldsymbol{\mathcal{V}}_L$ (defined from an independent and usually finer partition $\tau^h$ of $\Omega_L$), and $\boldsymbol{\mathcal{M}}^h \subset \boldsymbol{\mathcal{M}}$ (i.e. the trace space defined from $\tau^h$), the algebraic formulation of the above problem reads:

$$\begin{bmatrix} \mathbb{K}_0 & 0 & \mathbb{C}_G^T \\ 0 & \mathbb{K}_L & -\mathbb{C}_L^T \\ \mathbb{C}_G & -\mathbb{C}_L & 0 \end{bmatrix} \begin{bmatrix} \mathbf{U}_G \\ \mathbf{U}_L \\ \boldsymbol{\Lambda} \end{bmatrix} = \begin{bmatrix} \mathbf{F}_0 \\ \mathbf{F}_L \\ 0 \end{bmatrix} \tag{1.6}$$

where $\mathbf{U}_G$, $\mathbf{U}_L$, and $\boldsymbol{\Lambda}$ are nodal value vectors of FE fields $\mathbf{u}_G^H$, $\mathbf{u}_L^h$, and $\boldsymbol{\lambda}^h$, respectively, $\mathbb{K}_0$ and $\mathbb{K}_L$ are stiffness matrices in $\Omega_0$ and $\Omega_L$, respectively, and $\mathbb{C}_G$ and $\mathbb{C}_L$ are coupling mortar operators.

In practice, and in order to conform with domain decomposition techniques and parallel computing, the previous coupling problem is not solved in a monolithic way but rather by means of an iterative Dirichlet-Neumann solver. To do so, an asymmetric local-global algorithm with alternated interface data transfer is introduced. After initializing $\boldsymbol{\lambda}^{(0)} = \mathbf{0}$ (zero interface reaction), the continuous problem at iteration $n$ consists in finding $(\mathbf{u}_G^{(n)}, \mathbf{u}_L^{(n)}, \boldsymbol{\lambda}^{(n)}) \in \boldsymbol{\mathcal{V}}_0 \times \boldsymbol{\mathcal{V}}_L \times \boldsymbol{\mathcal{M}}$ verifying

- a global problem over $\Omega_0$, with given Neumann boundary conditions $\boldsymbol{\lambda}^{(n-1)}$ on $\Gamma$, providing $\mathbf{u}_G^{(n)}$:

$$\int_{\Omega_0} \mathbf{K}_0 \mathbb{e}(\mathbf{u}_G^{(n)}) : \mathbb{e}(\mathbf{v}_G) = \int_{\Omega_0} \mathbf{f}_d \cdot \mathbf{v}_G + \int_{\partial_F \Omega} \mathbf{F}_d \cdot \mathbf{v}_G - \int_\Gamma \boldsymbol{\lambda}^{(n-1)} \cdot \mathbf{v}_G \quad \forall \mathbf{v}_G \in \boldsymbol{\mathcal{V}}_0 \tag{1.7}$$

and associated stress field $\mathbb{o}_G^{(n)} = \mathbf{K}_0 \mathbb{e}(\mathbf{u}_G^{(n)})$;

- a local problem over $\Omega_L$ with given Dirichlet boundary conditions derived from $\mathbf{u}_G^{(n)}$ on $\Gamma$, providing $(\mathbf{u}_L^{(n)}, \boldsymbol{\lambda}^{(n)})$:

$$\begin{aligned} \mathbf{u}_{L|\Gamma}^{(n)} &= \mathbf{u}_{G|\Gamma}^{(n)} \\ \int_{\Omega_L} \mathbf{K}\mathbb{e}(\mathbf{u}_L^{(n)}) : \mathbb{e}(\mathbf{v}_L) - \int_\Gamma \boldsymbol{\lambda}^{(n)} \cdot \mathbf{v}_L &= \int_{\Omega_L} \mathbf{f}_d \cdot \mathbf{v}_L \quad \forall \mathbf{v}_L \in \boldsymbol{\mathcal{V}}_L \end{aligned} \tag{1.8}$$

and associated stress field $\mathbb{o}_L^{(n)} = \mathbf{K}\mathbb{e}(\mathbf{u}_L^{(n)})$.

The corresponding algebraic formulation reads:

$$\mathbb{K}_0 \mathbf{U}_G^{(n)} = \mathbf{F}_0 - \mathbb{C}_G^T \boldsymbol{\Lambda}^{(n-1)} \quad ; \quad \begin{bmatrix} \mathbb{K}_L & -\mathbb{C}_L^T \\ -\mathbb{C}_L & 0 \end{bmatrix} \begin{bmatrix} \mathbf{U}_L^{(n)} \\ \boldsymbol{\Lambda}^{(n)} \end{bmatrix} = \begin{bmatrix} \mathbf{F}_L \\ -\mathbb{C}_G \mathbf{U}_G^{(n)} \end{bmatrix} \tag{1.9}$$

*Remark. We assume here that meshes $\tau^H$ and $\tau^h$ are geometrically compatible even though they do not match on $\Gamma$, i.e. the interface is aligned with the edges of the local and global elements. As a result, interface data are fully transmitted from one model to the other: the continuity of displacements can be enforced exactly (while traction equilibrium is enforced weakly on the interface approximation space) and a general mortar method [Bernardi et al., 2005] is used to transfer interface data between local and global problems. The numerical experiments reported in the manuscript are mostly performed in this context. In the more general case of a non-conforming interface, the transfer would require special attention in the implementation process, evaluating reaction forces with suitable quadrature rules, as performed in [Bouclier et al., 2016] for NURBS geometry representations. Alternative matching conditions have also been introduced in the literature for non-intrusive couplings, such as these based on a more regular mortar method [Bouclier et al., 2017], on a Nitsche method [Bouclier and Passieux, 2018], or on the use of a transition mesh to address topology changes between models [Guguin et al., 2014, Guguin et al., 2016, Guinard et al., 2018].*

**Non-intrusive coupling strategy**

A drawback of the previous intrusive coupling technique is that the stiffness matrix $\mathbb{K}_0$, that depends on the geometrical definition of $\Omega_0$ (and thus $\Omega_L$), should be computed for each particular configuration of the local zone $\Omega_L$. Indeed, it requires the construction of a global mesh which is conforming with the potentially complex geometry of $\Omega_0$. Consequently, remeshing and new factorization of $\mathbb{K}_0$ are necessary each time the location or shape of $\Omega_L$ is changed (e.g. in case of crack propagation). This appears to be much time consuming, in particular for large domains with many dofs involved, and in a multi-query context. To circumvent this issue and enhance the numerical efficiency, the key idea of the non-intrusive local-global coupling strategy is to modify the global problem (1.3), defining the support of its solution $\mathbf{u}_G$ over the whole domain $\Omega$.

In order to derive the new global problem, the homogenized linear elasticity behavior is fictively prolongated to $\Omega_L$. Consequently, using additivity of the integral over $\Omega_0 \cup \Omega_L$, the initial global problem (1.3) is recast as:

Find $\mathbf{u}_G \in \boldsymbol{\mathcal{V}}$ such that

$$\begin{aligned}\int_\Omega \mathbf{K}_0\mathbb{e}(\mathbf{u}_G) : \mathbb{e}(\mathbf{v}_G) &= \int_{\Omega_0} \mathbf{f}_d \cdot \mathbf{v}_G + \int_{\partial_F\Omega} \mathbf{F}_d \cdot \mathbf{v}_G - \int_\Gamma \boldsymbol{\lambda} \cdot \mathbf{v}_G + \int_{\Omega_L} \mathbf{K}_0\mathbb{e}(\mathbf{u}_G) : \mathbb{e}(\mathbf{v}_G) \quad \forall \mathbf{v}_G \in \boldsymbol{\mathcal{V}} \\ &= \int_\Omega \mathbf{f}_d \cdot \mathbf{v}_G + \int_{\partial_F\Omega} \mathbf{F}_d \cdot \mathbf{v}_G + \int_\Gamma [\mathbb{\sigma}_{G|\Omega_L}\mathbf{n}_{\Omega_L} - \boldsymbol{\lambda}] \cdot \mathbf{v}_G \quad \forall \mathbf{v}_G \in \boldsymbol{\mathcal{V}} \quad \text{using equilibrium in } \Omega_L\end{aligned} \tag{1.10}$$

with $\mathbb{\sigma}_G = \mathbf{K}_0\mathbb{e}(\mathbf{u}_G)$, and $\mathbf{n}_{\Omega_L}$ being the outward unit normal vector of $\Omega_L$. We emphasize that the corresponding solution $\mathbf{u}_G$, even though defined over the whole domain $\Omega$, is usually non-physical in $\Omega_L$ and irrelevant to analyze local phenomena of interest correctly (all the more so when $\mathbf{u}_G$ is approximated using a coarse mesh). Furthermore, it is not unique in $\Omega_L$ and a specific solution is in practice selected from the choice of the initialization in the coupling algorithm. Nevertheless, these do not represent any issue as $\mathbf{u}_G$ is eventually replaced by the local fine-scale solution $\mathbf{u}_L$ in $\Omega_L$ for analysis, so that there is no impact on the local-global solution.

Using the new discretization space $\boldsymbol{\mathcal{V}}^H$, obtained from a coarse mesh $\tau^H$ defined over the whole domain $\Omega$, the non-intrusive procedure leads to the following change regarding the algebraic formulation of the global problem:

$$\mathbb{K}_0\mathbf{U}_G = \mathbf{F}_0 - \mathbb{C}_G^T\boldsymbol{\Lambda} \quad \Longrightarrow \quad \mathbb{K}_{0\Omega}\mathbf{U}_G = \mathbf{F}_0 - \mathbb{C}_G^T\boldsymbol{\Lambda} + \mathbb{K}_{0L}\mathbf{U}_G = \mathbf{F}_{0\Omega} - \mathbb{C}_G^T\boldsymbol{\Lambda} + \mathbf{R}_{LG} \tag{1.11}$$

where $\mathbb{K}_{0\Omega}$ (resp. $\mathbb{K}_{0L}$) is the stiffness matrix computed over the whole domain $\Omega$ (resp. over the subdomain $\Omega_L$) using the smooth linear operator $\mathbb{K}_0$, while $\mathbf{R}_{LG} = \mathbb{K}_{0L}\mathbf{U}_G - \mathbf{F}_{0L}$ corresponds to the discretized interface reaction forces coming from the fictitious part of the global model (referred as the auxiliary model), computed in practice from volume integrals.

Introducing again an iterative Dirichlet-Neumann solution scheme (fixed point algorithm), the non-intrusive local-global coupling method consists in finding, at each iteration $n$ of the process and after initializing $\mathbf{u}_G^{(0)} = \mathbf{0}$ and $\boldsymbol{\lambda}^{(0)} = \mathbf{0}$, the set $(\mathbf{u}_G^{(n)}, \mathbf{u}_L^{(n)}, \boldsymbol{\lambda}^{(n)}) \in \boldsymbol{\mathcal{V}} \times \boldsymbol{\mathcal{V}}_L \times \boldsymbol{\mathcal{M}}$ verifying

- a global problem over $\Omega$, with given internal reaction forces on $\Gamma$, providing $\mathbf{u}_G^{(n)}$:

$$\begin{aligned}\int_\Omega \mathbf{K}_0\mathbb{e}(\mathbf{u}_G^{(n)}) : \mathbb{e}(\mathbf{v}_G) &= \int_{\Omega_0} \mathbf{f}_d \cdot \mathbf{v}_G + \int_{\partial_F\Omega} \mathbf{F}_d \cdot \mathbf{v}_G - \int_\Gamma \boldsymbol{\lambda}^{(n-1)} \cdot \mathbf{v}_G + \int_{\Omega_L} \mathbf{K}_0\mathbb{e}(\mathbf{u}_G^{(n-1)}) : \mathbb{e}(\mathbf{v}_G) \quad \forall \mathbf{v}_G \in \boldsymbol{\mathcal{V}} \\ &= \int_\Omega \mathbf{f}_d \cdot \mathbf{v}_G + \int_{\partial_F\Omega} \mathbf{F}_d \cdot \mathbf{v}_G + \int_\Gamma [\mathbb{\sigma}_{G|\Omega_L}^{(n-1)}\mathbf{n}_{\Omega_L} - \boldsymbol{\lambda}^{(n-1)}] \cdot \mathbf{v}_G \quad \forall \mathbf{v}_G \in \boldsymbol{\mathcal{V}}\end{aligned} \tag{1.12}$$

  and associated stress field $\mathbb{\sigma}_G^{(n)} = \mathbf{K}_0\mathbb{e}(\mathbf{u}_G^{(n)})$;

- a local problem over $\Omega_L$ with given Dirichlet boundary conditions on $\Gamma$, providing ($\mathbf{u}_L^{(n)}$, $\boldsymbol{\lambda}^{(n)}$):

$$\begin{aligned} \mathbf{u}_{L|\Gamma}^{(n)} &= \mathbf{u}_{G|\Gamma}^{(n)} \\ \int_{\Omega_L} \mathbf{K}\mathbb{e}(\mathbf{u}_L^{(n)}) : \mathbb{e}(\mathbf{v}_L) - \int_\Gamma \boldsymbol{\lambda}^{(n)} \cdot \mathbf{v}_L &= \int_{\Omega_L} \mathbf{f}_d \cdot \mathbf{v}_L \quad \forall \mathbf{v}_L \in \boldsymbol{\mathcal{V}}_L \end{aligned} \tag{1.13}$$

  and associated stress field $\mathbb{s}_L^{(n)} = \mathbf{K}\mathbb{e}(\mathbf{u}_L^{(n)})$.

*Remark. Writing the global problem in an incremental way reads:*

$$\int_\Omega (\mathbb{s}_G^{(n)} - \mathbb{s}_G^{(n-1)}) : \mathbb{e}(\mathbf{v}_G) = \int_{\Omega_0} \mathbf{f}_d \cdot \mathbf{v}_G + \int_{\partial_F \Omega} \mathbf{F}_d \cdot \mathbf{v}_G - \int_\Gamma \boldsymbol{\lambda}^{(n-1)} \cdot \mathbf{v}_G - \int_{\Omega_0} \mathbb{s}_G^{(n-1)} : \mathbb{e}(\mathbf{v}_G) \quad \forall \mathbf{v}_G \in \boldsymbol{\mathcal{V}} \tag{1.14}$$

The corresponding algebraic formulation reads:

$$\begin{aligned} \mathbb{K}_{0\Omega}\mathbf{U}_G^{(n)} &= \mathbf{F}_0 - \mathbb{C}_G^T \boldsymbol{\Lambda}^{(n-1)} + \mathbb{K}_{0L}\mathbf{U}_G^{(n-1)} \quad ; \quad \begin{bmatrix} \mathbb{K}_L & -\mathbb{C}_L^T \\ -\mathbb{C}_L & 0 \end{bmatrix} \begin{bmatrix} \mathbf{U}_L^{(n)} \\ \boldsymbol{\Lambda}^{(n)} \end{bmatrix} = \begin{bmatrix} \mathbf{F}_L \\ -\mathbb{C}_G \mathbf{U}_G^{(n)} \end{bmatrix} \\ &= \mathbf{F}_{0\Omega} - \mathbb{C}_G^T \boldsymbol{\Lambda}^{(n-1)} + \mathbf{R}_{LG}^{(n-1)} \end{aligned} \tag{1.15}$$

We point out that the global stiffness matrix $\mathbb{K}_{0\Omega}$, as well as the global force vector $\mathbf{F}_{0\Omega}$, are fixed independently of the local model parameters (position and shape of $\Omega_L$, mesh size used in $\tau^h$). They correspond to quantities that would be initially computed considering a smooth behavior over the whole structure, i.e. without any analysis of local complex phenomena, and using a global coarse mesh. The global stiffness operator is therefore assembled and factorized only once, which refers to the non-intrusive feature of the coupling method.

Essentially, the non-intrusive coupling technique thus consists in alternating between local calculations over $\Omega_L$ with prescribed displacements on the coupling interface, and global correction calculations over the whole domain $\Omega$ which include inner corrective loads (in terms of equilibrium residual, i.e. reaction forces mismatch) in order to reduce the imbalance between concurrent models. Two independent numerical softwares may be used to perform the local and global calculations. A sketch of the associated local-global algorithm is given in Figure 1.4. The overall principle of this algorithm is to find (by means of an iterative procedure with corrections) an extra-load to be applied to the global model on the interface $\Gamma$, such that local and complementary models are in balance at the interface.

It can be shown that, under some conditions (e.g. multiscale elliptic problem, or high-fidelity model operator not stiffer than the coarse global (auxiliary) model one in the local zone of interest, which is the usual case in practical applications), the solution to the fixed point (1.12)-(1.13) converges to the solution to the initial coupling problem (1.3)-(1.5). We refer to [Gendre et al., 2009, Chevreuil et al., 2013, Duval et al., 2016, Nouy and Pled, 2018]

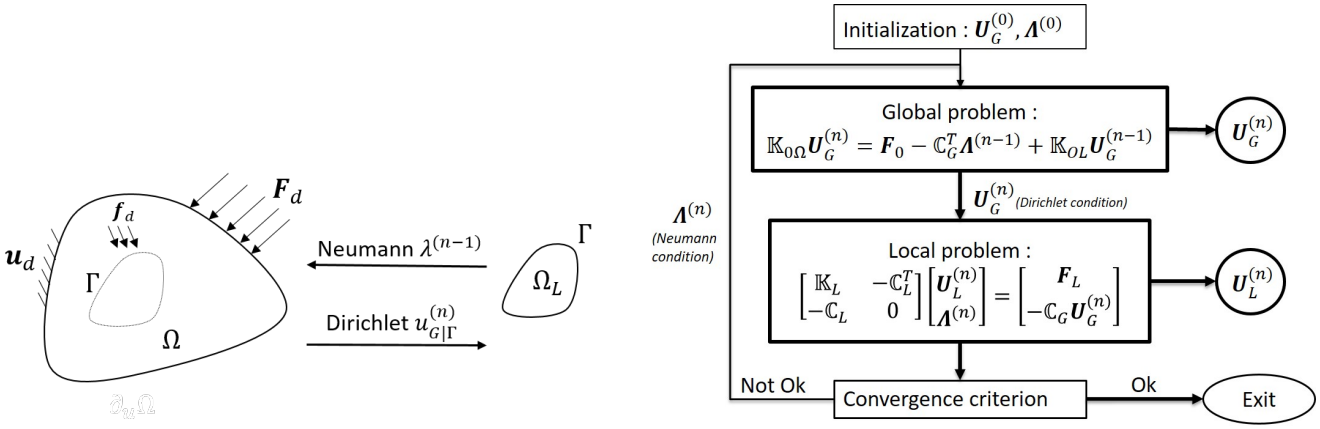


Figure 1.4: Illustration of the non-intrusive local-global coupling strategy.

for a review on these aspects, based on a global reformulation of the iterative non-intrusive local-global coupling strategy that can be interpreted as a quasi-Newton algorithm on reaction force equilibrium. The approach can also be registered among Schwarz alternating methods for which many convergence results exist [Gosselet et al., 2018].

The number of solver iterations is the price to pay in the non-intrusive coupling method compared with the intrusive version. Classically, a relative norm on the interface residual is used as a convergence indicator and stopping criterion in order to monitor the iterative procedure. Nevertheless, we mention that convergence acceleration techniques [Brezinski, 2000] can be used in this framework, such as the dynamic Aitken relaxation [Aitken, 1926, Irons and Tuck, 1969, Duval et al., 2016], or the update of the global operator (without factorizing it again) using the symmetric rank one (SR1) update [Conn et al., 1991] and/or the Shermann-Morison and Woodbury formulas [Gendre et al., 2009]. Relaxation may also be used to ensure convergence when auxiliary model is more compliant than the local model. Moreover, mixed interface conditions may be considered between local and global models [Gendre et al., 2009, Oumaziz et al., 2017, Oumaziz et al., 2018]. All these techniques will not be implemented in the present work.

*Remark. Basically, the local-global coupling framework is merely seen as a behavior substitution in $\Omega_L$ (numerical zoom), starting from an initial smooth behavior (with homogeneous operator $\mathbf{K}_0$) defined over the whole domain $\Omega$. We adopt here another vision, deriving the coupling problem from an initial reference model in which the complex material behavior (with heterogeneous operator $\mathbf{K}$) is introduced everywhere in $\Omega$. This reference model is next coarsened by replacing $\mathbf{K}$ with the homogeneous operator $\mathbf{K}_0$ in $\Omega_0$. This enables to have a consistent definition of the reference solution, from which error measures will be later defined (see next chapter).*

*Remark. In case of non-conforming meshes at the coupling interface, a transfer matrix should be used to connect local and global displacement fields. This matrix can be derived for instance from the mortar method [Liu et al., 2014, Duval et al., 2016]. We will not consider this case in the following, even though it does not bring major*

*technical issues for the overall strategy developed in the PhD.*

*Remark. Even though it is out of the scope of the PhD work, the non-intrusive global-local coupling technique may require additional technicalities when considering nonlinear time-dependent problems, with different time grids at the global and local levels. In particular, it is important in this case to provide sufficient synchronization of the time grids in order to preserve the consistency of the coupling. An illustrative study is performed in [Blanchard et al., 2019] in the context of viscoplastic models.*

### 1.1.3 Illustrative example

As a simple illustration of the non-intrusive local-global coupling strategy, we consider an elastic bar of length $L$, clamped on its left end ($x = 0$) and subjected to a given displacement $u_d$ on its right end ($x = L$). It is made of a material with constant Young's modulus $E$, except in a local zone $\omega = ]0, \ell[$ where the Young modulus is $\widetilde{E} < E$, which corresponds to a local weakening (Figure 1.5). The interface $\Gamma$ corresponds here to point $x = \ell$. We denote by $N$ the exact (constant) force in the beam and $u_{|\Gamma}$ the exact longitudinal displacement on the interface.
It is straightforward, using the relations $N = \widetilde{E}\dfrac{u_{|\Gamma}}{\ell} = E\dfrac{u_d - u_{|\Gamma}}{L - \ell}$, to obtain the exact analytical primal solution of the problem:

$$u_{|\Gamma} = \frac{E\ell u_d}{E\ell + \widetilde{E}(L-\ell)} = u_d \frac{\ell}{L} \frac{1}{1 - \frac{E-\widetilde{E}}{E}.\frac{L-\ell}{L}} = u_d \frac{\ell}{L}\left(1 + \frac{E-\widetilde{E}}{E}.\frac{L-\ell}{L} + \left(\frac{E-\widetilde{E}}{E}.\frac{L-\ell}{L}\right)^2 + \dots\right) \tag{1.16}$$

We now implement the non-intrusive local-global algorithm on this problem, considering the local model in $\omega$ and defining a global model with Young modulus $E$ over the whole domain. As detailed in Figure 1.5, global and local models can be introduced and processed in a direct manner: (i) a given displacement $u_{|\Gamma}$ on the interface $\Gamma$ yields a force $N_L = \widetilde{E}\dfrac{u_{|\Gamma}}{\ell}$ for the local model; (ii) a given (incremental) force $\delta F_{|\Gamma}$ on the interface $\Gamma$ yields a corresponding displacement $\delta u_{|\Gamma} = \dfrac{\delta F_{|\Gamma}\ell(L-\ell)}{EL}$ on the interface, and force $\delta N_G = -\delta F_{|\Gamma}\dfrac{\ell}{L}$ for $x > \ell$ for the incremental version of the global problem. Consequently, the various iterations of the local-global algorithm read as follows:

- Initial global solution at iteration 1:

$$u^{(1)}_{|\Gamma} = u_d\frac{\ell}{L} \quad ; \quad N^{(1)}_G = E\frac{u_d}{L} \tag{1.17}$$

- Local solution at iteration 1, with interface displacement $u^{(1)}_{|\Gamma} = u_d\dfrac{\ell}{L}$:

$$N^{(1)}_L = \widetilde{E}\frac{u^{(1)}_{|\Gamma}}{\ell} = \widetilde{E}\frac{u_d}{L} \tag{1.18}$$

- Global solution at iteration 2, with incremental interface force $\delta F_{|\Gamma}^{(1)} = N_G^{(1)} - N_L^{(1)} = (E - \widetilde{E})\dfrac{u_d}{L}$:

$$\delta u_{|\Gamma}^{(2)} = \frac{\delta F_{|\Gamma}^{(1)} \ell (L-\ell)}{EL} = u_d \frac{\ell}{L} \frac{E-\widetilde{E}}{E} \frac{L-\ell}{L} \quad ; \quad \delta N_{G,x>\ell}^{(2)} = -\delta F_{|\Gamma}^{(1)} \frac{\ell}{L} = -(E-\widetilde{E}) \frac{u_d}{L} \frac{\ell}{L} \tag{1.19}$$

- Local solution at iteration 2, with interface displacement $u_{|\Gamma}^{(2)} = u_{|\Gamma}^{(1)} + \delta u_{|\Gamma}^{(2)} = u_d \dfrac{\ell}{L}(1 + \dfrac{E-\widetilde{E}}{E} \dfrac{L-\ell}{L})$:

$$N_L^{(2)} = \widetilde{E} \frac{u_{|\Gamma}^{(2)}}{\ell} = \widetilde{E} \frac{u_d}{L} (1 + \frac{E-\widetilde{E}}{E} \frac{L-\ell}{L}) \tag{1.20}$$

- Global solution at iteration 3, with incremental interface force $\delta F_{|\Gamma}^{(2)} = N_G^{(1)} + \delta N_{G,x>\ell}^{(2)} - N_L^{(2)} = \dfrac{(E-\widetilde{E})^2}{E} \dfrac{u_d}{L} \dfrac{L-\ell}{L}$:

$$\delta u_{|\Gamma}^{(3)} = \frac{\delta F_{|\Gamma}^{(2)} \ell (L-\ell)}{EL} = u_d \frac{\ell}{L} \left( \frac{(E-\widetilde{E})}{E} \right)^2 \left( \frac{L-\ell}{L} \right)^2 \quad ; \quad \delta N_{G,x>\ell}^{(3)} = -\delta F_{|\Gamma}^{(2)} \frac{\ell}{L} = -\frac{(E-\widetilde{E})^2}{E} \frac{u_d}{L} \frac{L-\ell}{L} \frac{\ell}{L} \tag{1.21}$$

At convergence, we get:

$$\begin{aligned} u_{|\Gamma} &= u_{|\Gamma}^{(1)} + \delta u_{|\Gamma}^{(2)} + \delta u_{|\Gamma}^{(3)} + \cdots = u_d \frac{\ell}{L} \left( 1 + \frac{E-\widetilde{E}}{E} . \frac{L-\ell}{L} + \left( \frac{E-\widetilde{E}}{E} . \frac{L-\ell}{L} \right)^2 + \dots \right) \\ N_{G,x>\ell} &= N_G^{(1)} + \delta N_{G,x>\ell}^{(2)} + \delta N_{G,x>\ell}^{(3)} + \cdots = E \frac{u_d - u_{|\Gamma}}{L - \ell} \\ N_L &= \widetilde{E} \frac{u_{|\Gamma}}{\ell} \end{aligned} \tag{1.22}$$

which corresponds to the exact solution.

Global and local solutions along the iterations are plot in Figures 1.6 and 1.7, respectively. They are computed for the following values of parameters: $L$=1; $\ell$=0.3, $E$=10, $\widetilde{E}$=3, and $u_d$=1.

## 1.2 Control of modelling errors when using surrogate models in computational mechanics

### 1.2.1 Context and motivations

The always growing computing resources, associated with more and more precise and validated mathematical models, enable to simulate very complex physical phenomena nowadays. However, there are some families of physical problems for which the initial simulation model is still intractable by current numerical capabilities. A coarser

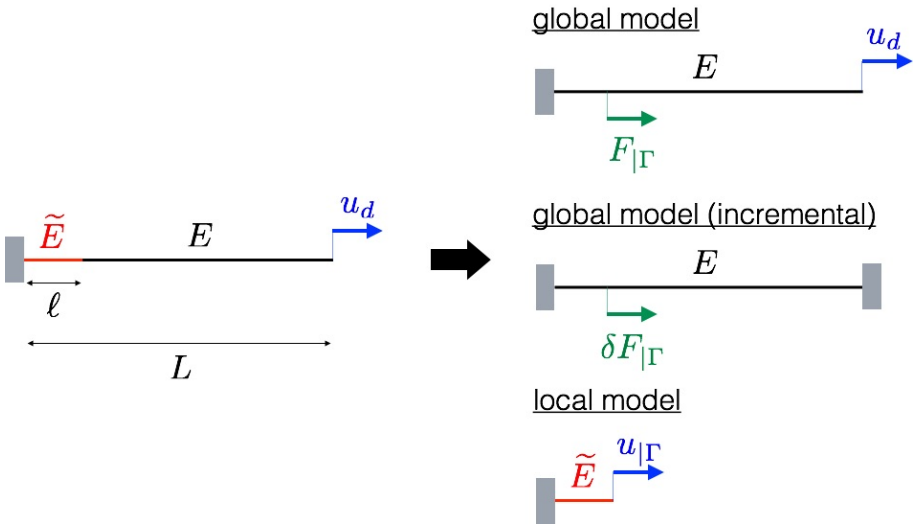


Figure 1.5: Non-intrusive local-global coupling performed on the considered bar.

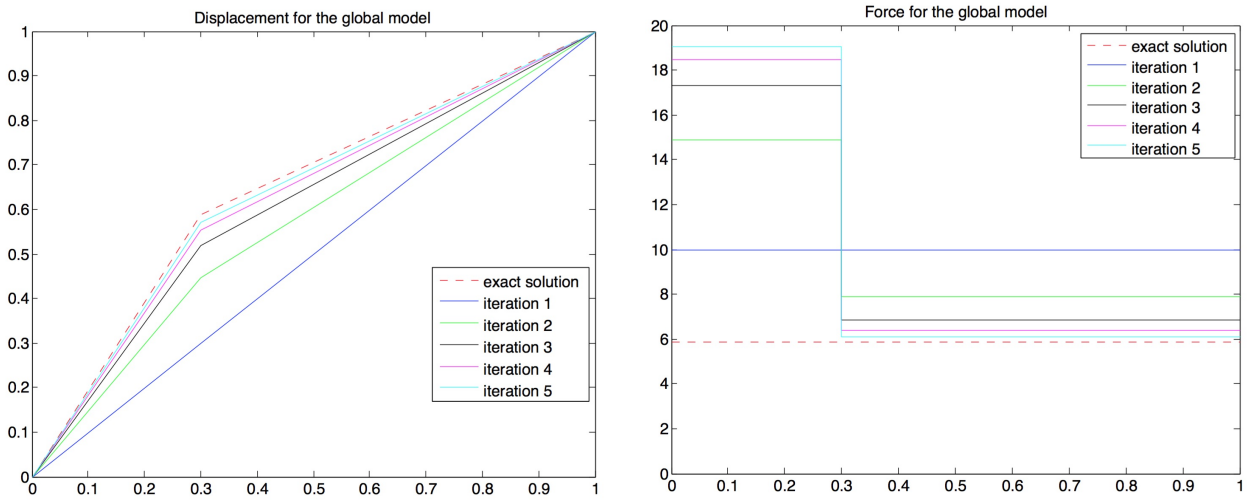


Figure 1.6: Global solution along the algorithm iterations: displacement (left) and force (right).

model (usually associated with some homogenization procedure or asymptotic limit, and sometimes involving the coupling of different types of equations) is thus mandatory and leads to a multiscale approach of the problem. On the other hand, the simulation of a physical phenomenon is usually performed in order to get information on a set of specific quantities of interest. From the analyst point of view, a critical issue is therefore to know whether or not the simulation model is sufficiently relevant for the assessment of such quantities of interest. In other words, goal-oriented information on modeling error is required.

During the last decade, and especially in the Computational Mechanics community, tools have been introduced in order to assess and control the quality of computerized models [Oden and Vemaganti, 2000, Oden and Prudhomme, 2002]. They were constructed from verification approaches which had been originally developed and implemented for *a posteriori* error estimation and mesh adaptation in the context of the finite element method [Verfürth, 1996,

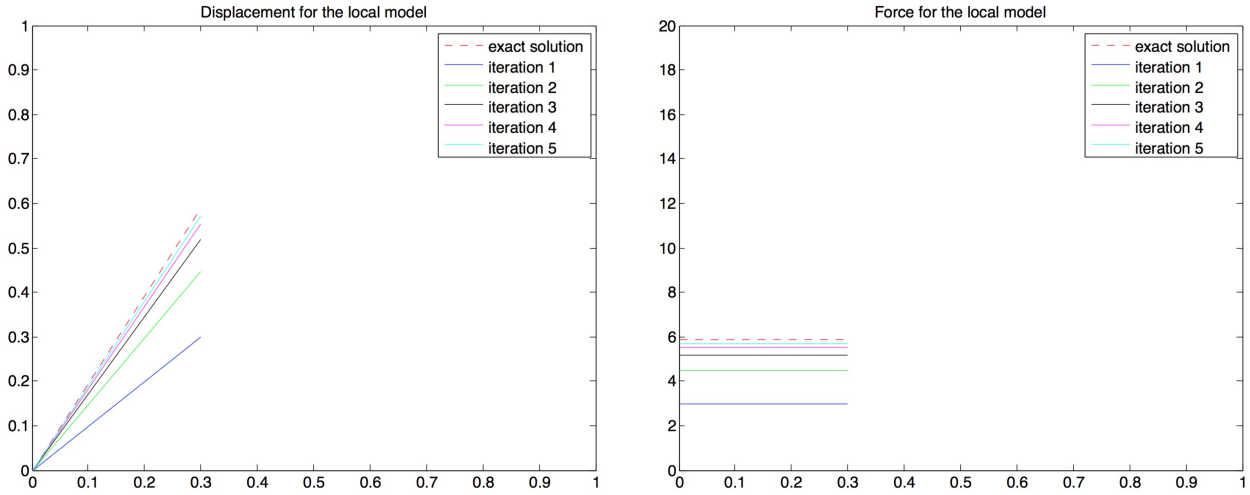


Figure 1.7: Local solution along the algorithm iterations: displacement (left) and force (right).

Ainsworth and Oden, 2000, Ladevèze and Pelle, 2005, Chamoin and Díez, 2016]; more specifically, they referred to the residual functional. Moreover, dedicated algorithms have also been introduced in order to adapt the surrogate model up to an acceptable error level. These tools dedicated to modelling error estimation were initially implemented in the context of hierarchical modeling with heterogeneous materials [Oden and Zohdi, 1997, Oden and Vemaganti, 2000, Vemaganti and Oden, 2001], before being applied in many applications with various multiscale contexts [Oden et al., 2005, Oden et al., 2006b, Romkes et al., 2006, Bauman et al., 2009, Prudhomme et al., 2009, Chamoin and Desvillettes, 2013, Zaccardi et al., 2013, Prudhomme and Bryant, 2015, Maier and Rannacher, 2018, Scarabosio et al., 2019, Tirvaudey et al., 2020b].

### 1.2.2 General methodology

In this section, we briefly present the general background for goal-oriented assessment of modeling errors initially developed in [Oden and Vemaganti, 2000, Oden and Prudhomme, 2002].

#### Definition of modeling error

We suppose that $u \in U$ is the solution to a general reference problem of the following weak form:

$$a(u; z) = l(z) \quad \forall z \in V \tag{1.23}$$

$a$ being potentially nonlinear with respect to $u$. In practical cases, this reference problem may be intractable and we are led to consider a surrogate problem (e.g. with model coupling) of the form: find $u_0 \in U_0$ such that

$$a_0(u_0; z_0) = l_0(z_0) \quad \forall z_0 \in V_0 \tag{1.24}$$

The solution $u_0$ is an affordable approximation of $u$. The case $\{a_0, l_0\} = \{a, l\}$ but $\{U_0, V_0\} \neq \{U, V\}$ corresponds to simple discretization with FEM for instance, while the reverse case corresponds to pure model coarsening; we consider this last case in the following.

We suppose that we are interested in a quantity of interest $Q(u)$ that is a localized specific feature (scalar output) derived from the solution $u$ to the reference model. It usually characterizes the local response at small scales, and is critical for design purposes. The modeling error in the quantity of interest $Q$ that we aim to assess thus reads $\mathcal{E}_Q = Q(u) - Q(u_0)$.

*Remark. In practice, the numerical simulations enable to compute an approximate solution $u_0^h$ of $u_0$ only, after FE discretization; we can thus define the total error on $Q$:*

$$Q(u) - Q(u_0^h) = [Q(u) - Q(u_0)] + [Q(u_0) - Q(u_0^h)] = \mathcal{E}_Q^{mod} + \mathcal{E}_Q^{dis} \tag{1.25}$$

*where $\mathcal{E}_Q^{mod}$ (resp. $\mathcal{E}_Q^{dis}$) is the error on $Q$ due to modeling (resp. due to discretization). Part of the error due to discretization can be assessed and controlled using well-known a posteriori error estimation techniques [Verfürth, 1996, Ainsworth and Oden, 2000, Chamoin and Díez, 2016].*

**Adjoint problem and goal-oriented error estimation**

For the purpose of estimating $\mathcal{E}_Q^{mod} = Q(u) - Q(u_0)$, the classical goal-oriented error estimation approach with the introduction of an adjoint problem is followed [Paraschivoiu et al., 1997, Rannacher and Suttmeier, 1997, Prudhomme and Oden, 1999, Oden and Prudhomme, 2001, Giles and Suli, 2002]. This auxiliary problem can be naturally derived from an optimal control point-of-view, considering $Q(u)$ as the solution to a constrained minimization problem [Becker and Rannacher, 2001]. The adjoint problem reads: find $p \in V$ such that:

$$a'(u; v, p) = Q'(u; v) \quad \forall v \in V \tag{1.26}$$

where $a'$ and $Q'$ are Gâteaux-derivatives of $a$ and $Q$, respectively:

$$a'(u; v, p) = \lim_{\theta \to 0} \frac{1}{\theta}[a(u + \theta v; p) - a(u; p)] \quad ; \quad Q'(u; v) = \lim_{\theta \to 0} \frac{1}{\theta}[Q(u + \theta v) - Q(u)] \tag{1.27}$$

The solution $p$ can be seen as an influence function that acts as a filter to capture only part of the error that impacts the quantity of interest; it thus fully depends on the choice of the quantity of interest.

*Remark. When $a$ and $Q$ are respectively bilinear and linear functionals, the adjoint problem reduces to:*

$$\textit{Find } p \in V \textit{ such that } a(v,p) = a^*(p,v) = Q(v) \quad \forall v \in V \tag{1.28}$$

*where $a^*$ is defined from the adjoint operator.*

The previous adjoint problem (1.26) is linear but unsolvable as the solution $u$ is not available. We shall thus consider the following approximate adjoint problem: find $p_0 \in V$ such that:

$$a'(u_0; v, p_0) = Q'(u_0; v) \quad \forall v \in V \tag{1.29}$$

Then, the error $Q(u) - Q(u_0)$ can be represented as (see [Oden and Prudhomme, 2002] for all details):

$$Q(u) - Q(u_0) = \mathcal{R}(u_0; p) + \Delta = \mathcal{R}(u_0; p_0) + \mathcal{R}(u_0; p - p_0) + \Delta \tag{1.30}$$

where $\mathcal{R}$ denotes the residual functional, that is $\mathcal{R}(u_0; v) = l(v) - a(u_0; v)$ (which represents the degree to which $u_0$ fails to satisfy the reference problem), and $\Delta$ is a remainder term of higher order in the errors $e_0 = u - u_0$ and $\epsilon_0 = p - p_0$. If $a$ and $Q$ are thrice differentiable, it can be explicitly written as:

$$\begin{aligned} \Delta =& \frac{1}{2} \int_0^1 \{a''(u_0 + se_0; e_0, e_0, p_0 + s\epsilon_0) - Q''(u_0 + se_0; e_0, e_0) \\ &+ [Q'''(u_0 + se_0; e_0, e_0, e_0) - 3a''(u_0 + se_0; e_0, e_0, \epsilon_0) - a'''(u_0 + se_0; e_0, e_0, e_0, p_0 + s\epsilon_0)](s-1)s\} ds \end{aligned} \tag{1.31}$$

However, the adjoint problem is still defined with respect to the full fine scale model and once again may be intractable for error estimation. Introducing a surrogate model for the adjoint problem (e.g. with model coupling), with solution $\tilde{p}_0$, and assuming the error $p - \tilde{p}_0$ is small (saturation assumption), we thus define the error estimate as:

$$\eta_Q^{mod} = \mathcal{R}(u_0; \tilde{p}_0) \approx Q(u) - Q(u_0) \tag{1.32}$$

which refers to the dual-weighted residual (DWR) method [Becker and Rannacher, 1996] for *a posteriori* error estimation. In this framework, the approximate solution $\tilde{p}_0$ should be chosen in a space richer than $u_0$ in order to get a relevant error estimate.

*Remark. When solving problems with FEM and taking discretization error into account, other estimates can be derived:*

- *First, an estimate of the total error on the quantity of interest reads:*

$$\mathcal{E}_Q \approx \mathcal{R}(u_0^h, \tilde{p}_0^h) = \eta_Q^{tot}, \tag{1.33}$$

*where $u_0^h$ and $\tilde{p}_0^h$ are computed solutions obtained after discretizations of coupled reference and adjoint problems.*

- *Second, if one wants to assess the discretization error only, a dedicated estimate is:*

$$\mathcal{E}_Q^{dis} \approx \mathcal{R}_0(u_0^h; \tilde{p}_0^h) := l_0(\tilde{p}_0^h) - a_0(u_0^h, \tilde{p}_0^h) == \eta_Q^{dis} \tag{1.34}$$

*i.e. an estimate defined taking the surrogate problem as the reference, and therefore based on the associated residual functional $\mathcal{R}_0$. The accuracy of such an estimate requires a discretization which is finer for computing $\tilde{p}_0^h$ than for computing $u_0^h$ (due to the Galerkin orthogonality property).*

*Let us notice that only estimates* (1.33) *and* (1.34) *are actually computable, as FE approximations of $u_0$ and $\tilde{p}_0$ are the only solutions at hand. Therefore, a relevant modeling error estimation process may consist in first assessing the discretization error $\mathcal{E}_Q^{dis}$ and checking that it is small in order to use the estimate $\mathcal{E}_Q^{mod} \approx \mathcal{E}_Q \approx \mathcal{R}(u_0^h; \tilde{p}_0^h)$.*

**Adaptive strategy**

When using a surrogate model, it is fundamental to be able to adapt it if need be, in order to reach a target accuracy. From the previous error estimation strategy, an adaptive scheme (referred to as *Goal algorithm* in the literature) can be derived for this purpose. The general objective of goal-oriented adaptivity is to construct a procedure that drives the definition of the surrogate model so as to control the error $Q(u) - Q(u_0)$ within some preset error tolerance $\gamma_{tol}$. This is generally achieved by generating a sequence of surrogate problems with solutions $u_0^{(k)}$ so that for some integer $\overline{k}$, the modeling error satisfies $|Q(u) - Q(u_0^{(\overline{k})})| \leq \gamma_{tol}$. At each iteration, the goal is to reduce the global quantity $\mathcal{R}(u_0^{(k)}; \tilde{p}_0^{(k)})$ by locally enriching the surrogate model, i.e. by locally switching to the high-fidelity model in those subregions where the coarser model is not accurate enough. This is possible by observing that the residual term $\eta_Q^{mod}$ is defined globally over the whole domain and can be decomposed into local contributions $\eta_c$ defined over predefined subdomains of $\Omega$. It seems natural to choose as subdomains the elements of the finite element mesh used to discretize the continuum model. Finally, prescribing a user-defined parameter $\gamma_a$ such that $0 < \gamma_a < 1$, the subdomains with contributions $\eta_c$ can be switched from the coarse model to the high-fidelity model whenever $\eta_c > \gamma_a \max_c \eta_c$. The proposed greedy algorithm for adaptation of the surrogate model reads as follows:

1. Specify the error tolerance for the quantity of interest $\gamma_{tol}$ and the refinement parameter $\gamma_a$
2. Solve the primal surrogate problem and compute $u_0^{(k)}$ for current model configuration $k$
3. Solve the approximate adjoint problem and compute $\tilde{p}_0^{(k)}$ for current model configuration $k$
1. Compute $\eta_Q^{mod} = \mathcal{R}(u_0^{(k)}; \tilde{p}_0^{(k)})$. If $|\eta_Q^{mod}/Q(u_0^{(k)})| < \gamma_{tol}$ then stop. Otherwise continue to next step
4. Decompose the residual term $\mathcal{R}(u_0^{(k)}; \tilde{p}_0^{(k)})$ into contributions $\eta_c$ over predefined subdomains
5. Switch subdomain with contribution $\eta_c$ to finer model if $\eta_c > \gamma_a \max_c \eta_c$, and go to step 2

Figure 1.8: Greedy algorithm for goal-oriented error estimation and control of modeling error.

### 1.2.3 Application to non-intrusive local-global couplings

As any numerical method, the non-intrusive local-global coupling method described in Section 1.1 is impacted by errors coming from various sources. These need to be controlled in order to certify the numerical accuracy of the method and permit its transfer and robust use in industrial activities, but also to compute right at the right cost with smart use of computing resources. In the non-intrusive coupling framework, and using notations of Section 1.1.2, error sources are of three types:

- *modeling error* due to the use of a surrogate model in $\Omega_0$, associated with a smooth material operator $\mathbf{K}_0$ and a fixed (i.e., not adaptive) coarse mesh $\tau^H$. It may generate pollution effects when dealing with the accuracy of quantities of interest defined inside $\Omega_L$. The amplitude of this error source can be reduced by increasing the size of the critical zone $\Omega_L$, and it vanishes when $\Omega_L = \Omega$;

- *discretization error* due to the use of a mesh $\tau^h$ in order to approximate the solution of the local problem (1.13). The amplitude of this error source can be reduced by decreasing the mesh size $h$ in $\tau^h$, and it vanishes when $h$ goes to zero;

- *convergence (or algebraic) error* due to the use of an iterative local-global algorithm. The amplitude of this error source can be reduced by increasing the number of local-global iterations, and it vanishes when $n$ tends to $+\infty$.

Numerical parameters associated to these error sources need to be carefully selected in order to get relevant simulation results in terms of output values used for decision-making. In practical applications of the non-intrusive coupling method, $\Omega_L$ and $\tau^h$ are usually defined empirically, from the *a priori* user experience, without any quantitative assessment of associated modeling and discretization errors. In addition, the convergence of the local-global iterative algorithm is classically controlled using stopping criteria (convergence indicators) based on the magnitude of a norm on the interface residual. This procedure may be very pessimistic and may use unnecessary computing resource, as: (i) the error tolerance on outputs of interest may be fulfilled even though the full local-global solution has not converged, so that the iterative algorithm could be stopped earlier without sacrificing the accuracy on these outputs; (ii) the convergence error, even large, may rapidly become negligible compared to other error sources, so that further iterations become useless to decrease the overall error.

Consequently, it is of interest to design tools that provide for a quantitative assessment of error measures as well as individual error contributions coming from various sources. Such tools could then be effectively used to drive an automated adaptive algorithm that optimally defines $\Omega_L$, $\tau^h$, and the required number of iterations (for a prescribed error tolerance), so that numerical performance in terms of computational cost is substantially enhanced. This is the topic of the remainder of this chapter, and of the next chapters, in which fully computable error estimators and indicators are developed.

In the current literature, and contrary to other multiscale or multi-model methods [Wohlmuth, 1999, Strouboulis et al., 2006, Larson and Malqvist, 2007, Abdulle and Nonnenmacher, 2009, Larsson and Runesson, 2011, Jhurani and Demkowicz, 2012, Henning et al., 2014, Chung et al., 2016, Paladim et al., 2017, Chamoin and Legoll, 2018, Chamoin and Legoll, 2021], there are very few works dealing with error estimation and adaptivity for non-intrusive local-global couplings. The work detailed in [Duval et al., 2018] is pioneering in this context; it constructs a cheap and global (i.e. in the energy norm) *a posteriori* error estimator based on an explicit residual technique. This estimator enables to control discretization and convergence (or algebraic) errors, and it may be used in practice to drive both mesh adaptation in the local model zone (supposed to have a fixed definition in [Duval et al., 2018]) and iteration stopping. Nevertheless, such a verification tool for non-intrusive local-global couplings does not provide a quantitative error assessment with computable bounds. Moreover, it does not consider modeling and pollution errors which are major concerns in model coupling; this is a drawback for robust design. Eventually, it may be too pessimistic when considering accuracy on outputs of interest, leading to unnecessary computing efforts.

In a very recent work [Tirvaudey et al., 2020b], there was a step forward in the certification of the non-intrusive local-global coupling method, so that the quality of simulation results can be better controlled for industrial purposes [Guinard et al., 2018]. Advanced tools were developed, in terms of fully computable *a posteriori* error estimator and indicators, in order to assess all error sources and drive effective adaptive procedures with low implementation effort. Error indicators were derived to separate contributions of each individual error source, including

modeling error with pollution effects. They were computed at each step of the iterative and adaptive local-global coupling process. They also fed a greedy adaptive algorithm that aims at automatically and iteratively meeting a given error tolerance with minimal computing effort, tuning at best the coupled numerical model (in terms of local zone $\Omega_L$ and local mesh $\tau^h$) as well as parameters of the coupling algorithm (number of local-global iterations). In particular, it was shown that the local-global iterations can be stopped when the convergence error (associated with goal-oriented unbalance at the coupling interface) becomes insignificant compared to other error contributions; this is an alternative to classical stopping criteria based on the decrease of a norm of the interface residual, and it avoids useless and costly iterations which would not improve the quality of the solution outputs. Eventually, the verification procedure proposed in [Tirvaudey et al., 2020b] indicates where to put the final coupling interface (according to the level of modeling error), and which discretization should be used in the local model zone (according to the level of discretization error), so that a trade-off is obtained between solution accuracy and numerical cost.
We emphasize that the non-intrusive feature of the local-global coupling substantially facilitates the implementation of the error estimation and adaptive procedures developed in [Tirvaudey et al., 2020b], as mesh refinement in the local model zone $\Omega_L$ and modifications in the geometry of this zone can be performed independently of the global model. Moreover, it brings flexibility in the analysis of various scenarios for optimal and certified modeling.

In the following, we detail the work performed in [Tirvaudey et al., 2020b], which can be seen as a specific extension of the DWR approach developed in [Oden and Vemaganti, 2000, Oden and Prudhomme, 2002] and presented previously.

**Error definition**

From the non-intrusive local-global coupling methodology previously described (see Section 1.1.2), and using discretization with meshes $\tau^H$ and $\tau^h$ for global and local models, respectively, an approximate continuous local-global displacement field $\mathbf{u}_{LG}^{hH(n)} \in \boldsymbol{\mathcal{V}}$ can be recovered at each iteration $n$ of the process. It is constructed as:

$$\mathbf{u}_{LG}^{hH(n)} = \begin{cases} \mathbf{u}_L^{h(n)} & \text{in } \Omega_L \\ \mathbf{u}_G^{H(n)} & \text{in } \Omega_0 \end{cases} \tag{1.35}$$

However, it should be noticed that the corresponding local-global stress field $\mathbb{\sigma}_{LG}^{hH(n)}$, defined as:

$$\mathbb{\sigma}_{LG}^{hH(n)} = \begin{cases} \mathbb{\sigma}_L^{h(n)} = \mathbf{K}\mathbb{\varepsilon}(\mathbf{u}_L^{h(n)}) & \text{in } \Omega_L \\ \mathbb{\sigma}_G^{H(n)} = \mathbf{K}_0\mathbb{\varepsilon}(\mathbf{u}_G^{H(n)}) & \text{in } \Omega_0 \end{cases} \tag{1.36}$$

does not respect equilibrium in any weak sense (before convergence) across the interface $\Gamma$.

Alternatively, a local-global stress field $\mathbb{\sigma}_{LG,N}^{hH(n)}$ being weakly equilibrated across the interface $\Gamma$ can be recovered

(the subscript $N$ refers to “Neumann" and is consistent with the phrasing used to indicate sub-iterations in domain decomposition methods). Indeed, we notice that the continuous weak forms of the equilibrium equation for the global problem (1.12) at iteration $n$ and local problem (1.13) at iteration $n-1$ can be respectively recast as:

$$\begin{aligned}\int_\Omega \boldsymbol{\sigma}_G^{(n)} : \boldsymbol{\varepsilon}(\mathbf{v}_G) - \int_{\Omega_L} \boldsymbol{\sigma}_G^{(n-1)} : \boldsymbol{\varepsilon}(\mathbf{v}_G) &= \int_{\Omega_0} \mathbf{f}_d \cdot \mathbf{v}_G + \int_{\partial_F\Omega} \mathbf{F}_d \cdot \mathbf{v}_G - \int_\Gamma \boldsymbol{\lambda}^{(n-1)} \cdot \mathbf{v}_G \quad \forall \mathbf{v}_G \in \boldsymbol{\mathcal{V}} \\ \int_{\Omega_L} \boldsymbol{\sigma}_L^{(n-1)} : \boldsymbol{\varepsilon}(\mathbf{v}_L) &= \int_{\Omega_L} \mathbf{f}_d \cdot \mathbf{v}_L + \int_\Gamma \boldsymbol{\lambda}^{(n-1)} \cdot \mathbf{v}_L \quad \forall \mathbf{v}_L \in \boldsymbol{\mathcal{V}}_L\end{aligned} \tag{1.37}$$

Therefore, by summing the two balance equations, the stress field $\boldsymbol{\sigma}_{LG,N}^{hH(n)}$ is defined as:

$$\boldsymbol{\sigma}_{LG,N}^{hH(n)} = \begin{cases} \boldsymbol{\sigma}_L^{h(n-1)} + [\boldsymbol{\sigma}_G^{H(n)} - \boldsymbol{\sigma}_G^{H(n-1)}] & \text{in } \Omega_L \\ \boldsymbol{\sigma}_G^{H(n)} & \text{in } \Omega_0 \end{cases} \tag{1.38}$$

It is equilibrated with the external loading $(\mathbf{f}_d, \mathbf{F}_d)$.
Nevertheless, the corresponding local-global displacement field denoted by $\mathbf{u}_{LG,N}^{hH(n)}$ and defined as:

$$\mathbf{u}_{LG,N}^{hH(n)} = \begin{cases} \mathbf{u}_L^{h(n-1)} + [\mathbf{u}_G^{H(n)} - \mathbf{u}_G^{H(n-1)}] & \text{in } \Omega_L \\ \mathbf{u}_G^{H(n)} & \text{in } \Omega_0 \end{cases} \tag{1.39}$$

is not continuous across $\Gamma$ (before convergence), that is, it does not belong to $\boldsymbol{\mathcal{V}}$.

*Remark. In the intrusive coupling procedure described in Section 1.1.2, the previously introduced local-global solution fields would merely become:*

$$\begin{aligned}\mathbf{u}_{LG}^{hH(n)} &= \begin{cases} \mathbf{u}_L^{h(n)} & \textit{in } \Omega_L \\ \mathbf{u}_G^{H(n)} & \textit{in } \Omega_0 \end{cases} \quad ; \quad \boldsymbol{\sigma}_{LG}^{hH(n)} = \begin{cases} \boldsymbol{\sigma}_L^{h(n)} & \textit{in } \Omega_L \\ \boldsymbol{\sigma}_G^{H(n)} & \textit{in } \Omega_0 \end{cases} \\ \mathbf{u}_{LG,N}^{hH(n)} &= \begin{cases} \mathbf{u}_L^{h(n-1)} & \textit{in } \Omega_L \\ \mathbf{u}_G^{H(n)} & \textit{in } \Omega_0 \end{cases} \quad ; \quad \boldsymbol{\sigma}_{LG,N}^{hH(n)} = \begin{cases} \boldsymbol{\sigma}_L^{h(n-1)} & \textit{in } \Omega_L \\ \boldsymbol{\sigma}_G^{H(n)} & \textit{in } \Omega_0 \end{cases}\end{aligned} \tag{1.40}$$

From the local-global displacement field $\mathbf{u}_{LG}^{hH(n)} \in \boldsymbol{\mathcal{V}}$ (resp. $\mathbf{u}_{LG,N}^{hH(n)} \notin \boldsymbol{\mathcal{V}}$), error fields $\mathbf{e}_{LG}^{hH(n)} = \mathbf{u} - \mathbf{u}_{LG}^{hH(n)} \in \boldsymbol{\mathcal{V}}$ and $\mathbf{e}_{LG,N}^{hH(n)} = \mathbf{u} - \mathbf{u}_{LG,N}^{hH(n)} \notin \boldsymbol{\mathcal{V}}$ can be defined. Such error fields describe the discrepancy between the exact solution to the reference problem (1.2) and the approximate local-global solution at hand. Error fields $\mathbf{e}_{LG}^{hH(n)}$ and $\mathbf{e}_{LG,N}^{hH(n)}$ are linked together by the relation:

$$\mathbf{e}_{LG,N}^{hH(n)} = \mathbf{e}_{LG}^{hH(n)} + [\mathbf{u}_{LG,D}^{hH(n)} - \mathbf{u}_{LG,N}^{hH(n)}] \tag{1.41}$$

with term

$$\mathbf{u}_{LG}^{hH(n)} - \mathbf{u}_{LG,N}^{hH(n)} = \begin{cases} \left[\mathbf{u}_L^{h(n)} - \mathbf{u}_G^{H(n)}\right] - \left[\mathbf{u}_L^{h(n-1)} - \mathbf{u}_G^{H(n-1)}\right] & \text{in } \Omega_L \\ \mathbf{0} \quad \text{in } \Omega_0 \end{cases} \tag{1.42}$$

highlighting the contribution to the error, inside $\Omega_L$, coming from iteration stopping.

Several scalar measures of the error field may then be used. Here, we consider a measure defined from a given linear quantity of interest $Q$. Nevertheless, global measures could also be used, such as the measure in the energy norm:

$$\|\cdot\|_{\mathbf{K}} = \sqrt{\int_\Omega \mathbf{K}\mathbb{e}(\cdot) : \mathbb{e}(\cdot)} \quad \left(\text{or } \|\cdot\|_{brok} = \sqrt{\int_{\Omega_L} \mathbf{K}\mathbb{e}(\cdot) : \mathbb{e}(\cdot) + \int_{\Omega_0} \mathbf{K}\mathbb{e}(\cdot) : \mathbb{e}(\cdot)} \quad \text{for } \mathbf{e}_{LG,N}^{hH(n)} \notin \boldsymbol{\mathcal{V}}\right) \tag{1.43}$$

In the following, we thus focus on the local error measure $Q(\mathbf{e}_{LG}^{hH(n)}) = Q(\mathbf{u}) - Q(\mathbf{u}_{LG}^{hH(n)})$ defined according to a given scalar quantity of interest $Q(\mathbf{u})$ that is a specific (and usually fine-scale) feature of the solution $\mathbf{u}$. We assume here that $Q : \boldsymbol{\mathcal{V}} \to \mathcal{R}$ is linear, even though nonlinear quantities of interest could also be considered with minor changes (see [Oden and Prudhomme, 2002]). We also naturally assume that the quantity $Q$ refers to features of $\mathbf{u}$ located in the initial configuration of $\Omega_L$, and critical for design or relevant to the understanding of physical phenomena when resorting to non-intrusive local-global couplings.

**Weak forms and residual functional**

In [Tirvaudey et al., 2020b], goal-oriented error estimation is developed in a similar way as in [Oden and Vemaganti, 2000, Oden and Prudhomme, 2002], based on the definition of an adjoint problem. The reference problem (1.2) can be recast as: find $\mathbf{u} \in \boldsymbol{\mathcal{V}}$ such that

$$a(\mathbf{u}, \mathbf{v}) = l(\mathbf{v}) \quad \forall \mathbf{v} \in \boldsymbol{\mathcal{V}} \tag{1.44}$$

with

$$a(\mathbf{u}, \mathbf{v}) = \int_\Omega \mathbf{K}\mathbb{e}(\mathbf{u}) : \mathbb{e}(\mathbf{v}) \quad ; \quad l(\mathbf{v}) = \int_\Omega \mathbf{f}_d \cdot \mathbf{v} + \int_{\partial_F \Omega} \mathbf{F}_d \cdot \mathbf{v} \tag{1.45}$$

Based on this weak form, the residual functional $\mathcal{R} : \boldsymbol{\mathcal{V}} \times \boldsymbol{\mathcal{V}} \to \mathcal{R}$ is introduced:

$$\mathcal{R}(\mathbf{w}, \mathbf{v}) = l(\mathbf{v}) - a(\mathbf{w}, \mathbf{v}) \tag{1.46}$$

The property (1.44) directly yields $\mathcal{R}(\mathbf{u}, \mathbf{v}) = 0$ for any $\mathbf{v} \in \boldsymbol{\mathcal{V}}$.

Further introducing the following notations:

$$\begin{aligned} &a_L(\mathbf{u},\mathbf{v}) = \int_{\Omega_L} \mathbf{K}\mathbb{\varepsilon}(\mathbf{u}) : \mathbb{\varepsilon}(\mathbf{v}) \quad ; \quad a_{0\Omega}(\mathbf{u},\mathbf{v}) = \int_{\Omega} \mathbf{K}_0\mathbb{\varepsilon}(\mathbf{u}) : \mathbb{\varepsilon}(\mathbf{v}) \quad ; \quad a_{0L}(\mathbf{u},\mathbf{v}) = \int_{\Omega_L} \mathbf{K}_0\mathbb{\varepsilon}(\mathbf{u}) : \mathbb{\varepsilon}(\mathbf{v}) \\ &b_\Gamma(\boldsymbol{\lambda},\mathbf{u}) = \int_\Gamma \boldsymbol{\lambda}\cdot\mathbf{u} \quad ; \quad l_L(\mathbf{v}) = \int_{\Omega_L} \mathbf{f}_d\cdot\mathbf{v} \quad ; \quad l_0(\mathbf{v}) = \int_{\Omega_0} \mathbf{f}_d\cdot\mathbf{v} + \int_{\partial_F\Omega} \mathbf{F}_d\cdot\mathbf{v} \end{aligned} \tag{1.47}$$

Additional weak forms are also defined for problems introduced in Section 1.1.2:

- the continuous weak form of the local-global non-intrusive coupling (without iterative fixed-point solution scheme at this stage), coming from (1.4), (1.5), and (1.10), reads: find $(\mathbf{u}_G,\mathbf{u}_L,\boldsymbol{\lambda}) \in \boldsymbol{\mathcal{V}}\times\boldsymbol{\mathcal{V}}_L\times\boldsymbol{\mathcal{M}}$ such that

$$\begin{aligned} &a_{0\Omega}(\mathbf{u}_G,\mathbf{v}_G) - a_{0L}(\mathbf{u}_G,\mathbf{v}_G) + a_L(\mathbf{u}_L,\mathbf{v}_L) - b_\Gamma(\boldsymbol{\lambda},\mathbf{v}_L-\mathbf{v}_G) + b_\Gamma(\boldsymbol{\mu},\mathbf{u}_L-\mathbf{u}_G) \\ &= l_0(\mathbf{v}_G) + l_L(\mathbf{v}_L) \quad \forall(\mathbf{v}_G,\mathbf{v}_L,\boldsymbol{\mu}) \in \boldsymbol{\mathcal{V}}\times\boldsymbol{\mathcal{V}}_L\times\boldsymbol{\mathcal{M}} \end{aligned} \tag{1.48}$$

  or in a more condensed writing:

$$a_{LG}\left((\mathbf{u}_G,\mathbf{u}_L,\boldsymbol{\lambda}),(\mathbf{v}_G,\mathbf{v}_L,\boldsymbol{\mu})\right) = l_{LG}(\mathbf{v}_G,\mathbf{v}_L,\boldsymbol{\mu}) \quad \forall(\mathbf{v}_G,\mathbf{v}_L,\boldsymbol{\mu}) \in \boldsymbol{\mathcal{V}}\times\boldsymbol{\mathcal{V}}_L\times\boldsymbol{\mathcal{M}} \tag{1.49}$$

  This provides the approximate solution $\mathbf{u}_{LG} \in \boldsymbol{\mathcal{V}}$ defined as $\mathbf{u}_{LG} = \begin{cases} \mathbf{u}_L & \text{in } \Omega_L \\ \mathbf{u}_G & \text{in } \Omega_0 \end{cases}$;

- introducing the FE space $\boldsymbol{\mathcal{V}}^H$, associated with coarse mesh $\tau^H$ over $\Omega$, the partially discretized version of (1.49) reads: find $(\mathbf{u}_G^H,\mathbf{u}_L,\boldsymbol{\lambda}) \in \boldsymbol{\mathcal{V}}^H\times\boldsymbol{\mathcal{V}}_L\times\boldsymbol{\mathcal{M}}$ such that

$$a_{LG}\left((\mathbf{u}_G^H,\mathbf{u}_L,\boldsymbol{\lambda}),(\mathbf{v}_G^H,\mathbf{v}_L,\boldsymbol{\mu})\right) = l_{LG}(\mathbf{v}_G^H,\mathbf{v}_L,\boldsymbol{\mu}) \quad \forall(\mathbf{v}_G^H,\mathbf{v}_L,\boldsymbol{\mu}) \in \boldsymbol{\mathcal{V}}^H\times\boldsymbol{\mathcal{V}}_L\times\boldsymbol{\mathcal{M}} \tag{1.50}$$

  This provides the approximate solution $\mathbf{u}_{LG}^H \in \boldsymbol{\mathcal{V}}$ defined as $\mathbf{u}_{LG}^H = \begin{cases} \mathbf{u}_L & \text{in } \Omega_L \\ \mathbf{u}_G^H & \text{in } \Omega_0 \end{cases}$;

- introducing the FE spaces $\boldsymbol{\mathcal{V}}_L^h$, and $\boldsymbol{\mathcal{M}}^h$, associated with the mesh $\tau^h$ used in $\Omega_L$, the fully discretized version of (1.49) reads: find $(\mathbf{u}_G^H,\mathbf{u}_L^h,\boldsymbol{\lambda}^h) \in \boldsymbol{\mathcal{V}}^H\times\boldsymbol{\mathcal{V}}_L^h\times\boldsymbol{\mathcal{M}}^h$ such that

$$a_{LG}\left((\mathbf{u}_G^H,\mathbf{u}_L^h,\boldsymbol{\lambda}^h),(\mathbf{v}_G^H,\mathbf{v}_L^h,\boldsymbol{\mu}^h)\right) = l_{LG}(\mathbf{v}_G^H,\mathbf{v}_L^h,\boldsymbol{\mu}^h) \quad \forall(\mathbf{v}_G^H,\mathbf{v}_L^h,\boldsymbol{\mu}^h) \in \boldsymbol{\mathcal{V}}^H\times\boldsymbol{\mathcal{V}}_L^h\times\boldsymbol{\mathcal{M}}^h \tag{1.51}$$

  This provides the approximate solution $\mathbf{u}_{LG}^{hH} \in \boldsymbol{\mathcal{V}}$ defined as $\mathbf{u}_{LG}^{hH} = \begin{cases} \mathbf{u}_L^h & \text{in } \Omega_L \\ \mathbf{u}_G^H & \text{in } \Omega_0 \end{cases}$;

- eventually, introducing the fixed-point scheme, the weak form at iteration $n$ stemming from (1.12)-(1.13) reads:

find $(\mathbf{u}_G^{H(n)}, \mathbf{u}_L^{h(n)}, \boldsymbol{\lambda}^{h(n)}) \in \boldsymbol{\mathcal{V}}^H \times \boldsymbol{\mathcal{V}}_L^h \times \boldsymbol{\mathcal{M}}^h$ such that

$$\begin{aligned} &a_{0\Omega}(\mathbf{u}_G^{H(n)}, \mathbf{v}_G^H) + a_L(\mathbf{u}_L^{h(n)}, \mathbf{v}_L^h) - b_\Gamma(\boldsymbol{\lambda}^{h(n)}, \mathbf{v}_L^h) + b_\Gamma(\boldsymbol{\mu}^h, \mathbf{u}_L^{h(n)} - \mathbf{u}_G^{H(n)}) \\ &= l_0(\mathbf{v}_G^H) + l_L(\mathbf{v}_L^h) + a_{0L}(\mathbf{u}_G^{H(n-1)}, \mathbf{v}_G^H) - b_\Gamma(\boldsymbol{\lambda}^{h(n-1)}, \mathbf{v}_G^H) \quad \forall (\mathbf{v}_G^H, \mathbf{v}_L^h, \boldsymbol{\mu}^h) \in \boldsymbol{\mathcal{V}}^H \times \boldsymbol{\mathcal{V}}_L^h \times \boldsymbol{\mathcal{M}}^h \end{aligned} \tag{1.52}$$

or in a more condensed writing:

$$a_{LG}^{(n)}\left((\mathbf{u}_G^{H(n)}, \mathbf{u}_L^{h(n)}, \boldsymbol{\lambda}^{h(n)}), (\mathbf{v}_G^H, \mathbf{v}_L^h, \boldsymbol{\mu}^h)\right) = l_{LG}^{(n)}(\mathbf{v}_G^H, \mathbf{v}_L^h, \boldsymbol{\mu}^h) \quad \forall (\mathbf{v}_G^H, \mathbf{v}_L^h, \boldsymbol{\mu}^h) \in \boldsymbol{\mathcal{V}}^H \times \boldsymbol{\mathcal{V}}_L^h \times \boldsymbol{\mathcal{M}}^h \tag{1.53}$$

This provides the approximate solution $\mathbf{u}_{LG}^{hH(n)} \in \boldsymbol{\mathcal{V}}$ defined in (1.35), and which is the available computed field when resorting to the non-intrusive local-global coupling framework.

We emphasize again that global solutions $\mathbf{u}_G$ (in (1.48)-(1.49)) and $\mathbf{u}_G^H$ (in (1.50)-(1.51)) are not unique in $\Omega_L$, even though $\mathbf{u}_G^{H(n)}$ (in (1.52)-(1.53)) is. However, non-uniqueness is not an issue as: (i) global solutions are eventually replaced by fine-scale local solutions $\Omega_L$ in the definition of the overall local-global solutions; (ii) contributions of global solutions in $\Omega_L$ vanish in the term $a_{0\Omega}(\cdot,\cdot) - a_{0L}(\cdot,\cdot)$ of the residual.

**Adjoint problem and error representation**

The adjoint problem of (1.44), associated with $Q$, is then introduced. It consists in finding $\widetilde{\mathbf{u}} \in \boldsymbol{\mathcal{V}}$ such that

$$a(\mathbf{v}, \widetilde{\mathbf{u}}) = a^*(\widetilde{\mathbf{u}}, \mathbf{v}) = Q(\mathbf{v}) \quad \forall \mathbf{v} \in \boldsymbol{\mathcal{V}} \tag{1.54}$$

$a^*$ being constructed from the adjoint model operator. In the present case, the model operator is self-adjoint so that $a^* = a$.

From the adjoint solution $\widetilde{\mathbf{u}}$, it is straightforward that for any approximation $\mathbf{u}_{app} \in \boldsymbol{\mathcal{V}}$ of $\mathbf{u}$, the error $Q(\mathbf{u}) - Q(\mathbf{u}_{app})$ can be represented as:

$$Q(\mathbf{u}) - Q(\mathbf{u}_{app}) = Q(\mathbf{u} - \mathbf{u}_{app}) = a(\mathbf{u} - \mathbf{u}_{app}, \widetilde{\mathbf{u}}) = \mathcal{R}(\mathbf{u}_{app}, \widetilde{\mathbf{u}}) \tag{1.55}$$

where $\mathbf{u}_{app}$ is any approximation of the reference problem. Then introducing any approximation $\widetilde{\mathbf{u}}_{app} \in \boldsymbol{\mathcal{V}}$ of the adjoint solution $\widetilde{\mathbf{u}}$, the error representation also reads:

$$Q(\mathbf{u}) - Q(\mathbf{u}_{app}) = \mathcal{R}(\mathbf{u}_{app}, \widetilde{\mathbf{u}}_{app}) + \mathcal{R}(\mathbf{u}_{app}, \widetilde{\mathbf{u}} - \widetilde{\mathbf{u}}_{app}) \tag{1.56}$$

*Remark. As it will be seen later, the quantity of interest is usually defined in a global way by means of extraction functions. It is written under the form:*

$$Q(\mathbf{u}) = \int_\Omega \varpi_\Sigma : \mathfrak{e}(\mathbf{u}) + \int_\Omega \mathbf{f}_\Sigma \cdot \mathbf{u} + \int_{\partial_F \Omega} \mathbf{F}_\Sigma \cdot \mathbf{u} + \int_\Omega \mathbf{K}\mathfrak{e}(\mathbf{u}_\Sigma) : \mathfrak{e}(\mathbf{u}) \tag{1.57}$$

*where $\varpi_\Sigma$, $\mathbf{f}_\Sigma$, $\mathbf{F}_\Sigma$, and $\mathbf{u}_\Sigma$ are extractors. These are defined explicitly or implicitly (depending on the quantity $Q$), and they can be mechanically interpreted as pre-stress, body force, traction force, and pre-displacement, respectively, in the loading of the adjoint problem. The field $\mathbf{u}_\Sigma$, vanishing on $\partial_F\Omega$, enables to extract components of the stress vector $\varpi(\mathbf{u})\mathbf{n}$ on $\partial_u\Omega$ (reaction forces).*

**Residual-based error estimator**

Using the previous error representation, a computable error estimate on $Q(\mathbf{u})$ is now developed when using the non-intrusive local-global coupling strategy. From (1.55), and noticing that $\mathbf{u}_{LG}^{hH(n)} \in \boldsymbol{\mathcal{V}}$, it first reads:

$$Q(\mathbf{u}) - Q(\mathbf{u}_{LG}^{hH(n)}) = \mathcal{R}(\mathbf{u}_{LG}^{hH(n)}, \widetilde{\mathbf{u}}) \tag{1.58}$$

For the term in the right-hand side to be computable, the adjoint solution $\widetilde{\mathbf{u}}$ should be replaced by an approximate solution $\widetilde{\mathbf{u}}_{app}$ as described in (1.56). Nevertheless, a relevant approximation should be computed so that $\mathcal{R}(\mathbf{u}_{LG}^{hH(n)}, \widetilde{\mathbf{u}}) \approx \mathcal{R}(\mathbf{u}_{LG}^{hH(n)}, \widetilde{\mathbf{u}}_{app})$ (i.e. $\mathcal{R}(\mathbf{u}_{LG}^{hH(n)}, \widetilde{\mathbf{u}} - \widetilde{\mathbf{u}}_{app}) \approx 0$ can then be neglected in this case). This is the saturation assumption. In practice, this means that in order to catch the various error sources accurately, the approximation space used to compute $\widetilde{\mathbf{u}}_{app}$ should be richer than that used for $\mathbf{u}_{LG}^{hH(n)}$. Considering $\widetilde{\mathbf{u}}_{app}$ in the same approximation space as $\mathbf{u}_{LG}^{hH(n)}$ would lead to a poor error estimate of the error on $Q$.

*Remark. Again, a typical and well-known case illustrating the previous statement is the mere finite element approximation $\mathbf{u}_{fem}$ of the solution $\mathbf{u}$ of* (1.44) *in a subspace $\boldsymbol{\mathcal{V}}_{fem} \subset \boldsymbol{\mathcal{V}}$. The Galerkin orthogonality $\mathcal{R}(\mathbf{u}_{fem}, \mathbf{v}) = 0$ for all $\mathbf{v} \in \boldsymbol{\mathcal{V}}_{fem}$ indicates that the discretization error estimate $\mathcal{R}(\mathbf{u}_{fem}, \widetilde{\mathbf{u}}_{app})$ is meaningless when $\widetilde{\mathbf{u}}_{app}$ is searched in $\boldsymbol{\mathcal{V}}_{fem}$. Considering a richer space $\boldsymbol{\mathcal{V}}_{fem}^+ \subset \boldsymbol{\mathcal{V}}$ (with finer mesh size) to compute $\widetilde{\mathbf{u}}_{app}$, the result $\mathcal{R}(\mathbf{u}_{fem}, \widetilde{\mathbf{u}}_{app}) = Q(\mathbf{u}_{fem}^+) - Q(\mathbf{u}_{fem})$ with $\mathbf{u}_{fem}^+ \in \boldsymbol{\mathcal{V}}_{fem}^+$ also shows that the estimate catches all the error on $Q(\mathbf{u})$ except the part $Q(\mathbf{u}) - Q(\mathbf{u}_{fem}^+)$.*

For the considered non-intrusive local-global coupling method, enriching the approximation space for the solution of the adjoint problem means: (i) sufficiently enlarging the zone $\Omega_L$ in which the original high-fidelity model is preserved (this enrichment is referred to with subscript "$L^+$" in the following); (ii) sufficiently refining the mesh $\tau^h$ used in this zone (this enrichment is referred to with superscript "$h^+$" in the following); (iii) being sufficiently close to convergence in the iterative algorithm (referred to with superscript "$\infty$" in the following). Consequently, after

computing $\widetilde{\mathbf{u}}_{L^+G}^{h^+H(\infty)} \in \boldsymbol{\mathcal{V}}$ using an enriched non-intrusive local-global coupling method, with local part $\widetilde{\mathbf{u}}_{L^+}^{h^+(\infty)} \in \boldsymbol{\mathcal{V}}_{L^+}^{h^+}$, an overall and fully computable error estimate of the error on $Q$ reads:

$$\eta_Q^{tot} = \mathcal{R}(\mathbf{u}_{LG}^{hH(n)}, \widetilde{\mathbf{u}}_{L^+G}^{h^+H(\infty)}) \tag{1.59}$$

*Remark. Due to the specific loading of the adjoint problem, which is concentrated inside $\Omega_L$, it is expected that the iterative local-global algorithm converges very fast when computing $\widetilde{\mathbf{u}}_{L^+G}^{h^+H(\infty)}$.*

*Remark. In order to further reduce the computational cost without sacrificing too much the quality of the error estimate, it would be possible to approximate the residual functional $\mathcal{R}$ (initially defined from the reference model) considering the enriched approximation space used to solve the adjoint problem. Nevertheless, such an approximation does not prevent from projections between meshes for the computation of $\mathcal{R}(\mathbf{u}_{LG}^{hH(n)}, \widetilde{\mathbf{u}}_{L^+G}^{h^+H(\infty)})$. This alternative is not investigated here.*

**Residual-based error indicators**

The estimate (1.59) comprises all error sources. As described in Section 1.2.3, these are threefold: modeling, discretization, convergence. Introducing solution fields defined in Section 1.2.3, the error on $Q$ can be split as:

$$Q(\mathbf{u}) - Q(\mathbf{u}_{LG}^{hH(n)}) = \underbrace{\left[Q(\mathbf{u}) - Q(\mathbf{u}_{LG}^{H})\right]}_{\mathcal{E}_Q^{mod}} + \underbrace{\left[Q(\mathbf{u}_{LG}^{H}) - Q(\mathbf{u}_{LG}^{hH})\right]}_{\mathcal{E}_Q^{dis}} + \underbrace{\left[Q(\mathbf{u}_{LG}^{hH}) - Q(\mathbf{u}_{LG}^{hH(n)})\right]}_{\mathcal{E}_Q^{conv}} \tag{1.60}$$

where $\mathcal{E}_Q^{mod}$, $\mathcal{E}_Q^{dis}$, and $\mathcal{E}_Q^{conv}$ correspond to modeling, discretization, and convergence parts of the error, respectively. We develop below some error indicators on each of these parts.

They are defined as follows:

- the indicator on convergence error, denoted by $\eta_Q^{conv}$, is constructed from a converged approximate adjoint solution $\widetilde{\mathbf{u}}_{LG}^{hH(\infty)} \in \boldsymbol{\mathcal{V}}$ with no enrichment in terms of mesh $\tau^h$ and local zone $\Omega_L$ used. It reads:

$$\eta_Q^{conv} = \mathcal{R}_{LG}(\mathbf{u}_{LG}^{hH(n)}, \widetilde{\mathbf{u}}_{LG}^{hH(\infty)}) \tag{1.61}$$

  where the residual $\mathcal{R}_{LG}$ is defined from operators $a_{LG}$ and $l_{LG}$ associated with the local-global coupling

problem (i.e., reference problem providing for $\mathbf{u}_{LG}^{H}$ and $\mathbf{u}_{LG}^{hH}$):

$$\begin{aligned}\mathcal{R}_{LG}(\mathbf{u}_{LG}^{hH(n)}, \widetilde{\mathbf{u}}_{LG}^{hH(\infty)}) =& l_0(\widetilde{\mathbf{u}}_{G}^{H(\infty)}) + l_L(\widetilde{\mathbf{u}}_{L}^{h(\infty)}) \\ & - a_{0\Omega}(\mathbf{u}_{G}^{H(n)}, \widetilde{\mathbf{u}}_{G}^{H(\infty)}) + a_{0L}(\mathbf{u}_{G}^{H(n)}, \widetilde{\mathbf{u}}_{G}^{H(\infty)}) - a_{L}(\mathbf{u}_{L}^{h(n)}, \widetilde{\mathbf{u}}_{L}^{h(\infty)})\end{aligned} \tag{1.62}$$

The indicator is such that $\eta_Q^{conv} \underset{n\to+\infty}{\longrightarrow} 0$. It should provide a quantitative indication on the convergence error $\mathcal{E}_Q^{conv}$, enabling to define a relevant stopping criterion for the local-global iterative solver.

- the indicator on discretization error, denoted by $\eta_Q^{dis}$, is constructed from a converged approximate solution $\widetilde{\mathbf{u}}_{LG}^{h^+H(\infty)} \in \boldsymbol{\mathcal{V}}$ computed with a finer local mesh $\tau^{h^+}$ alone, while the shape of $\Omega_L$ remains unchanged compared to that used for the computation of $\mathbf{u}_{LG}^{hH(n)}$. It reads:

$$\eta_Q^{dis} = \mathcal{R}_{LG}(\mathbf{u}_{LG}^{hH(n)}, \widetilde{\mathbf{u}}_{LG}^{h^+H(\infty)}) - \eta_Q^{conv} \tag{1.63}$$

and is such that $\eta_Q^{dis} \underset{h\to h^+}{\longrightarrow} \approx 0$. It should provide a relevant quantitative indication on the discretization error $\mathcal{E}_Q^{dis}$ provided $h^+$ is small enough.

- eventually, the indicator on modeling error, denoted by $\eta_Q^{mod}$, is constructed from an approximate solution $\widetilde{\mathbf{u}}_{L^+G}^{hH(\infty)} \in \boldsymbol{\mathcal{V}}$ computed with a larger zone $\Omega_{L^+}$ alone, while the mesh $\tau^h$ is unchanged compared to that used for the computation of $\mathbf{u}_{LG}^{hH(n)}$. It reads:

$$\eta_Q^{mod} = \mathcal{R}(\mathbf{u}_{LG}^{hH(n)}, \widetilde{\mathbf{u}}_{L^+G}^{hH(\infty)}) - \eta_Q^{conv} \tag{1.64}$$

and is such that $\eta_Q^{mod} \underset{\Omega_L\to\Omega_{L^+}}{\longrightarrow} \approx 0$. It should provide a relevant quantitative indication on the modeling error $\mathcal{E}_Q^{mod}$ provided $\Omega_{L^+}$ is large enough. An alternative construction of the indicator $\eta_Q^{mod}$, giving in practice slightly different values but decreasing the number of adjoint solutions, stems from the following (and still empirical) definition:

$$\eta_Q^{mod} = \eta_Q^{tot} - \eta_Q^{conv} - \eta_Q^{dis} \tag{1.65}$$

*Remark. It is worth noticing that numerical strategies which have to be implemented for the computation of the estimator $\eta_Q^{tot}$, as well as indicators $\eta_Q^{conv}$, $\eta_Q^{dis}$, and $\eta_Q^{mod}$, are in accordance with the non-intrusive framework. Indeed, the definitions of the enriched spaces which are used to compute the approximate adjoint solutions $\widetilde{\mathbf{u}}_{L^+G}^{h^+H(\infty)}$, $\widetilde{\mathbf{u}}_{LG}^{h^+H(\infty)}$, and $\widetilde{\mathbf{u}}_{L^+G}^{hH(\infty)}$ require modifications of $\boldsymbol{\mathcal{V}}_L^h$ alone, while $\boldsymbol{\mathcal{V}}^H$ is kept unchanged. This can be easily performed using the non-intrusive coupling methodology.*

*In addition, the non-intrusive framework applied to the solution of the adjoint problem enables to select specific error sources and analyze various modeling configurations in a suitable manner. By a flexible introduction of additional*

*patches to $\Omega_{L^+}$, located on some preselected zones (e.g. in the vicinity of geometrical details such as holes), the corresponding adjoint solution automatically filters targeted error sources due to orthogonality properties described in Section 1.2.3. Therefore, the critical phenomena that affect the accuracy on the quantity of interest, even though located far from the region over which the quantity of interest is defined (pollution effects), are easily detected. These phenomena would then need to be further modeled accurately, i.e. at the fine-scale level.*

**Adaptive strategy**

From the previously defined error estimator $\eta_Q^{tot}$ and indicators $\eta_Q^{conv}$, $\eta_Q^{dis}$, and $\eta_Q^{mod}$, it is possible to set up a relevant adaptive algorithm in order to drive the non-intrusive coupling algorithm. The one developed in [Tirvaudey et al., 2020b] is based on a greedy algorithm and closely related to those proposed in [Oden and Vemaganti, 2000, Vemaganti and Oden, 2001, Oden et al., 2006b, Romkes et al., 2006, Bauman et al., 2009, Prudhomme et al., 2009, Zaccardi et al., 2013] (so-called *Goals algorithms*). The approach, which refers to goal-oriented adaptivity, aims at automatically tuning the parameters of the local-global coupling method (shape of $\Omega_L$, mesh size in $\tau^h$, number of local-global iterations) in order to predict the quantity of interest $Q$ within a preset error tolerance $\gamma_{tol}$ while optimizing the computational cost. This is achieved by generating a sequence of approximate solutions $\mathbf{u}_{app}^{(k)}$ so that for some integer $k_0$, the overall error on $Q$ satisfies:

$$|Q(\mathbf{u}) - Q(\mathbf{u}_{app}^{(k_0)})| \leq \gamma_{tol}|Q(\mathbf{u}_{app}^{(k_0)})| \tag{1.66}$$

At each iteration of the adaptive process, and before stopping the full adaptive algorithm when the error tolerance is met (quantitative information given by $\eta_Q^{tot} \leq \gamma_{tol}|Q(\mathbf{u}_{app})|$), the goal is to reduce the major error source which is identified comparing indicators $\eta_Q^{conv}$, $\eta_Q^{dis}$, and $\eta_Q^{mod}$. Adaptations in discretization and modeling are conducted locally after decomposing the indicators over predefined subdomains in $\Omega_L$ and $\Omega_0$, respectively. In practice, subdomains in $\Omega_L$ are chosen as elements of $\tau^h$, while subdomains in $\Omega_0$ are defined from elements of the coarse mesh $\tau^H$ (even though larger subdomains could be used). This decomposition is possible by observing that indicators $\eta_Q^{dis}$ and $\eta_Q^{mod}$ correspond to residual terms defined from space integrals.

After initializing $\Omega_L$ (as a neighborhood of the region over which the quantity of interest is defined) and $\tau^h$ (with similar mesh size as for $\tau^H$), and after specifying the error tolerance $\gamma_{tol}$ for the quantity of interest, the proposed adaptive algorithm reads as follows:

0. Compute the adjoint solution $\widetilde{\mathbf{u}}_{L^+G}^{h^+H(\infty)}$ (using an appropriate enriched space);
1. Set $n = 1$;
2. Solve the primal surrogate problem for $\mathbf{u}_{LG}^{hH(n)}$;

3. Compute the estimate $\eta_Q^{tot}$;

4. If $|\eta_Q^{tot}/Q(\mathbf{u}_{LG}^{hH(n)})| \leq \gamma_{tol}$ then STOP. Otherwise proceed to Step 5;

5. Compute solutions $\widetilde{\mathbf{u}}_{L^+G}^{hH(\infty)}$, $\widetilde{\mathbf{u}}_{LG}^{h^+H(\infty)}$, and indicators $\eta_Q^{conv}$, $\eta_Q^{dis}$, and $\eta_Q^{mod}$:

   - if $\max(|\eta_Q^{conv}|, |\eta_Q^{dis}|, |\eta_Q^{mod}|) = |\eta_Q^{conv}|$, increment $n+1 \to n$ and go to Step 2;
   - if $\max(|\eta_Q^{conv}|, |\eta_Q^{dis}|, |\eta_Q^{mod}|) = |\eta_Q^{dis}|$, decompose $\eta_Q^{dis}$ and locally refine $\tau^h$ up to reaching $|\eta_Q^{dis}/Q(\mathbf{u}_{LG}^{hH(n)})| \leq \gamma_{tol}/3$, then go to Step 0;
   - if $\max(|\eta_Q^{conv}|, |\eta_Q^{dis}|, |\eta_Q^{mod}|) = |\eta_Q^{mod}|$, decompose $\eta_Q^{mod}$ and locally enlarge $\Omega_L$ up to reaching $|\eta_Q^{mod}/Q(\mathbf{u}_{LG}^{hH(n)})| \leq \gamma_{tol}/3$, then go to Step 0.

This adaptive algorithm prevents from useless local-global iterations for the primal problem (when discretization or modeling error is larger than convergence error). It also indicates, at the end of the adaptive process, a suitable definition of $\Omega_L$ and $\tau^h$ for reaching the error tolerance.

**Illustrative application**

The present illustration is taken from [Tirvaudey et al., 2020b]. A square plate (size $L \times L$ with $L = 1$) is considered, in which localized weakenings of the material stiffness are located. The structure, represented in Figure 1.9, is clamped on its left side and subjected to a uniform traction on its right side; other boundaries are free. The global mesh $\tau^H$ is made of 100 (10×10) first-order quadrangular elements. Local variations of the Young modulus $E(x, y)$ take the form of five zones, which act as inclusions inside the material, where the Young modulus is lower than its nominal value $E_0 = 1$. A specific case is considered where a zone on which the Young modulus is decreased has a large area and impacts more than one macro element of the global mesh $\tau^H$. The contrast is such that $E_{min} = 0.45$. The impacted macro elements are shown in Figure 1.9(b). The Poisson ratio is fixed and set to $\nu = 0.3$.
The quantity of interest is the average longitudinal displacement on the right edge $x = L$ where the traction loading is applied. The goal of the adaptation procedure is to find the optimal configuration for the coupled problem regarding this quantity of interest, and with respect to a given error tolerance. This tolerance is set to $\gamma_{tol} = 0.5\%$ (this value enables to detect the small impact of the modified Young modulus on the predicted value of the quantity of interest).

Starting from the initial solution given in Figure 1.10(a), where we observe effects of the clamping on left corners when using a coarse mesh, the adaptive procedure is performed. The values of the different relative estimator and indicators (i.e. normalized by the approximate value of the quantity of interest) are given at each adaptation step. These are $|\eta_Q^{tot}/Q(\mathbf{u}_{LG}^{hH(n)})|$, $|\eta_Q^{conv}/Q(\mathbf{u}_{LG}^{hH(n)})|$, $|\eta_Q^{dis}/Q(\mathbf{u}_{LG}^{hH(n)})|$, and $|\eta_Q^{mod}/Q(\mathbf{u}_{LG}^{hH(n)})|$.

For this example and as shown in Figure 1.10(b), eleven adaptive steps are required to reach a tolerance $\gamma_{tol} = 1\%$ on the quantity of interest; these are mostly related to model adaptation. In order to detail the adaptive

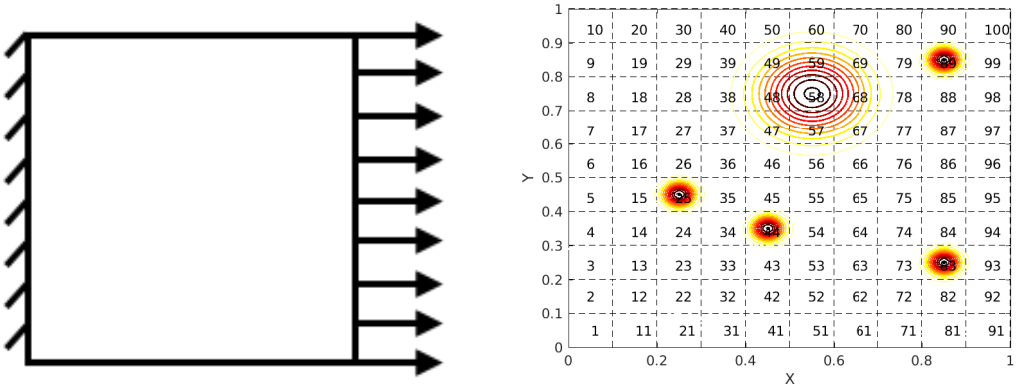

(a) Considered structure with boundary conditions.

(b) Position of the zones with degenerated Young modulus. The impacted macro elements are numbered $\{25, 44, 58, 83, 89\}$, and the local decrease of the Young modulus also impacts the neighbordhood of element 58.

Figure 1.9: Considered problem with local variations of the Young modulus (from [Tirvaudey et al., 2020b]).

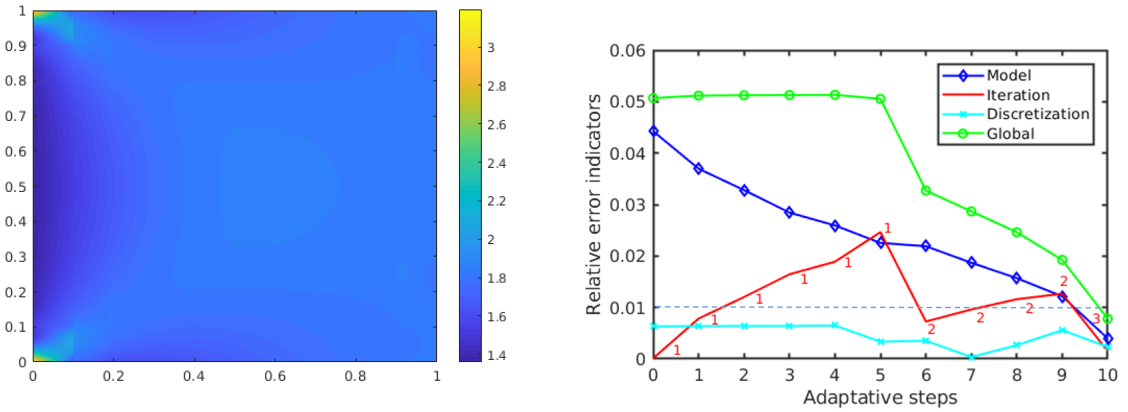


(a) Primal coupled solution at initial step.

(b) Evolution of error indicators along the adaptive process.

Figure 1.10: Initial coupling configuration and obtained results for adaptation (from [Tirvaudey et al., 2020b]).

process, we represent in Figure 1.11 the spatial distribution of the indicator $\eta_Q^{mod}$ on modeling error per macro element of $\tau^H$, the position of the local patches constituting $\Omega_L$ (grey zones), and each macro element (in black) that is included in the local zone $\Omega_L$ at the current adaptation step. At the end of the adaptive process, the configuration of the coupling problem is such that $\Omega_L$ is made of the element set $\{91-100, 58, 59, 57, 25, 83, 68, 48, 89\}$ (elements are listed in the order they are included in $\Omega_L$), 3 iterations are performed in the local-global coupling algorithm, and no refinement is needed.

Eventually, for this last configuration of the Young modulus distribution, the control of the error on another quantity of interest $Q$ is considered. It is the average of the strain component $\epsilon_{xx}$ in the macro element 68 (which is in the neighborhood of the large weakened zone). The local zone $\Omega_L$ initially consists of macro elements 58 and 68. Applying the adaptive process for this quantity indicates that the main error sources are initially due to coupling

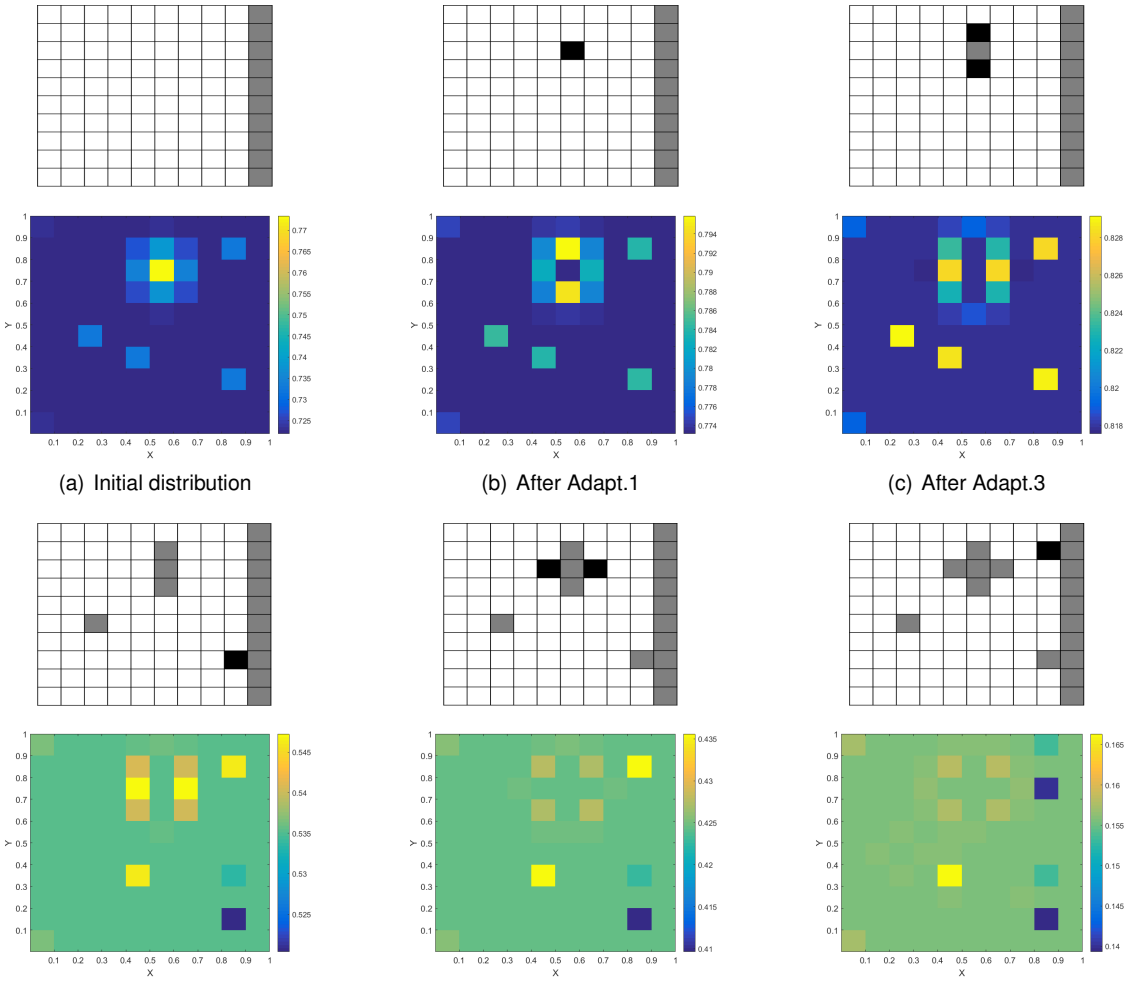

(a) Initial distribution (b) After Adapt.1 (c) After Adapt.3

(d) After Adapt.6 (e) After Adapt.8 (f) Final distribution.

Figure 1.11: Distribution of the indicator on modeling error at different steps of the adaptation procedure. In the top figures of each step, the local zone $\Omega_L$ is in grey and the newly added elements in the local zone are in black (from [Tirvaudey et al., 2020b]).

iterations and local discretization so that the mesh $\tau^h$ in the local zone $\Omega_L$ needs to be refined in order to reach the tolerance $\gamma_{tol} = 2\%$. This tolerance obtained after 4 iterations of the adaptive algorithm, also requires $n = 3$ local-global iterations but no extension of $\Omega_L$. We show in Figure1.12 several features of the goal-oriented adaptation strategy: the adjoint solution (that exhibits large localized gradients in the vicinity of the region of interest) is shown in Figure 1.12(a), the evolution of error estimator and indicators along the adaptive process are given in Figure 1.12(b), while the final local mesh $\tau^h$ and the final approximate local-global solution (requiring $n = 3$ local-global iterations) are shown in Figure 1.12(c) and Figure 1.12(d), respectively.

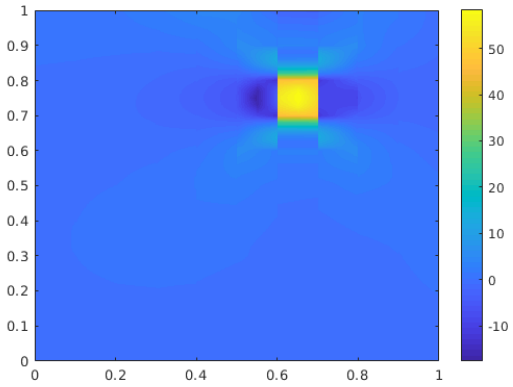

(a) Stress component $\sigma_{xx}$ of the adjoint problem.

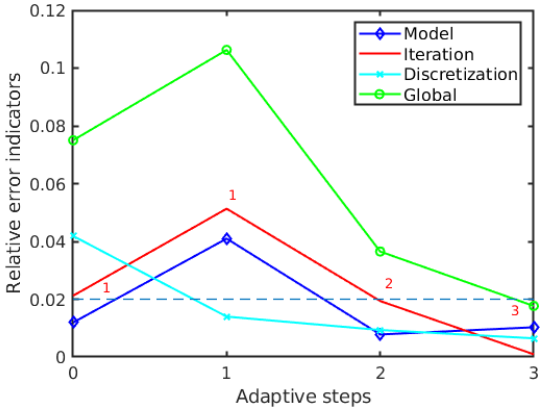


(b) Evolution of error indicators along the adaptive process.

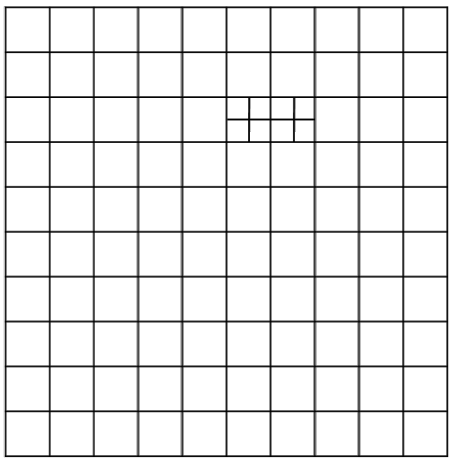

(c) Final mesh used to approximate the solution in the local-global coupling process.

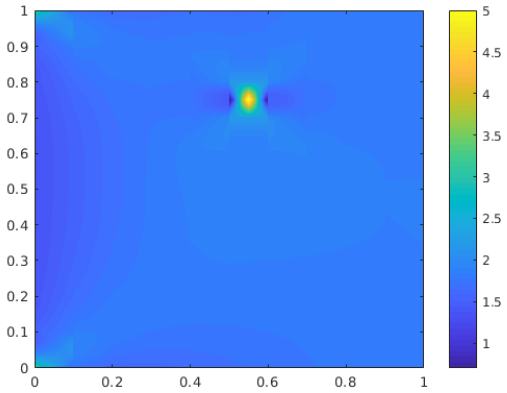

(d) Primal coupled solution after adaptation.

Figure 1.12: Results when considering as a quantity of interest the average of the strain component $\epsilon_{xx}$ in the vicinity of the large weakened zone: influence on the adjoint solution (a), and final stress field in the structure after applying the adaptive algorithm (from [Tirvaudey et al., 2020b]).

## 1.3 Partial conclusions

We presented in this bibliography chapter the non-intrusive local-global coupling method which is at the heart of the PhD work. We focused on its implementation and on its attractive features, compared to alternative approaches, for addressing industrial applications with sufficient flexibility. We also presented, in this context, the currently available strategy for error control with respect to some quantities of interest. This strategy, based on residual functionals and adjoint-based techniques, defines a fully computable error estimate (quantitatively certifying the quality of the approximation) as well as error indicators which are used in an adaptation process. These goal-oriented indicators enable to split error between iteration (i.e. lack of convergence at the coupling interface), modeling, and discretization sources so that useless over-computations are avoided (e.g. the iterative solver is usually stopped before reaching convergence in terms of the usual interface equilibrium). It is important to notice that the strategy is made

consistent with the non-intrusive framework of the coupling; it can thus be performed when coupling two different codes, and local analyses for error sources (by adding local patches when solving the adjoint problem) can advantageously benefit from this non-intrusive framework. Consequently, the adjoint solution does not require prohibitive computing resources but is rather conducted by defining individual and manageable problems (that differ by the position of local patches) which can be solved in parallel.

Nevertheless, the previous strategy for modeling error estimation and management has some limitations. In particular, error bounds are not mathematically guaranteed. Moreover, extension to nonlinear problems is only possible by using linearized operators, so that the error estimator and indicators may not be fully robust in some cases. Further developments should thus address: (i) the computation of robust (e.g. mathematically guaranteed) error bounds on quantities of interest, which was so far a scientific challenge for non-intrusive local-global coupling strategies; (ii) the application to structures with complex nonlinear material behaviors (such as damage or plasticity). These points are the main topics of the PhD work, addressed by a new strategy which is developed in the following chapters.

# Chapter 2

# New error estimation strategy based on CRE for non-intrusive local-global couplings

In this second chapter, we develop a new verification tool for non-intrusive local-global couplings. It is based on the constitutive relation error (CRE) concept, providing guaranteed and fully computable error bounds which are applicable to linear or nonlinear mechanical behaviors. The CRE concept has been the topic of many studies and applications for FE model verification. Out of early works, several developments have been proposed over the last two decades for various problems such as stochastics [Chamoin et al., 2012], transient dynamics [Waeytens et al., 2012] and vibratory dynamics [Wang et al., 2016], or plasticity [Ladevèze et al., 2012]. Applications to several variants of FEM have also been addressed such as XFEM [Panetier et al., 2010], domain decomposition [Parret-Fréaud et al., 2010, Rey et al., 2014b], model reduction [Ladevèze and Chamoin, 2011, Chamoin et al., 2017], non-conforming approximations (e.g. Discontinuous Galerkin) [Ern and Vohralik, 2015], isogeometric analysis [Thai et al., 2019], or multiscale analysis [Chamoin and Legoll, 2018]. Eventually, coupled with adjoint-based techniques, the CRE concept was effectively used for goal-oriented error estimation [Chamoin and Ladevèze, 2008, Ladevèze, 2008, Ladevèze and Chamoin, 2010, Ladevèze et al., 2013, Wang et al., 2016, Chamoin and Legoll, 2021]. We extend here this list to non-intrusive local-global couplings. The resulting error estimation technique is a real asset to the coupling method, allowing to effectively control and adapt the choice of several numerical parameters (e.g. associated with the convergence criterion in the global/local iterations) for a given target accuracy.

## 2.1 Basics on CRE

The energy-based CRE concept has been used for the robust verification of FEM models, that is the *a posteriori* estimation of discretization error, for more than thirty years. Pioneering ideas can be found in [Ladevèze, 1975, Ladevèze and Leguillon, 1983,Ladevèze and Rougeot, 1997,Destuynder and Métivet, 1999], and a general overview is given in [Ladevèze and Pelle, 2005, Ladevèze and Chamoin, 2015]. The CRE concept, based on dual analysis, has similitudes with other methods in the literature such as equilibrated residuals [Ainsworth and Oden, 2000] or flux-free [Pares et al., 2006, Gallimard, 2009] approaches. They all share the idea of constructing a fully equilibrated (i.e. statically admissible) dual field, which is actually the only way to recover guaranteed and fully computable error estimates for linear or nonlinear models of computational mechanics. It thus appears as the most powerful and robust tool in the huge literature on FEM verification. For the sake of clarity, we first introduce below the CRE concept in the context of linear elasticity models.

### 2.1.1 The CRE functional for linear elasticity

#### Reference model

We again consider an open bounded domain $\Omega \subset \mathbb{R}^d$, with boundary $\partial\Omega$, occupied by a linear elastic material (Figure 2.1). We assume that a displacement field $\mathbf{u}_d$ is prescribed on part $\partial_u\Omega$ of the boundary, and that tractions $\mathbf{F}_d$ are prescribed on the complementary part $\partial_F\Omega$ such that $\partial_u\Omega \cap \partial_F\Omega = \emptyset$ and $\overline{\partial_u\Omega \cup \partial_F\Omega} = \partial\Omega$. A body force field $\mathbf{f}_d$ may also be given in $\Omega$. Sufficient regularity is assumed for the prescribed data, that is $\mathbf{u}_d \in [H^{1/2}(\partial_u\Omega)]^d$, $\mathbf{F}_d \in [H^{-1/2}(\partial_F\Omega)]^d$, and $\mathbf{f}_d \in [H^{-1}(\Omega)]^d$. The associated (well-posed) problem is then classically written by splitting in 3 groups of equations:

- kinematic admissibility (defining the space $\boldsymbol{\mathcal{U}}_{ad}$ of compatible displacement fields verifying Dirichlet boundary conditions):

$$\mathbf{u} \in [H^1(\Omega)]^d \quad ; \quad \mathbf{u}_{|\partial_u\Omega} = \mathbf{u}_d \tag{2.1}$$

- static admissibility (defining the space $\boldsymbol{\mathcal{S}}_{ad}$ of $H(div,\Omega)$ stress fields satisfying equilibrium equations written here in the weak form referring to the principle of virtual works):

$$\boldsymbol{\sigma} \in [L^2(\Omega)]_s^{d(d+1)/2} \quad ; \quad \nabla\cdot\boldsymbol{\sigma} \in [L^2(\Omega)]^d \quad ; \quad \int_\Omega \boldsymbol{\sigma} : \boldsymbol{\varepsilon}(\mathbf{v}) = \int_\Omega \mathbf{f}_d\cdot\mathbf{v} + \int_{\partial_F\Omega} \mathbf{F}_d\cdot\mathbf{v} \quad \forall \mathbf{v} \in \boldsymbol{\mathcal{U}}_{ad}^0 \tag{2.2}$$

- constitutive relation (Hooke's law):

$$\boldsymbol{\sigma} = \mathbf{K}\boldsymbol{\varepsilon}(\mathbf{u}) \tag{2.3}$$

with $\mathbf{K}$ the symmetric positive definite Hooke tensor, and $\boldsymbol{\mathcal{U}}_{ad}^0$ the vectorial space associated with $\boldsymbol{\mathcal{U}}_{ad}$.

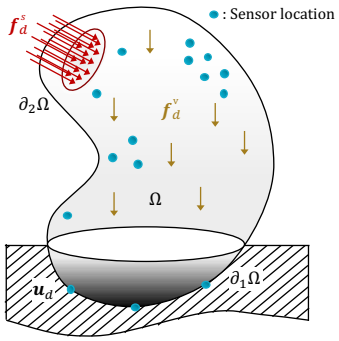


Figure 2.1: Configuration of the reference problem.

A classical primal FE approximation of the problem yields $\mathbf{u}_h \in \boldsymbol{\mathcal{U}}_{ad}^h \subset \boldsymbol{\mathcal{U}}_{ad}$ (with associated stress field $\boldsymbol{\sigma}_h = \mathbf{K}\boldsymbol{\varepsilon}(\mathbf{u}_h) \notin \boldsymbol{\mathcal{S}}_{ad}$) and leads to a discretization error field $\mathbf{e}_h = \mathbf{u} - \mathbf{u}_h$. A measure $\|\mathbf{e}_h\|_{\mathbf{K}}^2 = \int_\Omega \boldsymbol{\varepsilon}(\mathbf{e}_h) : \mathbf{K}\boldsymbol{\varepsilon}(\mathbf{e}_h)$ of this error in the energy norm can be defined, and the objective of FE model verification is to compute an *a posteriori* error estimate on $\|\mathbf{e}_h\|_{\mathbf{K}}$. This may be addressed in two ways:

- a primal variational approach, involving the potential energy $J_1(\mathbf{v}) = \frac{1}{2}\int_\Omega \mathbf{K}\boldsymbol{\varepsilon}(\mathbf{v}) : \boldsymbol{\varepsilon}(\mathbf{v}) - \int_\Omega \mathbf{f}_d \cdot \mathbf{v} - \int_{\partial_F\Omega} \mathbf{F}_d \cdot \mathbf{v}$ and the search space $\boldsymbol{\mathcal{U}}_{ad}$ of compatible displacement fields, leads to:

$$J_1(\mathbf{u}) = \inf_{\mathbf{v}\in\boldsymbol{\mathcal{U}}_{ad}} J_1(\mathbf{v}) \quad ; \quad \|\mathbf{e}_h\|_{\mathbf{K}}^2 = 2\left(J_1(\mathbf{u}_h) - J_1(\mathbf{u})\right) \geq 2\left(J_1(\mathbf{u}_h) - J_1(\mathbf{v})\right) \quad \forall \mathbf{v} \in \boldsymbol{\mathcal{U}}_{ad} \tag{2.4}$$

  so that a computable lower error bound on $\|\mathbf{e}_h\|_{\mathbf{K}}$ can be obtained from a field $\mathbf{u}^* \in \boldsymbol{\mathcal{U}}_{ad}$ at disposal (which should live in a larger space than $\boldsymbol{\mathcal{U}}_{ad}^h$ in order to get a meaningful bound);

- a dual variational approach, involving the complementary energy $J_2(\boldsymbol{\tau}) = \frac{1}{2}\int_\Omega \mathbf{K}^{-1}\boldsymbol{\tau} : \boldsymbol{\tau} - \int_{\partial_u\Omega} \boldsymbol{\tau}\mathbf{n} \cdot \mathbf{u}_d$ and the search space $\boldsymbol{\mathcal{S}}_{ad}$ of equilibrated stress fields, leads to:

$$J_2(\boldsymbol{\sigma}) = \inf_{\tau\in\boldsymbol{\mathcal{S}}_{ad}} J_2(\boldsymbol{\tau}) \quad ; \quad \|\mathbf{e}_h\|_{\mathbf{K}}^2 = 2\left(J_1(\mathbf{u}_h) + J_2(\boldsymbol{\sigma})\right) \leq 2\left(J_1(\mathbf{u}_h) + J_2(\boldsymbol{\tau})\right) \quad \forall \boldsymbol{\tau} \in \boldsymbol{\mathcal{S}}_{ad} \tag{2.5}$$

  so that a fully computable (i.e. without any unknown multiplicative constant) upper error bound on $\|\mathbf{e}_h\|_{\mathbf{K}}$ is obtained from a field $\hat{\boldsymbol{\sigma}} \in \boldsymbol{\mathcal{S}}_{ad}$ at disposal. This bound may be used as a guaranteed error estimate for the assessment of accuracy and as a criterion for mesh adaptivity.

**CRE functional and properties**

Introducing the energy norm $\|\bullet\|_{\mathbf{K}^{-1}}$ on stress fields, the previous upper bound on $\|\mathbf{e}_h\|_{\mathbf{K}}^2/2$ is written as:

$$J_1(\mathbf{u}_h) + J_2(\hat{\boldsymbol{\sigma}}) = \frac{1}{2}\int_\Omega (\hat{\boldsymbol{\sigma}} - \mathbf{K}\boldsymbol{\varepsilon}(\mathbf{u}_h)) : \mathbf{K}^{-1}(\hat{\boldsymbol{\sigma}} - \mathbf{K}\boldsymbol{\varepsilon}(\mathbf{u}_h)) = \frac{1}{2}\|\hat{\boldsymbol{\sigma}} - \mathbf{K}\boldsymbol{\varepsilon}(\mathbf{u}_h)\|_{\mathbf{K}^{-1}}^2 = \mathcal{E}_{CRE}^2(\mathbf{u}_h, \hat{\boldsymbol{\sigma}}) \geq 0 \tag{2.6}$$

It is interpreted as a measure of the residual on the constitutive relation for the admissible pair $(\mathbf{u}_h, \hat{\boldsymbol{\sigma}}) \in \boldsymbol{\mathcal{U}}_{ad} \times \boldsymbol{\mathcal{S}}_{ad}$; this is the definition of the CRE functional $\mathcal{E}_{CRE}$. The CRE concept thus applies to a so-called admissible pair $(\hat{\mathbf{u}}, \hat{\boldsymbol{\sigma}}) \in \boldsymbol{\mathcal{V}} \times \boldsymbol{\mathcal{S}}$ satisfying boundary conditions and balance equations of the model problem. Only the constitutive law (2.3) is relaxed for such an admissible couple $(\hat{\mathbf{u}}, \hat{\boldsymbol{\sigma}})$.

The bounding property given by $\mathcal{E}^2_{CRE}(\mathbf{u}_h, \hat{\boldsymbol{\sigma}})$ is also explained from the Prager-Synge theorem [Prager and Synge, 1947], that relates the computable CRE term with distances, in energy norms, to the unknown exact solution $(\mathbf{u}, \boldsymbol{\sigma})$ of (2.1)-(2.3):

$$\|\mathbf{u} - \mathbf{u}_h\|^2_{\mathbf{K}} + \|\boldsymbol{\sigma} - \hat{\boldsymbol{\sigma}}\|^2_{\mathbf{K}^{-1}} = 2.\mathcal{E}^2_{CRE}(\mathbf{u}_h, \hat{\boldsymbol{\sigma}}) \tag{2.7}$$

The potential of this theorem in the field of error evaluation, even if not originally applied in the FE context, has been known for a long time [Tottenham, 1970, Aubin and Bouchard, 1970].

*Remark. For any admissible pair $(\mathbf{v}, \boldsymbol{\tau}) \in \boldsymbol{\mathcal{U}}_{ad} \times \boldsymbol{\mathcal{S}}_{ad}$, the property $\mathcal{E}_{CRE}(\mathbf{v}, \boldsymbol{\tau}) = 0$ means that $(\mathbf{v}, \boldsymbol{\tau})$ corresponds to the exact solution $(\mathbf{u}, \boldsymbol{\sigma})$ of the problem. Using the CRE concept, the reference problem can thus be formulated as:*

$$(\mathbf{u}, \boldsymbol{\sigma}) = \underset{(\mathbf{v}, \boldsymbol{\tau}) \in \boldsymbol{\mathcal{U}}_{ad} \times \boldsymbol{\mathcal{S}}_{ad}}{\operatorname{argmin}} \mathcal{E}_{CRE}(\mathbf{v}, \boldsymbol{\tau}) \tag{2.8}$$

*Remark. We also have the following property, known as the hypercircle property (see [Ladevèze and Pelle, 2005]):*

$$\mathcal{E}^2_{CRE}(\mathbf{u}_h, \hat{\boldsymbol{\sigma}}) = 2\|\boldsymbol{\sigma} - \hat{\boldsymbol{\sigma}}^m\|^2_{\mathbf{K}^{-1}} \quad \textit{where} \quad \hat{\boldsymbol{\sigma}}^m = \frac{1}{2}(\hat{\boldsymbol{\sigma}} + \mathbf{K}\mathfrak{e}(\mathbf{u}_h)) \tag{2.9}$$

*It is a consequence of the Prager-Synge equality, and is in practice used for goal-oriented error estimation (see next chapter).*

Consequently, the quantity $\sqrt{2}\,\mathcal{E}_{CRE}(\mathbf{u}_h, \hat{\boldsymbol{\sigma}})$ is an upper bound on the error $\|\mathbf{u} - \mathbf{u}_h\|$. It is fully computable as soon as $\hat{\boldsymbol{\sigma}}$ is available. As shown below, it is possible to efficiently build some statically admissible stress field $\hat{\boldsymbol{\sigma}}$ such that this upper bound is accurate in the sense that $\sqrt{2}\,\mathcal{E}_{CRE}(\mathbf{u}_h, \hat{\boldsymbol{\sigma}})/\|\mathbf{u} - \mathbf{u}_h\|$ is close to 1.

*Remark. Depending on the precise way the flux $\hat{\boldsymbol{\sigma}}$ is constructed, a lower bound on $\|\mathbf{u} - \mathbf{u}_h\|$ can also be obtained (see e.g. [Ladevèze and Leguillon, 1983, Ladevèze and Pelle, 2005]). This lower bound is usually of the form $\mathcal{E}_{CRE}(\mathbf{u}_h, \hat{\boldsymbol{\sigma}}) \leq C\|\mathbf{u} - \mathbf{u}_h\|$, where $C$ is a constant independent of the mesh size $h$, showing that the estimate and exact error have the same asymptotic convergence rate.*

**Geometrical interpretation**

Two geometrical representations of the CRE philosophy are now given for the sake of better understanding (see Figure 2.2). The first one, classical, is in the space of stress fields with inner product $\langle \boldsymbol{\sigma}_1, \boldsymbol{\sigma}_2 \rangle = \int_\Omega \boldsymbol{\sigma}_1 \mathbf{K}^{-1} \boldsymbol{\sigma}_2$ and

associated energy norm. It illustrates the orthogonality property involved in the Prager-Synge theorem. The distance between $\hat{\mathfrak{o}}$ and $\mathfrak{o}_h$, that is $\sqrt{2}\mathcal{E}_{CRE}(\mathbf{u}_h, \hat{\mathfrak{o}})$, is an upper error bound on the discretization error $\|\mathbf{u} - \mathbf{u}_h\|_{\mathbf{K}}$.

The second representation, less classical but that is more convenient to interpret the CRE functional in terms of modelling error, is in the space of strain-stress couples $s = (\mathfrak{e}, \mathfrak{o})$. This space is equipped with the energy inner product $\langle s_1, s_2 \rangle = \int_\Omega (\mathfrak{e}_1 \mathbf{K} \mathfrak{e}_2 + \mathfrak{o}_1 \mathbf{K}^{-1} \mathfrak{o}_2)$ and associated energy norm. We denote $(\mathbf{A}_d)$ the space of (kinematically and statically) admissible couples, and $\mathbf{\Gamma}$ the space (linear here) associated with the constitutive law. The exact solution of the well-posed problem (2.1)-(2.3) is then defined by the intersection between $(\mathbf{\Gamma})$ and $(\mathbf{A}_d)$. It is easy to show that the value $\mathcal{E}_{CRE}$ exactly corresponds to the distance from the solution $\hat{s} = (\mathfrak{e}(\mathbf{u}_h), \hat{\mathfrak{o}}) \in (\mathbf{A}_d)$ at hand to $(\mathbf{\Gamma})$, with orthogonal projection. The stress field $\mathfrak{o}_m$ obtained after projection is the average field $\mathfrak{o}_m = \frac{1}{2}(\hat{\mathfrak{o}} + \mathfrak{o}_h)$. The Prager-Synge theorem reads in this framework:

$$\langle s - \hat{s}, s - \hat{s} \rangle = 2.\mathcal{E}^2_{CRE}(\hat{s})$$

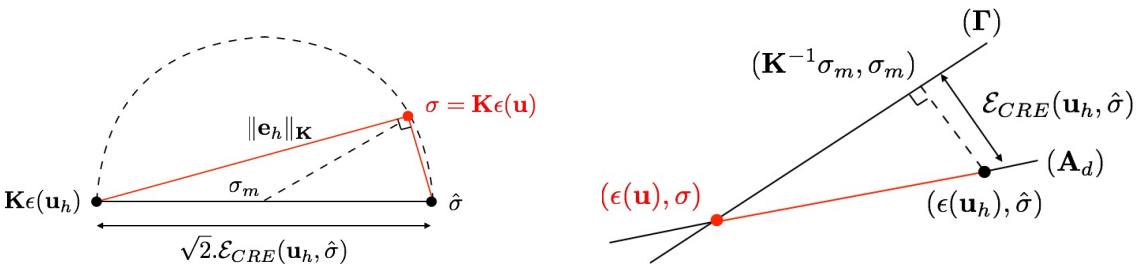


Figure 2.2: Geometrical representations of the CRE concept.

### 2.1.2 Construction of an equilibrated stress field

The quality of the upper error bound $\sqrt{2}\mathcal{E}_{CRE}(\mathbf{u}_h, \hat{\mathfrak{o}})$ depends on that of the statically admissible field $\hat{\mathfrak{o}}$. The suitable construction of such a fully equilibrated stress field is the key and technical point of the CRE concept. For this purpose, a first approach may consist in using equilibrated elements in a dual version of FEM [Fraeijs de Veubeke, 1965, Fraeijs de Veubeke and Hogge, 1972, Debongnie et al., 1995, Fraeijs de Veubeke, 2001, Moitinho de Almeida and Almeida Pereira, 2006, Kempeneers et al., 2009, Moitinho de Almeida and Maunder, 2017]. It is the most effective approach in practice, but also the most technical (as relying on non-conventional FE spaces in the general case, which are not suited to commercial codes) and expensive (as another global problem needs to be solved). Other approaches in the literature are based on the post-processing of the approximate FE field $\mathfrak{o}_h$ using:

- a hybrid flux (or Element Equilibration Technique - EET) technique [Ladevèze and Leguillon, 1983, Coorevits et al., 1992, Ladevèze and Maunder, 1996, Florentin et al., 2002, Ladevèze et al., 2010a, Pled et al., 2011, Rey et al., 2014a];

- a flux-free technique [Pares et al., 2006, Cottereau et al., 2009, Gallimard, 2009, Pares et al., 2009];
- Raviart-Thomas-Nédélec elements over a dual mesh [Ern et al., 2007, Vohralik, 2007, Vohralik, 2008, Ern and Vohralik, 2010, Vohralik, 2011].

We briefly describe here the hybrid flux (EET) technique that will be reused and adapted later. It is made of two steps (see Figure 2.3):

1. polynomial tractions $\hat{\mathbf{F}}_{K|\Gamma}$, equilibrated with the external loading ($\mathbf{f}_d$, $\mathbf{F}_d$), are built over edges $\Gamma$ on the boundary $\partial K$ of each element $K$. They should satisfy $\hat{\mathbf{F}}_{K|\Gamma} = \mathbf{F}_d$ if $\Gamma \subset \partial_F\Omega$, as well as equilibrium at the element level:
$$\int_K \mathbf{f}_d \cdot \mathbf{u}_R^* + \int_{\partial K} \hat{\mathbf{F}}_K \cdot \mathbf{u}_R^* = 0 \quad \forall \mathbf{u}_R^* \in \boldsymbol{\mathcal{U}}_R(K) \tag{2.10}$$
where $\boldsymbol{\mathcal{U}}_R(K)$ denotes the space of rigid body motions on $K$. In practice, tractions are defined as $\hat{\mathbf{F}}_{K|\Gamma} = \eta_K^\Gamma \hat{\mathbf{F}}_\Gamma$, with $\eta_K^\Gamma = \pm 1$ a signed scalar value that ensures continuity of the stress vector across element boundaries, and they are searched as a linear combination of FE shape functions: $\hat{\mathbf{F}}_{K|\Gamma}(\mathbf{x}) = \sum_{j\in J_\Gamma} \hat{\mathbf{F}}^j_{K|\Gamma}\phi_j(\mathbf{x})$; $J_\Gamma$ denotes the set of nodes connected to the edge $\Gamma$.
2. in each element $K$, a stress field $\hat{\sigma}_{h|K}$ is constructed that satisfies equilibrium:
$$\boldsymbol{\nabla}\cdot\hat{\sigma}_h + \mathbf{f}_d = \mathbf{0} \text{ in } K \quad ; \quad \hat{\sigma}_h\mathbf{n} = \hat{\mathbf{F}}_K \text{ on } \partial K \tag{2.11}$$
and that minimizes local complementary energy. The associated local problems are in practice solved with a quasi-explicit technique and polynomial basis [Ladevèze and Rougeot, 1997], or with a dual approach with degree enrichment (i.e. using higher-order elements generating space $\boldsymbol{\mathcal{U}}^h_{p+k}(K)$). The basis functions are then polynomial functions over the whole element $K$, up to a degree $p+k$ ($p$ being the order of the polynomial functions used to discretize $u_h$). Orthogonal hierarchical subspaces $\widetilde{\boldsymbol{\mathcal{U}}}^h_q(K)$ (for $q = p+1, p+2, \ldots, p+k$) can also be introduced to solve the dual version of (2.11) effectively [Ainsworth and Oden, 2000]. Numerical comparisons performed in [Babuska et al., 1994] showed that the approach based on exactly solving the dual local problem and the numerical approach we have just described (approximating it in $\boldsymbol{\mathcal{U}}^h_{p+k}(K)$) provide similar CRE values (i.e. error bounds) when choosing $k \geq 3$, even though the stress fields $\hat{\sigma}_{h|K}$ obtained with the latter approach do not exactly satisfy equilibrium equations (2.11) (and therefore do not provide for a mathematically guaranteed upper error bound). We also refer to [Strouboulis and Haque, 1992] for similar investigations.

The construction of $\hat{\mathbf{F}}_K$ in the first step leans on the following prolongation (energy) condition:
$$\int_K (\hat{\sigma}_h - \sigma_h)\boldsymbol{\nabla}\phi_i = \mathbf{0} \quad \Longrightarrow \quad \int_{\partial K} \hat{\mathbf{F}}_K\phi_i = \int_K (\sigma_h\boldsymbol{\nabla}\phi_i - \mathbf{f}_d\phi_i) \tag{2.12}$$

which is enforced for all elements $K$ and all nodes $i$ connected to $K$; $\phi_i$ is the FE shape function associated with node $i$. This condition, which automatically ensures the equilibration of $\hat{\mathbf{F}}_K$ over $K$ (using the property $\sum_i \phi_{i|K} = 1$), leads to the solution to a system of the form:

$$\sum_{r=1}^{R_n} \mathbf{b}^r_{K_n}(i) = \mathbf{Q}_{K_n}(i) \quad \text{with } \mathbf{Q}_{K_n}(i) = \int_{K_n} (\varpi_h \boldsymbol{\nabla}\phi_i - \mathbf{f}_d \phi_i)$$
$$\hat{\mathbf{b}}^r_{K_n}(i) = \int_{\Gamma_r} \eta^{\Gamma_r}_K \hat{\mathbf{F}}_{\Gamma_r} \phi_i \tag{2.13}$$

over the set of elements $K_n$ connected to each node $i$ (so-called patch, see Figure 2.3). $R_n$ is the number of edges of the element $K_n$ connected to node $i$. The existence of a solution for the unknowns $\hat{\mathbf{b}}^r_{K_n}(i)$ of the system (that are projections of tractions $\hat{\mathbf{F}}_\Gamma$ on FE shape functions) is ensured by the equilibrium property (in the FE sense) verified by $\varpi_h$, and uniqueness may be obtained minimizing a least-squares cost function [Ladevèze and Pelle, 2005].

*Remark. Several variants of the above hybrid-flux method, which is based on the prolongation condition, have been proposed in the literature [Florentin et al., 2002, Pled et al., 2012]. For instance, a "weak" prolongation condition may be applied to shape functions associated with non-vertex nodes alone. Tractions are then constructed as* $\hat{\mathbf{F}}_K = \mathbf{L} + \mathbf{H}$ *where* $\mathbf{H}$ *(high-degree component) is fully computed from the weak prolongation condition whereas* $\mathbf{L}$ *(low-degree component) is obtained by minimizing a global complementary energy. This procedure is in practice applied in zones with high gradients or high element aspect ratio in order to optimize the estimate. In the other zones, the above method, based on the prolongation condition, is used.*

*Another variant is to construct equilibrated tractions using the Partition of Unity Method (PUM) [Ladevèze et al., 2010a, Pled et al., 2011]. This variant provides results similar to those obtained with the method based on the prolongation condition, but is easier to implement in simulation softwares.*

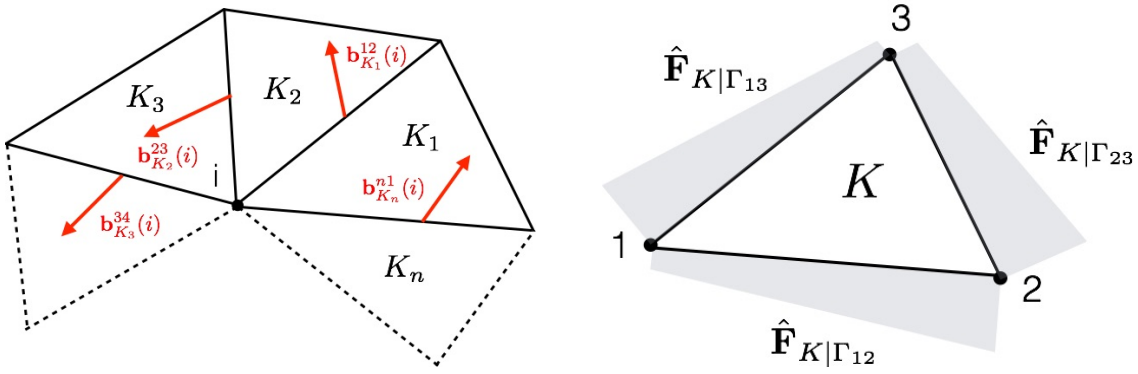


Figure 2.3: Illustration of the two steps of the hybrid-flux equilibration technique.

### 2.1.3 Extensions of CRE to complex models

When addressing model verification for nonlinear problems, there are much fewer contributions than for linear problems. It is important to distinguish between nonlinear *time-dependent* and nonlinear *time-independent* problems. For the latter case, we mention [Larsson et al., 2002] for the design of estimates for nonlinear elasticity problems, [Johnson and Hansbo, 1992] for Hencky-type plasticity problems, or [Gallimard et al., 1996, Rannacher and Suttmeier, 1999] for elastoplasticity. For the former case, viscoplasticity problems have been treated in [Fourment and Chenot, 1995, Larsson et al., 2003, Pelle and Ryckelynck, 2000], nonlinear dynamics has been considered in [Radovitzky and Ortiz, 1999], and other nonlinear contexts have been investigated in [Huerta and Diez, 2000]. In most cases, techniques devised for linear problems or time-independent nonlinear problems are used at each time step, so that the estimation is limited to spatial error.

The CRE concept, originally used for linear thermal and elasticity problems [Ladevèze and Leguillon, 1983], can be naturally extended to more complex problems embracing a larger class of nonlinear time-dependent constitutive models of the general functional form $\varpi_{|t} = \mathbf{A}(\dot{\varepsilon}_{|\tau}, \tau \leq t)$ (such as elasto-plasticity with or without softening). It thus provides robust error estimators for such models. This extension makes benefit of the duality and convex analysis tools developed in [Moreau, 1966, Nayroles, 1973]. It then enables all numerical error sources of FEM simulations to be controlled, which are space or time discretizations, as well as algebraic errors generated by iterative algorithms. This is a major step forward compared to classical residual-based error estimation techniques that consider a linearized (tangent) operator when dealing with nonlinear constitutive models.
For nonlinear material behaviors, such as hyper-elasticity, the key concept is the use of the convex dual potentials $\psi$ and $\psi^*$ that derive from continuum thermodynamics, and that define the material law as $\varpi = \frac{\partial \psi}{\partial \varepsilon}$ or $\varepsilon = \frac{\partial \psi^*}{\partial \varpi}$ [Repin, 1999]. Potentials $\psi$ and $\psi^*$ are dual in the Legendre-Fenchel sense, i.e.:

$$\psi^*(\varpi) = \sup_{\varepsilon} \{\varpi : \varepsilon - \psi(\varepsilon)\}$$

Linear elasticity corresponds to quadratic potentials $\psi(\varepsilon) = \frac{1}{2}\varepsilon : \mathbf{K}\varepsilon$ and $\psi^*(\varpi) = \frac{1}{2}\varpi : \mathbf{K}^{-1}\varpi$.

The definition of the CRE measure then refers to the previous Legendre-Fenchel duality (related to the symmetrized Bergman divergence used in statistics) and reads for an admissible pair $(\hat{\varepsilon}, \hat{\varpi}) \in (\mathbf{A}_d)$:

$$\mathcal{E}^2_{CRE}(\hat{\varepsilon}, \hat{\varpi}) = \int_\Omega (\psi(\hat{\varepsilon}) + \psi^*(\hat{\varpi}) - \hat{\varpi} : \hat{\varepsilon}) \geq 0 \tag{2.14}$$

A geometrical interpretation of this error measure is given in Figure 2.4: for a given point $(\hat{\varepsilon}, \hat{\varpi})$, $\psi(\hat{\varepsilon})$ is the area in blue, $\psi^*(\hat{\varpi})$ is the area in red, and $\hat{\varpi} : \hat{\varepsilon}$ is the area in grey. The CRE residual quantity $\psi(\hat{\varepsilon}) + \psi^*(\hat{\varpi}) - \hat{\varpi} : \hat{\varepsilon}$ is then the remaining blank area.

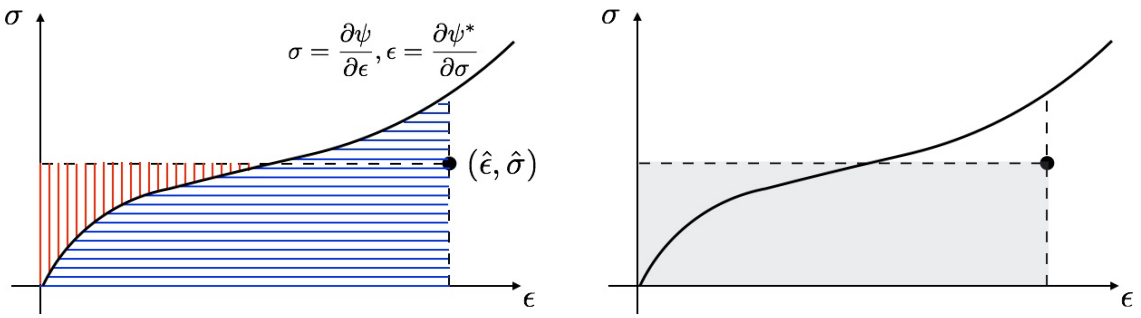


Figure 2.4: Geometrical representation of the CRE measure for nonlinear material behaviors.

For dissipative material behaviors with standard formulation, the clue is the use of internal variables associated with the continuum thermodynamics framework [Halphen and Nguyen, 1975, Germain et al., 1983], and describing past history. This framework leads to the introduction of two pairs of Legendre-conjugate convex potentials that describe the two complementary parts of the overall material behavior: (i) state equations $\mathbf{e}_e = \mathbf{\Lambda}(\mathbf{s}) = \frac{\partial \psi^*}{\partial \mathbf{s}}$; (ii) evolution laws $\dot{\mathbf{e}}_p = \mathbf{B}(\mathbf{s}) = \frac{\partial \varphi^*}{\partial \mathbf{s}}$. Generalized quantities $\mathbf{e}_e$, $\mathbf{e}_p$ and $\mathbf{s}$ include observable and internal variables.

The CRE measure is then constructed from residuals $\eta_\psi(\hat{\mathbf{e}}_e, \hat{\mathbf{s}}) = \psi(\hat{\mathbf{e}}_e) + \psi^*(\hat{\mathbf{s}}) - \hat{\mathbf{s}} \cdot \hat{\mathbf{e}}_e$ and $\eta_\varphi(\dot{\hat{\mathbf{e}}}_p, \hat{\mathbf{s}}) = \varphi(\dot{\hat{\mathbf{e}}}_p) + \varphi^*(\hat{\mathbf{s}}) - \hat{\mathbf{s}} \cdot \dot{\hat{\mathbf{e}}}_p$ on these two parts, with admissible solution $(\hat{\mathbf{e}}_e, \hat{\mathbf{e}}_p, \hat{\mathbf{s}})$ such that $\hat{\mathbf{e}}_e + \hat{\mathbf{e}}_p = \hat{\mathbf{e}}$. Terms $\mathbf{y} \cdot \mathbf{x}$ correspond to the duality product between variables $\mathbf{x}$ and $\mathbf{y}$. Residuals $\eta_\psi$ and $\eta_\varphi$ are local in space and time quantities, so that the global CRE functional over the whole space-time domain reads [Ladevèze, 1998, Ladevèze et al., 1999, Ladevèze, 2001, Ladevèze and Pelle, 2005]:

$$\mathcal{E}^2_{CRE|t} = \int_\Omega \eta_\psi(\hat{\mathbf{e}}_e, \hat{\mathbf{s}}) + \int_0^t \int_\Omega \eta_\varphi(\dot{\hat{\mathbf{e}}}_p, \hat{\mathbf{s}}) \tag{2.15}$$

More details on the extended CRE functional, with specific application to the elasto-plastic case, will be given in the following sections.

*Remark. A variant of the literature is to define the CRE measure from the residual on evolution laws alone, enforcing state equations in the definition of admissibility [Ladevèze and Moës, 1997, Ladevèze, 1998, Ladevèze and Moës, 1999]. This is the concept of dissipation error which has a clear mechanical meaning and emphasizes the dissipation properties of the model. n this context, state equations are inserted in admissibility conditions. This framework was widely used for model verification purposes [Pelle and Ryckelynck, 2000, Chamoin and Ladevèze, 2007, Chamoin and Ladevèze, 2008, Ladevèze, 2008, Ladevèze et al., 2012]. It will not be considered here.*

*On the other hand, a more general framework for the definition of the CRE error was proposed [Ladevèze, 2008] when constitutive laws are not given by potentials (but provided the constitutive operator still remains monotonic).*

*Eventually, an alternative CRE measure denoted Drucker's error can be defined for dynamics problems [Gallimard et al., 1996, Ladevèze, 1999]; it is based on the Drucker material stability principle [Drucker, 1964].*

## 2.2 Development of a CRE-based error estimator for non-intrusive couplings

In this section, we define some *a posteriori* error estimation tools, based on the Constitutive Relation Error (CRE) concept, for the non-intrusive local-global coupling method. Contrary to the residual-based approach shown in Chapter 1, this new approach provides for guaranteed (and still fully computable with no unknown constant) error bounds for both linear and nonlinear models. It is a suitable framework to certify the quality of the approximation solution stemming from the local-global non-intrusive coupling. We concentrate here on the recovery of admissible fields which is the main technical point of the approach.

### 2.2.1 Construction of admissible fields and CRE estimate

In order to implement the CRE approach at iteration $n$ of the local-global iterative procedure, an admissible pair should be recovered from the solution at hand. On the one hand, the displacement field $\mathbf{u}_{LG}^{hH(n)} \in \boldsymbol{\mathcal{V}}$ can be used as an admissible displacement field in a straightfoward manner. On the other hand, it is possible to recover an admissible stress field $\hat{\boldsymbol{\sigma}}_{LG,N}^{hH(n)} \in \boldsymbol{\mathcal{S}}$, using the *hybrid-flux* technique, from a specific post-processing of the approximate field $\boldsymbol{\sigma}_{LG,N}^{hH(n)} \notin \boldsymbol{\mathcal{S}}$ at hand (which verifies balance equations in a FE weak sense). Indeed:

- the discretized global problem at iteration $n$ provides for the global stress field $\boldsymbol{\sigma}_G^{H(n)}$ verifying the following equilibrium in the FE weak sense:

$$\int_\Omega \boldsymbol{\sigma}_G^{H(n)} : \mathbb{e}(\mathbf{v}_G^H) = \int_{\Omega_0} \mathbf{f}_d \cdot \mathbf{v}_G^H + \int_{\partial_F \Omega} \mathbf{F}_d \cdot \mathbf{v}_G^H - \int_\Gamma \boldsymbol{\lambda}^{h(n-1)} \cdot \mathbf{v}_G^H + \int_{\Omega_L} \boldsymbol{\sigma}_G^{H(n-1)} : \mathbb{e}(\mathbf{v}_G^H) \quad \forall \mathbf{v}_G^H \in \boldsymbol{\mathcal{V}}^H \tag{2.16}$$

  Introducing the field $\delta\boldsymbol{\sigma}_G^{H(n)} = \boldsymbol{\sigma}_G^{H(n)} - \boldsymbol{\sigma}_G^{H(n-1)}.I_{\Omega_L}$, with $I_{\Omega_L}$ the indicatrix function of subdomain $\Omega_L$, the previous FE equilibrium property reads:

$$\int_\Omega \delta\boldsymbol{\sigma}_G^{H(n)} : \mathbb{e}(\mathbf{v}_G^H) = \int_{\Omega_0} \mathbf{f}_d \cdot \mathbf{v}_G^H + \int_{\partial_F \Omega} \mathbf{F}_d \cdot \mathbf{v}_G^H - \int_\Gamma \boldsymbol{\lambda}^{h(n-1)} \cdot \mathbf{v}_G^H \quad \forall \mathbf{v}_G^H \in \boldsymbol{\mathcal{V}}^H \tag{2.17}$$

  Using this property together with the hybrid-flux equilibration procedure, a stress field $\widehat{\delta\boldsymbol{\sigma}_G^{H(n)}}$ verifying the following full equilibrium:

$$\int_\Omega \widehat{\delta\boldsymbol{\sigma}_G^{H(n)}} : \mathbb{e}(\mathbf{v}_G) = \int_{\Omega_0} \mathbf{f}_d \cdot \mathbf{v}_G + \int_{\partial_F \Omega} \mathbf{F}_d \cdot \mathbf{v}_G - \int_\Gamma \boldsymbol{\lambda}^{h(n-1)} \cdot \mathbf{v}_G \quad \forall \mathbf{v}_G \in \boldsymbol{\mathcal{V}} \tag{2.18}$$

  can be recovered in $\Omega$;

- the discretized local problem at iteration $n-1$ provides for the local stress field $\boldsymbol{\sigma}_L^{h(n-1)}$ verifying the following

equilibrium in the FE weak sense:

$$\int_{\Omega_L} \varpi_L^{h(n-1)} : \mathfrak{e}(\mathbf{v}_L^h) = \int_{\Omega_L} \mathbf{f}_d \cdot \mathbf{v}_L^h + \int_{\Gamma} \boldsymbol{\lambda}^{h(n-1)} \cdot \mathbf{v}_L^h \quad \forall \mathbf{v}_L^h \in \boldsymbol{\mathcal{V}}_L^h \tag{2.19}$$

Using this property together with the hybrid-flux equilibration procedure, a stress field $\hat{\varpi}_L^{h(n-1)}$ verifying the following full equilibrium:

$$\int_{\Omega_L} \hat{\varpi}_L^{h(n-1)} : \mathfrak{e}(\mathbf{v}_L) = \int_{\Omega_L} \mathbf{f}_d \cdot \mathbf{v}_L + \int_{\Gamma} \boldsymbol{\lambda}^{h(n-1)} \cdot \mathbf{v}_L \quad \forall \mathbf{v}_L \in \boldsymbol{\mathcal{V}}_L \tag{2.20}$$

can be recovered in $\Omega_L$.

Then, the field $\hat{\varpi}_{LG,N}^{hH(n)}$ defined as $\widehat{\delta\varpi}_G^{H(n)} + \hat{\varpi}_L^{h(n-1)}.I_{\Omega_L}$ is statically admissible, that is:

$$\int_{\Omega} \hat{\varpi}_{LG,N}^{hH(n)} : \mathfrak{e}(\mathbf{v}) = \int_{\Omega} \mathbf{f}_d \cdot \mathbf{v} + \int_{\partial_F \Omega} \mathbf{F}_d \cdot \mathbf{v} \quad \forall \mathbf{v} \in \boldsymbol{\mathcal{V}} \tag{2.21}$$

*Remark. It should be noticed that here again, the construction of the admissible stress field follows the non-intrusive framework and can be performed independently inside softwares addressing global and local problems. Nevertheless, it is required that each associated software be equipped with an equilibration procedure (e.g. based on the hybrid-flux technique).*

Consequently, using (2.7), we obtain the upper bound on the error $\|\mathbf{u} - \mathbf{u}_{LG}^{hH(n)}\|$ in the energy norm:

$$\|\mathbf{u} - \mathbf{u}_{LG}^{hH(n)}\|_{\mathbf{K}} \leq \sqrt{2}.\mathcal{E}_{CRE}(\mathbf{u}_{LG}^{hH(n)}, \hat{\varpi}_{LG,N}^{hH(n)}) = \eta_{CRE}^{tot} \tag{2.22}$$

The estimate $\eta_{CRE}^{tot}$ is guaranteed whether the local-global iterative solver has converged or not. It comprises all error sources; nevertheless, as such, the different error sources are not separated.

*Remark. The proposed approach for the implementation of CRE-based error estimation shares similarities with the work performed in [Parret-Fréaud et al., 2010, Rey et al., 2014b, Rey et al., 2015] in the context of sub-structured problems and domain decomposition solvers. They both rely on the construction of an admissible pair from two consecutive Dirichlet-Neumann steps of the iterative solver. Nevertheless, the technicality is different between the two approaches, as the global and local models co-exist in subzone $\Omega_L$ for the non-intrusive local-global coupling method.*

### 2.2.2 Technical implementation of the hybrid-flux technique

A technical and unconventional difficulty when implementing the hybrid-flux technique in the context of a non-intrusive local-global coupling is in the fact that this coupling generates internal element edge loadings for the global problem. These correspond to forces coming from the local problem at the previous iteration step and applied on the coupling interface $\Gamma$ (see (2.17)). We detail here the specific procedure that thus needs to be implemented to address this case, and which represents a variant of the classical hybrid-flux technique. As an example, we consider the configuration shown in Figure 2.5 with internal surface loading $\boldsymbol{\lambda}^h$ on the interface $\Gamma_{12}$ between elements $K_1$ and $K_2$.

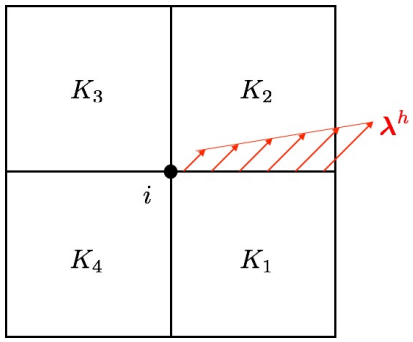


Figure 2.5: Illustration of an internal interface loading.

The FE equilibrium (with shape function $\phi_i$) on patch $\Omega_i$ reads:

$$\int_{\Omega_i} \boldsymbol{\varpi}^H : \mathfrak{e}(\phi_i) = \int_{\Omega_i} \mathbf{f}_d \phi_i + \int_{\Gamma_{12}} \boldsymbol{\lambda}^h \phi_i \tag{2.23}$$

From the prolongation condition $\int_K (\hat{\boldsymbol{\sigma}} - \boldsymbol{\varpi}^H) : \mathfrak{e}(\phi_i) = 0$ for any element $K$ in $\Omega_i$, it yields:

$$\int_{\partial K} \hat{\boldsymbol{\sigma}} \mathbf{n} \phi_i = \int_K \boldsymbol{\varpi}^H : \mathfrak{e}(\phi_i) - \int_K \mathbf{f}_d \phi_i = Q_K(i) \tag{2.24}$$

This leads to the following system over $\Omega_i$:

$$\begin{aligned}
\int_{\Gamma_{12}} \hat{\boldsymbol{\sigma}}_1 \mathbf{n}_{12} \phi_i - \int_{\Gamma_{14}} \hat{\boldsymbol{\sigma}}_1 \mathbf{n}_{41} \phi_i &= Q_{K_1}(i) \\
\int_{\Gamma_{23}} \hat{\boldsymbol{\sigma}}_2 \mathbf{n}_{23} \phi_i - \int_{\Gamma_{12}} \hat{\boldsymbol{\sigma}}_2 \mathbf{n}_{12} \phi_i &= Q_{K_2}(i) \\
\int_{\Gamma_{34}} \hat{\boldsymbol{\sigma}}_3 \mathbf{n}_{34} \phi_i - \int_{\Gamma_{23}} \hat{\boldsymbol{\sigma}}_3 \mathbf{n}_{23} \phi_i &= Q_{K_3}(i) \\
\int_{\Gamma_{14}} \hat{\boldsymbol{\sigma}}_4 \mathbf{n}_{41} \phi_i - \int_{\Gamma_{34}} \hat{\boldsymbol{\sigma}}_4 \mathbf{n}_{34} \phi_i &= Q_{K_4}(i)
\end{aligned} \tag{2.25}$$

Noticing that $\int_{\Gamma_{12}} \hat{\boldsymbol{\sigma}}_2 \mathbf{n}_{12} \phi_i = \int_{\Gamma_{12}} \hat{\boldsymbol{\sigma}}_1 \mathbf{n}_{12} \phi_i - \int_{\Gamma_{12}} \boldsymbol{\lambda}^h \phi_i$ (equilibrium of the interface $\Gamma_{12}$), the second equation of the

system can be recast as:

$$\int_{\Gamma_{23}} \hat{\mathfrak{o}}_2 \mathbf{n}_{23} \phi_i - \int_{\Gamma_{12}} \hat{\mathfrak{o}}_1 \mathbf{n}_{12} \phi_i = Q_{K_2}(i) - \int_{\Gamma_{12}} \boldsymbol{\lambda}^h \phi_i \tag{2.26}$$

so that we come down to a classical system (of the form (2.13)), replacing $Q_{K_2}(i)$ with $Q_{K_2}(i) - \int_{\Gamma_{12}} \boldsymbol{\lambda}^h \phi_i$. The usual hybrid-flux technique can then be employed based on this system.

Then, after solving individual local systems and recovering the equilibrated traction $\hat{\mathbf{F}}_{12} = \hat{\mathfrak{o}}_1 \mathbf{n}_{12}$ on $\Gamma_{12}$, we take $\hat{\mathfrak{o}}_2 \mathbf{n}_{12} = \hat{\mathbf{F}}_{12} - \boldsymbol{\lambda}^h$ (or $\hat{\mathfrak{o}}_2 \mathbf{n}_{21} = -\hat{\mathbf{F}}_{12} + \boldsymbol{\lambda}^h$) to solve the local Neumann problem and reconstruct an equilibrated stress field inside element $K_2$. A classical procedure is used for equilibrated stress reconstruction within other elements.

*Remark. In the local minimization associated with the solution of the local system (to get a unique solution),* $\hat{\mathfrak{o}}_1 \mathbf{n}_{12}$ *should thus be compared with* $(\mathfrak{o}_1^H \mathbf{n}_{12} + (\mathfrak{o}_2^H \mathbf{n}_{12} + \boldsymbol{\lambda}^h))/2$.

## 2.3 Construction of error indicators and adaptive algorithm

### 2.3.1 Error indicators on individual sources

Following previous notations, the global error estimate $\eta_{CRE}^{tot}$ defined in Section 2.2 can be recast as:

$$\begin{aligned} 2.\mathcal{E}_{CRE}^2(\mathbf{u}_{LG}^{hH(n)}, \hat{\mathfrak{o}}_{LG,N}^{hH(n)}) &= \|\hat{\mathfrak{o}}_{LG,N}^{hH(n)} - \mathbf{K}\mathfrak{C}(\mathbf{u}_{LG}^{hH(n)})\|_{\mathbf{K}^{-1}}^2 \\ &= \|\hat{\mathfrak{o}}_{LG,N}^{hH(n)} - \mathbf{K}\mathfrak{C}(\mathbf{u}_{LG}^{hH(n)})\|_{\mathbf{K}^{-1}|\Omega_0}^2 + \|\hat{\mathfrak{o}}_{LG,N}^{hH(n)} - \mathbf{K}\mathfrak{C}(\mathbf{u}_{LG}^{hH(n)})\|_{\mathbf{K}^{-1}|\Omega_L}^2 \end{aligned} \tag{2.27}$$

The first term:

$$\|\hat{\mathfrak{o}}_{LG,N}^{hH(n)} - \mathbf{K}\mathfrak{C}(\mathbf{u}_{LG}^{hH(n)})\|_{\mathbf{K}^{-1}|\Omega_0}^2 = \|\widehat{\delta\mathfrak{o}}_G^{H(n)} - \mathbf{K}\mathfrak{C}(\mathbf{u}_G^{H(n)})\|_{\mathbf{K}^{-1}|\Omega_0}^2 \tag{2.28}$$

corresponds to modeling error. It is 0 when there is no discretization or modeling error in $\Omega_0$, and no pollution error coming from the use of a coarse mesh in $\Omega_L$ when solving the global problem.

The second term reads:

$$\begin{aligned} \|\hat{\mathfrak{o}}_{LG,N}^{hH(n)} - \mathbf{K}\mathfrak{C}(\mathbf{u}_{LG}^{hH(n)})\|_{\mathbf{K}^{-1}|\Omega_L}^2 &= \|\widehat{\delta\mathfrak{o}}_G^{H(n)} + \hat{\mathfrak{o}}_L^{h(n-1)} - \mathbf{K}\mathfrak{C}(\mathbf{u}_L^{h(n)})\|_{\mathbf{K}^{-1}|\Omega_L}^2 \\ &= \|\widehat{\delta\mathfrak{o}}_G^{H(n)} - (\hat{\mathfrak{o}}_L^{h(n)} - \hat{\mathfrak{o}}_L^{h(n-1)}) + \hat{\mathfrak{o}}_L^{h(n)} - \mathbf{K}\mathfrak{C}(\mathbf{u}_L^{h(n)})\|_{\mathbf{K}^{-1}|\Omega_L}^2 \end{aligned} \tag{2.29}$$

It is made of a first term $\|\widehat{\delta\mathfrak{o}}_G^{H(n)} - (\hat{\mathfrak{o}}_L^{h(n)} - \hat{\mathfrak{o}}_L^{h(n-1)})\|_{\mathbf{K}^{-1}|\Omega_L}^2$, corresponding to iteration error, that vanishes when $n \to +\infty$, and a second term $\|\hat{\mathfrak{o}}_L^{h(n)} - \mathbf{K}\mathfrak{C}(\mathbf{u}_L^{h(n)})\|_{\mathbf{K}^{-1}|\Omega_L}^2$, corresponding to discretization error, that vanishes when $h \to 0$. Consequently, we get:

$$\eta_{CRE}^{tot} \leq \eta_{CRE}^{conv} + \eta_{CRE}^{dis} + \eta_{CRE}^{mod} \tag{2.30}$$

with error indicators defined as:

$$\begin{aligned}
\eta_{CRE}^{conv} &= \|\widehat{\delta\mathfrak{S}}_G^{H(n)} - (\hat{\mathfrak{S}}_L^{h(n)} - \hat{\mathfrak{S}}_L^{h(n-1)})\|_{\mathbf{K}^{-1}|\Omega_L} \\
\eta_{CRE}^{dis} &= \|\hat{\mathfrak{S}}_L^{h(n)} - \mathbf{K}\mathfrak{C}(\mathbf{u}_L^{h(n)})\|_{\mathbf{K}^{-1}|\Omega_L} \\
\eta_{CRE}^{mod} &= \|\widehat{\delta\mathfrak{S}}_G^{H(n)} - \mathbf{K}\mathfrak{C}(\mathbf{u}_G^{H(n)})\|_{\mathbf{K}^{-1}|\Omega_0}
\end{aligned} \tag{2.31}$$

The error indicators defined in (2.31) can also interpreted as follows:

- the indicator on convergence error $\eta_{CRE}^{conv}$ quantifies the change between two successive iterations in the fine-scale part of the stress field in $\Omega_L$;
- the indicator on discretization error $\eta_{CRE}^{dis}$ comes down to define admissibility and CRE functional from an intermediate reference model with coarse discretized model in $\Omega$, unbalance on $\Gamma$, but continuous solution in $\Omega_L$;
- the indicator on modeling error $\eta_{CRE}^{mod}$ comes down to define admissibility and CRE functional from an intermediate reference model with high-fidelity model over the whole domain $\Omega$, unbalance on $\Gamma$, but already discretized with $\tau^h$ in $\Omega_L$.

*Remark. Indicators $\eta_{CRE}^{dis}$ and $\eta_{CRE}^{mod}$ can be computed independently inside softwares dealing with local and global problems, respectively. We will check in the numerical results that they are mostly driven by the discretization and surrogate model, respectively, so that they slightly vary during iterations with fixed mesh $\tau^h$ and local zone $\Omega_L$.*

*Remark. The indicator $\eta_{CRE}^{conv}$ requires to combine in the local zone $\Omega_L$ some admissible stress fields coming from global and local models, and defined at integration points of corresponding FE meshes. For that purpose, a technical step with field transfer is implemented in the numerical experiments. It is based on the procedure described in [Dureisseix and Bavestrello, 2006], that permits information transfer between non-matching finite element meshes by means of a geometric approach (seen as an extension of the mortar technique).*

*Remark. For error splitting and definition of error indicators using CRE, we here again follow a different approach from that presented in [Rey et al., 2014b, Rey et al., 2015, Rey et al., 2016] in the context of domain decomposition, and inspired from [Vohralik, 2007]. In those works, the algebraic error source is separated from other sources by introducing a discontinuous displacement field $\mathbf{u}_N^{(n)}$ associated with a FE equilibrated stress field $\mathfrak{S}_N$. This leads to a bound under the form $\|\mathbf{u} - \mathbf{u}_N^{(n)}\|_{brok} \leq C + \mathcal{E}_{CRE}(\mathbf{u}_N^{(n)}, \hat{\mathfrak{S}}_N^{(n)})$ where the term $C$ corresponds to algebraic error and is defined from the preconditioner norm of the residual.*

### 2.3.2 Greedy adaptive algorithm

A greedy adaptive algorithm can be set up from the computation (at each iteration of the local-global coupling algorithm) of error estimator and indicators. Considering here the control of the error in the energy norm (with specified error tolerance $\gamma_{tol}$), and after initializing $\Omega_L$ and $\tau_h$, the algorithm reads as follows:

0. Set $n = 1$;
1. Solve the primal surrogate problem for $\mathbf{u}_{LG}^{hH(n)}$;
2. Recover the admissible stress field $\hat{\mathfrak{G}}_{LG,N}^{hH(n)}$ and compute the estimate $\eta_{CRE}^{tot}$;
3. If $\eta_{CRE}^{tot}/\|\mathbf{u}_{LG}^{hH(n)})\|_{\mathbf{K}} \leq \gamma_{tol}$ then STOP. Otherwise proceed to Step 4;
4. Compute indicators $\eta_{CRE}^{conv}$, $\eta_{CRE}^{dis}$, and $\eta_{CRE}^{mod}$:
   - if $\max(\eta_{CRE}^{conv}, \eta_{CRE}^{dis}, \eta_{CRE}^{mod}) = \eta_{CRE}^{conv}$, increment $n+1 \to n$ and go to Step 1;
   - if $\max(\eta_{CRE}^{conv}, \eta_{CRE}^{dis}, \eta_{CRE}^{mod}) = \eta_{CRE}^{dis}$, decompose $\eta_{CRE}^{dis}$ and locally refine $\tau^h$ up to reaching $\eta_{CRE}^{dis}/\|\mathbf{u}_{LG}^{hH(n)})\|_{\mathbf{K}} \leq \gamma_{tol}/3$, then go to Step 1;
   - if $\max(\eta_{CRE}^{conv}, \eta_{CRE}^{dis}, \eta_{CRE}^{mod}) = \eta_{CRE}^{mod}$, decompose $\eta_{CRE}^{mod}$ and locally enlarge $\Omega_L$ up to reaching $\eta_{CRE}^{mod}/\|\mathbf{u}_{LG}^{hH(n)})\|_{\mathbf{K}} \leq \gamma_{tol}/3$, then go to Step 1.

## 2.4 Numerical results

### 2.4.1 Elasticity problem on a plate with a hole

In a first application, we use the non-intrusive local-global coupling technique to perform local analysis in the vicinity of a hole. In the global model, the hole is not represented. This hole is represented in the local model which is centered on it. The initial geometry and configuration of the global and local domains are given in Figure 2.6. The global domain is meshed using a structured mesh made of T3 triangular elements, while the local domain is meshed using smaller T3 triangular elements.

We consider two loading cases (Figure 2.7): on both we apply a uniform traction force along the direction $x$ on the right side of the plate. As Dirichlet boundary conditions, for the first loading case we restrain the translation along the $y$ axis on the bottom edge and the translation along the $x$ axis on the left edge. For the second loading case, we restrain the translation along $x$ and $y$ axes on the left edge.

The material properties for the whole domain are set as homogeneous, isotropic and linear elastic with a Young modulus $E = 1MPa$ and a Poisson ratio $\nu = 0.3$. We have the same material for both global model and local model.

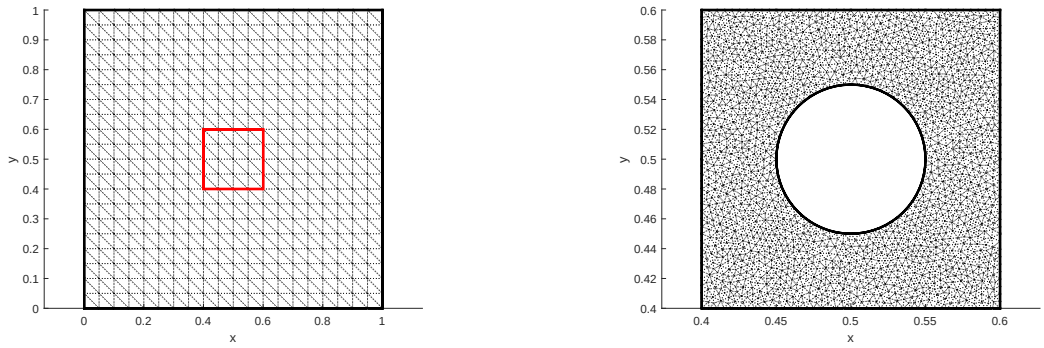


(a) Global mesh (with the coupling interface).

(b) Initial local mesh.

Figure 2.6: Initial coupling configuration and mesh.

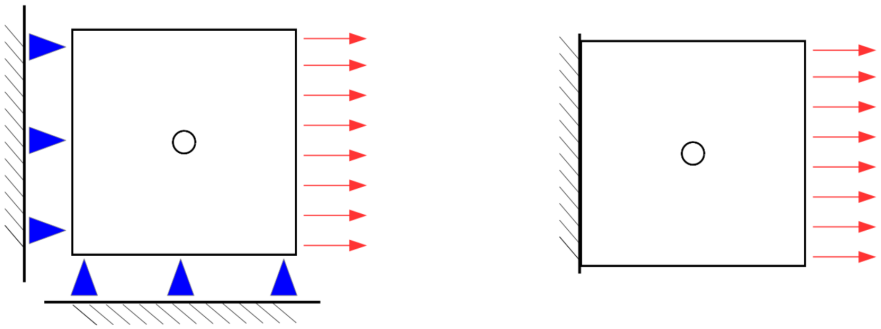

(a) Case study 1.

(b) Case study 2.

Figure 2.7: Case studies.

The solution is obtained using the non-intrusive coupling, at convergence we obtain the solution shown in Figure 2.8. Note that we use a very fine mesh for the local model.

The classical methodology for non-intrusive coupling consists in adding an iteration for the algorithm until the convergence is reached (i.e. the interface residual is smaller than a tolerance). In this context, we evaluate the error indicators, based on the CRE, at each iteration (cf Figure 2.9(a)). We observe that the modeling error contribution penalizes the overall error and the classical methodology is not optimal to decrease the global error, as enlarging the local domain would lead to better results after 3 iterations of the non-intrusive coupling algorithm.

To show the capability of the adaptive algorithm, we consider the same initial problem, with the exception that the initial local model mesh is initially coarser, cf Figure 2.10). The CRE-based greedy adaptive strategy is used to drive the solution of the local-global problem (cf Chapter 2.3.2).

The evolution of the relative error indicators are given in Figure 2.9(b) and the evolution of the local domain size is given in Figure 2.11. As we can see at steps 6 and 8 the local domain is enlarged, and the local mesh is refined at steps 2, 4, 5, 7 and 9.

The final configuration obtained after 10 adaptive steps is given in Figure 2.12 and a global relative error of 2%

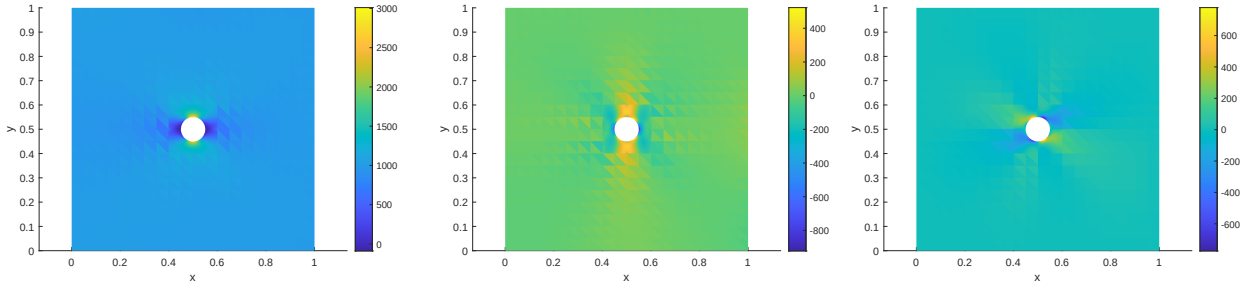

(a) Component $\varpi_{11}$ (b) Component $\varpi_{22}$ (c) Component $\varpi_{12}$

Figure 2.8: Local-global solution - Stress field.

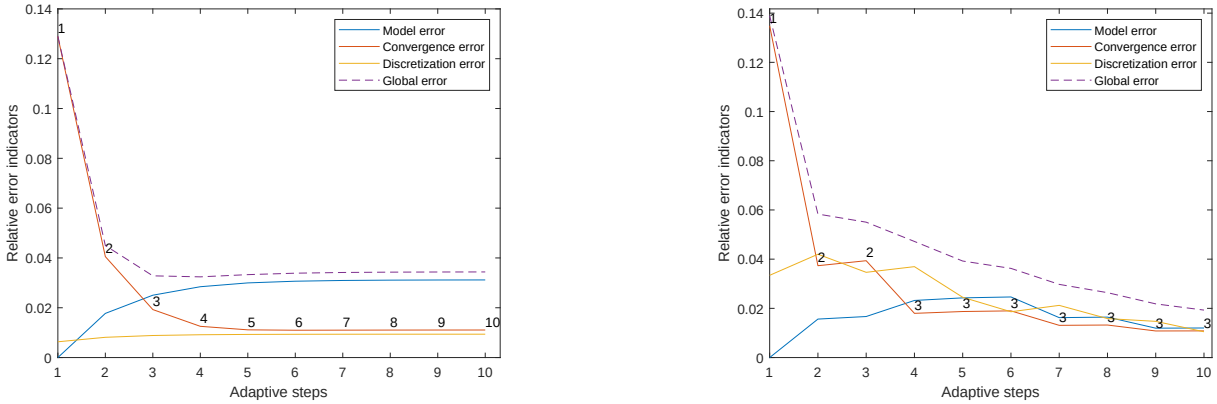


(a) Classical strategy (b) Adaptive strategy

Figure 2.9: Evolution of relative error indicators at each step.

is reached which is better than the classical strategy which reached an error of 3.5 %, while starting with a coarser local domain. The adaptive strategy thus shows better performance to reduce the global error than the classical strategy.

*Remark. For the practical computation of the convergence error* $\eta_{CRE}^{conv} = \|\widehat{\delta\varpi}_G^{H(n)} - (\hat{\varpi}_L^{h(n)} - \hat{\varpi}_L^{h(n-1)})\|_{\mathbf{K}^{-1}|\Omega_L}$ *we here separate it into two contributions:* $\eta_{CRE}^{conv} \leq \|\widehat{\delta\varpi}_G^{H(n)}\|_{\mathbf{K}^{-1}|\Omega_L} + \|(\hat{\varpi}_L^{h(n)} - \hat{\varpi}_L^{h(n-1)})\|_{\mathbf{K}^{-1}|\Omega_L}$ *in order to avoid to project the stress field* $\widehat{\delta\varpi}_G^{H(n)}$ *on the local domain* $\Omega_L$*. Since each contribution converges to 0 when sufficiently iterating, the property of this error indicator is preserved. Figure 2.13 shows the impact of projection of the global stress field on the local domain. The method without projection penalizes the convergence error when the number of iterations is small. The computation of the convergence error is faster without the projection step.*

To compute the error indicators based on the constitutive relation error, we need to recover an admissible stress field for the global domain and the local domain. As explained in Section 2.2, we use a post-processing of the FE solution obtained from the non-intrusive coupling, based on dedicated hybrid-flux technique. Figures 2.14 and 2.15

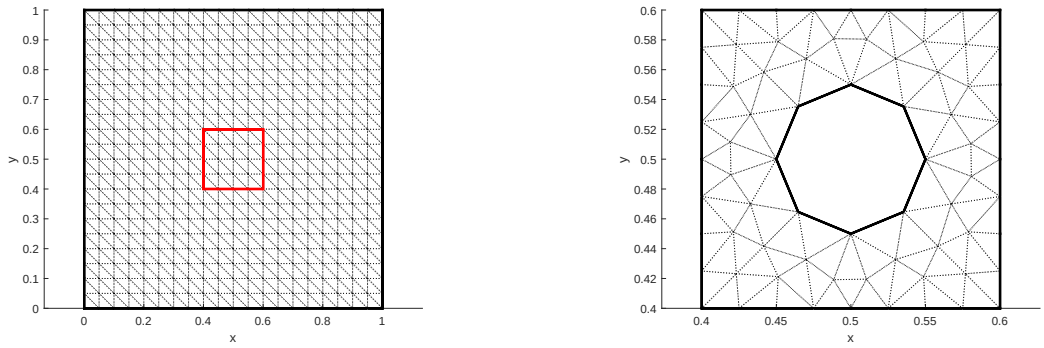


(a) Global mesh (with the coupling interface).

(b) Initial local mesh.

Figure 2.10: Initial coupling configuration and mesh for the adaptive strategy.

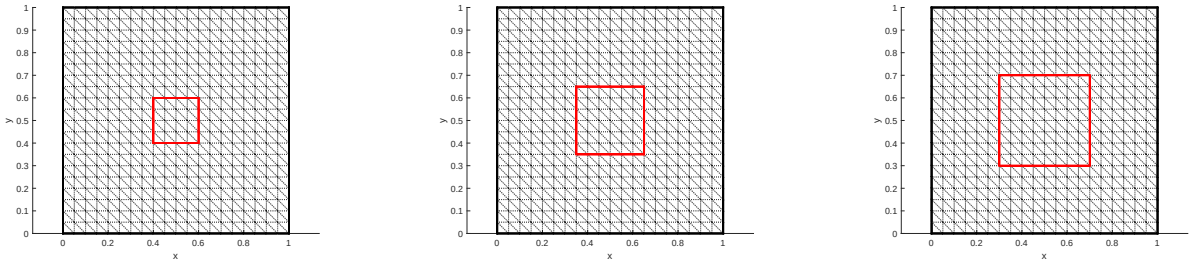


(a) Configuration at step 1

(b) Configuration at step 7

(c) Configuration at step 10

Figure 2.11: Evolution of the coupling configuration for the adaptive strategy.

respectively show the admissible stress field for the global domain and the local domain at the last adaptive step.

From these admissible stress fields, the error indicators can be computed. For the discretization and modeling errors, local error contributions can be evaluated. These allow to choose the optimal enrichment. For the discretization error we could create a map defining the element size such that the local error contribution is homogeneous for discretization error, but for our study we refined homogeneously the local mesh. For the modeling error, in order to reduce it we chose either to add a new patch or to enlarge an already existing patch where the modeling error is the most important. Figure 2.16 shows local error contributions for the discretization and modeling errors at the 5th adaptive step. As we can see the maximal local contribution for the modeling error is located near the local patch, in the vicinity of the interface between the global model and the local model. The maximal local contribution for the discretization error is located near the hole where there is larger stress concentration.

The first case study shows that our methodology is efficient to tackle the problem where we a priori know where the error source is located.

In the second case study (with different boundary conditions), we focus on the flexibility of our methodology. We consider the same initial configuration for the adaptive strategy. The evolution of error indicators is given in Figure 2.17 and the evolution of the configuration is given in Figure 2.18. The final solution is given in Figure 2.19.

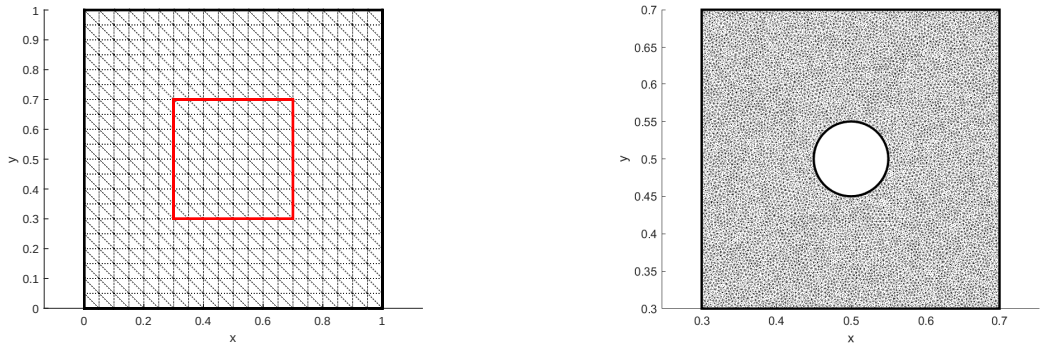


(a) Global mesh (with the coupling interface). (b) Final local mesh.

Figure 2.12: Final coupling configuration and mesh for the adaptive strategy.

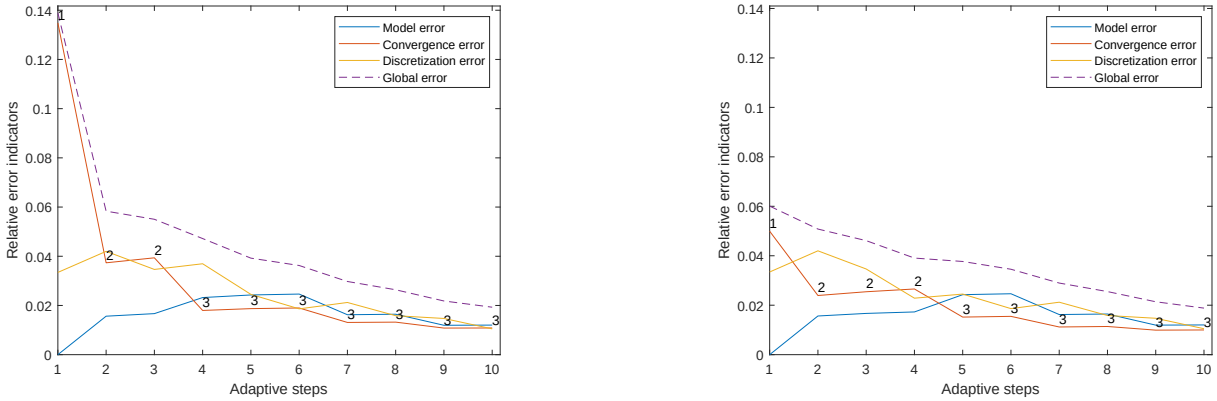


(a) Without projection (b) With projection

Figure 2.13: Evolution of relative error indicators at each step.

As we can see there are two more singularities in the local-global solution in addition to stress concentration near the hole where the initial local patch is located. The two other singularities are placed at the bottom left and top left corners of the plate. There is no local patch in these regions initially.

We observe in Figure 2.20 that the local contribution for the modeling error is maximal in these corners.

In order to reduce the modeling error, our adaptive strategy starts by adding a patch where the global model is too coarse to describe the problem. Indeed, the singularity could not be captured by the global coarse mesh. Modeling error contribution can be associated with a discretization error with the global mesh. After those patches are added, they can be enlarged in order to reduce the overall modeling error.

Furthermore, we can see in Figure 2.17 that enlarging the local domain could reduce the convergence error. Indeed, the convergence rate of the algorithm which is tied to the convergence error is linked to the complexity of the correction term computed from the flux unbalanced at the coupling interface. If the singularity is close to the coupling interface (Saint-Venant's Principle) or the shape of the coupling interface is too complex, then the correction

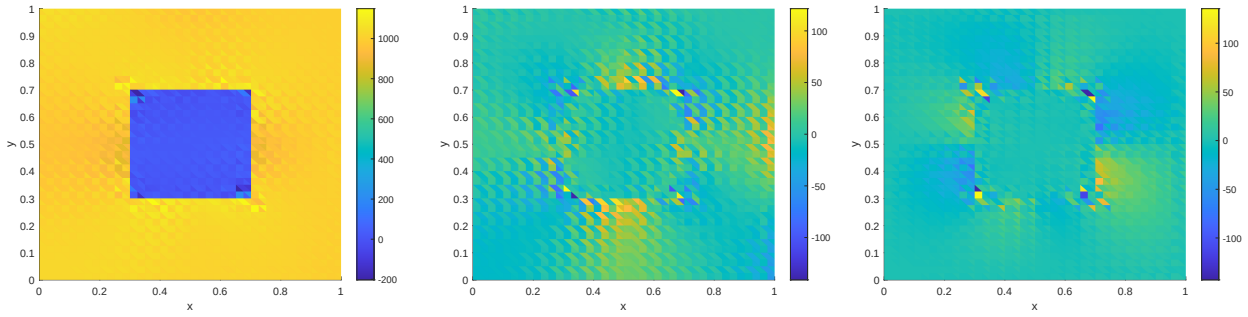


(a) Component $\sigma_{11}$ (b) Component $\sigma_{22}$ (c) Component $\sigma_{12}$

Figure 2.14: Global admissible stress field.

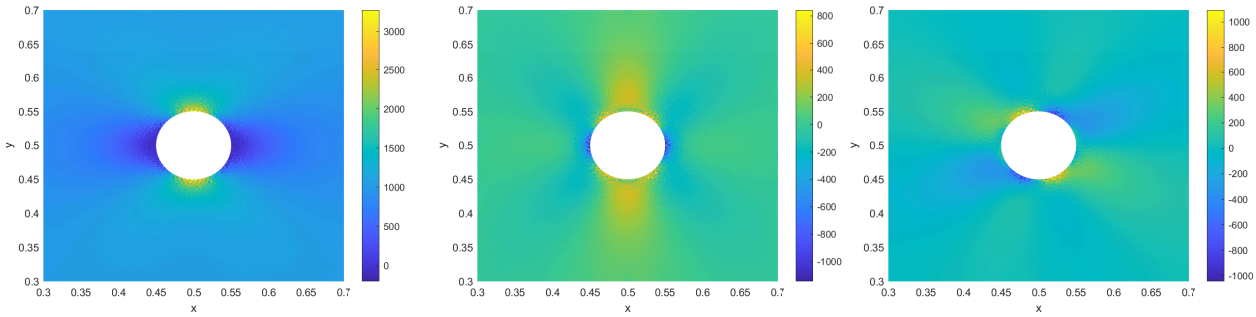


(a) Component $\sigma_{11}$ (b) Component $\sigma_{22}$ (c) Component $\sigma_{12}$

Figure 2.15: Local admissible stress field.

term is complex too, and needs more iterations or a finer description of the interface in order to describe it. Since it is not possible to refine the mesh in the global domain $\Omega_0$ (and particularly along its trace on the coupling interface), the solution is to enlarge the local domain into a smooth shape. The complexity and value of the correction term impact both the modeling error (in the vicinity of the coupling interface) and the convergence error and can suggest to enlarge the local domain. The modeling error is also impacted by the mesh size on the complementary domain, thus we can detect where the model is too coarse, and add a new local patch where the modeling error is the largest.

This study thus shows the flexibility of the proposed method as we were able to select the optimal definition of the local domain where the global description was not satisfying.

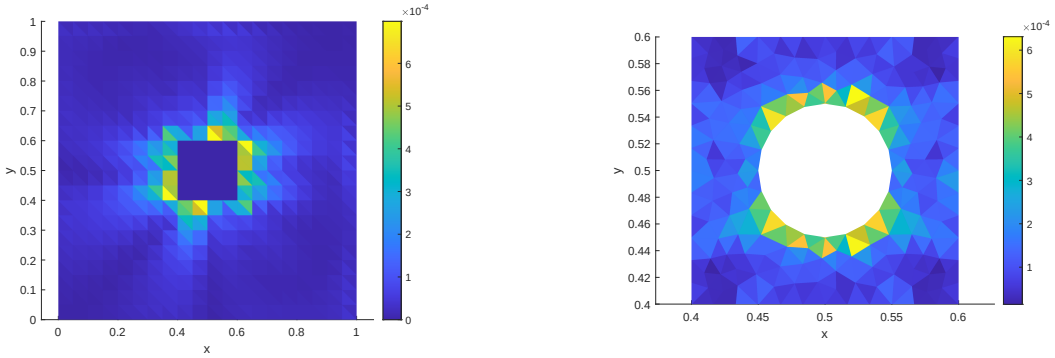


(a) Local modeling error contribution

(b) Local discretiation error contribution

Figure 2.16: Local error contributions.

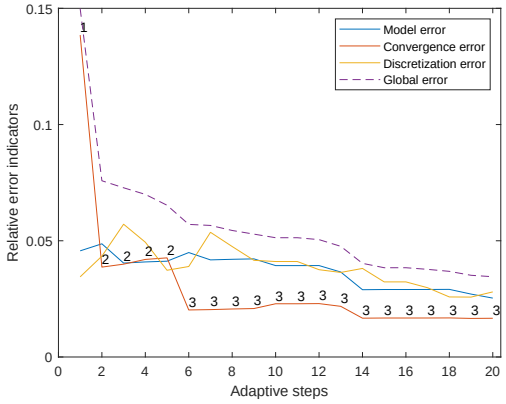


Figure 2.17: Evolution of relative error indicators at each step.

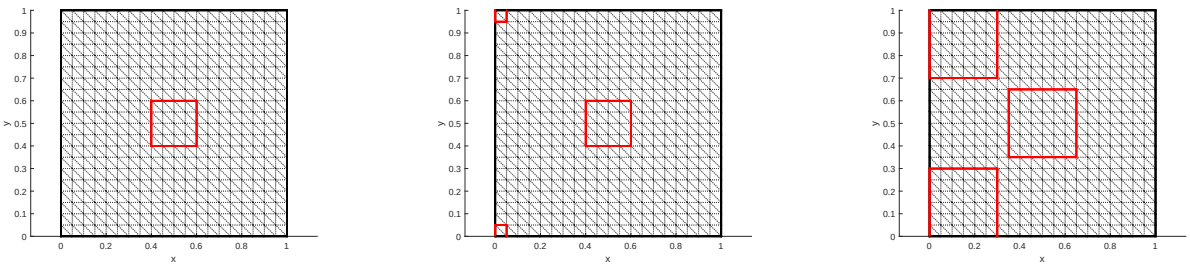

(a) Configuration at step 1

(b) Configuration at step 8

(c) Configuration at step 20

Figure 2.18: Evolution of the coupling configuration for the adaptive strategy.

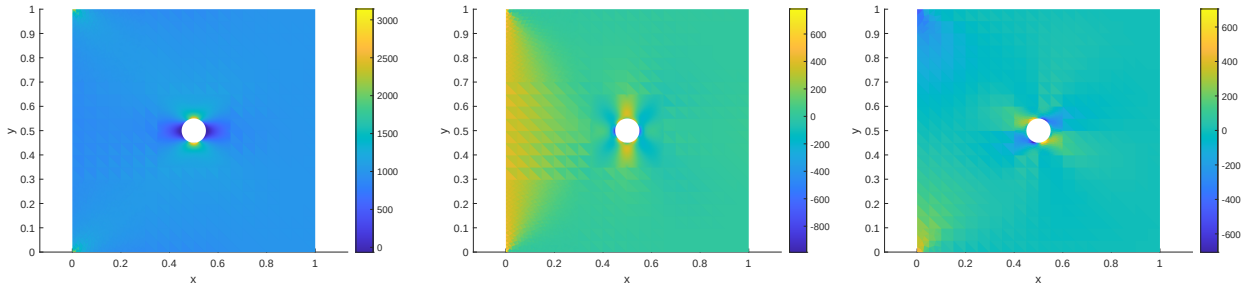

(a) Component $\varpi_{11}$ (b) Component $\varpi_{22}$ (c) Component $\varpi_{12}$

Figure 2.19: Local-global solution - Stress field (case study 2).

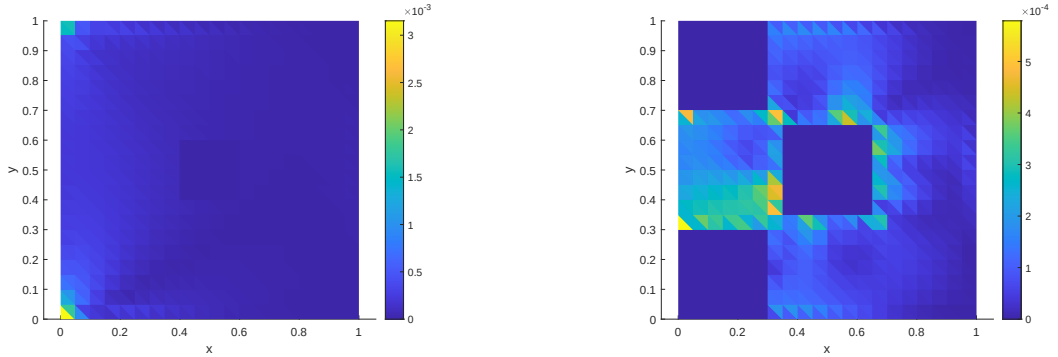

(a) Local modeling error contribution - step 1 (b) Local modeling error contribution - step 20

Figure 2.20: Local error contributions at different steps.

### 2.4.2 Elasticity problem on a L-shaped structure

We now show performance of the approach on a L-shape domain. Linear/linear coupling is performed in which the local model, defined in the vicinity of the singularity, has a refined mesh. The initial configuration and mesh are shown in Figure 2.21. As in the previous example the global domain is meshed using a structured mesh made of T3 triangular elements. The local domain is meshed using T3 triangular elements.

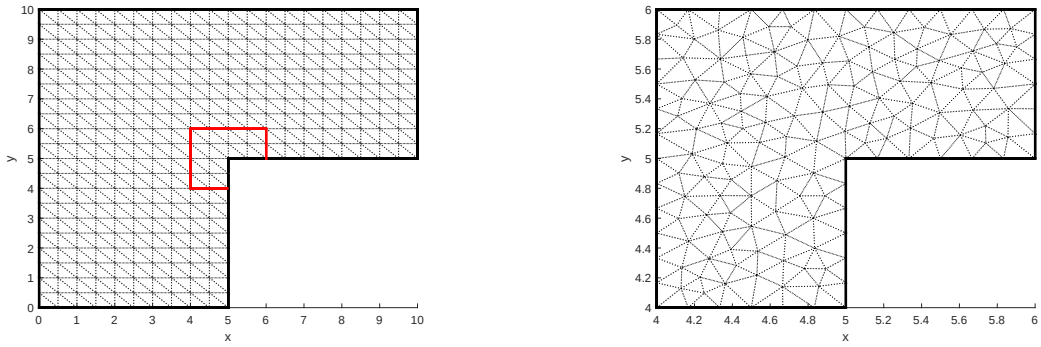


(a) Global mesh (with the coupling interface). (b) Initial local mesh.

Figure 2.21: Initial coupling configuration and mesh.

We consider an homogeneous, isotropic and linear elastic material on the local and global domains (Young's modulus $E = 1Mpa$ and Poisson's coefficient $\nu = 0.3$).

We restrain the translation along both axes on the bottom edge and we apply a uniform traction force along the $y$ direction on the far right side. The solution obtained at the last adaptive step is shown in Figure 2.22.

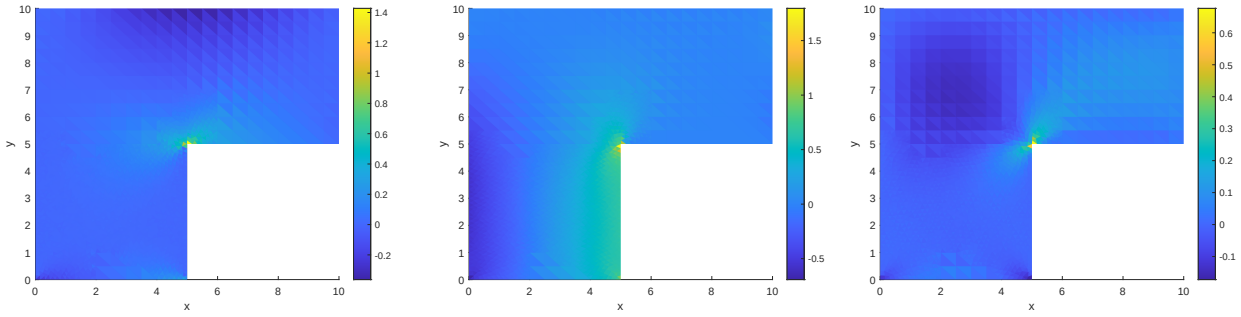


(a) Component $\sigma_{11}$ (b) Component $\sigma_{22}$ (c) Component $\sigma_{12}$

Figure 2.22: Local-global solution - Stress field.

We can see that the solution presents one major singularity in the central corner and two smaller singularities in the bottom corners connected to the Dirichlet boundary condition.

Let us study the performance of our adaptive strategy on this case study. Figure 2.23 shows the evolution of the error indicators at each adaptive step.

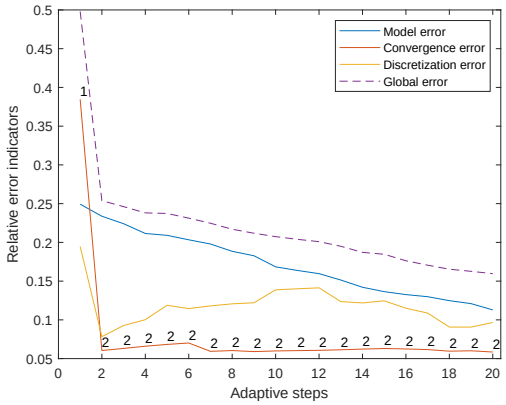


Figure 2.23: Evolution of relative error indicators at each step.

As we can see the major source of error is the modeling error from the second adaptive step until the last step. It is the predominant error after the initial convergence error is reduced drastically by adding one iteration. Figure 2.24 shows the evolution of the local domain at different adaptive steps.

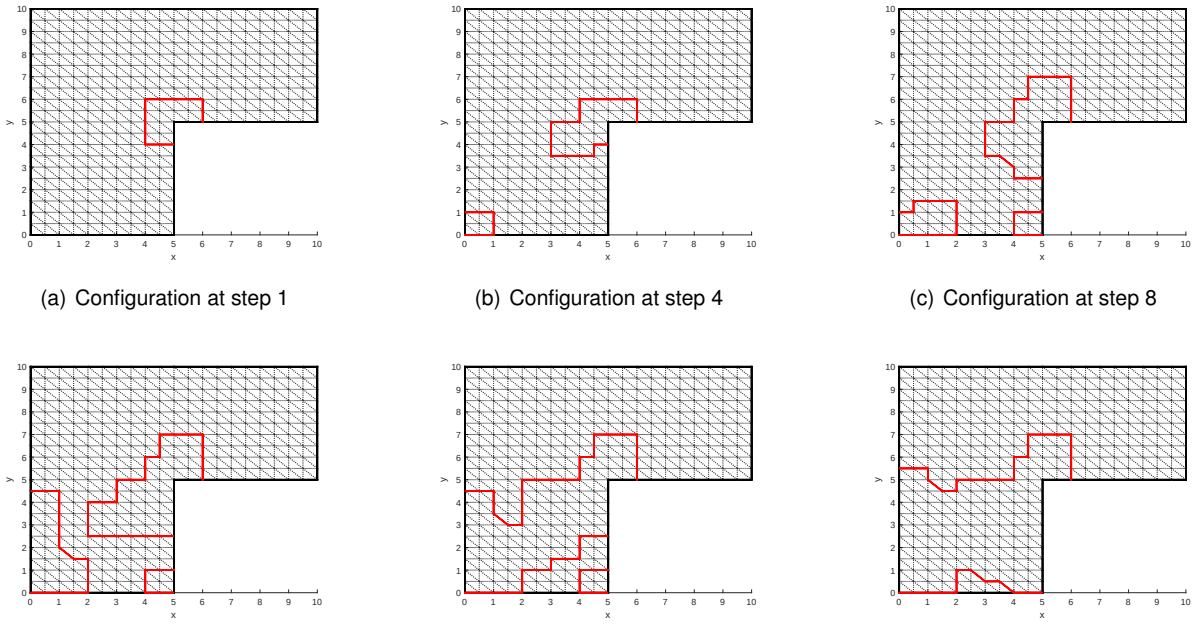

(a) Configuration at step 1 (b) Configuration at step 4 (c) Configuration at step 8

(d) Configuration at step 12 (e) Configuration at step 16 (f) Configuration at step 20

Figure 2.24: Evolution of the coupling configuration for the adaptive strategy.

The initial local patch is placed near the central singularity and is later growing in order to reduce the modeling error. Our strategy is then able to create multiple local patches and to merge them when they are colliding. Figure 2.25 shows the modeling error distribution along the iterations.

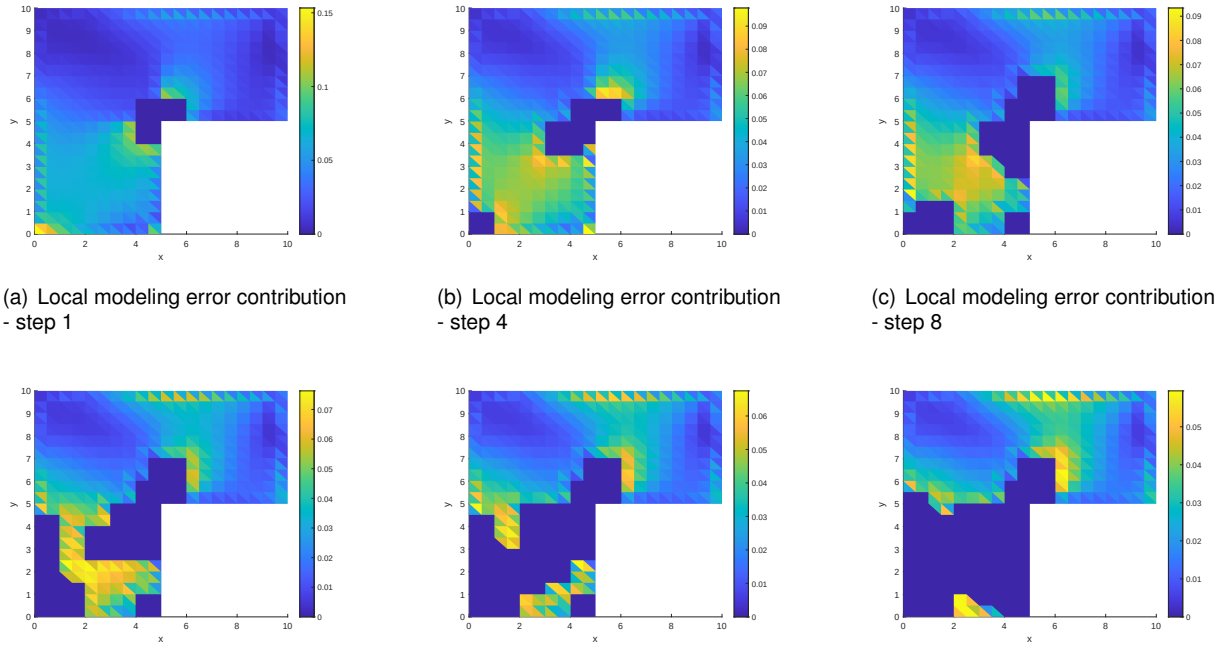

(a) Local modeling error contribution - step 1

(b) Local modeling error contribution - step 4

(c) Local modeling error contribution - step 8

(d) Local modeling error contribution - step 12

(e) Local modeling error contribution - step 16

(f) Local modeling error contribution - step 20

Figure 2.25: Local error contributions at different steps.

### 2.4.3 Coupling with a nonlinear local model

We reuse the L-shaped geometry, but we now consider that the high-fidelity model is a nonlinear elasto-plasticity model. It is conserved in the local region of interest where high gradients are located, while it is replaced with a linear elasticity model in the remainder of the structure.

#### Thermodynamical framework

In the context of a high-fidelity nonlinear elasto-plastic model, and using the thermodynamical framework with standard formulation, we introduce the Helmholtz free energy potential $\psi$:

$$\psi := \psi(T, \mathfrak{e}, \mathfrak{e}_p, \mathbf{X}) = \psi(T, \mathfrak{e}_e, \mathbf{X}) \tag{2.32}$$

that depends on state variables, i.e. observable variables (temperature $T$ and strain tensor $\mathfrak{e}$) and internal variables: (i) the inelastic part $\mathfrak{e}_p$ of the strain tensor, such that $\mathfrak{e} = \mathfrak{e}_e + \mathfrak{e}_p$ ($\mathfrak{e}_e$ being the elastic strain); (ii) additional internal variables $X_i$ (gathered in a vector $\mathbf{X}$) describing additional phenomena such as hardening. The potential $\psi$ is assumed to be convex (and concave with respect to $T$ in a more general case) in order to get a sufficient condition to satisfy stability conditions. Introducing thermodynamical forces $Y_i$ (gathered in a vector $\mathbf{Y}$) associated with internal

variables $X_i$ in a duality pairing, the state equations of the material behavior read:

$$\varpi = \partial_{\mathfrak{e}_e} \rho\psi \quad ; \quad Y_i = \partial_{V_i} \psi \tag{2.33}$$

Defining the dual free energy potential, denoted $\psi^\star$, as the Legendre-Fenchel transform of $\psi$:

$$\psi^\star\left(T, \varpi, \mathbf{Y}\right) = \sup_{\mathfrak{e}_e, \mathbf{X}} \left(\varpi : \mathfrak{e}_e + \mathbf{Y} \cdot \mathbf{X} - \psi(T, \mathfrak{e}_e, \mathbf{X})\right) \tag{2.34}$$

we naturally get $\psi\left(T, \mathfrak{e}_e, \mathbf{X}\right) + \psi^\star\left(T, \varpi, \mathbf{Y}\right) - \varpi : \mathfrak{e}_e - \mathbf{Y} \cdot \mathbf{X} \geq 0$. It can also be shown, using convex analysis [Moreau, 1966], that state equations can be equivalently recast as:

$$\psi\left(T, \mathfrak{e}_e, \mathbf{X}\right) + \psi^\star\left(T, \varpi, \mathbf{Y}\right) - \varpi : \mathfrak{e}_e - \mathbf{Y} \cdot \mathbf{X} = 0 \tag{2.35}$$

*Remark. The free energy $\psi$ is usually written as the sum of an elastic contribution $\psi_e$ and a plastic contribution $\psi_p$:*

$$\psi(\mathfrak{e}_e, \mathbf{X}) = \psi_e(\mathfrak{e}_e) + \psi_p(\mathbf{X}) \tag{2.36}$$

*Also, it is shown in [Ladevèze, 1999] that for a large class of material behaviors, sets $\mathbf{X}$ and $\mathbf{Y}$ can be defined (using a change of variables if required) such that state equations are linear i.e. the free energy is quadratic (normal formulation).*

The intrinsic dissipation involved in the Clausius-Duhem inequality (merging first and second principles) can thus be recast in the following condensed format:

$$\varpi : \dot{\mathfrak{e}}_p - \mathbf{Y} \cdot \dot{\mathbf{X}} \geq 0 \tag{2.37}$$

This inequality imposes a consistency condition on the pair of variables $((\mathfrak{e}_p, \mathbf{X}), (\varpi, \mathbf{Y}))$ in order to ensure that intrinsic dissipation (reflecting dissipative evolution phenomena associated with the nonlinear material behavior) remains positive. To satisfy the previous condition, it is usual and convenient to introduce a dissipation pseudo-potential, denoted $\varphi(\dot{\mathfrak{e}}_p, -\dot{\mathbf{X}})$, as well as its dual potential (defined using the Legendre-Fenchel transform):

$$\varphi^\star(\varpi, \mathbf{Y}) = \sup_{\dot{\mathfrak{e}}_p, \dot{\mathbf{X}}} \left(\varpi : \dot{\mathfrak{e}}_p - \mathbf{Y} \cdot \dot{\mathbf{X}} - \varphi(\dot{\mathfrak{e}}_p, -\dot{\mathbf{X}})\right) \tag{2.38}$$

Then, evolution laws are defined from the gradients of potential $\varphi$ (or $\varphi^\star$), involving a nonlinear operator $\mathcal{B}$:

$$\begin{bmatrix} -\dot{\mathbf{X}} \\ \dot{\mathfrak{e}}_p \end{bmatrix} = \mathcal{B}\left(\begin{bmatrix} \mathbf{Y} \\ \varpi \end{bmatrix}\right) = \partial_{(\varpi, \mathbf{Y})} \varphi^\star(\varpi, \mathbf{Y}) \tag{2.39}$$

so that the inequality (2.37), which reads:

$$\begin{bmatrix} \mathbf{Y} \\ \varpi \end{bmatrix} \cdot \mathcal{B}\left( \begin{bmatrix} \mathbf{Y} \\ \varpi \end{bmatrix} \right) \geq 0 \tag{2.40}$$

comes down to positive (but possibly multivalued) properties of the operator $\mathcal{B}$ and is naturally satisfied when dissipation pseudo-potentials are chosen convex, with $\varphi(\mathbf{0},\mathbf{0}) = \varphi^*(\mathbf{0},\mathbf{0}) = 0$.

*Remark. As $\varphi^*$ may be not differentiable at some points (usual case in elasto-plasticity), evolution laws should more generally be written $\dot{\mathbf{e}}_p \in \partial_{\mathbf{s}}\varphi^*$ where $\partial_{\mathbf{s}}\varphi^*$ denotes the sub-differential of $\varphi^*$, defined as:*

$$\partial_{\mathbf{s}}\varphi^* = \{\dot{\mathbf{e}}_p \text{ such that } \varphi^*(\overline{\mathbf{s}}) - \varphi^*(\mathbf{s}) \geq \dot{\mathbf{e}}_p \cdot (\overline{\mathbf{s}} - \mathbf{s}) \quad \forall \overline{\mathbf{s}}\} \tag{2.41}$$

*Introducing the convex yield function $f(\mathbf{s}) \leq 0$ associated with the indicatrix function $\varphi^*$ (that is $\varphi^* = 0$ if $f < 0$ and $\varphi^* = +\infty$ if $f = 0$), one gets:*

$$\dot{\mathbf{e}}_p = \dot{\lambda}\frac{\partial f}{\partial \mathbf{s}} \quad \text{with } \dot{\lambda} \geq 0 \text{ and } \dot{\lambda} f = 0 \text{ (consistency condition)} \tag{2.42}$$

*This defines associated models as surface $f$ (defining the elasticity domain) also corresponds to the flow potential. It is equivalent to the Hill principle of maximal work indicating that the rate $\dot{\mathbf{e}}_p$ maximizes the intrinsic dissipation $\Phi_1 = \mathbf{s} \cdot \dot{\mathbf{e}}_p$; in this case, $\dot{\lambda}$ corresponds to a multiplier in Kuhn-Tucker conditions with constraint $f \leq 0$.*

**Definition of the CRE functional**

Then, as mentioned in Section 2.1.3, a general CRE measure can be derived from the previous thermodynamical formulation of nonlinear behaviors, based on Legendre-Fenchel residuals $\eta_\psi$ and $\eta_\varphi$ on state equations and evolution laws, respectively [Ladevèze, 1998, Ladevèze et al., 1999, Ladevèze, 2001, Ladevèze and Pelle, 2005]. These read:

$$\begin{aligned} \eta_\psi(\mathbb{e}_e, \mathbf{V}, \varpi, \mathbf{Y}) &= \psi(\mathbb{e}_e, \mathbf{V}) + \psi^\star(\varpi, \mathbf{Y}) - \langle (\varpi, \mathbf{Y}) \, , \, (\mathbb{e}_e, \mathbf{V}) \rangle \geq 0 \\ \eta_\varphi(\dot{\mathbb{e}}_p, -\dot{\mathbf{V}}, \varpi, \mathbf{Y}) &= \varphi(\dot{\mathbb{e}}_p, -\dot{\mathbf{V}}) + \varphi^\star(\varpi, \mathbf{Y}) - \left\langle (\varpi, \mathbf{Y}) \, , \, (\dot{\mathbb{e}}_p, -\dot{\mathbf{V}}) \right\rangle \geq 0 \end{aligned} \tag{2.43}$$

and vanish when corresponding constitutive equations are satisfied. Denoting $\hat{\mathbf{\Sigma}} = (\hat{\mathbb{e}}_e, \hat{\mathbb{e}}_p, \hat{\mathbf{X}}, \hat{\varpi}, \hat{\mathbf{Y}})$ the whole set of (admissible) variables, the local in space and time CRE measure $e_{CRE}$ is eventually defined as:

$$e^2_{CRE}(\hat{\mathbf{\Sigma}}) = \eta_\psi\left(\hat{\mathbf{\Sigma}}\right) + \int_0^t \eta_\varphi\left(\hat{\mathbf{\Sigma}}\right) \mathrm{d}t \quad \forall \mathbf{x} \in \Omega, \forall t \in I_t \tag{2.44}$$

A global measure $\mathcal{E}^2_{CRE} = \int_\Omega \int_{I_t} e^2_{CRE}$ is then obtained by integration over the space-time domain.

**Considered material behavior**

For the numerical application of this section, we consider a Prandtl-Reuss plastic model with linear isotropic hardening, for which $\mathbf{e}_e = [\mathfrak{e}_e, p]^T$, $\mathbf{e}_p = [\mathfrak{e}_p, -p]^T$, and $\mathbf{s} = [\mathfrak{s}, R]^T$, with $p = \int_0^t \|\dot{\mathfrak{e}}_p\| dt$ the cumulative inelastic strain ($\| \bullet \| = (\bullet : \bullet)^{1/2}$) and $R$ the associated thermodynamic force (isotropic hardening variable on additional yield stress). The associated free energy potential reads:

$$\psi(\mathfrak{e}_e, p) = \frac{1}{2}\mathbf{K}\mathfrak{e}_e : \mathfrak{e}_e + g(p) \tag{2.45}$$

with $g(p) = \frac{1}{2}kp^2$ a function that characterizes the linear hardening law ($k$ is a strictly positive material parameter). We thus obtain the following state laws:

$$\mathfrak{s} = \frac{\partial \psi}{\partial \mathfrak{e}_e} = \mathbf{K}\mathfrak{e}_e \quad ; \quad R = \frac{\partial \psi}{\partial p} = g'(p) \tag{2.46}$$

and the dual potential reads:

$$\psi^*(\mathfrak{s}, R) = \frac{1}{2}\mathbf{K}^{-1}\mathfrak{s} : \mathfrak{s} + g^*(R) \tag{2.47}$$

with $g^*$ the Legendre-Fenchel transform of function $g$.

The dissipation potential $\varphi^*(\mathfrak{s}, R)$ is the indicator function of the elasticity domain $C_f = \{(\mathfrak{s}, R), z(\mathfrak{s}, R) \leq 0, R \geq 0\}$, that is:

$$\varphi^*(\mathfrak{s}, R) = \chi_{C_f}(\mathfrak{s}, R) = \begin{cases} 0 & \text{if } (\mathfrak{s}, R) \in C \\ +\infty & \text{if } (\mathfrak{s}, R) \notin C \end{cases} \tag{2.48}$$

with $z = \|\mathfrak{s}^D\| - (R + R_0)$ for linear hardening, $\mathfrak{s}^D$ the deviatoric part of the stress tensor, and $R_0 \geq 0$ the yield stress. Introducing the convex set $C_e = \{(\dot{\mathfrak{e}}_p, -\dot{p}), \|\dot{\mathfrak{e}}_p\| - \dot{p} \leq 0, \mathrm{Tr}[\dot{\mathfrak{e}}_p] = 0\}$ with associated indicator function $\chi_{C_e}$, the dual dissipation potential reads (for linear hardening):

$$\varphi(\dot{\mathfrak{e}}_p, -\dot{p}) = R_0\|\dot{\mathfrak{e}}_p\| + \chi_{C_e}(\dot{\mathfrak{e}}_p, -\dot{p}) \tag{2.49}$$

**Numerical analysis**

When solving the local problem (with given external loads and under prescribed interface displacements) at a given iteration $n$ of the coupling algorithm, a classical nonlinear iterative solver is used. Reaction forces $\boldsymbol{\lambda}^{(n)}$ are then deduced and used to solve the global problem at the next iteration $n + 1$.

We recover an admissible solution $\hat{\boldsymbol{\Sigma}}$ by using the hybrid-flux technique at each time increment, before interpolating linearly between increments.

The error estimator is then defined as $\mathcal{E}_{CRE}(\hat{\boldsymbol{\Sigma}}) = \sqrt{\int_\Omega \int_{I_t} e^2_{CRE}(\hat{\boldsymbol{\Sigma}})}$, where $e^2_{CRE}$ is given in (2.44).

In a similar way as in the linear case, using a consistent splitting, error indicators are next defined as:

$$\eta_{CRE}^{conv} = \sqrt{\int_{\Omega_L}\int_{I_t} (\widehat{\delta\mathfrak{v}}_G^{H(n)} - (\hat{\mathfrak{v}}_L^{h(n)} - \hat{\mathfrak{v}}_L^{h(n-1)})) : \mathbf{K}^{-1}(\widehat{\delta\mathfrak{v}}_G^{H(n)} - (\hat{\mathfrak{v}}_L^{h(n)} - \hat{\mathfrak{v}}_L^{h(n-1)})) + \frac{1}{k}((\hat{R}_L^{h(n)} - \hat{R}_L^{h(n-1)}))^2}$$
$$\eta_{CRE}^{dis} = \sqrt{\int_{\Omega_L}\int_{I_t} e_{CRE}^2(\hat{\boldsymbol{\Sigma}}_L^{h(n)})} \tag{2.50}$$
$$\eta_{CRE}^{mod} = \sqrt{\int_{\Omega_0}\int_{I_t} e_{CRE}^2(\hat{\boldsymbol{\Sigma}}_G^{H(n)})}$$

*Remark. The control of the sub-iterations for solving the nonlinear local problem could also be performed by defining a specific indicator based on a suitable definition of admissible fields. For instance, only one sub-iteration is performed in [Blanchard et al., 2019] between two consecutive global iterations of the coupling algorithm. Here, this is not investigated, and we assume that convergence is reached when solving the local problem.*

### Results

We now show performance of the approach on the previous L-shape domain. Linear/nonlinear coupling is performed in which the local model, defined in the vicinity of the singularity, has a refined mesh. The initial configuration and mesh are shown in Figure 2.26. As in the previous example the global domain is meshed using a structured mesh made of T3 triangular elements. The local domain is meshed using smaller T3 triangular elements.

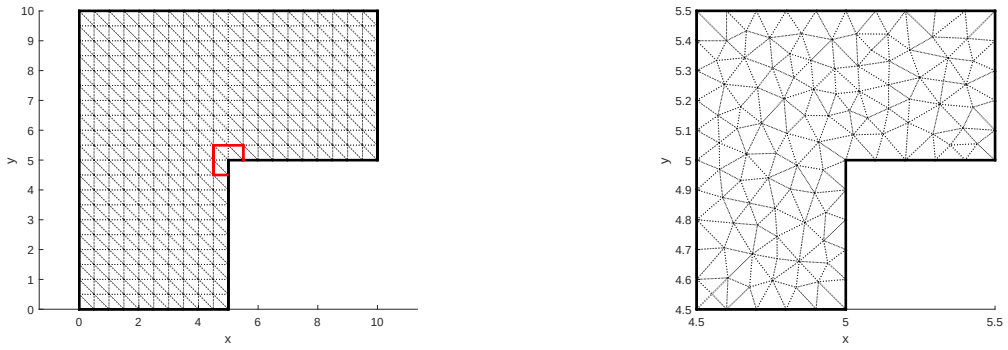


(a) Global mesh (with the coupling interface). (b) Initial local mesh.

Figure 2.26: Initial coupling configuration and mesh.

We consider an homogeneous, Prandtl-Reuss plastic model with linear isotropic hardening on the local domain and an homogeneous, isotropic and linear elastic model in the global domain (Young's modulus $E = 1Mpa$, Poisson's coefficient $\nu = 0.3$, Hardening coefficient $H = 0.05 * E$ and elastic limit $R_0 = 0.88Mpa$ ). In this study we assume a two dimensional model with plane strain.

The loading case is the same as defined in Figure 2.22 with a uniform traction force along the $y$ direction on the far right side with a constant value of $f = 1.1E^6 N/m$.

We have computed a reference solution considering a nonlinear model on the whole domain and with a very fine mesh. In further results, the accumulated plasticity will be the focus. The reference solution with the stress field is given in Figure 2.27.

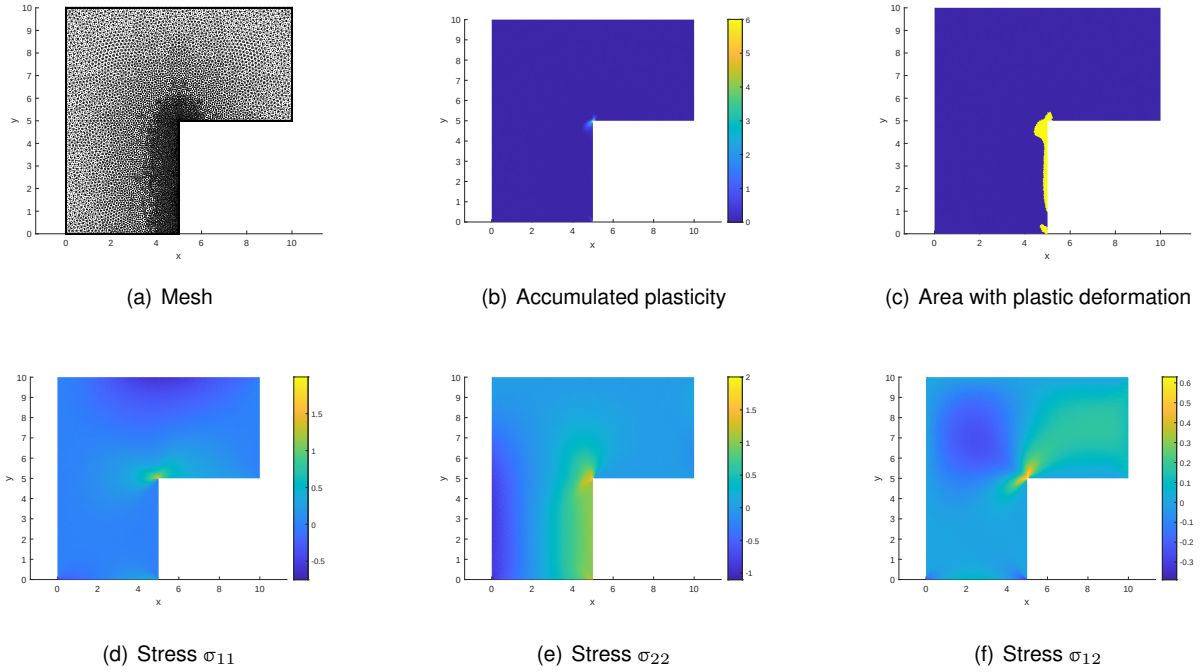

(a) Mesh (b) Accumulated plasticity (c) Area with plastic deformation

(d) Stress $\sigma_{11}$ (e) Stress $\sigma_{22}$ (f) Stress $\sigma_{12}$

Figure 2.27: Reference solution with Prandlt-Reuss elasto-plastic model.

As we can see the initial configuration of the local and global domain does not contain all the area with plastic deformation and we have only one iteration for the non-intrusive local-global coupling algorithm. We obtain the following result shown in Figure 2.28.

The error indicators presented in this chapter are able to evaluate the contribution of the size of the local domain, the discretization of the local domain and the number of local-global iterations in regards to the global error with nonlinear behavior, and can be used to drive the algorithm optimally. In our case the convergence error is the most important initially, then the model error is the second most important. Figure 2.29 shows the evolution of error indicators at each step of the adaptation algorithm.

Notice that the last step was not driven by the adaptive algorithm but instead we added more iterations for the non-intrusive coupling method in order to check the decrease of the indicator on iterations.

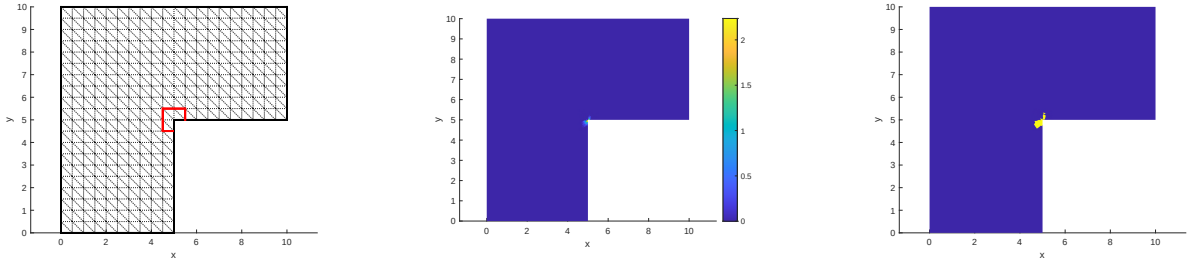

(a) Mesh (b) Accumulated plasticity (c) Area with plastic deformation

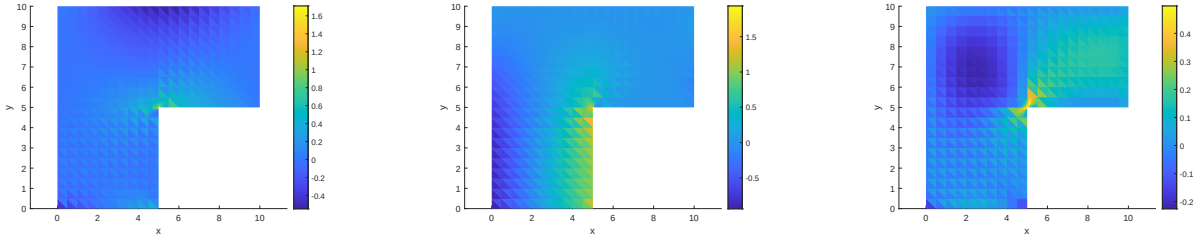

(d) Stress $\sigma_{11}$ (e) Stress $\sigma_{22}$ (f) Stress $\sigma_{12}$

Figure 2.28: Initial solution with Prandlt-Reuss elasto-plastic model with non-intrusive local-global coupling method.

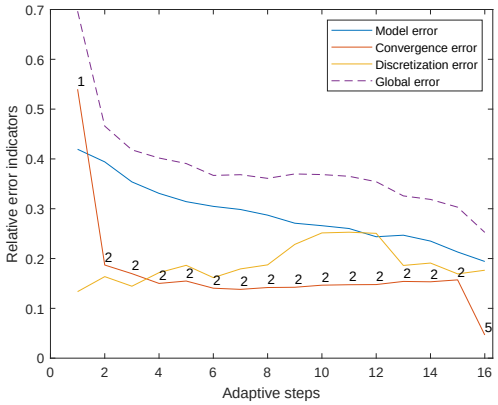


Figure 2.29: Evolution of relative error indicators at each step.

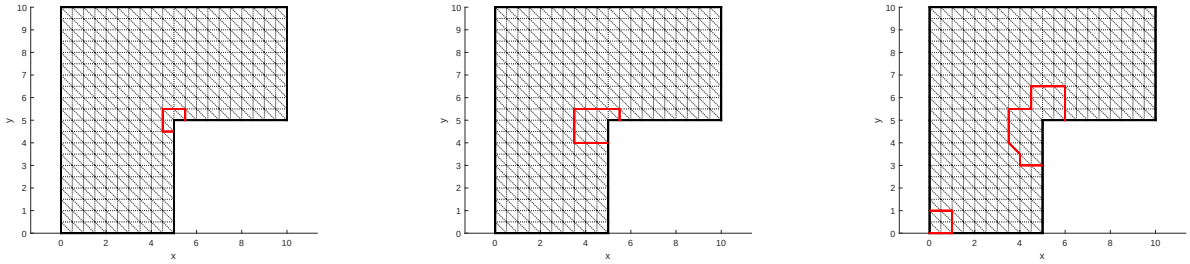

(a) Configuration at step 1 (b) Configuration at step 3 (c) Configuration at step 6

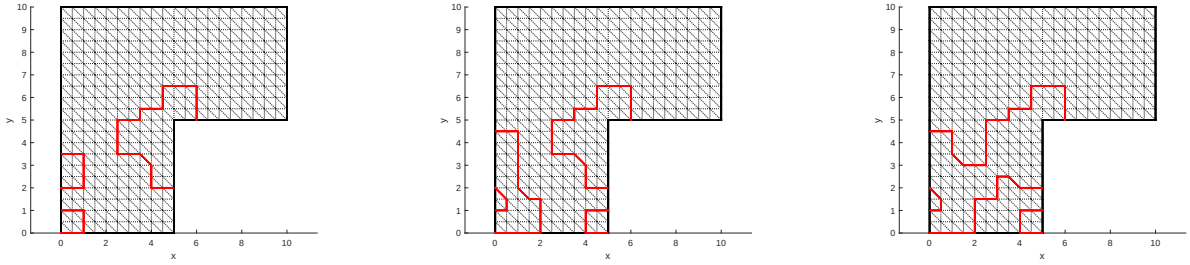

(d) Configuration at step 9 (e) Configuration at step 12 (f) Configuration at step 15

Figure 2.30: Evolution of the coupling configuration for the adaptive strategy.

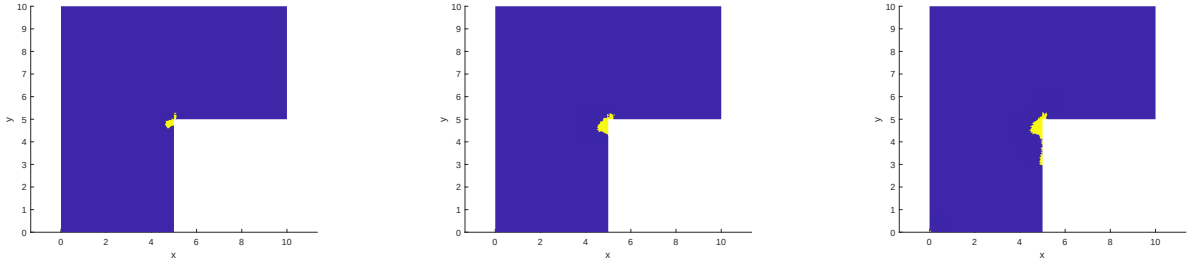

(a) Step 1 (b) Step 3 (c) Step 6

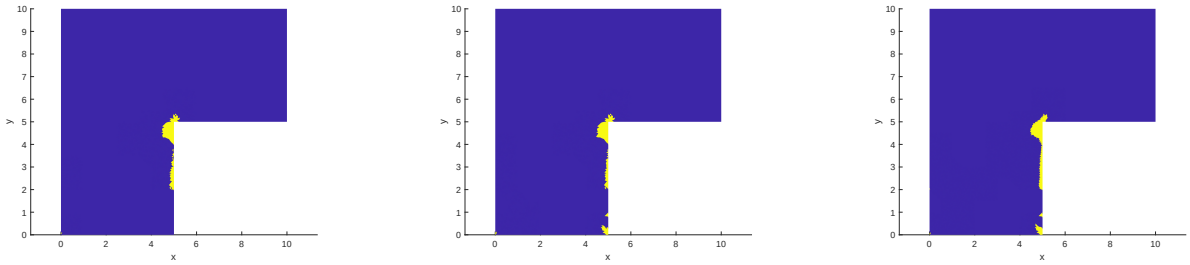

(d) Step 9 (e) Step 12 (f) Step 15

Figure 2.31: Evolution of the area with plastic deformation for the adaptive strategy.

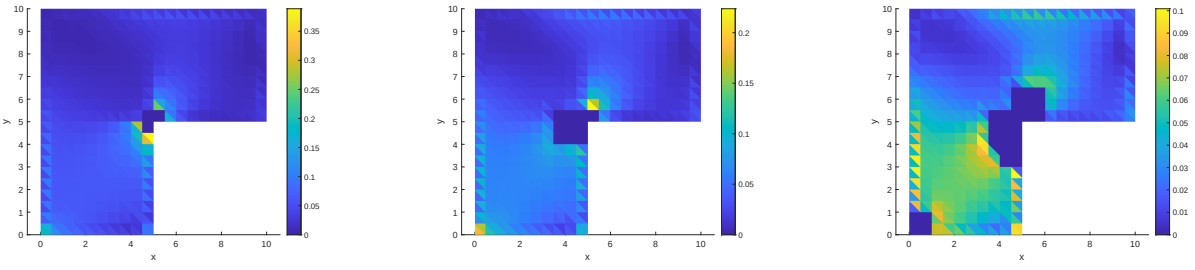

(a) Step 1 (b) Step 3 (c) Step 6

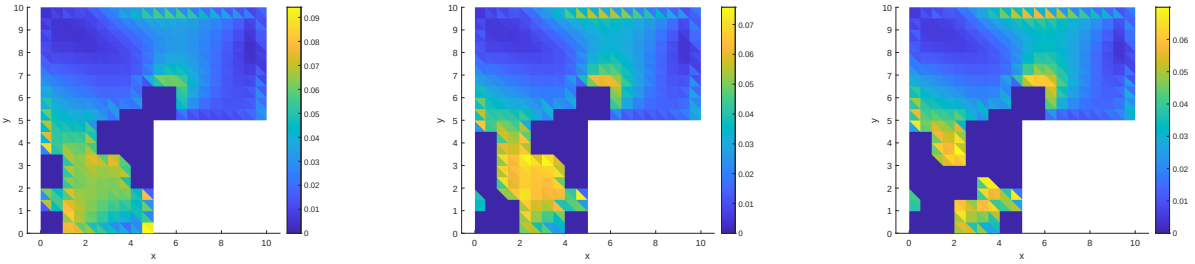

(d) Step 9 (e) Step 12 (f) Step 15

Figure 2.32: Evolution of the modeling error spatial distribution for the adaptive strategy.

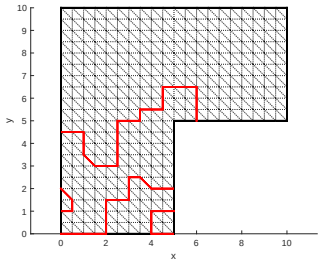

(a) Mesh

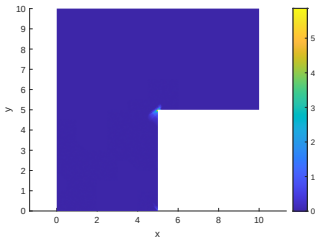

(b) Accumulated plasticity

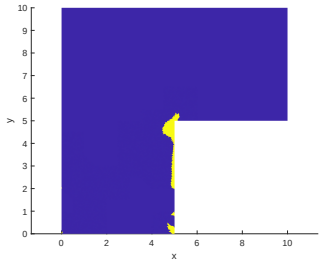

(c) Area with plastic deformation

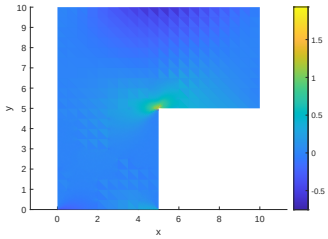

(d) Stress $\sigma_{11}$ (global local solution)

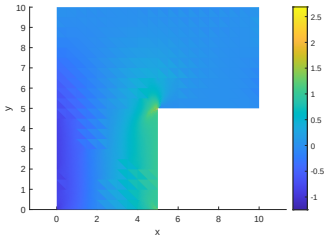

(e) Stress $\sigma_{22}$ (global local solution)

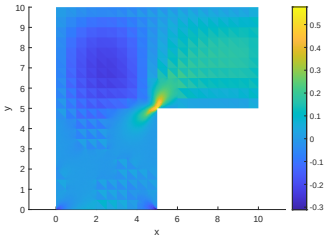

(f) Stress $\sigma_{12}$ (global local solution)

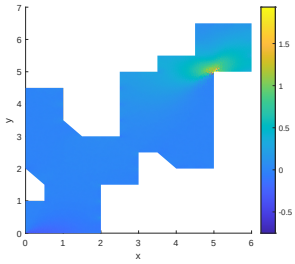

(g) Stress $\sigma_{11}$ (local solution)

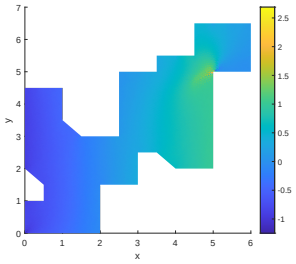

(h) Stress $\sigma_{22}$ (local solution)

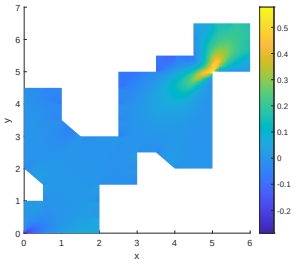

(i) Stress $\sigma_{12}$ (local solution)

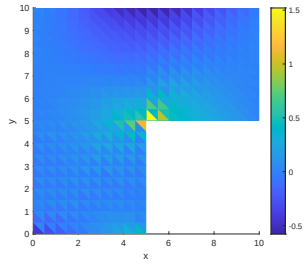

(j) Stress $\sigma_{11}$ (global solution)

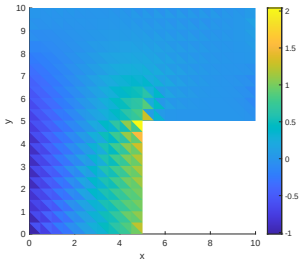

(k) Stress $\sigma_{22}$ (global solution)

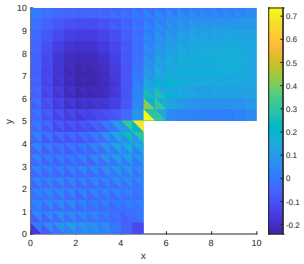

(l) Stress $\sigma_{12}$ (global solution)

Figure 2.33: Final solution with Prandlt-Reuss elasto-plastic model with non-intrusive local-global coupling method.

The final solution is shown in Figure 2.33 and the evolution of the local domain and area with plastic deformation are shown in Figures 2.30 and 2.31. The adaptive algorithm first adds one iteration to the non-intrusive local-global coupling then enlarges the local domain in the vicinity of the singularity where the plasticity is the largest. The evolution of the final modeling error spatial distribution is shown in Figure 2.32. We can notice that the local domain does not contain all the area with plastic deformation computed in the reference. Indeed the contribution to the modeling error when not considering the plasticity in those remaining area is lower than the discretization error in other regions, the accumulated plasticity would have been small and had a low impact on the overall solution.

## 2.5 Partial conclusions

In this chapter, we designed a new verification tool, based on the CRE concept and providing robust and fully computable error estimator and indicators, in order to control the accuracy of local-global coupling strategies. The tool provides mathematically guaranteed error bounds, and is therefore conservative, compared to residual-based approaches. It also optimally defines the coupling parameters by means of an adaptive procedure, avoiding useless over-computations and thus meeting the objective to control right at the right cost. It applies to linear as well as nonlinear structural mechanics models. A main aspect was the construction of an admissible stress field, in the context of the non-intrusive coupling procedure in which internal loadings are involved. Another aspect was to derive relevant error indicators associated which each error source (i.e. coupling iterations, use of a surrogate model, and discretization). Up to now, the verification tool focuses on global error; however, such an energy-norm driven error estimation may fail to provide the required accuracy on some quantities of interest defined in the local zone where the high-fidelity model is preserved. On the other hand, complex features of the solution on some parts of the domain may not influence the local quantity of interest, and much computational resource could thus be gained. In other words, goal-oriented error estimation would make more sense in the context of local analysis with the non-intrusive local-global coupling method. Consequently, in the next chapter we extend the proposed CRE-based verification tool to the control of such quantities of interest.

# Chapter 3

# Goal-oriented strategy in the adaptive control of non-intrusive couplings

In this third chapter, we propose an extension of tools developed in Chapter 2 for the control of some local quantities which are of interest for engineering design purposes. This is performed by using the classical adjoint-based technique defined in [Becker and Rannacher, 2001, Giles and Suli, 2002] and widely used in a posteriori error estimation [Paraschivoiu et al., 1997, Rannacher and Suttmeier, 1997, Peraire and Patera, 1998, Cirak and Ramm, 1998, Prudhomme and Oden, 1999, Strouboulis et al., 2000b, Oden and Prudhomme, 2001, Ohnimus et al., 2001, Cao and Kelly, 2003]. This technique relies on the solution of an auxiliary problem associated with the studied quantity of interest. With a CRE-based approach, a guaranteed error bound on the quantity of interest is then obtained from a specific post-processing of admissible solutions for primal and adjoint problems. An adaptive strategy is again defined from the computed error estimator and indicators.

## 3.1 Goal-oriented CRE-based verification framework

Again, for the sake of simplicity, we consider a linear elasticity reference model similar to (2.1)- (2.3) to detail the computation of CRE-based guaranteed error bounds on quantities of interest. A more general procedure, valid in the nonlinear context, can be found in [Ladevèze, 2008, Ladevèze et al., 2012]. We deal with a quantity of interest $Q(\mathbf{u})$, that is a linear functional of the solution $\mathbf{u}$, and we focus on the error on this quantity when approximating $\mathbf{u}$ with $\mathbf{u}_0$ (using FEM and/or a surrogate model), that is $Q(\mathbf{u}) - Q(\mathbf{u}_0)$. For nonlinear quantities of interest, and out of classical linearization techniques, a dedicated approach can be found in [Ladevèze and Chamoin, 2010].

### 3.1.1 Adjoint problem

Following the general definition given in (1.54), we introduce the adjoint problem of the elasticity problem (self-adjoint operator), associated with quantity $Q$. It consists in finding the pair $(\tilde{\mathbf{u}}, \tilde{\boldsymbol{\sigma}})$ satisfying the following equations:

- kinematic admissibility:

$$\tilde{\mathbf{u}} \in [H^1(\Omega)]^d \quad ; \quad \mathbf{u}_{|\partial_u \Omega} = \mathbf{0} \tag{3.1}$$

- static admissibility (with external loading defined from $Q$):

$$\tilde{\boldsymbol{\sigma}} \in [L^2(\Omega)]_s^{d(d+1)/2} \quad ; \quad \nabla \cdot \tilde{\boldsymbol{\sigma}} \in [L^2(\Omega)]^d \quad ; \quad \int_\Omega \tilde{\boldsymbol{\sigma}} : \mathbb{e}(\mathbf{v}) = Q(\mathbf{v}) \quad \forall \mathbf{v} \in \boldsymbol{\mathcal{U}}_{ad}^0 \tag{3.2}$$

- constitutive relation (Hooke's law):

$$\tilde{\boldsymbol{\sigma}} = \mathbf{K}\mathbb{e}(\tilde{\mathbf{u}}) \tag{3.3}$$

The quantity of interest is usually defined in a global way by means of extraction functions, under the form:

$$Q(\mathbf{u}) = \int_\Omega \boldsymbol{\sigma}_\Sigma : \mathbb{e}(\mathbf{u}) + \int_\Omega \mathbf{f}_\Sigma \cdot \mathbf{u} + \int_{\partial_F \Omega} \mathbf{F}_\Sigma \cdot \mathbf{u} + \int_\Omega \mathbf{K}\mathbb{e}(\mathbf{u}_\Sigma) : \mathbb{e}(\mathbf{u}) \tag{3.4}$$

Quantities $\boldsymbol{\sigma}_\Sigma$, $\mathbf{f}_\Sigma$, $\mathbf{F}_\Sigma$ and $\mathbf{u}_\Sigma$ constitute the mechanical loading of the adjoint problem. They correspond to pre-stress, body force, traction force, and pre-displacement, respectively, and are specific to the quantity $Q$.
The solution $(\tilde{\mathbf{u}}, \tilde{\boldsymbol{\sigma}})$ indicates the sensitivity of $Q$ to the overall numerical error; it thus acts as a filter and conveys the locality of the targeted information.

### 3.1.2 Error bound on the overall error

After computing an approximate solution $\widetilde{\mathbf{u}}_0 \in \boldsymbol{\mathcal{V}}$ of $\widetilde{\mathbf{u}}$, then after recovering an admissible stress field $\hat{\widetilde{\boldsymbol{\sigma}}} \in \widetilde{\boldsymbol{\mathcal{S}}}$ verifying the adjoint balance equations (3.2), it is possible to define bounds on the error on the quantity of interest $Q$ [Chamoin and Ladevèze, 2008, Ladevèze, 2008]. Indeed, it is straightforward to show that:

$$\begin{aligned}
Q(\mathbf{u}) - Q(\mathbf{u}_0) = \int_\Omega \mathbb{e}(\mathbf{u} - \mathbf{u}_0) : \widetilde{\boldsymbol{\sigma}} \\
&= \int_\Omega \mathbb{e}(\mathbf{u} - \mathbf{u}_0) : \hat{\widetilde{\boldsymbol{\sigma}}} \quad (\hat{\widetilde{\boldsymbol{\sigma}}} \in \widetilde{\boldsymbol{\mathcal{S}}}) \\
&= \int_\Omega \mathbb{e}(\mathbf{u} - \mathbf{u}_0) : (\hat{\widetilde{\boldsymbol{\sigma}}} - \mathbf{K}\mathbb{e}(\widetilde{\mathbf{u}}_0)) + \int_\Omega \mathbb{e}(\mathbf{u} - \mathbf{u}_0) : \mathbf{K}\mathbb{e}(\widetilde{\mathbf{u}}_0) \\
&= \int_\Omega \mathbb{e}(\mathbf{u} - \mathbf{u}_0) : (\hat{\widetilde{\boldsymbol{\sigma}}} - \mathbf{K}\mathbb{e}(\widetilde{\mathbf{u}}_0)) + \int_\Omega (\hat{\boldsymbol{\sigma}} - \mathbf{K}\mathbb{e}(\mathbf{u}_0)) : \mathbb{e}(\widetilde{\mathbf{u}}_0) \quad (\hat{\boldsymbol{\sigma}} \in \boldsymbol{\mathcal{S}}) \\
&= \int_\Omega (\boldsymbol{\sigma} - \mathbf{K}\mathbb{e}(\mathbf{u}_0)) : \mathbf{K}^{-1}(\hat{\widetilde{\boldsymbol{\sigma}}} - \mathbf{K}\mathbb{e}(\widetilde{\mathbf{u}}_0)) + Q_{corr,1}
\end{aligned} \tag{3.5}$$

where $Q_{corr,1} = \int_\Omega (\hat{\sigma} - \mathbf{K}\mathbb{e}(\mathbf{u}_0)) : \mathbb{e}(\widetilde{\mathbf{u}}_0)$ is a fully computable correction term on $Q(\mathbf{u}_0)$.
Using the Cauchy-Schwarz inequality together with the Prager-Synge equality (2.7) yields the following guaranteed bound:

$$|Q(\mathbf{u}) - Q(\mathbf{u}_0) - Q_{corr,1}| \leq ||\sigma - \mathbf{K}\mathbb{e}(\mathbf{u}_0)||_{\mathbf{K}^{-1}}.||\hat{\widetilde{\sigma}} - \mathbf{K}\mathbb{e}(\widetilde{\mathbf{u}}_0)||_{\mathbf{K}^{-1}} \leq 2.\mathcal{E}_{CRE}(\mathbf{u}_0, \hat{\sigma}).\mathcal{E}_{CRE}(\widetilde{u}_0, \hat{\widetilde{\sigma}}) \tag{3.6}$$

A more accurate (i.e. twice sharper) bounding can be obtained introducing average stress fields $\hat{\sigma}^* = \frac{1}{2}[\hat{\sigma} + \mathbf{K}\mathbb{e}(\mathbf{u}_0)]$ and $\hat{\widetilde{\sigma}}^* = \frac{1}{2}[\hat{\widetilde{\sigma}} + \mathbf{K}\mathbb{e}(\widetilde{\mathbf{u}}_0)]$. Indeed, rewriting (3.5) as:

$$Q(\mathbf{u}) - Q(\mathbf{u}_0) - Q_{corr,1} = \int_\Omega (\sigma - \hat{\sigma}^*) : \mathbf{K}^{-1}(\hat{\widetilde{\sigma}} - \mathbf{K}\mathbb{e}(\widetilde{\mathbf{u}}_0)) + \int_\Omega (\hat{\sigma}^* - \mathbf{K}\mathbb{e}(\mathbf{u}_0)) : \mathbf{K}^{-1}(\hat{\widetilde{\sigma}} - \mathbf{K}\mathbb{e}(\widetilde{\mathbf{u}}_0)) \tag{3.7}$$

and using the Cauchy-Schwarz inequality together with (2.9), the following enhanced bound holds:

$$|Q(\mathbf{u}) - Q(\mathbf{u}_0) - Q_{corr,2}| \leq \|\sigma - \hat{\sigma}^*\|_{\mathbf{K}^{-1}}.\|\hat{\widetilde{\sigma}} - \mathbf{K}\mathbb{e}(\widetilde{\mathbf{u}}_0)\|_{\mathbf{K}^{-1}} = \mathcal{E}_{CRE}(\mathbf{u}_0, \hat{\sigma}).\mathcal{E}_{CRE}(\widetilde{\mathbf{u}}_0, \hat{\widetilde{\sigma}}) \tag{3.8}$$

with $Q_{corr,2} = Q_{corr,1} + \int_\Omega (\hat{\sigma}^* - \mathbf{K}\mathbb{e}(\mathbf{u}_0)) : \mathbf{K}^{-1}(\hat{\widetilde{\sigma}} - \mathbf{K}\mathbb{e}(\widetilde{\mathbf{u}}_0)) = \int_\Omega (\hat{\sigma} - \mathbf{K}\mathbb{e}(\mathbf{u}_0)) : \mathbf{K}^{-1}\hat{\widetilde{\sigma}}^*$. This enables to define a computable bounding on the exact value $Q(\mathbf{u})$ of the quantity of interest, under the form:

$$Q^- \leq Q(\mathbf{u}) \leq Q^+ \tag{3.9}$$

with

$$\begin{aligned} Q^- &= Q(\mathbf{u}_0) + Q_{corr,2} - \mathcal{E}_{CRE}(\mathbf{u}_0, \hat{\sigma}).\mathcal{E}_{CRE}(\widetilde{\mathbf{u}}_0, \hat{\widetilde{\sigma}}) \\ Q^+ &= Q(\mathbf{u}_0) + Q_{corr,2} + \mathcal{E}_{CRE}(\mathbf{u}_0, \hat{\sigma}).\mathcal{E}_{CRE}(\widetilde{\mathbf{u}}_0, \hat{\widetilde{\sigma}}) \end{aligned} \tag{3.10}$$

This bounding partially takes error cancellations into account (through the computable term $Q_{corr,2}$). The quantity $Q(\mathbf{u}_0) + Q_{corr,2}$ can be interpreted as a corrected approximate value of the quantity of interest.

The previously introduced local error bounds take all error sources (modeling, discretization, algebraic error) into account. They do not use orthogonality properties, and therefore enable to decouple discretizations of direct and adjoint problems. In practice, accurate bounds $Q^-$ and $Q^+$ are obtained by an enrichment of the adjoint solution [Chamoin and Ladevèze, 2008], so that $\mathcal{E}_{CRE}(\widetilde{u}_0, \hat{\widetilde{\sigma}})$ tends to 0 and $Q_{corr,2}$ tends to $Q(\mathbf{u}) - Q(\mathbf{u}_0)$. Noticing that the adjoint loading $(\sigma_\Sigma, \mathbf{f}_\Sigma, \mathbf{F}_\Sigma, \mathbf{u}_\Sigma)$ usually applies on a local subdomain of $\Omega$, and therefore leads to an adjoint solution with localized high gradients (Saint-Venant principle), the idea is to use local enrichment (with analytical or pre-computed numerical functions) in the vicinity of the space region of interest where the quantity $Q$ is defined. In the context of local-global couplings, this enrichment can be easily done using the non-intrusive framework, keeping the same global mesh for direct and adjoint problems but adding additional local patches to solve the adjoint problem

efficiently if need be.

*Remark. The bounding result on $Q$ can be recast such that the estimate is spatially split in local contributions (i.e. for mesh adaptivity purposes). We indeed get from* (3.10)*:*

$$|Q(\mathbf{u}) - Q(\mathbf{u}_0)| \leq |Q_{corr,2} + \theta_{max}\mathcal{E}_{CRE}.\tilde{\mathcal{E}}_{CRE}| = \eta^{tot}_{Q,CRE} = |\sum_K \eta_{Q,K}| \tag{3.11}$$

*where $\theta_{max} \in \{-1, +1\}$ is the maximizer, and $\eta_{Q,K}$ is a local contribution over each element $K$ defined as:*

$$\eta_{Q,K} = \int_K (\hat{\mathfrak{S}} - \mathbf{K}\mathfrak{e}(\mathbf{u}_0)) : \mathbf{K}^{-1}\hat{\widetilde{\mathfrak{S}}}^* + \frac{1}{2}\theta_{max}\left(\frac{\tilde{\mathcal{E}}_{CRE}}{\mathcal{E}_{CRE}}.\mathcal{E}^2_{CRE|K} + \frac{\mathcal{E}_{CRE}}{\tilde{\mathcal{E}}_{CRE}}.\tilde{\mathcal{E}}^2_{CRE|K}\right) \tag{3.12}$$

## 3.2 Application to non-intrusive coupling

### 3.2.1 Computation of a goal-oriented error estimator

In the present context, the adjoint solution is approximated as the primal solution, using the non-intrusive local-global coupling technique (potentially with the same coupling configuration). This technique yields the approximate solution $(\tilde{\mathbf{u}}^{hH(n)}_{LG}, \tilde{\mathfrak{S}}^{hH(n)}_{LG,N})$ at iteration $n$. Then, in a similar way as for error estimation in the energy norm performed in Chapter 2, an admissible adjoint stress field $\hat{\widetilde{\mathfrak{S}}}^{hH(n)}_{LG,N} \in \widetilde{\boldsymbol{\mathcal{S}}}$ is recovered from a specific post-processing of the field $\widetilde{\mathfrak{S}}^{hH(n)}_{LG,N} \notin \widetilde{\boldsymbol{\mathcal{S}}}$ at hand. We thus obtain from (3.8):

$$|Q(\mathbf{u}) - Q(\mathbf{u}^{hH(n)}_{LG}) - Q_{corr,2}| \leq \mathcal{E}_{CRE}(\mathbf{u}^{hH(n)}_{LG}, \hat{\mathfrak{S}}^{hH(n)}_{LG,N}).\mathcal{E}_{CRE}(\widetilde{\mathbf{u}}^{hH(n)}_{LG}, \hat{\widetilde{\mathfrak{S}}}^{hH(n)}_{LG,N}) \tag{3.13}$$

with $Q_{corr,2} = \frac{1}{2}\int_\Omega (\hat{\mathfrak{S}}^{hH(n)}_{LG,N} - \mathbf{K}\mathfrak{e}(\mathbf{u}^{hH(n)}_{LG})) : \mathbf{K}^{-1}(\hat{\widetilde{\mathfrak{S}}}^{hH(n)}_{LG,N} + \mathbf{K}\mathfrak{e}(\widetilde{\mathbf{u}}^{hH(n)}_{LG}))$ a computable quantity, so that guaranteed bounds on $Q(\mathbf{u})$ (or on the error $Q(\mathbf{u}) - Q(\mathbf{u}^{hH(n)}_{LG})$) are obtained. We indicate again that the quantity $Q(\mathbf{u}^{hH(n)}_{LG}) + Q_{corr,2}$ represents an enhancement of the approximate value $Q(\mathbf{u}^{hH(n)}_{LG})$ of the quantity of interest, by means of the correction term $Q_{corr,2}$.

### 3.2.2 Definition of error indicators

As described in Chapter 1, error sources in non-intrusive local-global coupling are threefold: modeling, discretization, convergence. In the goal-oriented context, and using solution fields defined in Section 1.2.3, the error on $Q$ at a given iteration $n$ can be split as:

$$Q(\mathbf{u}) - Q(\mathbf{u}^{hH(n)}_{LG}) = \underbrace{\left[Q(\mathbf{u}) - Q(\mathbf{u}^{H}_{LG})\right]}_{\mathcal{E}^{mod}_Q} + \underbrace{\left[Q(\mathbf{u}^{H}_{LG}) - Q(\mathbf{u}^{hH}_{LG})\right]}_{\mathcal{E}^{dis}_Q} + \underbrace{\left[Q(\mathbf{u}^{hH}_{LG}) - Q(\mathbf{u}^{hH(n)}_{LG})\right]}_{\mathcal{E}^{conv}_Q} \tag{3.14}$$

where $\mathcal{E}_Q^{mod}$, $\mathcal{E}_Q^{dis}$, and $\mathcal{E}_Q^{conv}$ correspond to modeling, discretization, and convergence parts of the error, respectively. Reusing the study performed in Chapter 2 for error splitting, the following error indicators on each of these error parts are defined:

$$
\begin{aligned}
\eta_{Q,CRE}^{conv} &= \left| \frac{1}{2} \int_{\Omega_L} (\widehat{\delta\sigma}_G^{H(n)} - (\hat{\sigma}_L^{h(n)} - \hat{\sigma}_L^{h(n-1)})) : \mathbf{K}^{-1} (\hat{\tilde{\sigma}}_{LG,N}^{hH(n)} + \mathbf{K}\mathfrak{C}(\tilde{\mathbf{u}}_{LG}^{hH(n)})) \right| \\
&\quad + \frac{1}{2} \| \widehat{\delta\sigma}_G^{H(n)} - (\hat{\sigma}_L^{h(n)} - \hat{\sigma}_L^{h(n-1)}) \|_{\mathbf{K}^{-1}|\Omega_L} . \| \widehat{\delta\tilde{\sigma}}_G^{H(n)} - (\hat{\tilde{\sigma}}_L^{h(n)} - \hat{\tilde{\sigma}}_L^{h(n-1)}) \|_{\mathbf{K}^{-1}|\Omega_L} \\
\eta_{Q,CRE}^{dis} &= \left| \frac{1}{2} \int_{\Omega_L} (\hat{\sigma}_L^{h(n)} - \mathbf{K}\mathfrak{C}(\mathbf{u}_L^{h(n)})) : \mathbf{K}^{-1} (\hat{\tilde{\sigma}}_{LG,N}^{hH(n)} + \mathbf{K}\mathfrak{C}(\tilde{\mathbf{u}}_{LG}^{hH(n)})) \right| \\
&\quad + \frac{1}{2} \| \hat{\sigma}_L^{h(n)} - \mathbf{K}\mathfrak{C}(\mathbf{u}_L^{h(n)}) \|_{\mathbf{K}^{-1}|\Omega_L} . \| \hat{\tilde{\sigma}}_L^{h(n)} - \mathbf{K}\mathfrak{C}(\tilde{\mathbf{u}}_L^{h(n)}) \|_{\mathbf{K}^{-1}|\Omega_L} \\
\eta_{Q,CRE}^{mod} &= \left| \frac{1}{2} \int_{\Omega_0} (\widehat{\delta\sigma}_G^{H(n)} - \mathbf{K}\mathfrak{C}(\mathbf{u}_G^{H(n)})) : \mathbf{K}^{-1} (\hat{\tilde{\sigma}}_{LG,N}^{hH(n)} + \mathbf{K}\mathfrak{C}(\tilde{\mathbf{u}}_{LG}^{hH(n)})) \right| \\
&\quad + \frac{1}{2} \| \widehat{\delta\sigma}_G^{H(n)} - \mathbf{K}\mathfrak{C}(\mathbf{u}_G^{H(n)}) \|_{\mathbf{K}^{-1}|\Omega_0} . \| \widehat{\delta\tilde{\sigma}}_G^{H(n)} - \mathbf{K}\mathfrak{C}(\tilde{\mathbf{u}}_G^{H(n)}) \|_{\mathbf{K}^{-1}|\Omega_0}
\end{aligned}
\tag{3.15}
$$

### 3.2.3 Adaptive algorithm

A greedy adaptive algorithm can be set up, from the computation (at each iteration of the local-global solver) of the previously defined goal-oriented error estimator and indicators, for the control of the accuracy on the quantity of interest. The objective is to optimally drive the non-intrusive local-global coupling method, tuning parameters so that useless computations are avoided when targeting a selected quantity of interest of the problem.

Specifying the error tolerance $\gamma_{tol}$, and after initializing $\Omega_L$ and $\tau_h$, the algorithm reads as follows:

0. Set $n = 1$;
1. Solve the primal and adjoint surrogate problems for $\mathbf{u}_{LG}^{hH(n)}$ and $\tilde{\mathbf{u}}_{LG}^{hH(n)}$;
2. Recover the admissible stress fields $\hat{\sigma}_{LG,N}^{hH(n)}$ and $\hat{\tilde{\sigma}}_{LG,N}^{hH(n)}$, and compute the estimate $\eta_{Q,CRE}^{tot}$;
3. If $\eta_{Q,CRE}^{tot} / |Q(\mathbf{u}_{LG}^{hH(n)})| \leq \gamma_{tol}$ then STOP. Otherwise proceed to Step 4;
4. Compute indicators $\eta_{Q,CRE}^{conv}$, $\eta_{Q,CRE}^{dis}$, and $\eta_{Q,CRE}^{mod}$:
   - if $\max(\eta_{Q,CRE}^{conv}, \eta_{Q,CRE}^{dis}, \eta_{Q,CRE}^{mod}) = \eta_{Q,CRE}^{conv}$, increment $n+1 \to n$ and go to Step 1;
   - if $\max(\eta_{Q,CRE}^{conv}, \eta_{Q,CRE}^{dis}, \eta_{Q,CRE}^{mod}) = \eta_{Q,CRE}^{dis}$, decompose $\eta_{Q,CRE}^{dis}$ and locally refine $\tau^h$ up to reaching $\eta_{Q,CRE}^{dis} / |Q(\mathbf{u}_{LG}^{hH(n)})| \leq \gamma_{tol}/3$, then go to Step 1;
   - if $\max(\eta_{Q,CRE}^{conv}, \eta_{Q,CRE}^{dis}, \eta_{Q,CRE}^{mod}) = \eta_{Q,CRE}^{mod}$, decompose $\eta_{Q,CRE}^{mod}$ and locally enlarge $\Omega_L$ up to reaching $\eta_{Q,CRE}^{mod} / |Q(\mathbf{u}_{LG}^{hH(n)})| \leq \gamma_{tol}/3$, then go to Step 1.

## 3.3 Numerical results

### 3.3.1 Plate with a hole

We consider the same problem as in Chapter 2, but we now focus on the control of the error on a local quantity of interest (max of stress component or VM stress).

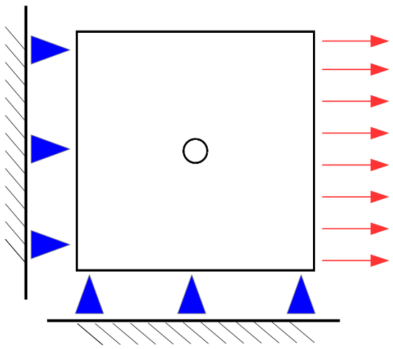

Figure 3.1: Case study.

When considering the Von Mises equivalent stress as the (nonlinear) quantity of interest, a linearization procedure is here performed. In order words, proving the error is sufficiently small, we write the error as:

$$Q(\mathbf{u}) - Q(\mathbf{u}_0) = Q'(\mathbf{u}_0; \delta\mathbf{u}) + O(\|\delta\mathbf{u}\|^2_{loc}) \tag{3.16}$$

with $Q'(\mathbf{u}_0;\mathbf{v}) = \lim_{\theta\to 0}\theta^{-1}(Q(\mathbf{u}_0+\theta\mathbf{v})-Q(\mathbf{u}_0))$ the Gâteaux derivative, $\delta\mathbf{u} = \mathbf{u}-\mathbf{u}_0$, and $\|\cdot\|_{loc}$ a $L^2$-norm defined in the local region where the quantity of interest is located. The linear part $Q'$ is then kept alone for the loading of the adjoint problem.

In the specific case of the Von Mises equivalent stress, denoting $\mathbb{S} = \boldsymbol{\sigma} - \frac{1}{3}\mathrm{Tr}[\boldsymbol{\sigma}]\mathbb{I}$ the deviatoric part of the stress tensor $\boldsymbol{\sigma}$ and $k_{VM}$ the normalizing constant ($k_{VM} = 3/2$ in 3D, $k_{VM} = 2$ in 2D), we get $Q(\mathbf{u}) = \sqrt{k_{VM}\mathbb{S}(\mathbf{u}) : \mathbb{S}(\mathbf{u})}$ and the linearization reads:

$$\begin{aligned}
Q(\mathbf{u}) = Q(\mathbf{u}_0+\delta\mathbf{u}) &= \sqrt{k_{VM}\mathbb{S}(\mathbf{u}_0+\delta\mathbf{u}) : \mathbb{S}(\mathbf{u}_0+\delta\mathbf{u})} \\
&= \sqrt{k_{VM}(\mathbb{S}(\mathbf{u}_0) : \mathbb{S}(\mathbf{u}_0) + 2\mathbb{S}(\mathbf{u}_0) : \mathbb{S}(\delta\mathbf{u}) + \mathbb{S}(\delta\mathbf{u}) : \mathbb{S}(\delta\mathbf{u}))} \\
&= Q(\mathbf{u}_0)\sqrt{1 + k_{VM}\frac{2\mathbb{S}(\mathbf{u}_0) : \mathbb{S}(\delta\mathbf{u})}{Q^2(\mathbf{u}_0)} + O(\|\delta\mathbf{u}\|^2_{loc})} \\
&= Q(\mathbf{u}_0)\left(1 + k_{VM}\frac{\mathbb{S}(\mathbf{u}_0) : \mathbb{S}(\delta\mathbf{u})}{Q^2(\mathbf{u}_0)} + O(\|\delta\mathbf{u}\|^2_{loc})\right)
\end{aligned} \tag{3.17}$$

Therefore, the loading employed in the weak form of the adjoint problem reads:

$$Q'(\mathbf{u}_0;\mathbf{v}) = k_{VM}\frac{\mathbb{S}(\mathbf{u}_0) : \mathbb{S}(\mathbf{v})}{Q(\mathbf{u}_0)} \tag{3.18}$$

It is associated with the tangent pre-strain extraction operator (evaluated at $\mathbf{u}_0$) $\mathfrak{e}_\Sigma = \mathbf{K}^{-1}\mathfrak{o}_\Sigma$ such that $\mathfrak{e}_\Sigma : \mathfrak{o}(\mathbf{v}) = k_{VM}\frac{\mathbb{S}(\mathbf{u}_0):\mathbb{S}(\mathbf{v})}{Q(\mathbf{u}_0)}$. It leads to accurate error bounds on $Q$, provided the error is small, event though bounds are not guaranteed any more.

For this study the quantity of interest is the maximal Von Mises Stress nearby of the hole top region. It is a local quantity of interest so we can assess that only the region in the vicinity of the hole might affect the accuracy of the quantity of interest computation.

The loading case and boundary conditions are the same as described in Chapter 2 for the first case study (cf. Figure 3.1).

A reference solution is at hand from Chapter 2, and is shown in Figure 3.2. From this reference solution, the adjoint solution can be computed (both are coupled through the adjoint loading).

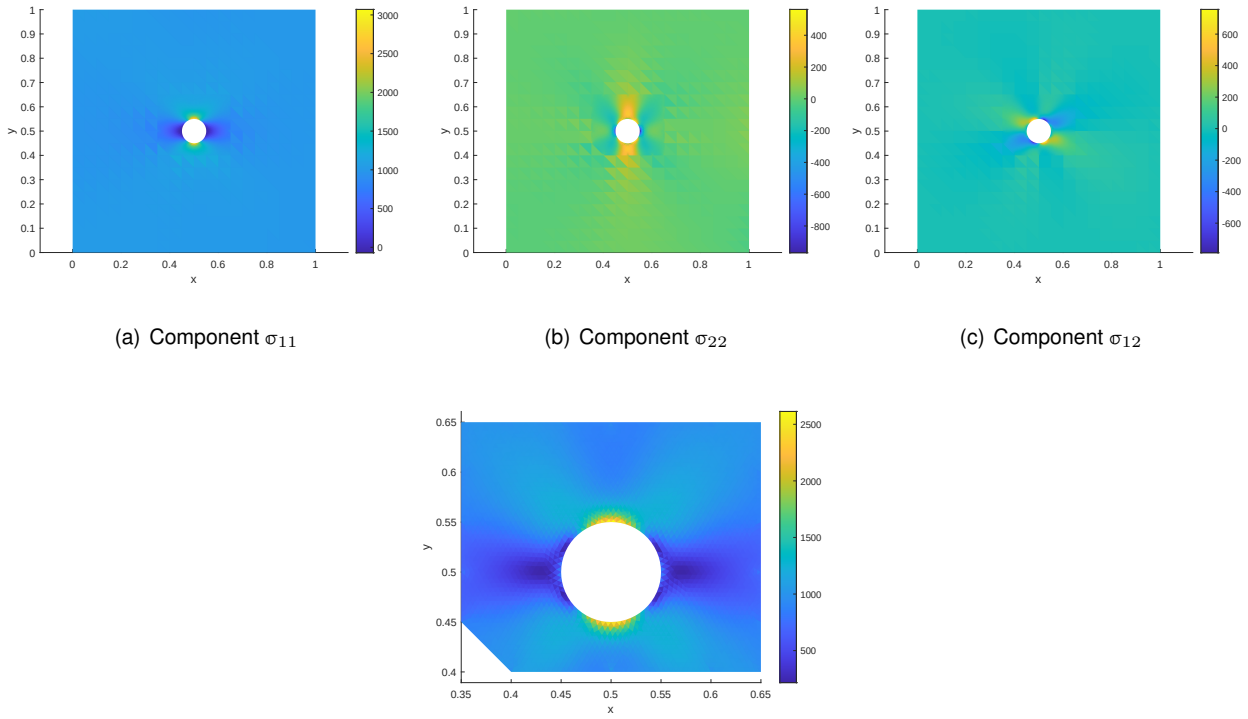

(a) Component $\mathfrak{o}_{11}$ (b) Component $\mathfrak{o}_{22}$ (c) Component $\mathfrak{o}_{12}$

(d) $\mathfrak{o}_{VM}$

Figure 3.2: Local-global primal solution - Stress field.

*Remark. In practice the adjoint solution is computed at the same time as the primal solution during the adaptive algorithm. The adjoint solution has the same local patch and the same local discretization as the primal solution. We are only enriching the number of iterations for the local global non-intrusive couplings algorithm between primal and adjoint solutions.*

The adjoint solution is shown in Figure 3.3. As we can see it is localized in the region of the quantity of interest.

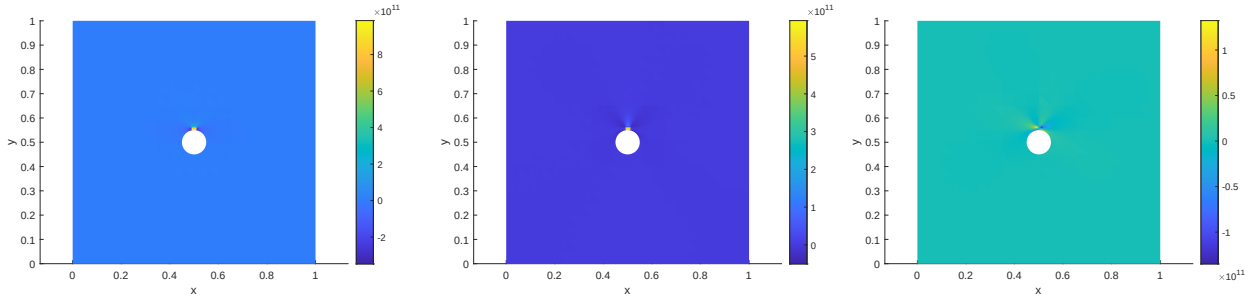

(a) Component $\widetilde{\sigma}_{11}$ (b) Component $\widetilde{\sigma}_{22}$ (c) Component $\widetilde{\sigma}_{12}$

Figure 3.3: Local-global adjoint solution - Stress field.

Using the error indicators defined in this chapter for a goal-orientated framework, the adaptive control and driving of the non-intrusive coupling is performed. The evolution of error indicators is shown in Figure 3.4. As we can see in the first adaptive steps, we alternatively add an iteration in the local global non-intrusive algorithm and refine the local mesh. After the 9th step the modeling error is dominating, but the global error decreases slowly. Figure 3.5 shows the evolution of the local mesh during the adaptive control.

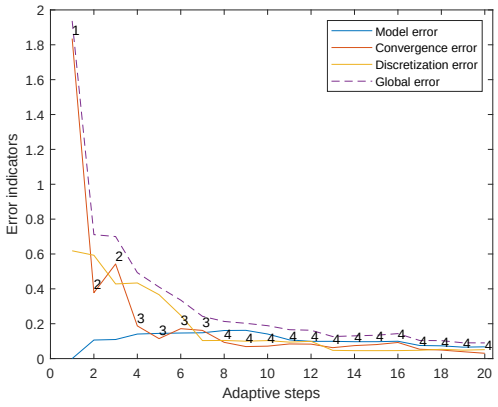


Figure 3.4: Evolution of relative error indicators at each adaptive step.

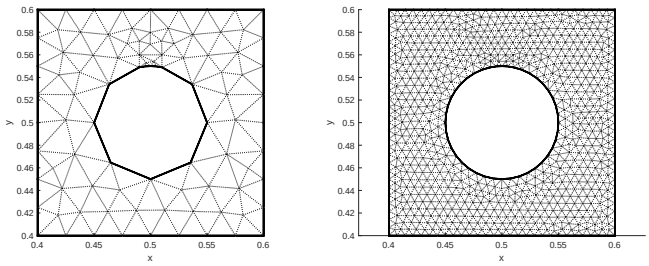


(a) Step 1

(b) Step 8

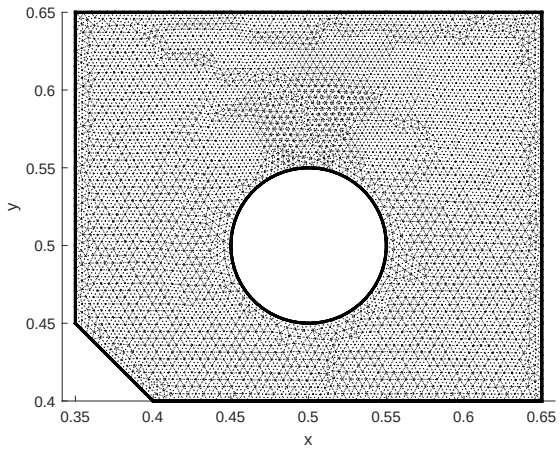


(c) Step 20

Figure 3.5: Evolution of the local mesh for the adaptive strategy.

### 3.3.2 L-shaped domain

We consider the same problem as in Chapter 2, but we now focus on the control of the error on two types of quantities of interest : the mean of a stress component and the mean of displacement component in a local region.

We have computed a reference solution in Chapter 2 (cf. Figure 3.6 ) for the primal solution. This reference solution is obtained after the global error is lower than a threshold.

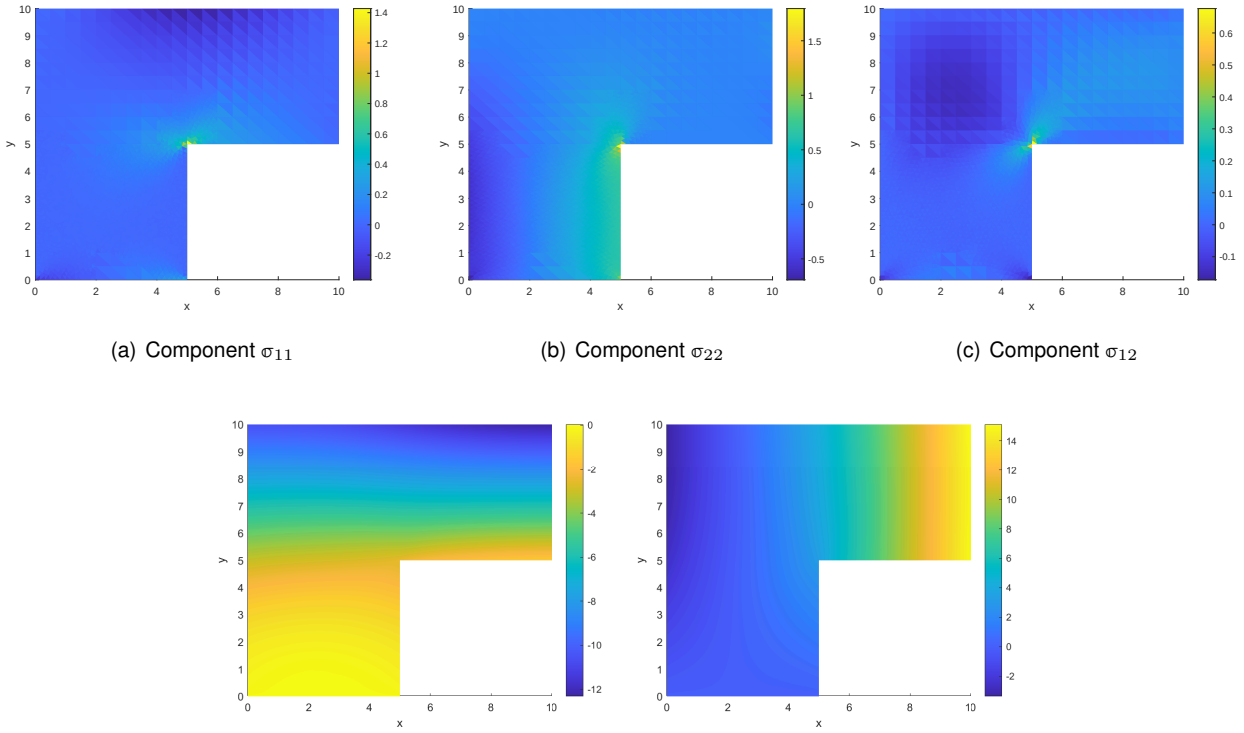

(a) Component $\sigma_{11}$ (b) Component $\sigma_{22}$ (c) Component $\sigma_{12}$

(d) $U_X$ (e) $U_Y$

Figure 3.6: Local-global primal solution - Stress field.

We are considering two quantities of interest in this study :

- The mean of the component $\sigma_{12}$ of the stress field in the vicinity of the singularity;
- The mean of the horizontal $U_X$ displacement on the far-right side of the L-shape structure.

We can forecast that in the case of the first quantity of interest the adaptive strategy should only require local enrichment near the area of interest whereas the second quantity of interest may require enrichment in some regions far from the one where the quantity of interest is defined.

### Local stress field component $\sigma_{12}$ as a quantity of interest

In this case, the loading of the adjoint problem is a pre-strain applied in the area of interest. The initial local patch is located near the singularity where the quantity of interest is embedded. Figure 3.7 show this initial patch.

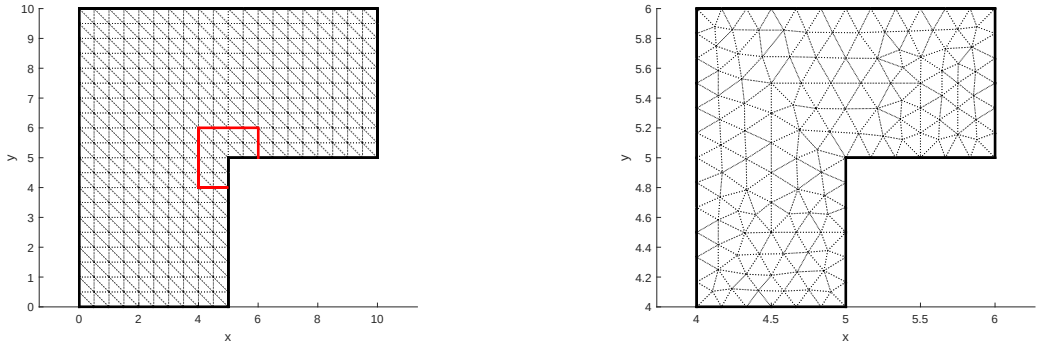


(a) Global mesh (with the coupling interface). (b) Initial local mesh.

Figure 3.7: Initial coupling configuration and mesh.

The approximate adjoint solution associated with this quantity of interest is shown in Figure 3.8

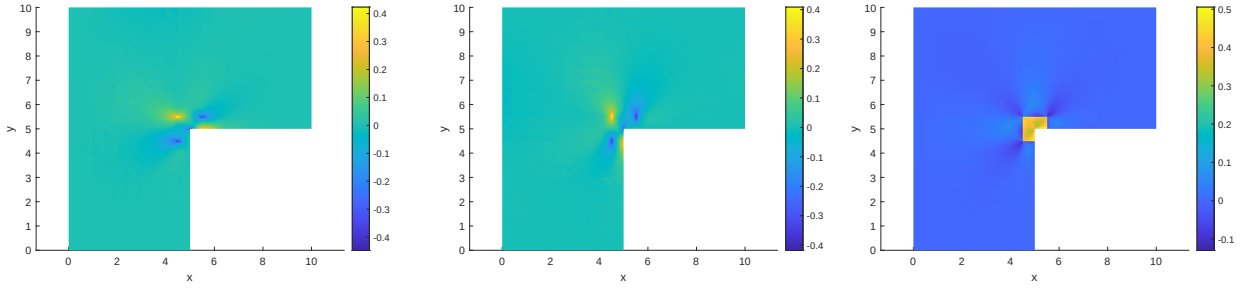


(a) Component $\widetilde{\sigma}_{11}$ (b) Component $\widetilde{\sigma}_{22}$ (c) Component $\widetilde{\sigma}_{12}$

Figure 3.8: Local-global adjoint solution - Stress field.

As we can see the adjoint solution shows only high-gradient phenomena near the area of interest. As assessed previously, the enrichment of the local global solution should be restrained in this area. Only the number of iterations, the discretization of the local domain and the size of the local domain should be updated according to the error indicators. No new local patch should be created. The evolution of the error indicators is shown in Figure 3.9.

As we can see, the modeling error is prominent and an enlargement of the local patch is first required. The evolution of the local patch is shown in Figure 3.10.

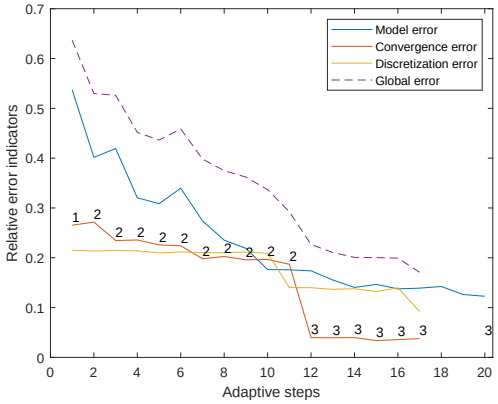


Figure 3.9: Evolution of relative error indicators at adaptive each step.

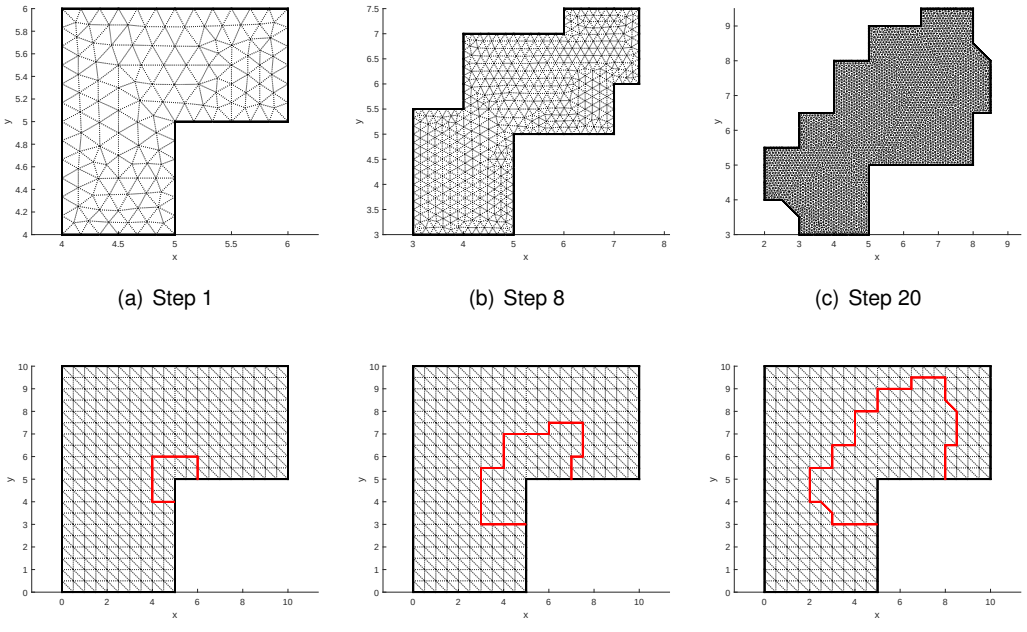

(a) Step 1 (b) Step 8 (c) Step 20

(d) Step 1 (e) Step 8 (f) Step 20

Figure 3.10: Evolution of the local mesh for the adaptive strategy.

**Displacement component $U_X$ as a quantity of interest**

In this case, the loading of the adjoint problem is a traction force on the far-right side of the structure along the direction $x$. There are two local patches initially, the first patch is located near the right side of the structure where the quantity of interest is defined and a second patch in the corner of the L-shape structure. The initial configuration is shown in Figure 3.11.

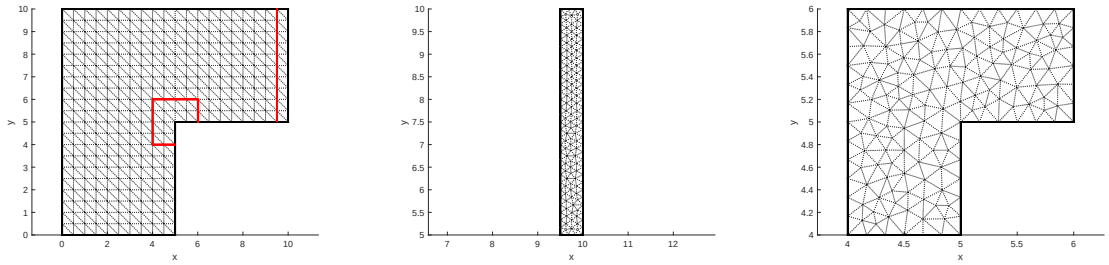

(a) Global mesh (with the coupling interface).

(b) Initial local mesh 1.

(c) Initial local mesh 2.

Figure 3.11: Initial coupling configuration and mesh.

The approximate adjoint solution associated with this quantity of interest is shown in Figure 3.12.

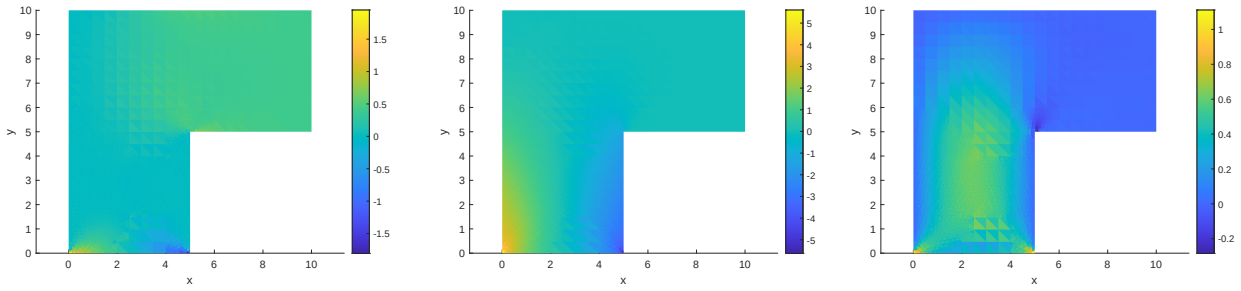

(a) Component $\widetilde{\sigma}_{11}$

(b) Component $\widetilde{\sigma}_{22}$

(c) Component $\widetilde{\sigma}_{12}$

Figure 3.12: Local-global adjoint solution - Stress field.

The adjoint solution shows that the quantity of interest is impacted by the solution on the whole domain. Also, in order to drive the adaptive strategy optimally, new patches may be necessary. The evolution of the error indicators is shown in Figure 3.13. As we can see, the modeling error is the most important, the computation of the local contribution for the modeling error is required in order to choose where to add new local patches. Figures 3.14 and 3.15 show, respectively, the local contribution for the modeling error and the evolution of the local-global model.

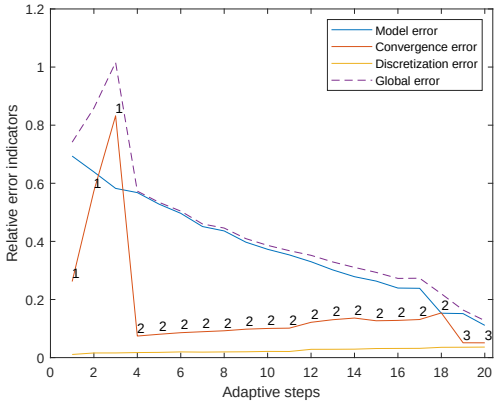


Figure 3.13: Evolution of relative error indicators at adaptive each step.

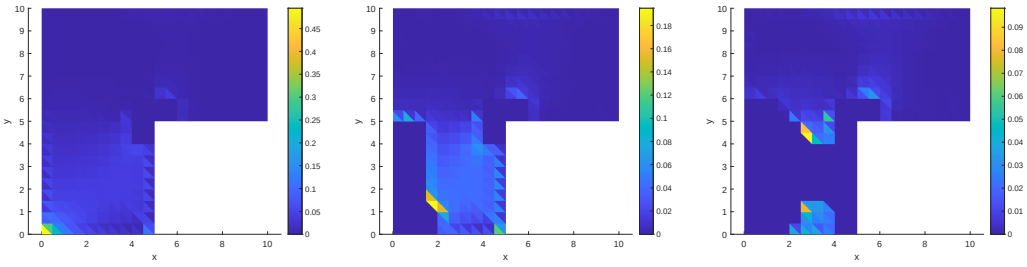

(a) Step 1 (b) Step 8 (c) Step 20

Figure 3.14: Evolution of modeling error contribution.

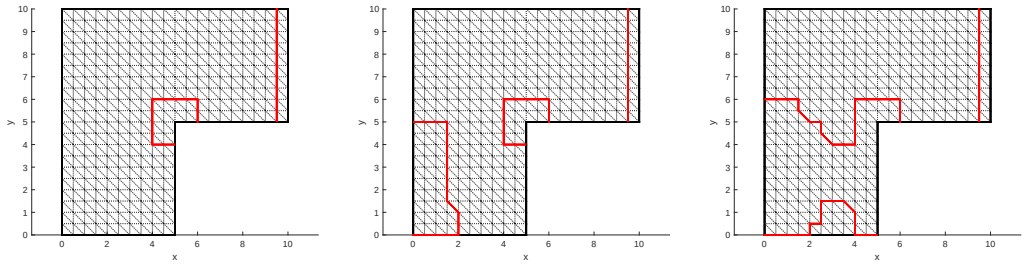

(a) Step 1 (b) Step 8 (c) Step 20

Figure 3.15: Evolution of the local mesh for the adaptive strategy.

### 3.3.3 Plate with regular distribution of holes

In this final application, we consider a plate with a regular (periodic) distribution of 160 holes with constant radius $r = 0.15$, and submitted to a bending loading. The dimensions of the plate and boundary conditions are detailed in Fig. 3.16. The Young modulus is $E = 1$ and the Poisson ratio is $\nu = 0.3$. The reference solution, in terms of $\epsilon_{yy}$ component of the strain field, is given in Fig. 3.17(a); all the 160 holes are considered in this case, and an overkill computation is performed. A main objective is to define which holes have to be eventually represented in order to ensure the accuracy on a given quantity of interest.

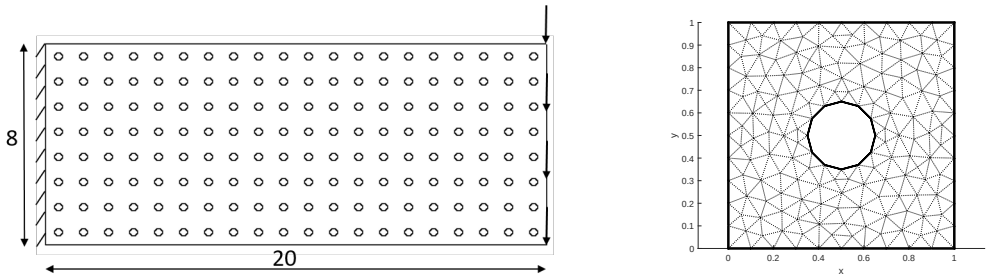


(a) Configuration of the studied problem.

(b) Zoom on the local mesh used to represent each hole.

Figure 3.16: Description of the bending plate problem. The reference geometry (a) is composed of 160 holes that may be each represented by a patch (b) in the numerical approximation.

Using the local-global coupling framework, the solution is approximated considering:

- a global model made of the plate without any hole and with an homogenized Young modulus $E_0 = (1 - \pi r^2)E$ (effective modulus obtained from a weighted average). The global mesh $\tau^H$ used for this model is composed of 8×20 first-order quadrangle elements;
- a local model in a zone $\Omega_L \subset \Omega$ made of a set of patches, each patch representing a squared domain including a hole (Fig. 3.16(b)). The size of one local patch is 1×1 (that is, the size of a macro element), the Young modulus is $E = 1$, and the unstructured mesh is composed of first-order triangular elements.

In the adaptive process, we consider that the local mesh $\tau^h$ is fine enough so that discretization error in $\Omega_L$ is neglected. Consequently, the adaptive procedure aims at setting the optimal number $n$ of iterations in the coupling procedure as well as the holes which need to be represented using a patch (definition of the size of $\Omega_L$). The quantity of interest is the average vertical displacement on the right side ($x = 20$) of the structure. Naturally, the initial local zone $\Omega_L$ is then placed in the vicinity of this edge (see Fig. 3.19(a)). It is made of the layer of 8 macro elements of $\tau^H$ which are connected to the right edge of $\Omega$; out of the 8 associated holes, the other holes are not represented. We show in Fig. 3.17(b) the approximate coupled solution obtained when considering this coupling

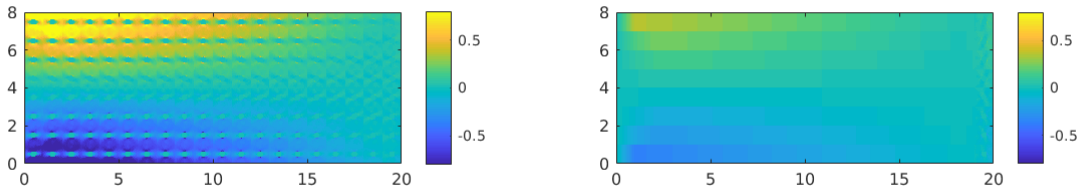


(a) Reference solution.

(b) Approximate solution (initial coupling configuration).

Figure 3.17: Map of the $\varepsilon_{yy}$ strain component for the considered plate problem: (a) when all the holes are considered (reference solution, no coupling); (b) when a local-global coupling strategy is used with a local zone made of one layer of macro elements (holes are represented in this zone alone).

configuration.

This benchmark has been studied by Marie Tirvaudey in [Tirvaudey et al., 2020b] using residual-based error estimator. The following results are obtained with the method developed using the CRE.

The adaptive process is performed, starting from the previous coupling configuration with one iteration in the local-global algorithm. Using the non-intrusive framework, potential critical zones are analyzed by placing additional patches in the adjoint problem in order to catch the associated error sources. The obtained set of adjoint problems can be solved in parallel. We can also solve and equilibrate the non-enriched adjoint problem, then local reanalysis is performed (CA: Dirichlet boundary conditions from the global solution, SA: Neumann boundary conditions from equilibrated tractions).

The adaptation results are shown in Fig. 3.18, where the evolutions of the relative error estimator and indicators (in terms of iteration and modeling sources) are shown along the adaptive process (Fig. 3.18(a)), as well as the final approximate coupled solution verifying the tolerance on the quantity of interest (Fig. 3.18(b)). This solution is obtained after 35 iterations of the adaptive process; it requires $n = 2$ iterations in the coupling algorithm and an enlarged local zone $\Omega_L$ taking into account pollution effects from the coarse global model. The adaptive process can be detailed as follows:

- from Step 1 to Step 8, modeling error is predominant so that patches are added to $\Omega_L$;
- at Step 9, an additional iteration is performed in the coupling algorithm;
- from Step 18 to Step 35, news patches are added to $\Omega_L$. The size of this zone at Step 35 is shown in Fig. 3.19(c);

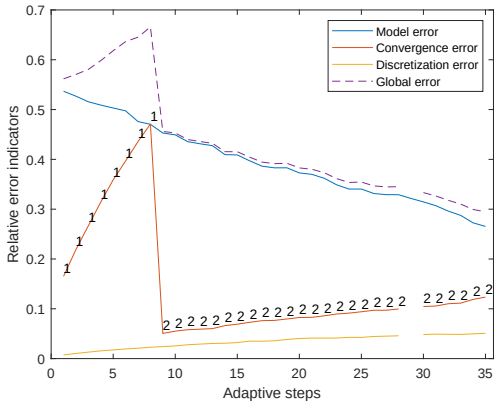


(a) Evolution of the error estimator and indicators along the adaptive process.

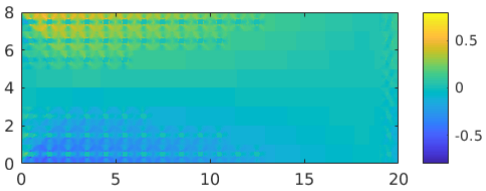

(b) Map of the $\epsilon_{yy}$ strain component for the final coupling solution.

Figure 3.18: Evolution of error quantities and final coupling configuration for the control on the plate with holes.

- at Step 36, the algorithm was stopped, as the generation of the local mesh crashed.

We emphasize that we chose here to add only one patch to $\Omega_L$ at each iteration of the adaptive process, so that the required number of iterations to reach the error tolerance is quite large. An alternative to decrease the number of iterations would be to add several patches in the same time (selecting macro elements of $\tau^H$ in which modeling error is larger than a threshold). Nevertheless, optimality of the final coupling configuration would be lost with this procedure, and this is why we chose not to apply it in this work.

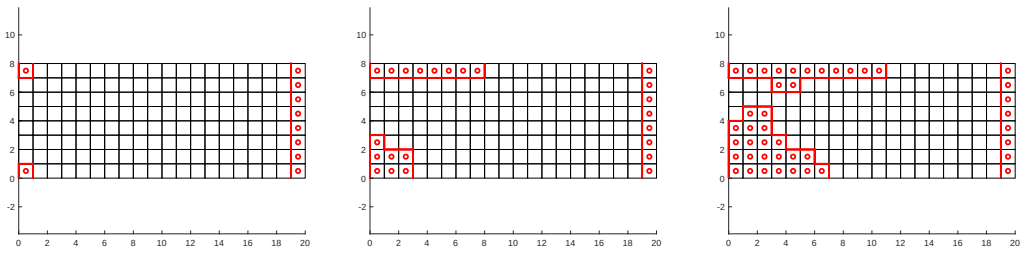

(a) Step 3 (b) Step 15 (c) Step 35

Figure 3.19: Evolution of the local domain for the adaptive strategy.

Furthermore our results present some strange behavior. Indeed, the symmetric distribution of the local domain is not respected. This can be explained by the non-symmetry of the global mesh which can affect the computation of the global stress field and therefore the admissible stress field (which is no more symmetric).

## 3.4 Partial conclusions

In this chapter, we extended the CRE strategy for goal-oriented error estimation in the context of local-global non-intrusive couplings. It avoids useless over-computations, e.g. the iterative solver is usually stopped before reaching convergence in terms of the usual interface equilibrium). It is important to notice that the strategy is made consistent with the non-intrusive framework of the coupling; it can thus be performed when coupling two different codes, and local analyses for error sources (by adding local patches when solving the adjoint problem) can advantageously benefit from this non-intrusive framework. Consequently, the adjoint solution does not require prohibitive computing resources but is rather conducted by defining individual and manageable problems (that differ by the position of local patches) which can be all solved in parallel at a global cost similar to that of the primal coupling problem.

In the next chapter, the proposed error estimation procedure is integrated in a larger and more flexible framework in which reduced order modeling is used in the local model, in order to further reduce CPU costs in multi-query analyses.

# Chapter 4

# Local use of PGD reduced order modeling

The non-intrusive coupling is a convenient way to perform local analysis. Due to natural multi-query aspects of the iterative coupling algorithm, in addition to potential parametric studies (optimization, uncertainty quantification...), reduced order modeling (ROM) appears as an attractive complementary approach. In this fourth chapter, we propose to introduce PGD model reduction in the framework of non-intrusive local-global couplings. We thus perform a coupling between a global solution raised from FEM and a local solution evaluated in the online phase (and in a cheap manner) from virtual charts constructed in a preliminary offline phase, and associated to a parametrized modeling (in terms of boundary conditions or geometry configuration) of the local region of interest. This strategy enables both to accelerate the iterative coupling procedure, as well as to effectively address local parametric analyses. Full error control is again performed in this context, adding to local discretization error the new error source coming from local PGD approximation.

## 4.1 Basics on PGD

### 4.1.1 Model reduction framework

Applied mathematics, computational mechanics, and computer sciences contributed in the last two decades to new modeling and simulation procedures in which reduced-order modeling (ROM) techniques are one of the major achievements. These advanced techniques address complex high-dimensional engineering problems, with a large set of parameters, which are out of reach or remain very costly despite the constant enhancements in computing resources. Indeed, solving the parametric problem for any configuration may require a huge and often unreasonable computational effort using brute force numerical methods, due to multi-query computations from a potentially high-dimensional parameter space and with large linear systems to solve. The issue comes from the exponential growth of complexity when using grid-based discretization strategies (this is the so-called curse of dimensionality).

To address this issue, model reduction tools are suited as they permit to capture the manifold of solutions over the whole parameter domain with dramatically reduced CPU cost and memory resources without sacrificing too much of the solution accuracy. Model reduction is an attractive and advanced numerical approach which has been widely developed during the last decade [Chinesta et al., 2017]. ROM techniques, unlike meta-modeling techniques, do not simplify physics models but rather decrease their computational complexity by using specific numerical tools that generate an adequate approximate solution from a low-dimensional basis (manifold), facilitating the map from the input space to the set of outputs. They lean on the fact that the (full-order) solution of a complex high-dimensional model can often be accurately approximated by the (reduced-order) solution of a surrogate model. This latter is obtained through the projection of the initial model onto a low-dimensional (reduced) subspace spanned by global basis functions, so that dimensionality can be drastically reduced. Consequently, such tools have the potential to circumvent the curse of dimensionality and make the approximation of high-dimensional solutions computationally tractable. They have been in rapid expansion over the last decade and their performance, in terms of savings in computational time and memory storage, are impressive (several orders of magnitude).

Most ROM procedures consist of the generation, in an intensive offline (learning) stage, of a relevant reduced-order basis that captures the dominant dynamics of the physical model. This basis can then be operated in an online phase to obtain approximate solutions at low cost. We may list here:

- the POD method [Chatterjee, 2000, Kunisch and Volkwein, 2001, Gunzburger et al., 2007], which is similar to the Singular Value Decomposition (SVD), the Principal Component analysis (PCA), or the Karhunen-Loeve Decomposition (KLD);
- the Reduced Basis (RB) method [Maday and Ronquist, 2002, Barrault et al., 2004, Rozza et al., 2008, Drohmann et al., 2012];
- the PGD method [Chinesta et al., 2011, Chinesta et al., 2014], which will be specifically detailed below.

In the case of nonlinear problems, a second reduction procedure aiming at reducing the evaluation step over a lower dimensional space is needed; this may be performed with several methods such as the Empirical Interpolation Method (EIM) [Barrault et al., 2004, Maday and Mula, 2013, Radermacher and Reese, 2016] or the hyper-reduction method [Ryckelynck, 2009], to name a few.
ROM is effective to address multi-query procedures and parametrized problems encountered in many computational engineering activities such as optimization (sensitivity analysis), inverse analysis, uncertainty propagation, or optimal control [Grepl et al., 2007, Nguyen et al., 2010, Ghnatios et al., 2012, Maday et al., 2015, Cui et al., 2015, Nadal et al., 2015, Yu and Chakravorty, 2015, Manzoni et al., 2016, Chen et al., 2017, Karcher et al., 2018].

We focus here on the Proper Generalized Decomposition (PGD) technique, which is an appealing model reduction technique based on low-rank modal approximation (canonical tensor format) [Chinesta et al., 2010, Leygue and Verron, 2010, Nouy, 2010a, Chinesta et al., 2011, Chinesta et al., 2013, Chinesta et al., 2014, Chinesta and Cueto, 2014]. In contrast to the POD or RB methods in which the reduced-order basis is extracted from pre-computed solutions of the system (learning phase), PGD is part of a priori methods that follow a different path by progressively building an approximate representation of the solution, without assuming any prior basis or knowledge on the problem dynamics (i.e. snapshots). PGD is equivalent to POD (it thus provides optimal modes with respect to the chosen norm) when solving elliptic pdes up to dimension 2 [Falco et al., 2013]; in other cases, there is no evidence that the solution is optimal.

PGD operates in an iterative strategy in which a representation of the multidimensional solution is defined as a linear combination of separated variables functions (called modes), after defining all model parameters as extra-coordinates of the problem. With such a modal representation, the complexity scales linearly with the number of dimensions. Modes are computed on the fly in an *offline* step, by means of a progressive construction of successive best rank-one approximations that leads to the solution of eigenvalue problems. The obtained PGD approximation explicitly depends on all model parameters and constitutes a handbook of solutions. It can further be particularized for any value of the parameters in an *online* phase, with cheap and fast computations on light computing platforms, in order to perform real-time parametric or sensitivity analysis for optimization, inverse identification, or optimal control purposes. In this framework, parameter sensitivities can be performed in a straightforward manner, without resorting to classical adjoint state methods.

During the last decade, the PGD was successfully implemented and extensively used to solve multidimensional problems and perform efficient simulations. We may cite:

- stochastic problems [Nouy, 2008, Nouy, 2010b];
- multiphysics problems [Néron and Ladevèze, 2010, Dumon et al., 2011];
- plates and shells [Bognet et al., 2012];
- highly transient evolutions [Favoretto et al., 2019];
- data assimilation and inverse analysis [Ghnatios et al., 2012, Gonzalez et al., 2012, Louf and Champaney, 2013, Beringhier and Gigliotti, 2015, Nadal et al., 2015, Berger et al., 2016, Chamoin and Díez, 2016, Marchand et al., 2016, Berger et al., 2017, Signorini et al., 2017, Badias et al., 2018, Rubio et al., 2018, Rubio et al., 2019a, Rubio et al., 2019b];
- problems with parametrized geometry [Chevreuil et al., 2013, Ammar et al., 2014, Modesto et al., 2015, Zlotnik et al., 2015, Courard et al., 2016, Signorini et al., 2017, Chamoin and Thai, 2019, Sevilla et al., 2020].

A review on PGD applications can be found in [Chinesta et al., 2014]. Some approaches have also been proposed to apply the PGD to nonlinear models, using Newton-type algorithms [Chinesta et al., 2011], the LATIN-PGD method [Ladevèze, 1989, Ladevèze, 1999, Ladevèze et al., 2010b, Vitse et al., 2014, Neron et al., 2015, Ladevèze, 2016, Vitse et al., 2019], or alternative methods [Ryckelynck, 2009]. In addition, the coupling between PGD models was investigated in [Néron et al., 2016]. Eventually, the certification of PGD has been investigated in several recent works [Ammar et al., 2010, Ladevèze and Chamoin, 2011, Moitinho de Almeida, 2013, Alfaro et al., 2015, Chamoin et al., 2017, Chamoin and Thai, 2019, Reis et al., 2020].

### 4.1.2 PGD algorithm

Several approaches based on Galerkin, Petrov-Galerkin or minimal residual formulations may be implemented to compute PGD modes [Nouy, 2010a]. The standard approach is the so-called *progressive Galerkin* approach, which starts from a global weak formulation of the multi-dimensional problem and introduces successive order 1 corrections. Consider a general linear $D$-dimensional problem of the form:

$$\mathcal{A}u = g \quad , \quad u \in \mathcal{X} = \mathcal{X}_1 \otimes \mathcal{X}_2 \otimes \cdots \otimes \mathcal{X}_D \tag{4.1}$$

where $\mathcal{A}$ is an operator defined on the tensor space $\mathcal{X}$. PGD consists in searching an approximation $u_m$ of $u$ in a low-dimensional tensor subspace of $\mathcal{X}$ made of canonical format tensors of rank $m$:

$$u_m = \sum_{i=1}^{m} w_i^1 \otimes w_i^2 \cdots \otimes w_i^D \quad , \quad w_i^\mu \in \mathcal{X}_\mu \tag{4.2}$$

We introduce the global weak formulation of the problem:

$$\text{Find } u \in \mathcal{X} \text{ such that } B(u,v) = F(v) \quad \forall v \in \mathcal{X} \tag{4.3}$$

with

$$A(u,v) = \int_{\Omega_1}\int_{\Omega_2}\cdots\int_{\Omega_D} a(u,v) \quad ; \quad L(v) = \int_{\Omega_1}\int_{\Omega_2}\cdots\int_{\Omega_D} l(v) \tag{4.4}$$

and ($a$, $l$) the forms associated with the formulation in space. Assuming the rank $m-1$ decomposition $u_{m-1}$ is known, the rank $m$ decomposition $u_m = u_{m-1} + w^1 \otimes w^2 \cdots \otimes w^D$ is searched such that:

$$A(u_m, \delta v) = L(\delta v) \quad \forall \delta v = \delta w^1 \otimes w^2 \cdots \otimes w^D + w^1 \otimes \delta w^2 \cdots \otimes w^D + \cdots + w^1 \otimes w^2 \cdots \otimes \delta w^D \tag{4.5}$$

The test function $\delta v$ lives in the tangent space with $\delta w^\mu \in \mathcal{X}_\mu$. This formulation naturally leads to a nonlinear system where a set of coupled low-dimensional problems have to be solved:

$$\begin{aligned}
A(w^1 \otimes w^2 \cdots \otimes w^D, \delta w^1 \otimes w^2 \cdots \otimes w^D) &= R_{m-1}(\delta w^1 \otimes w^2 \cdots \otimes w^D) \quad \forall \delta w^1 \in \mathcal{X}_1 \\
A(w^1 \otimes w^2 \cdots \otimes w^D, w^1 \otimes \delta w^2 \cdots \otimes w^D) &= R_{m-1}(w^1 \otimes \delta w^2 \cdots \otimes w^D) \quad \forall \delta w^2 \in \mathcal{X}_2 \\
&\vdots = \vdots \\
A(w^1 \otimes w^2 \cdots \otimes w^D, w^1 \otimes w^2 \cdots \otimes \delta w^D) &= R_{m-1}(w^1 \otimes w^2 \cdots \otimes \delta w^D) \quad \forall \delta w^D \in \mathcal{X}_D
\end{aligned} \tag{4.6}$$

with $R_{m-1}(v) = L(v) - A(u_{m-1}, v)$. As it can be interpreted as an eigenvalue problem, this system may be solved using specific iterative algorithms inspired from classical power iterations algorithms dedicated to eigenvalue problems or dominant subspace methods [Nouy, 2010a]. It is in practice addressed with an iterative fixed-point (or alternating directions) strategy, by solving individual problems sequentially until convergence is reached (residual below a prescribed tolerance, stagnation of modal functions) or up to a given number of iterations. All modal functions are normalized so that the magnitude of a PGD mode is supported by space function alone. Additional ingredients may be added in the modal construction in order to optimize numerical performance, such as the orthogonalization of space modal functions (with Gram-Schmidt procedure), or the update of previous extra-parameter modal functions before starting again the power iterations algorithm in order to satisfy a stronger Galerkin orthogonality condition (this preliminary stage actually corresponds to a low-cost POD step).

### 4.1.3 Case of geometry parametrization

We follow here the approach defined in [Ammar et al., 2014, Zlotnik et al., 2015, Chamoin and Thai, 2019] and based on a geometric transformation to a reference configuration by means of a parametrized mapping. The mapping is defined as a function of a finite number of parameters, and is similar to isoparametric analysis in the FEA context. Alternative techniques have been investigated in order to address evolving geometries; let us cite fictitious domain or immersed boundary methods where the computational domain is extended from the actual shape to a fixed exterior domain [Haslinger and Makinen, 2003, Canuto and Kozubek, 2007, Nouy et al., 2011, Nouy and Pled, 2018], and boundary tracking methods with explicit description of the boundary [Courard et al., 2016].

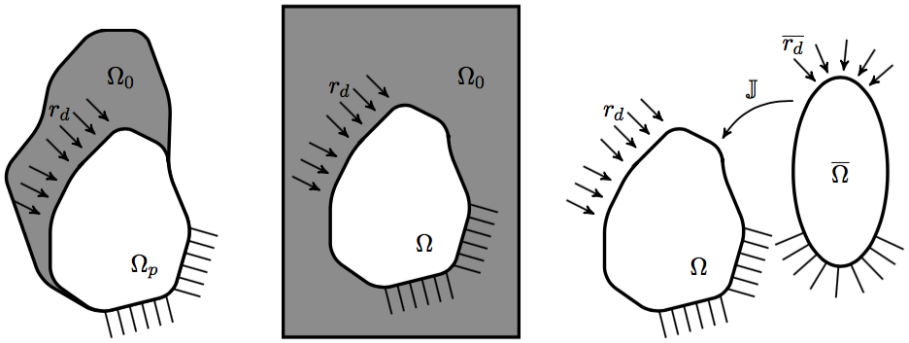


Figure 4.1: Possible numerical methods to deal with evolving geometries: boundary tracking method (left), immersed boundary method (center), and mapping from a reference shape (right).

The problem is reformulated by introducing a parameter-dependent mapping $M(\mathbf{p}_{geo}) : \Omega_{ref} \mapsto \Omega(\mathbf{p}_{geo})$ from a fixed reference physical domain $\Omega_{ref}$ (with coordinates $\mathbf{x}_{ref}$) to the current geometrically parametrized domain $\Omega(\mathbf{p}_{geo})$ (with coordinates $\mathbf{x}$). It involves the transformation matrix $\mathbb{T}(\mathbf{p}_{geo})$ such that $\mathbf{x} = \mathbb{T}\mathbf{x}_{ref}$ and is associated with Jacobian matrix $\mathbb{J} = \partial\mathbf{x}/\partial\mathbf{x}_{ref}$ and Jacobian $J = det(\mathbb{J})$. Components of the weak form are then pulled back to the reference configuration using the following properties:

$$\int_{\Omega} f(\mathbf{x}) = \int_{\Omega_{ref}} f(\mathbb{T}\mathbf{x}_{ref})J \quad ; \quad \frac{\partial f}{\partial \mathbf{x}} = \mathbb{J}^{-T}\frac{\partial f}{\partial \mathbf{x}_{ref}} \tag{4.7}$$

Such a geometrical transformation then allows the problem to be recast in a tensor product space and PGD to be applied in a direct manner.

## 4.2 PGD in local-global couplings

### 4.2.1 Parametrization of the local model

The interest in using PGD model reduction in the non-intrusive local-global coupling is to make the solution of local problems (1.13) more effective in a multi-query context. We remind that they read:

$$\begin{bmatrix} \mathbb{K}_L & -\mathbb{C}_L^T \\ -\mathbb{C}_L & 0 \end{bmatrix} \begin{bmatrix} \mathbf{U}_L \\ \mathbf{\Lambda} \end{bmatrix} = \begin{bmatrix} \mathbf{F}_L \\ -\mathbb{C}_G\mathbf{U}_G \end{bmatrix} \quad \text{or} \quad \begin{bmatrix} \mathbb{K}_L & \mathbb{C}_L^T \\ \mathbb{C}_L & 0 \end{bmatrix} \begin{bmatrix} \mathbf{U}_L \\ \mathbf{\Lambda} \end{bmatrix} = \begin{bmatrix} \mathbf{F}_L \\ \mathbb{C}_G\mathbf{U}_G \end{bmatrix} \tag{4.8}$$

with $\mathbb{K}_L$ the local stiffness matrix, and $(\mathbb{C}_L, \mathbb{C}_G)$ some coupling (mortar) matrices.

For these problems, we define parameters related to Dirichlet boundary conditions $\mathbf{U}_G$ (i.e. data exchanged with the global modal at the interface, using coupling operators that may deal with incompatible interfaces), as well as geometry parameters impacting matrices $(\mathbb{K}_L, \mathbb{C}_L, \mathbb{C}_G)$ and related to both local structural configuration inside the local zone (e.g. size and position of a hole) and geometry of the coupling patch. Denoting by $\mathbf{p}_{geo}$ the set of

geometry parameters, the constrained problem to be solved after parametric mapping (to come back to a fixed geometry) is of the form:

$$\begin{bmatrix} \mathbb{K}_L(\mathbf{p}_{geo}) & \mathbb{C}_L(\mathbf{p}_{geo})^T \\ \mathbb{C}_L(\mathbf{p}_{geo}) & 0 \end{bmatrix} \begin{pmatrix} \mathbf{U}_L \\ \mathbf{\Lambda} \end{pmatrix} = \begin{pmatrix} \mathbf{F}_L(\mathbf{p}_{geo}) \\ \mathbb{C}_G(\mathbf{p}_{geo})\mathbf{U}_G \end{pmatrix} \tag{4.9}$$

The associated construction of local virtual charts $\mathbf{U}_L(\mathbf{U}_G, \mathbf{p}_{geo})$ is made difficult as the number of parameters increases quickly, and therefore the use of reduced order modeling is natural.

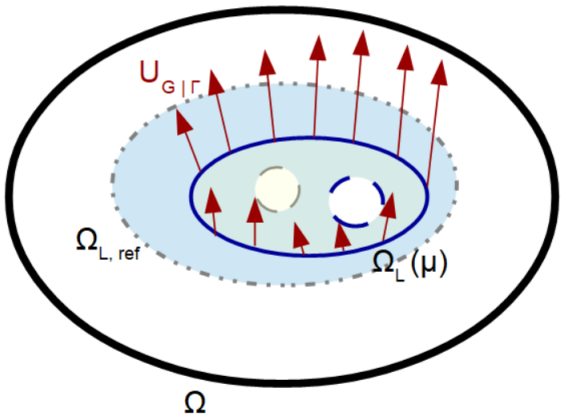


Figure 4.2: Geometric parameter and boundary condition parameter.

The Figure 4.2 represent the global and local domain and the parameter sets used in the PGD. There is two groups of parameters : the first one is the geometric parameters who define the current geometric from the reference configuration and the second one is the boundary condition imposed from the global model on the coupling interface (a FEM basis can be used to describe this displacement field).

### 4.2.2 PGD solution with specific algorithm

Addressing the previous constrained local problem, involving Lagrange multipliers and associated with an indefinite saddle point problem, with PGD is not a trivial task. A difficulty is in the application of PGD for constrained problems written with a Lagrangian (mixed) formulation. The main challenge in applying a constraint functional within the PGD framework arises from the fact that the coupled problem is decoupled into subproblems with respect to each variable, while the constraint should be applied to the solution globally. Another difficulty is in the combination of parameters on geometry and boundary conditions, with boundary conditions explicitly depending on the geometry of the local domain. Here we resort to the work in [Ainsworth, 2001] that specifically provides the following assumptions under which the constrained problem is well-posed:

1. $\mathbb{C}_G\mathbf{U}_G \in Range(\mathbb{C}_L)$; this condition simply ensures that constraints are not so restrictive as to rule out any possibility of a solution. That is, at least one function from the FE space satisfies the constraints $\mathbb{C}_L\mathbf{U}_L =$

$\mathbb{C}_G\mathbf{U}_G$;

2. $Ker(\mathbb{K}_L) \cap Ker(\mathbb{C}_L) = \{0\}$; this condition ensures that if a solution exists, then it is unique (if the condition is false, then there is a non-zero vector $\mathbf{W}_L$ such that $\mathbb{K}_L\mathbf{W}_L = \mathbb{C}_L\mathbf{W}_L = 0$, so that if $(\mathbf{U}_L, \mathbf{\Lambda})$ is solution then $(\mathbf{U}_L + \alpha\mathbf{W}_L, \mathbf{\Lambda})$ is also solution for any choice of $\alpha$;

3. $\mathbb{C}_L$ is of full rank; this condition simply means that the constraints are linearly independent. In particular, it implies that the following matrices are well defined:

$$\mathbb{P}_L = \mathbb{C}_L^T(\mathbb{C}_L\mathbb{C}_L^T)^{-1}\mathbb{C}_L \quad ; \quad \mathbb{Q}_L = \mathbb{I} - \mathbb{C}_L^T(\mathbb{C}_L\mathbb{C}_L^T)^{-1}\mathbb{C}_L \quad ; \quad \mathbb{R}_L = \mathbb{C}_L^T(\mathbb{C}_L\mathbb{C}_L^T)^{-1} \tag{4.10}$$

The matrix $\mathbb{Q}_L$ (and in fact $\mathbb{P}_L$ too) is idempotent that is $\mathbb{Q}_L^2 = \mathbb{Q}_L$, and satisfies $\mathbb{C}_L\mathbb{Q}_L = 0$.

It is then shown that, under the previous conditions, a direct characterization of the unique solution $\mathbf{U}_L$ is provided by $\tilde{\mathbb{K}}_L\mathbf{U}_L = \tilde{\mathbf{F}}_L$ with

$$\tilde{\mathbb{K}}_L = \mathbb{C}_L^T\mathbb{C}_L + \mathbb{Q}_L^T\mathbb{K}_L\mathbb{Q}_L \quad ; \quad \tilde{\mathbf{F}}_L = \mathbb{C}_L^T\mathbb{C}_G\mathbf{U}_G + \mathbb{Q}_L^T(\mathbf{F}_L - \mathbb{K}_L\mathbb{R}_L\mathbb{C}_G\mathbf{U}_G) \tag{4.11}$$

and the corresponding Lagrange multiplier vector is $\mathbf{\Lambda} = \mathbb{R}_L^T(\mathbf{F}_L - \mathbb{K}_L\mathbf{U}_L)$.
The proof is given in Appendix A. Note that if the original matrix $\mathbb{K}_L$ is symmetric, then so is the reduced matrix $\tilde{K}_L$, meaning that the possibility of using a conjugate gradient solver is not sacrificed through the imposition of constraints.

Consequently, the parametrized local problem is recast as:

$$\mathbb{Z}(\mathbf{p}_{geo})\mathbf{U}_L(\mathbf{p}_{geo}, \mathbf{U}_G) = \mathbb{C}(\mathbf{p}_{geo})\mathbf{U}_G + \mathbf{F}(\mathbf{p}_{geo}) \tag{4.12}$$

with

$$\mathbb{Z} = \mathbb{C}_L^T\mathbb{C}_L + \mathbb{Q}_L^T\mathbb{K}_L\mathbb{Q}_L \quad ; \quad \mathbb{C} = (\mathbb{C}_L^T - \mathbb{Q}^T\mathbb{K}_L\mathbb{R}_L)\mathbb{C}_G \quad ; \quad \mathbf{F} = \mathbb{Q}_L^T\mathbf{F}_L \tag{4.13}$$

The solution $\mathbf{U}_L(\mathbf{p}_{geo}, \mathbf{U}_G)$ is searched using PGD, with separated-variable form:

$$\mathbf{U}_L(\mathbf{p}_{geo}, \mathbf{U}_G) = \sum_{i=1}^{N_{pgd}} \mathbf{f}^i.g^i(\mathbf{p}_{geo}).\prod_{j=1}^{n_{U_G}} \gamma^{i,j}(U_G^j) \tag{4.14}$$

where $U_G^j$ are nodal components of $\mathbf{U}_G$ i.e. $\mathbf{U}_G = \sum_{j=1}^{n_{U_G}} U_G^j\mathbf{e}_j$.

The PGD formulation is implemented after decomposing operators as $\mathbb{Z}(\mathbf{p}_{geo}) = \sum_{i=1}^{n_Z} \varphi^i(\mathbf{p}_{geo})\mathbb{Z}^i$, $\mathbb{C}(\mathbf{p}_{geo}) = \sum_{i=1}^{n_C} \chi^i(\mathbf{p}_{geo})\mathbb{C}^i$, and $\mathbf{F}(\mathbf{p}_{geo}) = \sum_{i=1}^{n_F} \psi^i(\mathbf{p}_{geo})\mathbf{F}^i$ (truncated SVD decomposition). Introducing the global weak form

associated with (4.12):

$$\int_{\mathcal{P}_{geo}} \int_{I_G} \delta \mathbf{U}^T (\mathbb{Z}(\mathbf{p}_{geo}) \mathbf{U}_L(\mathbf{p}_{geo}, \mathbf{U}_G) - \mathbb{C}(\mathbf{p}_{geo}) \mathbf{U}_G - \mathbf{F}(\mathbf{p}_{geo})) = 0 \quad \forall \delta \mathbf{U} \tag{4.15}$$

a progressive approach is followed to compute the last mode of the decomposition at order $N_{pgd}$. Using the following test function in the tangent space:

$$\delta \mathbf{U} = \delta \mathbf{f}.g(\mathbf{p}_{geo}). \prod_{j=1}^{n_{U_G}} \gamma^j(U_G^j) + \mathbf{f}.\delta g(\mathbf{p}_{geo}). \prod_{j=1}^{n_{U_G}} \gamma^j(U_G^j) + \dots \tag{4.16}$$

it yields the following elementary problems:

- problem in space

$$\begin{aligned}
\left[ (\sum_{i=1}^{n_S}) \mathbb{S}^i \int_{\mathcal{P}_{geo}} g(\mathbf{p}_{geo}) \phi^i(\mathbf{p}_{geo}) g(\mathbf{p}_{geo})) \prod_{k=1}^{n_{U_G}} \int_{I_G^k} (\gamma^k(U_G^k))^2 \right] \mathbf{f} &= (\sum_{i=1}^{n_F} \mathbf{F}^i \int_{\mathcal{P}_{geo}} g(\mathbf{p}_{geo}) \psi^i(\mathbf{p}_{geo})) \prod_{k=1}^{n_{U_G}} \int_{I_G^k} 1.\gamma^k(U_G^k) \\
&- \sum_{j=1}^{N_{pgd}-1} \left[ (\sum_{i=1}^{n_S}) \mathbb{S}^i \int_{\mathcal{P}_{geo}} g(\mathbf{p}_{geo}) \phi^i(\mathbf{p}_{geo}) g^j(\mathbf{p}_{geo})) \prod_{k=1}^{n_{U_G}} \int_{I_G^k} \gamma^k(U_G^k).\gamma^{j,k}(U_G^k) \right] \mathbf{f}^j \\
&+ \left[ \sum_{i=1}^{n_C} \mathbb{C}^i \int_{\mathcal{P}_{geo}} g(\mathbf{p}_{geo}) \chi^i(\mathbf{p}_{geo}) \right] (\sum_{j=1}^{n_{U_G}} (\prod_{k \neq j} \int_{I_G^k} \gamma^k(U_G^k)).(\int_{I_G^j} U_G^j \gamma^j(U_G^j)) \mathbf{e}_j)
\end{aligned} \tag{4.17}$$

- problem in the geometry parameters (with discretization $g(\mathbf{p}_{geo}) = \mathbb{N}(\mathbf{p}_{geo})\hat{\mathbf{g}}$):

$$\begin{aligned}
\left[ \prod_{k=1}^{n_{U_G}} \int_{I_G^k} (\gamma^k)^2 . \sum_{i=1}^{n_S} (\mathbf{f}^T \mathbb{S}^i \mathbf{f}) \mathbb{M}_p(\hat{\phi}^i \otimes \hat{\mathbf{g}} \right] &= \prod_{k=1}^{n_{U_G}} \int_{I_G^k} 1.\gamma^k(U_G^k). \sum_{i=1}^{n_F} (\mathbf{f}^T \cdot \mathbf{F}^i). \mathbb{M}_p \hat{\phi}^i) \\
&- \sum_{j=1}^{N_{pgd}-1} \left[ \prod_{k=1}^{n_{U_G}} \int_{I_G^k} \gamma^k(U_G^k).\gamma^{j,k}(U_G^k).(\sum_{i=1}^{n_S} (\mathbf{f}^T \mathbb{S}^i \mathbf{f}) \mathbb{M}_p(\hat{\phi}^i \otimes \hat{\mathbf{g}}^j)) \right] \\
&+ \sum_{i=1}^{n_C} (\mathbf{f}^T . \mathbb{C}^i) \left( \sum_{j=1}^{n_{U_G}} (\prod_{k \neq j} \int_{I_G^k} \gamma^k(U_G^k)).(\int_{I_G^j} U_G^j \gamma^j(U_G^j)) \mathbf{e}_j \right) \mathbb{M}_p \hat{\chi}^i
\end{aligned} \tag{4.18}$$

- problem in the boundary conditions

$$\begin{aligned}
&\left[(\sum_{i=1}^{n_S}(\mathbf{f}^T\mathbb{S}^i\mathbf{f})\int_{\mathcal{P}_{geo}} g(\mathbf{p}_{geo})\phi^i(\mathbf{p}_{geo})g(\mathbf{p}_{geo}))\prod_{k\neq K}\int_{I_G^k}(\gamma^k(U_G^k))^2\right]\gamma^K(U_G^K) = \\
&\qquad (\sum_{i=1}^{n_F}(\mathbf{f}^T\mathbf{F}^i)\int_{\mathcal{P}_{geo}} g(\mathbf{p}_{geo})\psi^i(\mathbf{p}_{geo}))\prod_{k\neq K}\int_{I_G^k} 1.\gamma^k(U_G^k) \\
-\sum_{j=1}^{N_{pgd}-1}&\left[(\sum_{i=1}^{n_S}(\mathbf{f}^T\mathbb{S}^i\mathbf{f}^j)\int_{\mathcal{P}_{geo}} g(\mathbf{p}_{geo})\phi^i(\mathbf{p}_{geo})g^j(\mathbf{p}_{geo}))\prod_{k\neq K}\int_{I_G^k}\gamma^k(U_G^k).\gamma^{j,k}(U_G^k)\right]\gamma^{j,K}(U_G^K) \\
&+\left[\sum_{i=1}^{n_C}(\mathbf{f}^T.\mathbb{C}^i)\int_{\mathcal{P}_{geo}} g(\mathbf{p}_{geo})\chi^i(\mathbf{p}_{geo})\right]\left(\sum_{j\neq K}(\prod_{k\neq j}\int_{I_G^k}\gamma^k(U_G^k)).(\int_{I_G^j}U_G^j\gamma^j(U_G^j))\mathbf{e}_j\right. \\
&\qquad \left.+(\prod_{k\neq K}\int_{I_G^k}\gamma^k(U_G^k).U_G^K.\mathbf{e}_K\right)
\end{aligned} \tag{4.19}$$

*Remark. We decide here to apply local PGD after implementing the local-global coupling strategy. An alternative option would be to first implement PGD for the monolithic problem before using model coupling to compute PGD modes. The first option appears more effective as PGD modes contain more local information.*

*Remark. Several strategies were developed and analyzed in [Kergrene et al., 2017] to use PGD on problems with affine constraints, by means of penalization, (augmented-) Lagrangian, or double Lagrangian, and with various implementations such as direct or iterative Uzawa method [Uzawa, 1958]. For local problems* (4.8)*, the direct Uzawa method manipulates the first equation to get* $\mathbf{U}_L = \mathbb{K}_L^{-1}(\mathbf{F}_L - \mathbb{C}_L^T\mathbf{\Lambda})$ *and yields* $\mathbb{C}_L(\mathbb{K}_L^{-1}(\mathbf{F}_L - \mathbb{C}_L^T\mathbf{\Lambda})) = \mathbb{C}_L\mathbb{K}_L^{-1}\mathbf{F}_L - \mathbb{C}_L\mathbb{K}_L^{-1}\mathbb{C}_L^T\mathbf{\Lambda} = \mathbb{C}_G\mathbf{U}_G$ *after incorporating in the second equation. We thus get* $\mathbb{S}_L\mathbf{\Lambda} = \mathbb{C}_L\mathbb{K}_L^{-1}\mathbf{F}_L - \mathbb{C}_G\mathbf{U}_G$*, with* $\mathbb{S}_L = \mathbb{C}_L\mathbb{K}_L^{-1}\mathbb{C}_L^T$ *the Schur complement, and the initial local problem is recast as (upper triangular matrix):*

$$\begin{bmatrix} \mathbb{K}_L(\mathbf{p}_{geo}) & \mathbb{C}_L^T \\ 0 & \mathbb{S}_L \end{bmatrix}\begin{pmatrix} \mathbf{U}_L \\ \mathbf{\Lambda} \end{pmatrix} = \begin{pmatrix} \mathbf{F}_L \\ \mathbb{C}_L\mathbb{K}_L^{-1}\mathbf{F}_L - \mathbb{C}_G\mathbf{U}_G \end{pmatrix} \tag{4.20}$$

*As direct Uzawa performs a triangularization by blocks, the constraint is decoupled from the rest of the problem and the problem can be solved by a backward substitution by blocks. However, it still requires to explicitly invert the stiffness matrix* $\mathbb{K}_L$*. Iterative Uzawa provides a way to avoid explicitly calculating the inverse* $\mathbb{K}_L^{-1}$*, solving the constraint equation in an iterative manner (e.g. with a descent algorithm).*

*The considered strategies were applied to two classes of problems with a 2D Poisson equation: the pure Neumann case (with constraint to recover uniqueness of the solution), and the Robin case (where the constraint forces the solution to move way from the already existing unique global minimizer of the energy functional). It was shown that the Uzawa method provides good performance when the Schur complement is small, while Lagrangian/augmented Lagrangian methods offer satisfactory results otherwise.*

*These do not apply to the current Lagrangian formulation, and an alternative strategy is thus introduced. Another alternative would be to prescribe Dirichlet boundary conditions by enforcing them in a first PGD mode.*

*Remark. The method in [Yu et al., 2018] is used to compute the SVD form (with separation of variables) for stiffness operator, right-hand side, and stress matrix which are large sparse matrices at the global level, in order to circumvent having to set the number of SVD modes a priori, and to be able to work with fixed accuracy without knowing the snapshot matrix rank. As the same connectivity table is used for all geometrical configurations, position of nul terms is the same and can be extracted to build snapshot matrices that only contain useful terms.*

*Remark. The number of prescribed values $U_G^j$ usually grows very quickly with the size of the domain boundary, which may make the PGD convergence difficult. However, in our application, the prescribed displacements come from the solution of a coarse global solution, so that the number of independent parameters can be drastically reduced.*

*Remark. Even though a discretization over the parameter space is introduced to numerically compute and store modal functions, it is not associated with a given numerical approximation method that we would have to design. Indeed, the associated mesh size can be taken a small as needed with low CPU cost (no ODE or PDE is solved).*

### 4.2.3 Online use of the local PGD solution

The previously constructed local PGD solution is used online as a virtual chart for the local solution in the non-intrusive coupling. For any new value of the parameter set, coming from new boundary conditions (along iterations for the coupling algorithm), new geometrical configuration of the local zone $\Omega_L$ (along iterations in the adaptive procedure), or new structural configuration inside the local zone (in design optimization or uncertainty quantification for instance), the local solution is computed in a straightforward manner by a direct evaluation of the local PGD solution.

### 4.2.4 Error control with local PGD models

As any numerical method, the use of PGD in the non-intrusive coupling is associated with an additional error source which needs to be effectively assessed and controlled to ensure the quality of the results for robust optimization and design. For this purpose, we still resort to the CRE concept, using a strategy similar to that developed in [Ladevèze and Chamoin, 2011, Chamoin and Ladevèze, 2012, Ladevèze and Chamoin, 2012, Chamoin et al., 2017, Chamoin and Thai, 2019] for addressing *a posteriori* error estimation when constructing the PGD model. This strategy is based on the specific processing of the approximate PGD solution at hand to recover admissible fields. It enables to evaluate the error level over the whole parametric space and to split error sources between PGD truncation and discretization errors, by introducing specific error indicators. This helps driving a greedy adaptive algorithm to save

CPU time and memory space for a prescribed error tolerance (i.e. optimizing the computational effort by defining a suitable PGD approximation in terms of required number of terms in the modal representation of the solution, but also in terms of the discretization meshes used to compute modes). In the following the CRE-based error estimation tools and adaptive algorithm are used to control the error due to PGD truncation, ensuring that it remains much lower than discretization error in the local zone $\Omega_L$.

## 4.3 Numerical results

In this part we focus on the numerical results for the construction of the approximate local PGD solution when we consider geometric parameters describing some details inside the local domain (for example the radius of a hole in the local domain or the position of this hole). The coupling interface between the local domain and the global domain is unchanged with those parameters.

The result of this method for geometric parameters describing the local domain (position, dimension or shape) is very similar to the previous one but the coupling interface between the local domain and the global domain is changed. As there is not the same discretization of this interface for each size of the local domain, if we use our local PGD solution as a virtual chart in the local-global non intrusive framework, a projection is needed for the global solution inside the local domain to the support of the parametric description of the local domain.

For this application, we use the non-intrusive local-global coupling technique to perform local analysis in the vicinity of a hole. In the global model, the hole is not represented. This hole is represented in the local model which is centered on it. The initial geometry and configuration of the global and local domains are given in Figure 4.3. The global domain is meshed using a structured mesh made of T3 triangular elements. The local domain is meshed using T3 triangular elements.

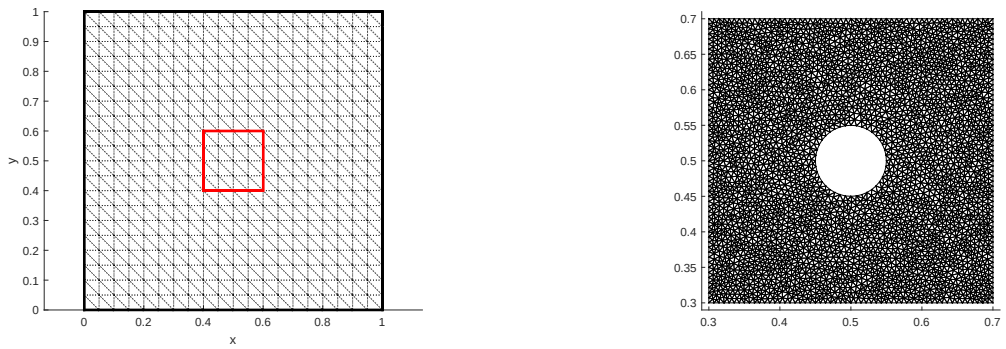


(a) Global mesh (with the coupling interface).

(b) Initial local reference mesh.

Figure 4.3: Initial coupling configuration and mesh.

The loading case we study is the following (Figure 4.4): we apply a uniform traction force along the direction $x$

on the right side of the plate. As Dirichlet boundary conditions, the translation along the $y$ axis on the bottom edge and the translation along the $x$ axis on the left edge are restrained.

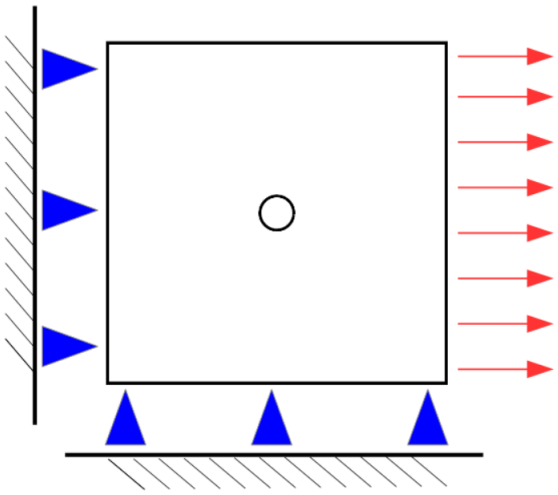

Figure 4.4: Case study.

The material for the whole domain is set as an homogeneous, isotropic and linear elastic with a Young modulus $E = 200GPa$ and a Poisson ratio $\nu = 0.3$. The same material is used for both global model and local model. We will consider two geometric parameters for our study : the radius of the hole in the local domain and the position of the hole (y coordinate).

Figure 4.5 shows the parameterization of the local domain and its Dirichlet boundary conditions. The red and blue arrows represent the parameters that come from the coarse description and define the Dirichlet boundary conditions, the number next to each arrow is the identification number of this particular boundary condition component.

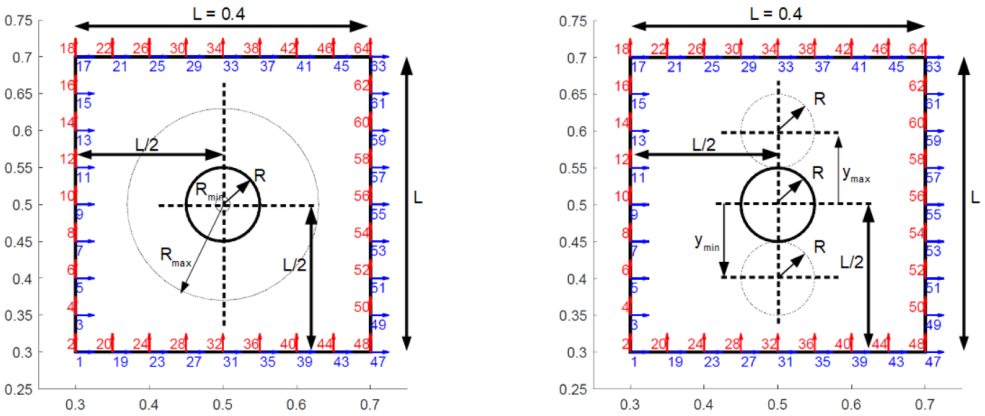


(a) Radius as a geometric parameter.

(b) Position as a geometric parameter.

Figure 4.5: Dirichlet Boundary conditions and parameterization of the local domain.

The description of the local domain is obtained from the transformation of the fixed reference physical domain shown in Figure 4.3(b). The evolution of the local mesh in the range of the parameter set is shown in Figure 4.6 (for

the radius) and in Figure 4.7 (for the vertical position).

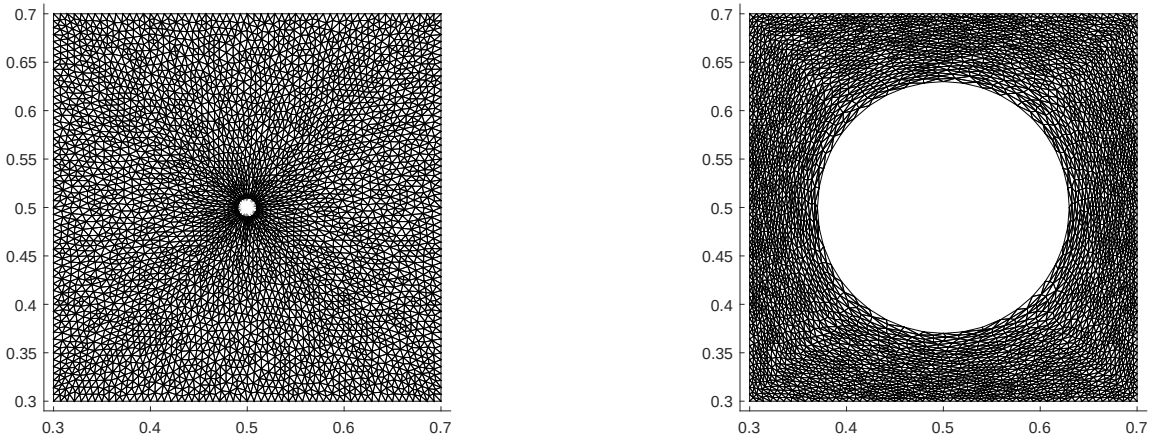


(a) Physical domain for Radius = 0.01.

(b) Physical domain for Radius = 0.13.

Figure 4.6: Radius of the hole as a parameter.

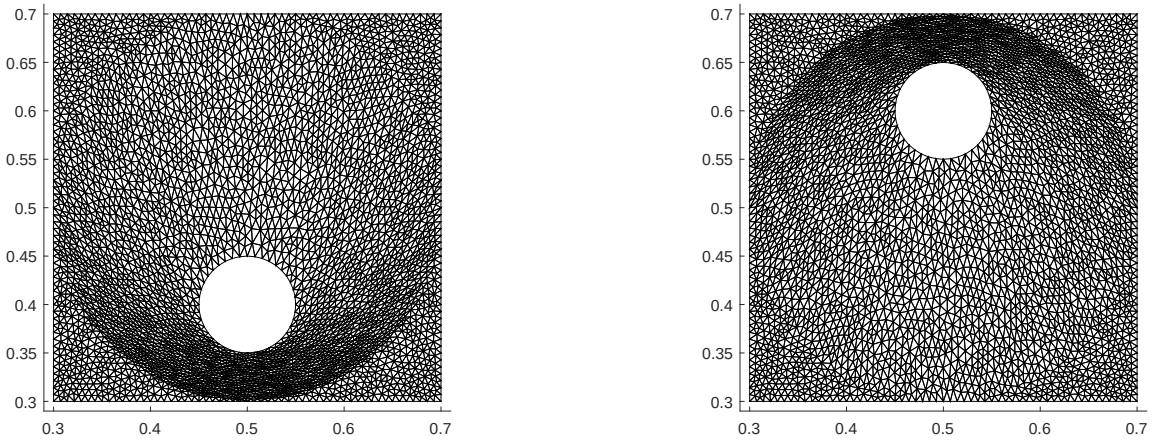


(a) Physical domain for Position = -0.1.

(b) Physical domain for Position = 0.1.

Figure 4.7: Position of the hole as a parameter.

As we can see the transformation we used consists in moving the nodes of the mesh such that we respect the configuration described by the parameter (position and radius of the hole). Therefore the connectivity table of the element is unchanged and the stiffness operator has the same support for each value of the parameter. Nevertheless, if the current geometrically parametrized domain is not similar enough to the fixed reference physical domain, the aspect ratio of the mesh element can impact numerical results.

Then we evaluate for a set of parameters the stiffness operator and right-hand side of the discretized problem. A

separated form of the stiffness operator and right-hand side are computed using the singular value decomposition.

A PGD solution is then computed for each boundary condition. We have a linear problem, so we can simplify the local solution such as :

$$\mathbf{U}_L(\mathbf{p}_{geo}, \mathbf{U}_G) = \sum_{j=1}^{n_{U_G}} \left( \sum_{i=1}^{N_{pgd}} \mathbf{f}_j^i . g_j^i(\mathbf{p}_{geo}) \right) . U_G^j \tag{4.21}$$

For each boundary condition, 5 to 6 PGD modes are needed to approximate the solution with sufficient accuracy. Figures 4.9 to 4.12 show some examples for these modes. The relative Frobenius norm of the modes is shown in Figure 4.8 for the radius as a parameter and for the first boundary condition. The other boundary conditions show similar evolutions.

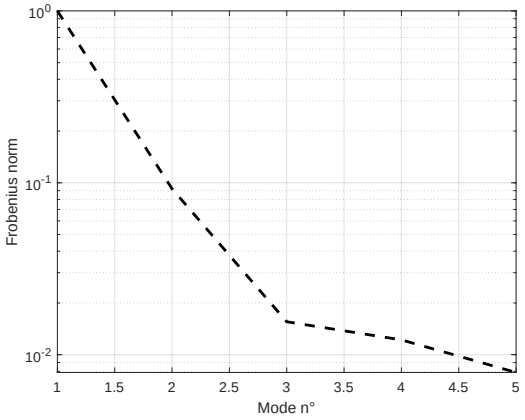


Figure 4.8: Evolution of the Frobenius norm of the PGD modes.

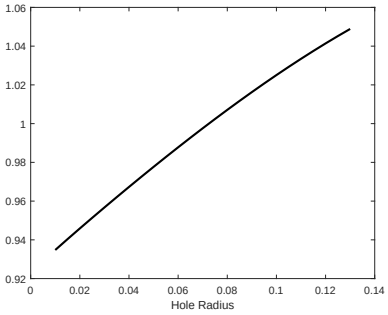


(a) geometric parameter function

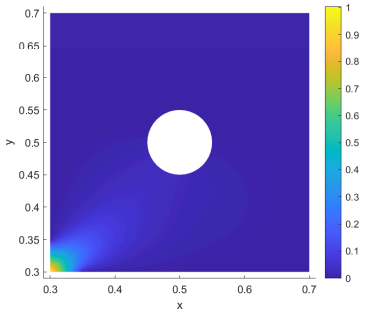


(b) space function $U_x$

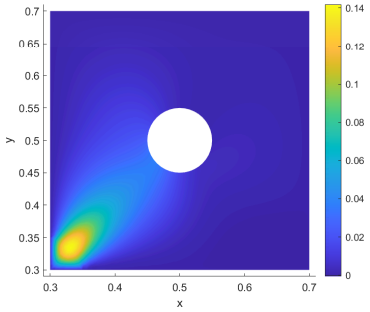


(c) space function $U_y$

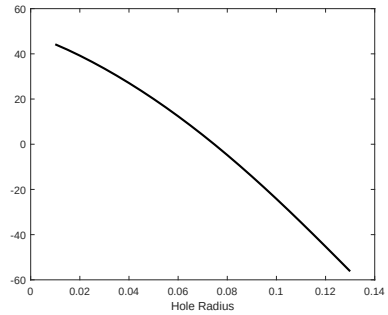


(d) geometric parameter function

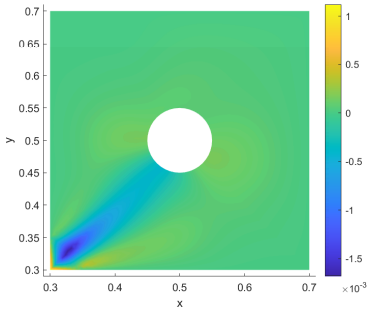


(e) space function $U_x$

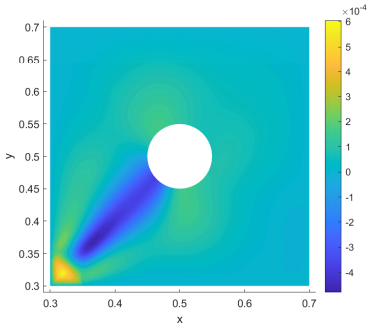


(f) space function $U_y$

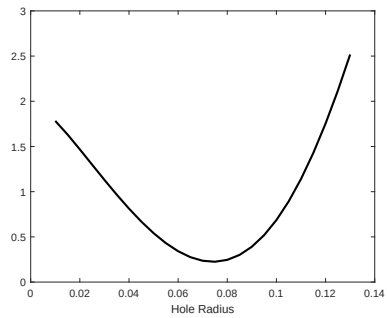


(g) geometric parameter function

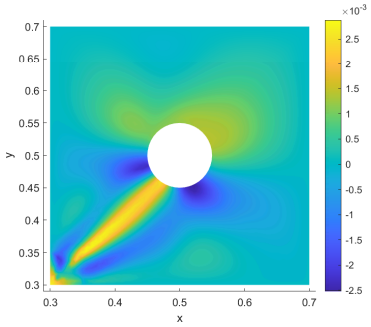


(h) space function $U_x$

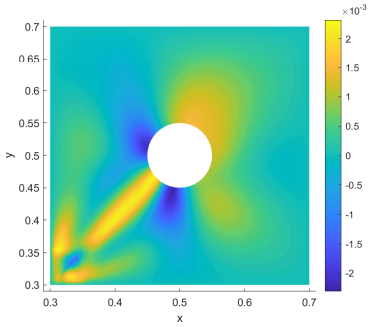


(i) space function $U_y$

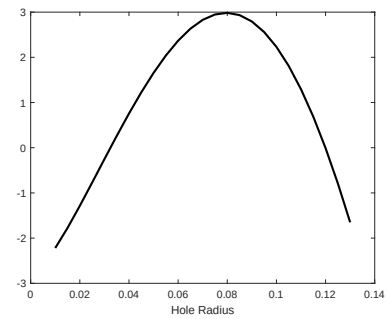


(j) geometric parameter function

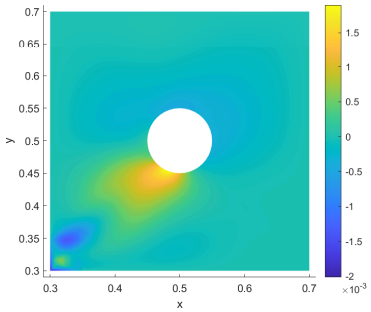


(k) space function $U_x$

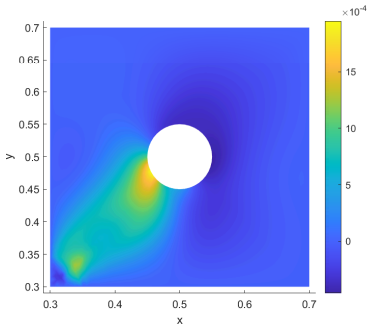


(l) space function $U_y$

Figure 4.9: Parameter: radius - Boundary condition 1 - Mode 1 to 4.

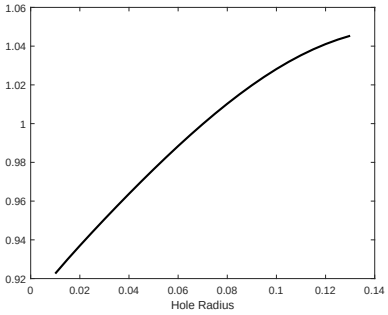


(a) geometric parameter function

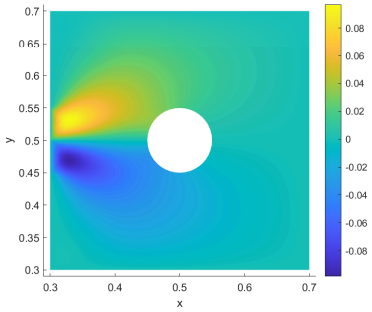


(b) space function $U_x$

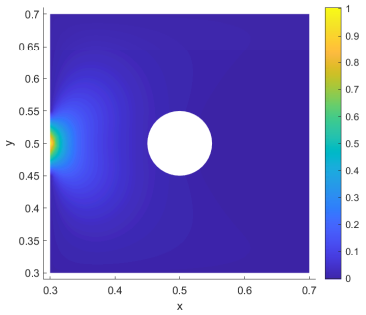


(c) space function $U_y$

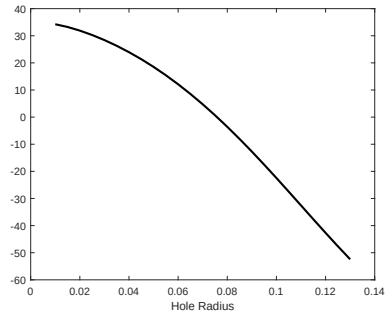


(d) geometric parameter function

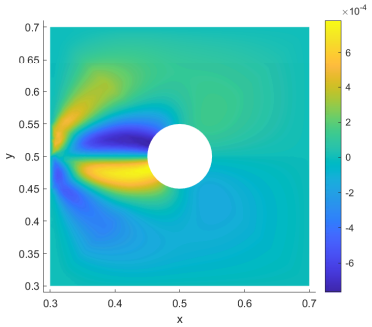


(e) space function $U_x$

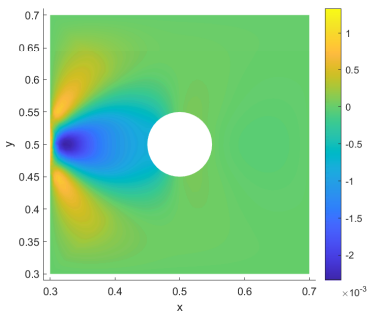


(f) space function $U_y$

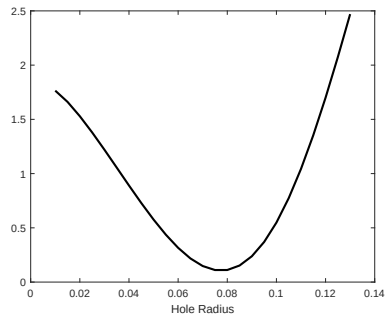


(g) geometric parameter function

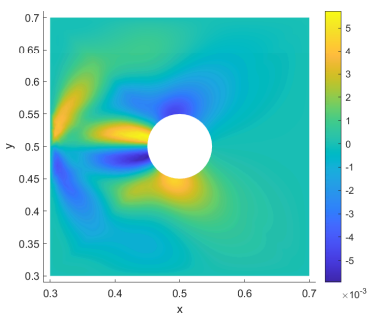


(h) space function $U_x$

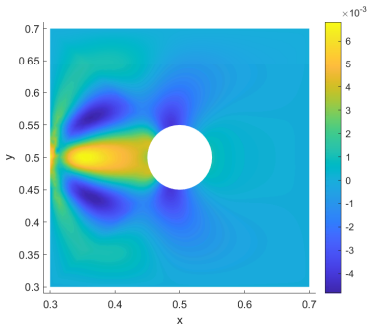


(i) space function $U_y$

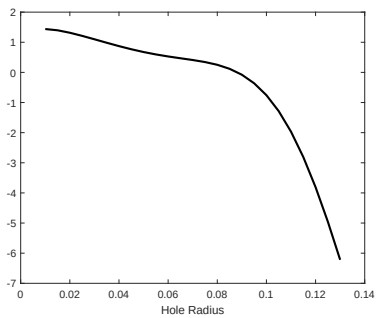


(j) geometric parameter function

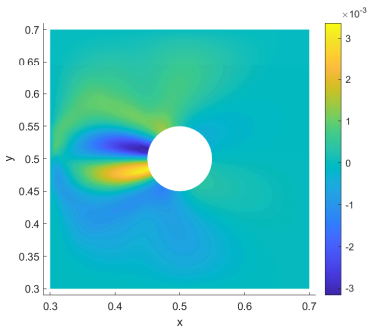


(k) space function $U_x$

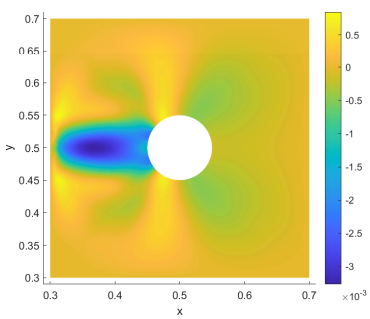


(l) space function $U_y$

Figure 4.10: Parameter: radius - Boundary condition 10 - Mode 1 to 4.

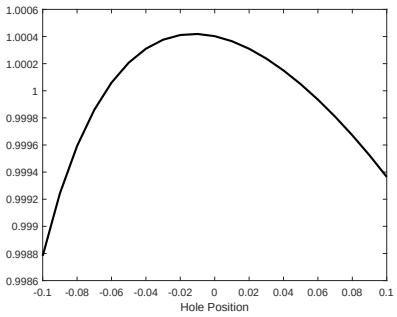


(a) geometric parameter function

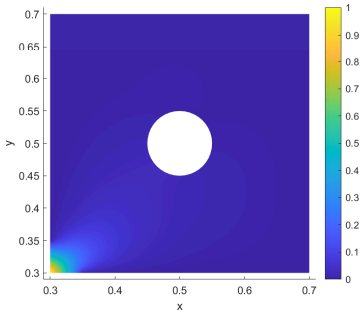


(b) space function $U_x$

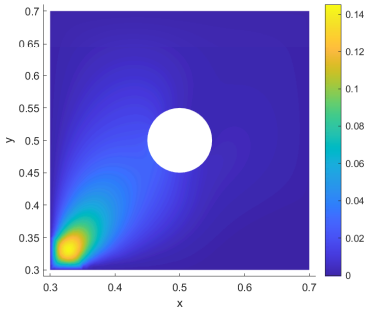


(c) space function $U_y$

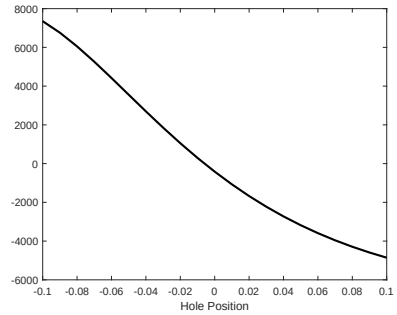


(d) geometric parameter function

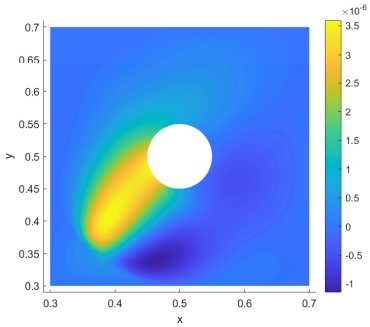


(e) space function $U_x$

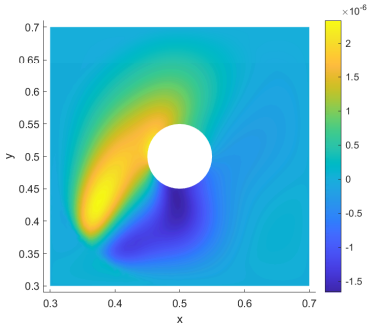


(f) space function $U_y$

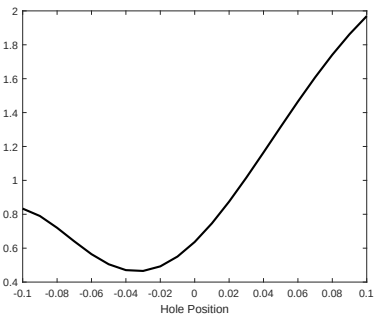


(g) geometric parameter function

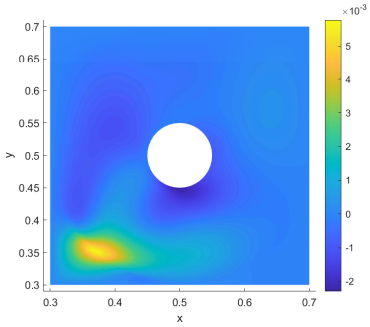


(h) space function $U_x$

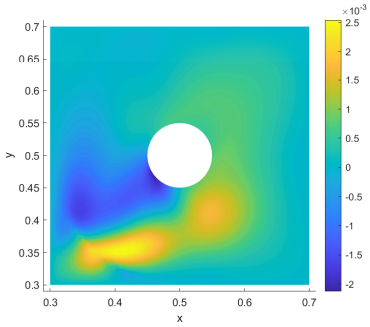


(i) space function $U_y$

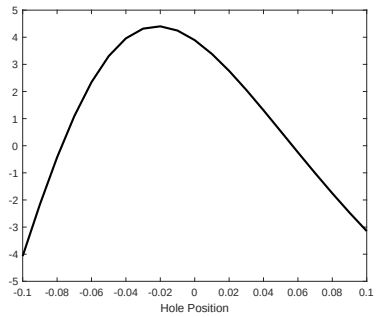


(j) geometric parameter function

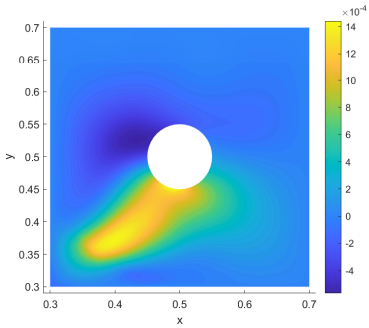


(k) space function $U_x$

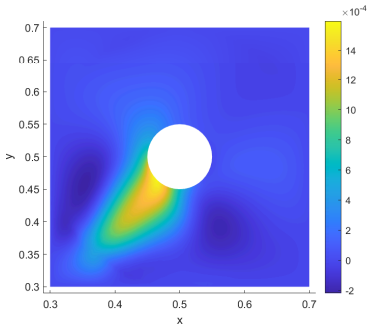


(l) space function $U_y$

Figure 4.11: Parameter: position - Boundary condition 1 - Mode 1 to 4.

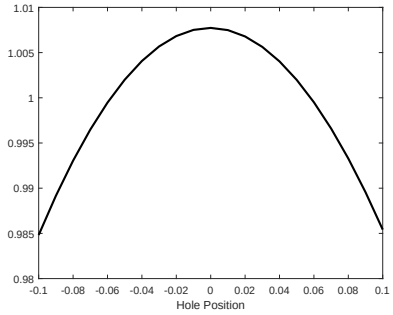


(a) geometric parameter function

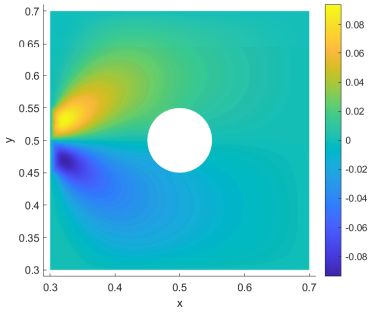


(b) space function $U_x$

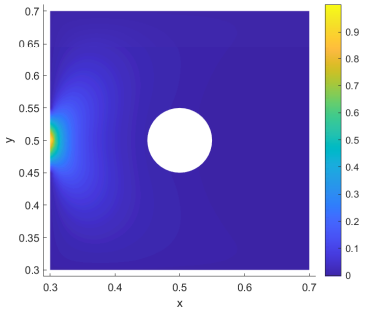


(c) space function $U_y$

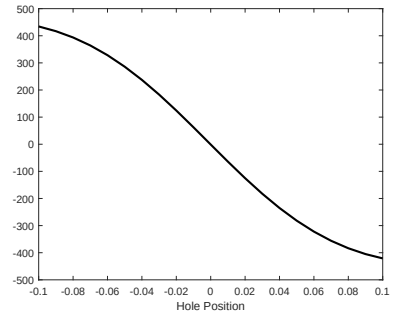


(d) geometric parameter function

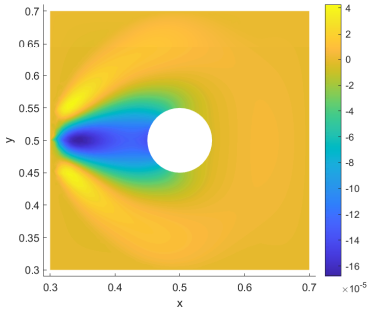


(e) space function $U_x$

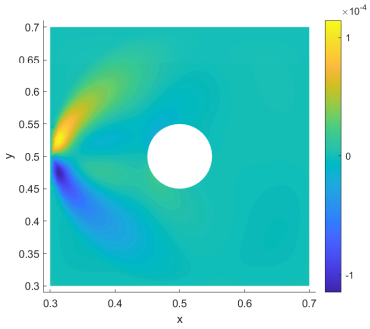


(f) space function $U_y$

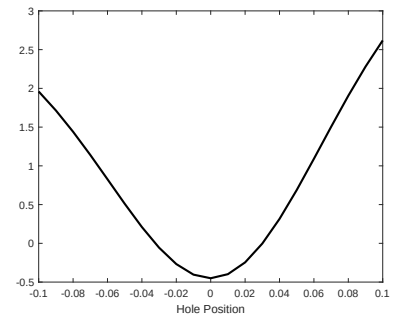


(g) geometric parameter function

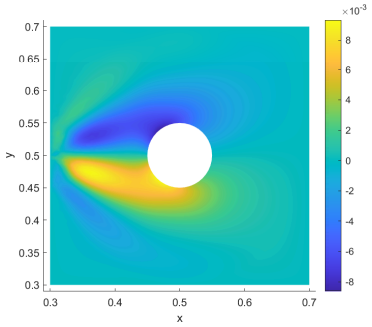


(h) space function $U_x$

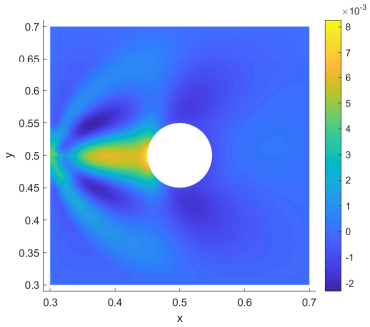


(i) space function $U_y$

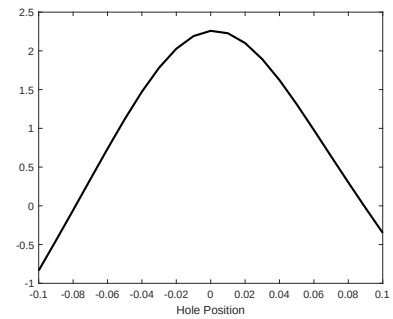


(j) geometric parameter function

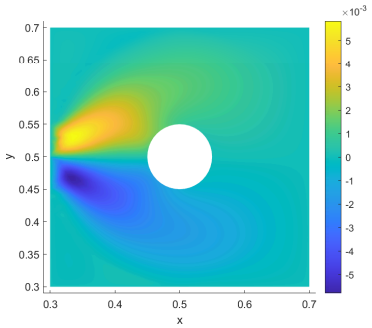


(k) space function $U_x$

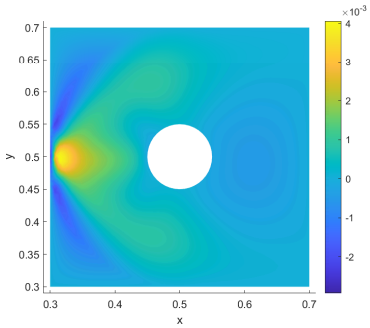


(l) space function $U_y$

Figure 4.12: Parameter: position - Boundary condition 10 - Mode 4.

With this local PGD solution we are able to compute the global local solution for any value of the parameter set inside the range of the PGD chart. Figure 4.13 shows an evaluation of the local domain as a solution of the local-global non-intrusive framework, the geometric parameter considered is the radius of the hole

*Remark. In order to obtain better results for the computation of local PGD solution, decomposing the Dirichlet boundary condition into rigid body displacements is necessary. This can be done at low cost by computing the average displacement and average rotation of the coupling interface.*

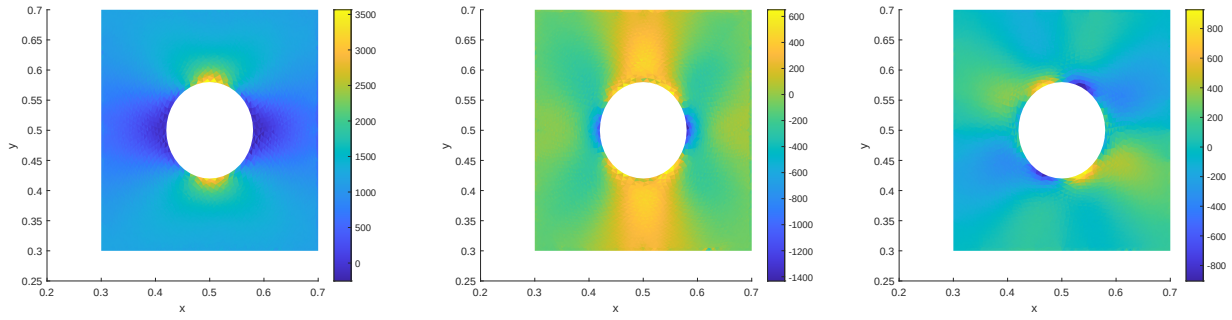


(a) Component $\sigma_{11}$ (b) Component $\sigma_{22}$ (c) Component $\sigma_{12}$

Figure 4.13: Local solution - parameter: $Radius = 0.008$.

The strength of using a virtual chart for the local solution is to be able to compute quickly and efficiently the solution for a vast query of geometric parameters. We are then able to perform a parametric optimization. For example, the maximum von Mises Stress with respect to the radius of the hole or its position can be obtained (cf. Figure 5.4 ).

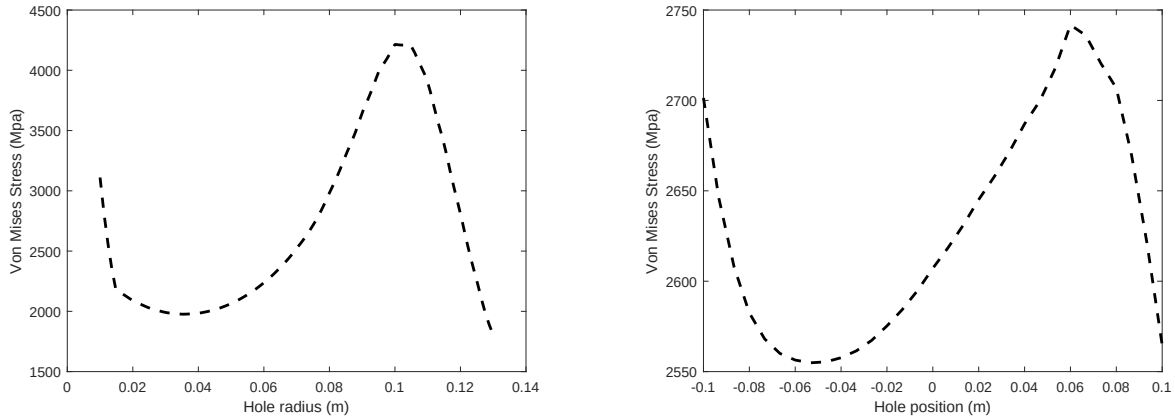


(a) Hole radius as a geometric parameter. (b) Hole position as a geometric parameter.

Figure 4.14: Evolution of a quantity of interest (maximum Von Mises stress) with respect to geometric parameter.

We can notice that the PGD solution is less accurate on the border of the parametric domain. Multiple reasons

can explain these results : firstly the PGD approximation is intrinsically less accurate on the parametric domain border, secondly the mesh could have been deformed too much and a locking element phenomenon can be observed, and finally the local detail may be too close to the coupling interface and the coarse discretization on the interface is then polluting the solution inside the local domain.

## 4.4 Partial conclusions

In this chapter, we developed a local model reduction technique in order to simplify computations associated with the local domain in the framework of the non-intrusive local-global couplings. It appears as a relevant tool when performing local design modifications, or in the adaptive procedure.

The overall coupling-PGD method with error control may also constitute a relevant tool for robust and multi-query analysis in structural engineering activities, with local analysis on large and complex parts.

In the next chapter, the interest of the method is shown for optimization and robust design.

# Chapter 5

# Application to robust design

In this last chapter, we implement the previously developed tools in order to conduct, in an effective manner, optimal or robust design (in a certain sense) which is a main concern in industry. We show the potential of certified and parametrized non-intrusive local-global coupling for this purpose by considering an academic example (plate with a hole).

## 5.1 Introduction to robust design

### 5.1.1 Context

We place in the framework of tolerant and reactive structural design. In many situations, available information during the design is not precise as it corresponds to an early step of the life cycle of the structure, and as it is necessary to let sufficient flexibility for manufacturing (e.g. in terms of local geometrical details). A set of possible design configurations thus needs to be considered. Uncertainties in structural mechanics, and in particular during the early phases of analysis and design, can play an extremely important role, affecting not only the safety and reliability of structures and their mechanical components, but also the level of their performance. Taking into account uncertainties in the early stages of the design, by means of numerical simulations (e.g. to detect failure), aims at modernizing industrial approaches by enabling the justification of larger tolerance intervals, and thus reducing costs.
A typical case is aerospace industry that needs, in a competitive context, to adapt by reducing the duration of development cycles for products such as space launchers (Figure 5.1), implementing effective development processes that lead to innovative and optimized products. This decrease leads to parallelism and use of an iterative process in structural design activities. During such iterations, the parameters of the product are adjusted to satisfy specifications. It is then mandatory to have fast and reactive strategies in order to ensure at any time that the initially defined product is tolerant to variations of design parameters which are encountered during the development. Con-

sequently, aerospace industrialists currently face the challenge to perform accurate simulations for modern designs, in order to quantify sensitivity of design modifications (in material properties, manufacturing conditions, external loading...) on the response of a structural system, and avoid overly conservative assumptions afterwards, such as large factors of safety. The goal is to better master margins related to an imprecise initial definition of the structure, defining then progressively refining them during the product definition. A difficulty in this challenge is that structural components within the design are based on varied length scales. Design features such as fillets, laminate layers, or small holes for instrumentation would typically require the use of hyper-refined models that are infeasible in practice. An associated requirement is thus to optimize computation times to conduct the simulation-based analysis.

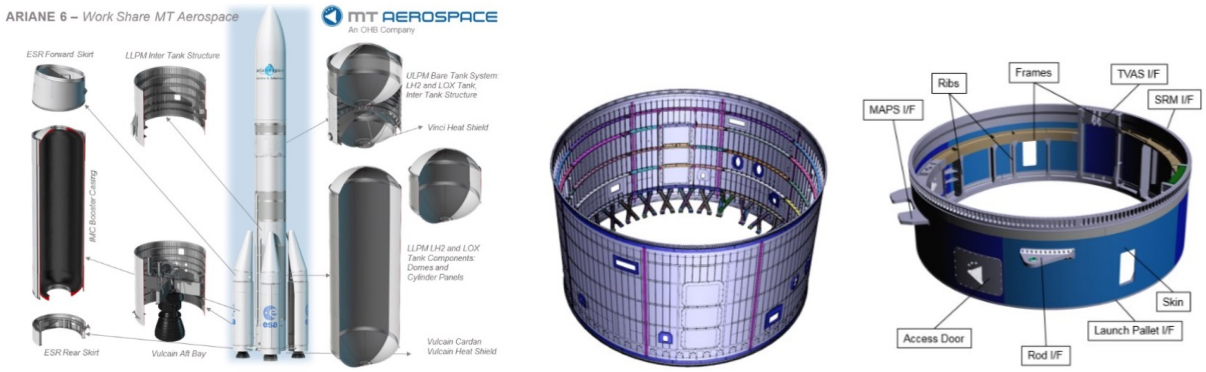


Figure 5.1: Structural components in the Ariane 6 programme, with focus on geometrical details on two of them (courtesy of Ariane Group).

During the last two decades, several non-deterministic methods have been developed to address design uncertainties on mechanical structures. They can be classified in two families:

1. methods based on reliability, that enable to assess the probability distribution of the response with respect to distributions of random parameters; they are mainly used for risk analysis by computing the probability of failure $P_f$ (or its complement to 1, the reliability). Variation is not minimized in such approaches, which rather concentrate on rare events at the tail of the probability distribution (see Figure 5.2), making the probability of failure not go higher than a threshold. Such methods, gathered in the family of Reliability-Based Design Optimization (RBDO) methods, usually consider the notion of reliability index for measuring the safety of structures in presence of uncertainties [Kang and Luo, 2010]. They lead to optimal design that gives solutions which are much above the average solution and are more sensitive to parameter uncertainty. Structural responses will thus much deviate from the predicted optimal state, and will be more easily close to failure;

2. robust methods that minimize effects of variabilities in system performance, the objective being to optimize the mean performance with low variation, while maintaining feasibility with probabilistic constraints (e.g. threshold on probability failure). This is realized by optimizing the design in order to make the performance little sensitive

to the different variation sources. Consequently robust design concentrates on probability density close to mean values (see Figure 5.2). Robust methods are gathered in the family of Robust Design Optimization (RDO) methods.

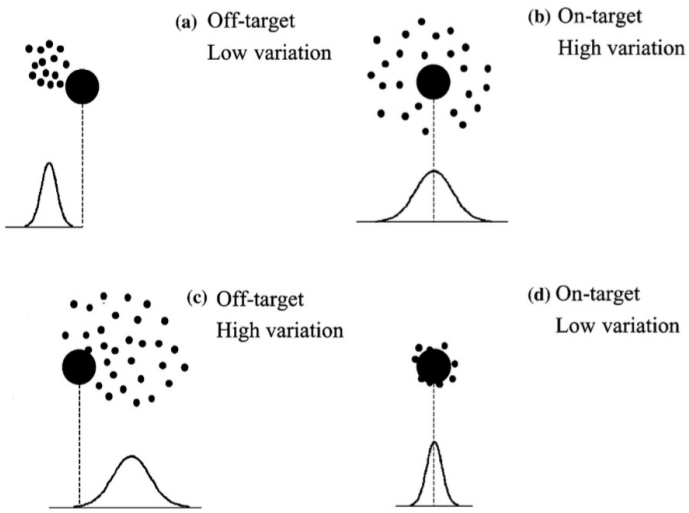


Figure 5.2: Different types of performance variations (from [Zang et al., 2005]).

### 5.1.2 Robust design

Concepts and foundations of robust design have been developed in the 50s by Taguchi, and an overview can be found in [Zang et al., 2005, Guedri et al., 2012, Carneiro and Antonio, 2019]. As said before, the objective of robust design is to optimize the mean and to minimize the variability (i.e. decrease sensitivity) resulting from uncertainties (in material or geometrical properties), represented by noise factors (variabilities from nominal values) or signal factors (set of design configurations). Effects of this uncertainty on conception shall thus be minimized.
Design optimization is thus conducted by minimizing the determinant of the covariance matrix of the response functionals (performance $P$) of the system. It is usually obtained through sensitivity analysis, as $Var(P) = \mathbf{S}\mathbb{V}\mathbf{S}^T$ with $\mathbf{S}$ the sensitivity vector such that $S_i = \partial P/\partial x_i|x_0$, and $\mathbb{V}$ the covariance matrix of random variables.

## 5.2 Numerical implementation

### 5.2.1 Use of certified and parametrized non-intrusive local-global coupling

The tools developed in previous chapters are suited to parametric study and uncertainty propagation associated with optimal or robust design, and therefore for margin estimation. Usually, in order to conduct reliable or robust design, sensitivity analysis is performed with the adjoint state method, and uncertainty quantification is performed with the

Monte-Carlo algorithm (repeated random sampling) on costly simulation models. Using the local-global coupling enables to address local variabilities and manage the model more easily. With an unchanged initial global model while making the design evolve on local zones of interest, it brings larger flexibility for local design modifications compared to classical FEA. Furthermore, the local use of PGD model reduction with parametrized configurations enables to perform sensitivity analysis and uncertainty quantification in a straightforward manner, with low computational effort. Eventually, the use of certified simulations enables to get confidence in the analysis.

### 5.2.2 Illustrative case

We apply the methodology and analyze it on a 2D case which is simplified but still representative of scientific and conceptual difficulties. It is a plate with a hole, submitted to known traction loading. We want to maximize the hole radius (that increases local stress), or reversely for a given nominal radius we define the margin on the loading.

We consider design uncertainties related to the exact position and radius (manufacturing precision) of the hole. With given uncertainty levels, we wish to propagate uncertainty and compute solutions associated with reliable or robust design. The quantity of interest if the maximal Von Mises stress in the vicinity of the hole, where singularities occur. Figure 5.3 shows an example for the nominal geometry and the manufactured geometry, with variabilities.

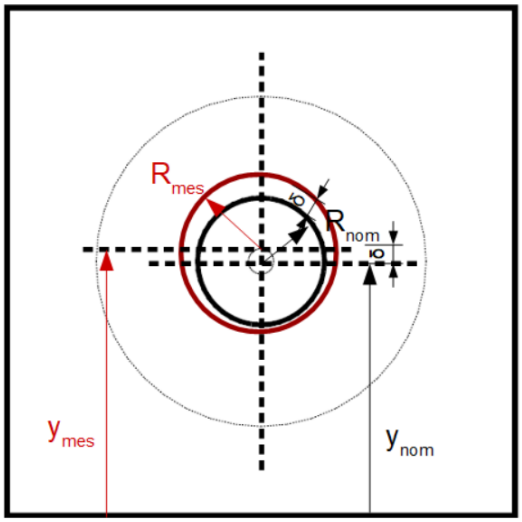


Figure 5.3: Example of nominal geometry and real or manufactured geometry.

The first analysis considered is the reliability. The reliability is defined such that from a nominal design, we define a safety coefficient on the loading to have less than 1% failure rate with prescribed parameter uncertainties on hole radius or position.

The second analysis considered is the robustness. The robustness consists in modifying the design so that variance of the response is lower than a threshold.

The chosen objective function is the signal to noise ratio (SNR) [Zang et al., 2005], defined as $SNR = -10\log(MSD)$

with MSD the mean squared deviation on maximal stress.

### 5.2.3 Results

We give the loading (or safety margin) to respect reliability or robustness criteria with a given tolerance. In each case, we compute the SNR. In robust analysis, we expect to have a reduced radius (or lower loading) that is lower performance. The Signal to Noise Ratio is defined as follow :

$$SNR = -10\log(MSD) = -10log_{10}\left(\frac{1}{n}\sum_{i=1}^{n}(y_i - t)^2\right) \tag{5.1}$$

The control parameter $t$ can be chosen such as that $t = \overline{y}$, ie. the target value $t$ is the mean of the population $\{y_i\}$.

This study aims to define the admissibility domain for the conception parameter in regards to the reliability and robustness of the design.

In this part we are exploiting the result of Chapter 4. For a reminder we have obtained the evolution of the maximum Von Mises Stress with respect to geometric parameters (radius and position of a hole inside the local domain). The case study is the same as described in Chapter 4, the result can be seen in Figure 5.4.

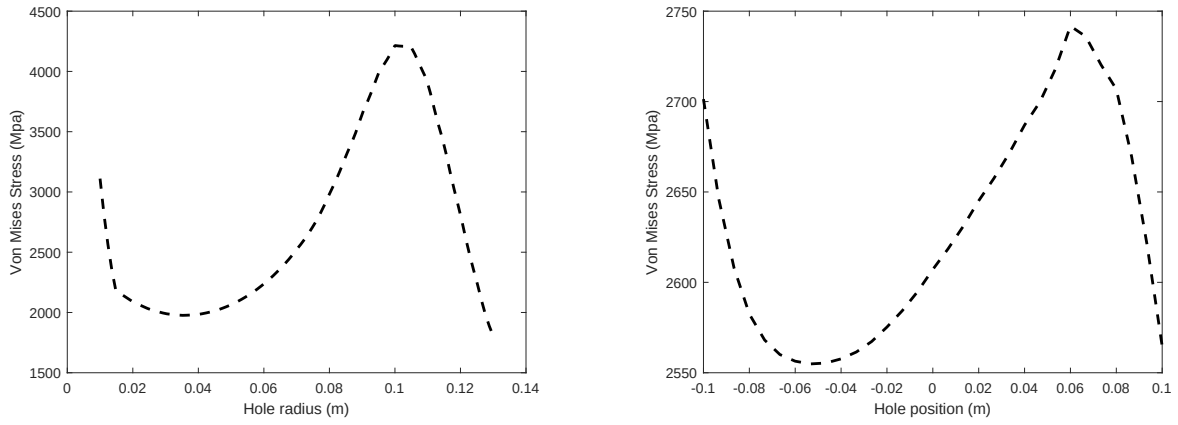


(a) Hole radius as a geometric parameter.

(b) Hole position as a geometric parameter.

Figure 5.4: Evolution of a quantity of interest (maximum Von Mises stress) as a function of a geometric parameter.

We will only consider the range $[0.045; 0.09]$ for the hole radius parameter and $[-0.06; 0.06]$ for the hole position parameter in order to avoid uncontrolled behaviour at the edge of the parametric domain for the PGD solution.

In order to compute the reliability of our system to the regards with failure (the maximum Von Mises stress is above a certain threshold) we use a Monte Carlo method. For this method we suppose that the parameters follow a normal distribution centered on a known mean value with a standard variation set as 1/25 of the parameter range considered. The failure occurs if the maximum Von Mises stress is larger than 2675 MPa. Figure 5.5 shows

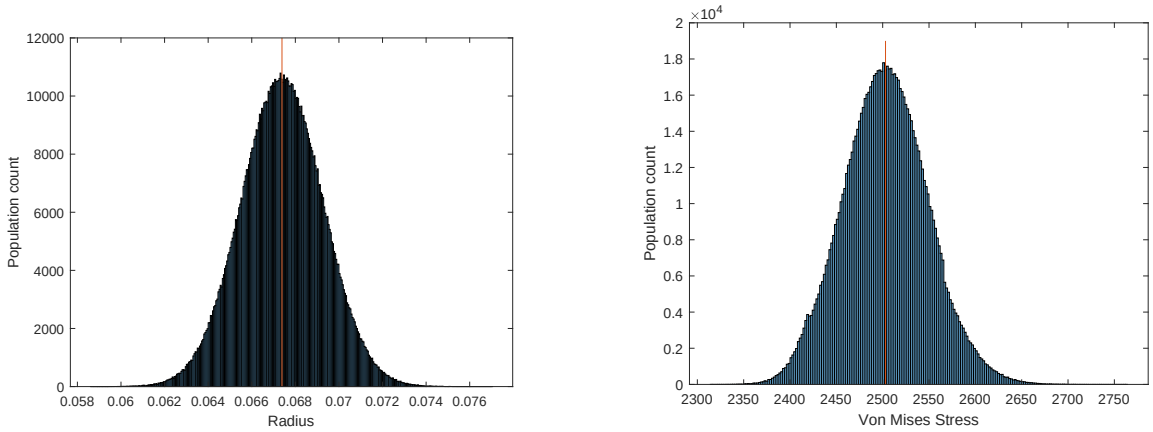


(a) Monte Carlo experiment for the Radius.

(b) Distribution of the quantity of interest for the Monte Carlo experiment.

Figure 5.5: Monte-Carlo experiment for the radius as a parameter ($R_{nom} = 0.067$).

distribution of the parameter and the quantity of interest for a given nominal radius for the hole.

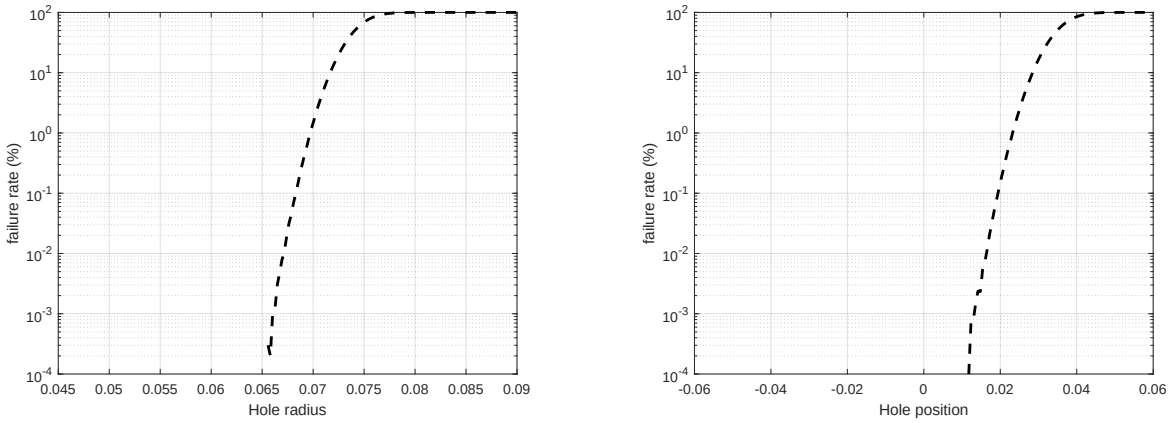


(a) Hole radius as a geometric parameter.

(b) Hole position as a geometric parameter.

Figure 5.6: Evolution of failure rate for a design.

We can see that the optimal radius and position of the hole to guaranty a failure rate less than 1% are respectively $R_{opti} = 0.068$ and $y^c_{opti} = 0.018$. Now we will study the robustness of our design.

In our application a design is considered robust if its SNR is greater than -30dB. Figure 5.7 shows the result for both hole radius and position as a geometric parameter. We can see that for respecting the robustness condition the hole radius needs to be smaller than 0.055 which is lower than the radius computed for the reliability condition. The SNR is always larger than -30dB for the hole position as a geometric parameter. Indeed maximum Von Mises stress is lightly impacted by the hole position in the range studied.

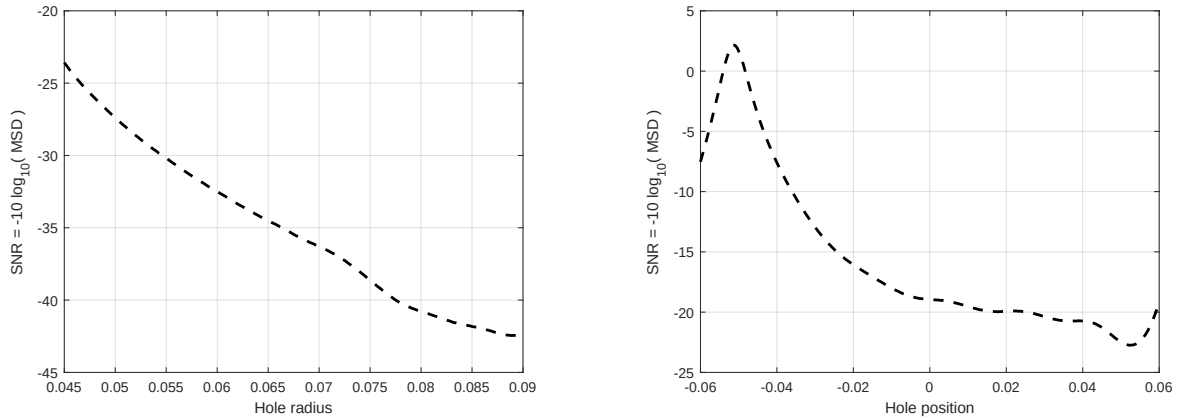


(a) Hole radius as a geometric parameter.

(b) Hole position as a geometric parameter.

Figure 5.7: Evolution of robustness for a design.

## 5.3 Partial conclusions

In this chapter, we illustrated a potential application of the numerical methodology developed in these PhD work. It dealt with local optimization and robust design, considering variability in the manufacturing. We showed that the non-intrusive coupling technique as well as the PGD model reduction offer large flexibility to address this problem.

# Conclusions & prospects

In this PhD work, we investigated some advanced numerical approaches in the context of non-intrusive local-global model coupling procedures. These approaches aimed at bringing confidence and efficiency, out of flexibility naturally offered by non-intrusive local-global model couplings when analyzing localized phenomena. We first developed a robust verification technique, valid for linear or nonlinear material laws, constructed from the Constitutive Relation Error concept. This technique represents a scientific advance in the wide literature on multiscale methods, and appears as a relevant tool for certifying the quality of approximate solutions obtained from such model couplings; it is the main contribution of the PhD work. In this context, we defined a guaranteed and reliable CRE-based error estimator which was derived through a unified thermodynamics framework. This fully computable estimate is valid for both linear and nonlinear constitutive models given by a standard formulation, and takes into account all error sources encountered in non-intrusive local-global model couplings (coming from the use of surrogate models, discretization techniques, and iterative algorithms). We also designed specific error indicators on individual error sources, in order to quantify these and drive an adaptive algorithm that adjusts the coupling parameters and permits an optimized allocation of computing ressources in terms of trade-off between accuracy and numerical cost. The developments were implemented and analyzed on several numerical examples, effectively controlling global error or error on specific quantities of interest (goal-oriented vision) with prescribed tolerance. In particular, it was often shown that the iterative coupling algorithm can be stopped long before reaching interface equilibrium. The overall verification framework, which is in line with the non-intrusive feature of the model coupling method, thus participates in achieving right computation at right cost, which has become a fundamental requirement in practical engineering analyses.

In a second part of the PhD work, the verification procedure was complemented by a local use of PGD-based model reduction. The objective was to effectively address multi-query computations performed at the local scale, coming from the iterative coupling algorithm itself but also from the solution of parametrized local problems. Such a parametrization naturally appears when implementing the adaptive process, with varying size of the local domain, and when considering optimization problems with local topology changes. Performance but also limits of the association between PGD and non-intrusive local-global model coupling were assessed through several numerical experiments with various quantities of interest.

In a last part of the PhD work, we applied the developed verification and model reduction tools in the context of robust design, targeting and controlling values of outputs of interest for design purposes as well as their fluctuations with design uncertainties. This part of the work, dealing with tolerance analysis, was a first illustration of the potential of the proposed approach for industrial applications.

Several prospects to this work may be envisioned:

- A short term prospect is the implementation of the proposed numerical framework on 3D industrial applications (e.g. for the local analysis of plasticity or damage), with model couplings resorting to commercial software. Out of requiring the availability of an equilibration technique (in order to assess the discretization error source), all other aspects should be transferable in a straightforward manner;

- Similar developments could be performed when considering volume coupling interfaces between models, which are better suited when very different physics or scales are coupled. As an example, the non-intrusive Arlequin-type coupling designed in the PhD of R. Ruyssen [Ruyssen, 2021], or the non-intrusive version of the Partition of Unity method [Plews et al., 2012], could advantageously benefit from the proposed CRE-based verification procedure. Here again, it seems there is no specific technical difficulty when addressing this new context;

- The algebraic error generated by solvers of local problems (when considering nonlinear models) was here neglected, by reaching local convergence, but it could be additionally added in the overall adaptive process;

- In the same spirit, another interesting extension of the work could deal with the consideration and control of error in the data transfer at the coupling interface, when applying the non-intrusive local-global model coupling with geometrically incompatible meshes;

- In terms of considered physics, time-dependent models could be considered. It seems a relatively simple extension could be made to dynamics models, considering available CRE tools in this case. More elaborated developments would be needed when considering models with concentrated moving sources [Cosimo et al., 2017], exhibiting advection phenomena when placed in the the frame linked to the source. A non-intrusive coupling technique with moving local zone may be a good option in this case to avoid costly remeshing techniques. Indeed, it would separate local and global scales for meshes and operators, and there is good hope that local model reduction performs well as the local solution is quasi-stationary (in the frame linked to the source). However, technical difficulties arise for managing the coupling with the global scale in such cases with moving sources (and incompatible meshes). Some first ideas on this topic are given in Appendix, and a typical application of interest could be manufacturing processes such as welding or additive manufacturing, with the aim of monitoring the process and control the quality of the obtained product;

- Eventually, it would be fruitful to investigate local model enrichment from assimilated data (hybrid approach), in order to learn model ignorance or account for variabilities, and therefore increase the reliability of model-based simulations. Observations on complex physical system would then feed their local virtual representation as well as their uncertain environment.

All these prospects will be topics of future research works.

# Appendices

# Appendix A

# Proof of the properties used in Chapter 5

**Part 1:** we show that $\tilde{\mathbb{K}}_L \mathbf{U}_L = \tilde{\mathbf{F}}_L$ has a unique solution. This follows at once if we show that the only solution of $\tilde{\mathbb{K}}_L \mathbf{W}_L = 0$ is the trivial solution $\mathbf{W}_L = 0$. By the definition of $\tilde{\mathbb{K}}_L$, it follows that $\mathbf{W}_L$ satisfies:

$$0 = \mathbb{C}_L^T \mathbb{C}_L \mathbf{W}_L + \mathbb{Q}_L^T \mathbb{K}_L \mathbb{Q}_L \mathbf{W}_L \tag{A.1}$$

Multiplying by $\mathbb{Q}_L^T$, recalling that $\mathbb{Q}_L^T \mathbb{C}_L^T = (\mathbb{C}_L \mathbb{Q}_L)^T = 0$ and that $\mathbb{Q}_L^2 = \mathbb{Q}_L$, we deduce that $\mathbb{Q}_L^T \mathbb{K}_L \mathbb{Q}_L \mathbf{W}_L = 0$ and so $\mathbb{Q}_L \mathbf{W}_L \in Ker(\mathbb{K}_L)$. (A.1) then reduces to

$$0 = \mathbb{C}_L^T \mathbb{C}_L \mathbf{W}_L \tag{A.2}$$

Consequently $\mathbb{C}_L \mathbf{W}_L = 0$ or, equally well, $\mathbf{W}_L \in Ker(\mathbb{C}_L)$. From the definition of $\mathbb{Q}_L$, it follows that $\mathbf{W}_L = \mathbb{Q}_L \mathbf{W}_L \in Ker(\mathbb{K}_L)$. We conclude that $\mathbf{W}_L \in Ker(\mathbb{K}_L) \cap Ker(\mathbb{C}_L)$, and thanks to Assumption 2, it follows $\mathbf{W}_L = 0$.

**Part 2:** it suffices to show there exists a Lagrange multiplier $\mathbf{\Lambda}$ such that the pair $(\mathbf{X}_L, \mathbf{\Lambda})$ satisfies the coupled system, where $\mathbf{X}_L$ is the solution of the equation:

$$\mathbb{C}_L^T \mathbb{C}_L \mathbf{X}_L + \mathbb{Q}_L^T \mathbb{K}_L \mathbb{Q}_L \mathbf{X}_L = \mathbb{C}_L^T \mathbb{C}_G \mathbf{U}_G + \mathbb{Q}_L^T (\mathbf{F}_L - \mathbb{K}_L \mathbb{R}_L \mathbb{C}_G \mathbf{U}_G) \tag{A.3}$$

Multiplying (A.3) by $\mathbb{Q}_L^T$ and arguing as before reveals that

$$\mathbb{Q}_L^T \mathbb{K}_L \mathbb{Q}_L \mathbf{X}_L = \mathbb{Q}_L^T (\mathbf{F}_L - \mathbb{K}_L \mathbb{C}_G \mathbf{U}_G) \quad \text{or} \quad \mathbb{Q}_L^T (\mathbb{K}_L \mathbb{Q}_L \mathbf{X}_L - \mathbf{F}_L + \mathbb{K}_L \mathbb{R}_L \mathbb{C}_G \mathbf{U}_G) = 0 \tag{A.4}$$

It follows that $\mathbb{K}_L \mathbb{Q}_L \mathbf{X}_L - \mathbf{F}_L + \mathbb{K}_L \mathbb{R}_L \mathbb{C}_G \mathbf{U}_G \in Ker(\mathbb{Q}_L^T) = Range(\mathbb{C}_L^T)$ ,where the final step is a standard result of

linear algebra. Inserting this information in (A.3) reveals that

$$\mathbb{C}_L^T \mathbb{C}_L \mathbf{X}_L = \mathbb{C}_L^T \mathbb{C}_G \mathbf{U}_G \quad \text{or} \quad \mathbb{C}_L^T (\mathbb{C}_L \mathbf{X}_L - \mathbb{C}_G \mathbf{U}_G) = 0 \tag{A.5}$$

It follows that $\mathbb{C}_L \mathbf{X}_L - \mathbb{C}_G \mathbf{U}_G \in Ker(\mathbb{C}_L^T) = Range(\mathbb{C}_L)^\perp$. Conversely, Assumption 1 implies $\mathbb{C}_G \mathbf{U}_G \in Range(\mathbb{C}_L)$ and hence $\mathbb{C}_L \mathbf{X}_L - \mathbb{C}_G \mathbf{U}_G \in Range(\mathbb{C}_L)$. Together, these conditions show that $\mathbb{C}_L \mathbf{X}_L - \mathbb{C}_G \mathbf{U}_G = 0$, and it follows that $\mathbf{X}_L$ satisfies the constraint equation $\mathbb{C}_L \mathbf{X}_L = \mathbb{C}_G \mathbf{U}_G$.

Now,

$$\mathbf{F}_L - \mathbb{K}_L \mathbf{X}_L = \mathbf{F}_L - \mathbb{K}_L (\mathbb{Q}_L + \mathbb{R}_L \mathbb{C}_L) \mathbf{X}_L = \mathbf{F}_L - \mathbb{K}_L \mathbb{Q}_L \mathbf{X}_L - \mathbb{K}_L \mathbb{R}_L \mathbb{C}_G \mathbf{U}_G \tag{A.6}$$

since $\mathbb{C}_L \mathbf{X}_L = \mathbb{C}_G \mathbf{U}_G$. Hence, $\mathbf{F}_L - \mathbb{K}_L \mathbf{X}_L \in Range(\mathbb{C}_L^T)$ and it follows that there exists a $\mathbf{\Lambda}$ satisfying the first condition of the coupled problem.

**Part 3:** The Lagrange multiplier satisfies the equation:

$$\mathbb{C}_L^T \mathbf{\Lambda} = \mathbf{F}_L - \mathbb{K}_L \mathbf{X}_L \tag{A.7}$$

and multiplying by $(\mathbb{C}_L \mathbb{C}_L^T)^{-1} \mathbb{C}_L$ implies that

$$\mathbf{\Lambda} = (\mathbb{C}_L \mathbb{C}_L^T)^{-1} \mathbb{C}_L (\mathbf{F}_L - \mathbb{K}_L \mathbf{X}_L) \tag{A.8}$$

and the result follows on noting $(\mathbb{C}_L \mathbb{C}_L^T)^{-1} \mathbb{C}_L = \mathbb{R}_L^T$.

# Appendix B

# Analytical solution for a plate with a hole

## Section 1

We consider a plate with horizontal traction loading $T_x$. Considering one quarter of the plate (due to symmetry), with radius $R$ and length $L$, the exact solution reads:

$$\begin{aligned}
\sigma_{rr}(r,\theta) &= \frac{T_x}{2}(1-\frac{R^2}{r^2}) + \frac{T_x}{2}(1+3\frac{R^4}{r^4}-4\frac{R^2}{r^2})\cos(2\theta) \\
\sigma_{\theta\theta}(r,\theta) &= \frac{T_x}{2}(1+\frac{R^2}{r^2}) - \frac{T_x}{2}(1+3\frac{R^4}{r^4})\cos(2\theta) \\
\sigma_{r\theta}(r,\theta) &= -\frac{T_x}{2}(1+2\frac{R^2}{r^2}-3\frac{R^4}{r^4})\sin(2\theta)
\end{aligned} \tag{B.1}$$

Holes conduct to a weakening of the structure due to local overstress. Here we compute stress intensity factors for each geometry, starting with a circular hole in a plate in traction before addressing elliptic holes. The study is for small perturbations, isotropic material, with linearized elasticity, and 2D problem.

The tool of choice to address the problem is Airy functions. For 2D problems (coordinates ($x_1$,$x_2$)) with linearized isotropic elasticity and no body force, the solution comes down to search a stress function $\chi(x_1,x_2)$ such that:

$$\sigma_{11} = \frac{\partial^2\chi}{\partial x_2^2} \quad ; \quad \sigma_{22} = \frac{\partial^2\chi}{\partial x_1^2} \quad ; \quad \sigma_{12} = -\frac{\partial^2\chi}{\partial x_1 \partial x_2} \tag{B.2}$$

and compatibility equations indicate that $\chi$ is biharmonic: $\Delta^2\chi = \chi_{1111} + \chi_{2222} + 2\chi_{1122} = 0$.

In a polar system, the stress function $\chi(r,\theta)$ is such that:

$$\sigma_{rr} = \frac{1}{r}\frac{\partial\chi}{\partial r} + \frac{1}{r^2}\frac{\partial^2\chi}{\partial\theta^2} \quad ; \quad \sigma_{\theta\theta} = \frac{\partial^2\chi}{\partial r^2} \quad ; \quad \sigma_{r\theta} = -\frac{\partial}{\partial r}(\frac{1}{r}\frac{\partial\chi}{\partial\theta}) \tag{B.3}$$

with, again:

$$\Delta^2\chi = (\frac{\partial^2}{\partial r^2} + \frac{1}{r}\frac{\partial}{\partial r} + \frac{1}{r^2}\frac{\partial^2}{\partial \theta^2})(\frac{\partial^2\chi}{\partial r^2} + \frac{1}{r}\frac{\partial\chi}{\partial r} + \frac{1}{r^2}\frac{\partial^2\chi}{\partial \theta^2}) = 0 \tag{B.4}$$

A quite large family of biharmonic functions is:

$$\begin{aligned}\chi(r,\theta) &= A_0 \log r + B_0 r^2 \log r + C_0 r^2 + D_0 \\ &+ (A_1 r \log r + B_1 r^3 + C_1 r + \frac{D_1}{r})\cos\theta + (A_1^* r \log r + B_1^* r^3 + C_1^* r + \frac{D_1^*}{r})\sin\theta \\ &+ \sum_{k=2}^{\infty}(A_k r^k + B_k r^{-k} + C_k r^{k+2} + D_k r^{-k+2})\cos(k\theta) \\ &+ \sum_{k=2}^{\infty}(A_k^* r^k + B_k^* r^{-k} + C_k^* r^{k+2} + D_k^* r^{-k+2})\sin(k\theta)\end{aligned} \tag{B.5}$$

It enables to solve many 2D linear elasticity problems with loading conditions which are periodic in $\theta$. Constants have to be determined from boundary conditions.

We first consider plate of width $2h$ with a circular hole of radius $a$, with plane stress assumption, submitted to simple traction loading (Figure B.1). The hole axis is $\mathbf{e}_3$ and the traction axis is $\mathbf{e}_1$. Length and height $L$ of the plate are assumed sufficiently large compared to $a$ for the stress state far from the hole not be affected by the hole and is considered as the homogeneous state $\sigma^\infty = \sigma^\infty \mathbf{e}_1 \otimes \mathbf{e}_1$ where $\sigma^\infty$ is the imposed stress (data of the problem. In the problem, the hole boundary and surfaces $z = \pm h$ are free.

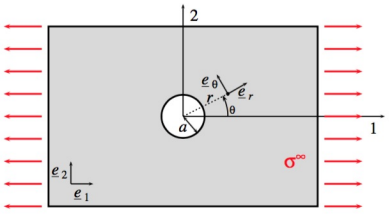


Figure B.1: Plate with a hole with simple traction loading.

Substituting $\mathbf{e}_1 = \cos\theta\mathbf{e}_r - \sin\theta\mathbf{e}_\theta$, we get far from the hole:

$$\sigma_{rr}^\infty = \frac{\sigma^\infty}{2}(1+\cos 2\theta) \quad ; \quad \sigma_{\theta\theta}^\infty = \frac{\sigma^\infty}{2}(1-\cos 2\theta) \quad ; \quad \sigma_{r\theta}^\infty = -\frac{\sigma^\infty}{2}\sin 2\theta \tag{B.6}$$

By integration, we get that an associated stress function is $\chi = \frac{\sigma^\infty}{2}(1-\cos 2\theta)\frac{r^2}{2}$.

This invites to search, among the previous family, a stress function at each point of the plate under the form:

$$\chi(r,\theta) = A\log r + Br^2\log r + Cr^2 + (A_2 r^2 + B_2 r^4 + \frac{C_2}{r^2} + D_2)\cos 2\theta \tag{B.7}$$

This results in the following form for stress components:

$$\begin{aligned}
\sigma_{rr} &= \frac{A}{r^2} + 2B\log r + B + 2C + (-2A_2 - \frac{6C_2}{r^4} - \frac{4D_2}{r^2})\cos 2\theta \\
\sigma_{\theta\theta} &= -\frac{A}{r^2} + 2B\log r + 3B + 2C + (2A_2 + 12B_2 r^2 + \frac{6C_2}{r^4})\cos 2\theta \\
\sigma_{r\theta} &= 2\sin 2\theta(A_2 + 3B_2 r^2 - \frac{3C_2}{r^4} - \frac{D_2}{r^2})
\end{aligned} \tag{B.8}$$

From the stress field far from the hole, we get $B = 0$, $C = \sigma^\infty/4$, $A_2 = -\sigma^\infty/4$, and $B_2 = 0$. Boundary conditions at the hole yield a linear system for unknowns $A$, $C_2$ and $D_2$, with solution $A = -a^2\sigma^\infty/2$, $C_2 = -a^4\sigma^\infty/4$, and $D_2 = a^2\sigma^\infty/2$. We thus get:

$$\begin{aligned}
\sigma_{rr} &= \frac{\sigma^\infty}{2}(1 - \frac{a^2}{r^2}) + \frac{\sigma^\infty}{2}(1 + \frac{3a^4}{r^4} - \frac{4a^2}{r^2})\cos 2\theta \\
\sigma_{\theta\theta} &= \frac{\sigma^\infty}{2}(1 + \frac{a^2}{r^2}) - \frac{\sigma^\infty}{2}(1 + \frac{3a^4}{r^4})\cos 2\theta \\
\sigma_{r\theta} &= -\frac{\sigma^\infty}{2}(1 - \frac{3a^4}{r^4} + \frac{2a^2}{r^2})\sin 2\theta \\
\chi &= -\frac{\sigma^\infty}{2}a^2\log r + \frac{\sigma^\infty}{4}r^2 + \frac{\sigma^\infty}{4}(-r^2 + 2a^2 - \frac{a^4}{r^2})\cos 2\theta
\end{aligned} \tag{B.9}$$

Decrease in $1/r^2$ ensures that heterogeneities develop in the vicinity of the hole alone, and that the field can be considered as homogeneous far from the hole. There are overstresses close to the hole (see figures), with factor 3 on the orthoradial component, that can lead to cracking.

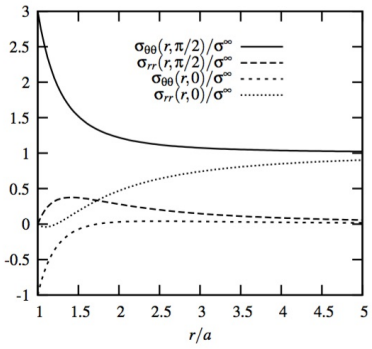


Figure B.2: Profiles of radial and orthoradial components normalized by the applied stress, along the pole ($\theta = 0$) and equator ($\theta = \pi/2$), as a function of the relative distance $r/a$ to the hole.

By integration, we obtain the displacement field (up to rigid body motions):

$$\begin{aligned}
u_r &= \frac{\sigma^\infty}{2E}\left((1-\nu)r + (1+\nu)(\frac{a^2}{r} + (r - \frac{a^4}{r^3})\cos 2\theta) + \frac{4a^2}{r}\cos 2\theta\right) \\
u_\theta &= -\frac{\sigma^\infty}{2E}\left((1+\nu)(1 + \frac{a^4}{r^4})r + (1-\nu)\frac{2a^2}{r}\right)\sin 2\theta
\end{aligned} \tag{B.10}$$

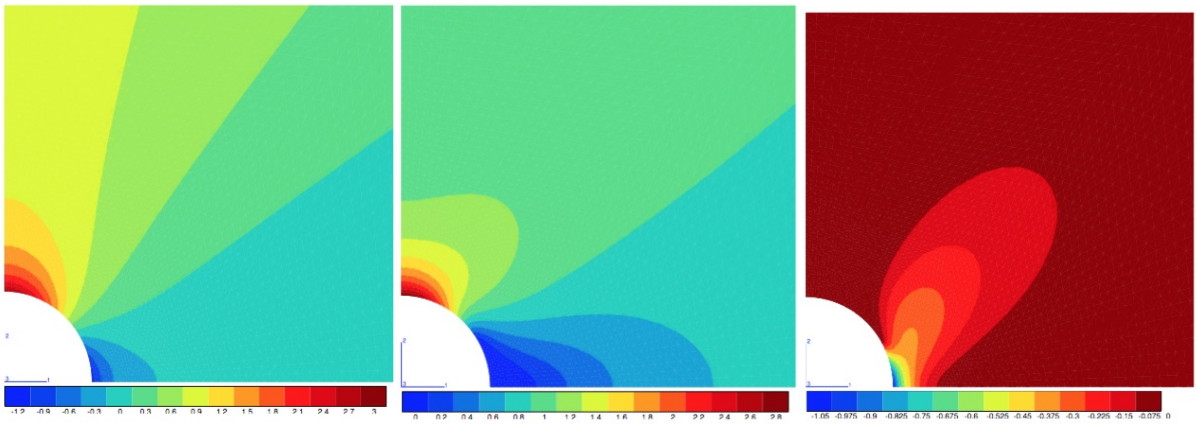

Figure B.3: Representation of the stress field around the hole, with component $\sigma_{\theta\theta}$, largest principal stress at each point, and smallest principal stress at each point. All these stresses are normalized by the value of the axial stress far from the hole.

# Appendix C

# First insights for the extension to the case of moving sources

We focus here on challenging problems characterized by steep moving gradients (as produced by a highly concentrated moving source), and which usually require numerical issues with small time steps and fine mesh sizes, as well as remeshing procedures. Typical applications are complex (multiphysics) manufacturing processes involving moving localized nonlinear physical phenomena that depend on many parameters, such as welding [Gastebois, 2015].

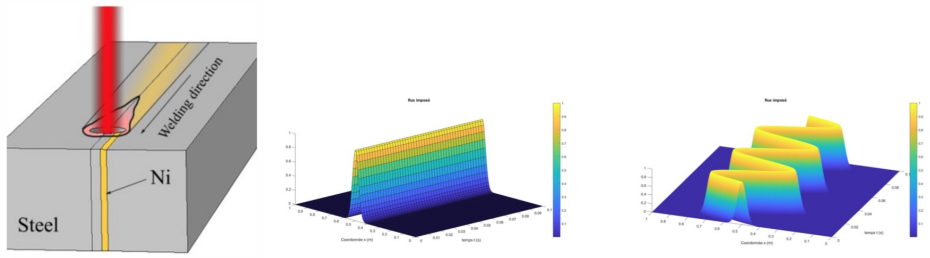


Figure C.1: Example of a welding application (left), and configuration with fixed or moving sources (right).

A typical academic example is the Idelsohn benchmark which is a 1D transient diffusion problem with moving localized source. It reads:

$$\begin{aligned} \rho c_p \partial_t u - \nabla \cdot k \nabla u &= f(x,t) \quad \text{in } \Omega \times I \\ u &= u_D \quad \text{on } \Gamma_D \times I \\ u &= u_0 \quad \text{on } \Gamma_D \times \{0\} \end{aligned} \tag{C.1}$$

with $\Omega = [0, \pi]$, $T = 1$, $u(0,t) = u(\pi,t) = 0$ and $u(x,0) = 0$. The value of the thermal conductivity is $k = 0.05$, density

is $\rho = 1$ and specific heat capacity $c_p = 1$. The source term (heat added per unite volume) is here described as:

$$\begin{aligned} &f(x,t) = 0 \quad t < t_i \text{ or } t > t_f \\ &f(x,t) = A\cos(\frac{\pi}{L}(x - x_0(t))) \quad t_i < t < t_f \text{ and } -\frac{L}{2} < x - x_0(t) < \frac{L}{2} \end{aligned} \tag{C.2}$$

where $x_0(t) = x_i + \frac{x_f - x_i}{t_f - t_i}(t - t_i)$, $A = 100$, $L = 0.15$, $t_i = 0.2$, $t_f = 0.7$, $x_i = 2\pi/7$ and $x_f = 5\pi/7$. $V = \frac{x_f - x_i}{t_f - t_i}$ is the source velocity. It can also be described as $f(x,t) = f_m e^{-(x - x_0(t))^2/\sigma^2}$, where $\sigma$ is a parameter that controls the heat concentration. When placing in the reference frame moving with the local source, the problem introduces an advection term.

We investigate below a non-intrusive global-local coupling approach when coupling a global diffusion-reaction model with a local advection-diffusion-reaction model. A difficulty is in the incompatibility between meshes and the moving feature of the interface between models.

## Non-intrusive local-global coupling

The local-global approach consists here in separating physical phenomena on two independent models: a global model, with coarse mesh on which the behavior of the global structure is described; a local model with fine mesh on which the neighborhood of the heat source is described. We assume that all nonlinear phenomena are restricted to the support of the local model. The difficulty is in the coupling of the two models.

In an intrusive coupling version, with non-overlapping decomposition between global domain $\Omega_c$ and fixed local domain $\Omega_f$ and heat source moving within its support), the variational formulation of the coupling reads: find $u^c \in H^1_c$, $u^f \in H^1_f$ and $\lambda \in H^{-1/2}_\Gamma$ such that:

$$\begin{aligned} m_c(\delta u^c, u^c) + k_c(\delta u^c, u^c) + c(\delta u^c, \lambda) &= q_c \quad \forall \delta u^c \in H^1_c \\ m_f(\delta u^f, u^f) + k_f(\delta u^f, u^f) + c(\delta u^f, \lambda) &= (\delta u^f, Q) \quad \forall \delta u^f \in H^1_f \\ c(\delta\lambda, u^c - u^f) &= 0 \quad \forall \delta\lambda \in H^{-1/2}_\Gamma \end{aligned} \tag{C.3}$$

with $m_i(v,u) = \int_{\Omega_i} v\frac{\partial u}{\partial t}$, $k_i(v,u) = \int_{\Omega_i} \nabla v.k\nabla u$, $c(v,\lambda) = \int_\Gamma v\lambda$, and $(v,Q) = \int_{\Omega_f} vQ$. $q_c$ denotes the contribution from boundary conditions in the global problem, and $Q$ is the moving heat source.

After discretization in space and time (with a $\theta$-method), we get the linear system:

$$\begin{bmatrix} \mathbb{M}^c + \theta\Delta t\mathbb{K}^c & 0 & \mathbb{B}^{c,T} \\ 0 & \mathbb{M}^f + \theta\Delta t\mathbb{K}^f & \mathbb{B}^{f,T} \\ \mathbb{B}^c & \mathbb{B}^f & 0 \end{bmatrix} \begin{pmatrix} \mathbf{u}_n^c \\ \mathbf{u}_n^f \\ \boldsymbol{\lambda} \end{pmatrix} = \begin{pmatrix} \theta\Delta t q_n^c + (1-\theta)\Delta t q_{n-1}^c + (\mathbb{M}^c - (1-\theta)\Delta t\mathbb{K}^c)\mathbf{u}_{n-1}^c \\ \theta\Delta t q_n^f + (1-\theta)\Delta t q_{n-1}^f + (\mathbb{M}^f - (1-\theta)\Delta t\mathbb{K}^f)\mathbf{u}_{n-1}^f \\ 0 \end{pmatrix} \tag{C.4}$$

To address the displacement of the source term with a moving local domain (with fixed mesh topology that moves following the heat source), different variants can be considered. A straightforward solution is to use the previous discrete formulation, but this requires to project the solution at the previous time step to the configuration adopted by the local domain. Two projections are needed, one for building $u_{n-1}^c$ and one for building $u_{n-1}^f$. A (diffusive) collocation methodology or mortar-like projections (conserving energy) can be used for this. Figure C.2 shows an example of a projection performed

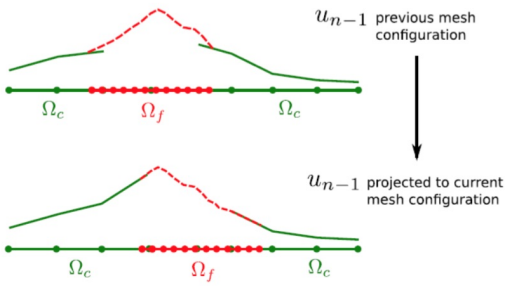


Figure C.2: Projection between time steps using a collocation method.

The fact that the local domain moves attached to the heat source can be exploited to avoid one of the projections. The movement of this domain can be described by adopting an Arbitrary Lagrangian Eulerian (ALE) description [Donea et al., 2004], for which the fundamental relation material time derivatives, referential time derivatives, and spatial gradient reads:

$$\frac{\partial f}{\partial t}_{|X} = \frac{\partial f}{\partial t}_{|x} + c \cdot \nabla f \tag{C.5}$$

with $c$ the relative velocity between the material domain and the reference domain ($\nabla c = 0$ in the local domain, so that well-posedness is ensured [Quarteroni and Valli, 1994, Morton, 1996]). It shows that the time derivative of the physical quantity $f$ for a given particle $X$, that is, its material derivative, is its local derivative (with the reference coordinate $\chi$ held fixed) plus a convective term taking into account the relative velocity $c$ between the material and the reference system. It thus involves a convection term to model the displacement of the source in local coordinates (reference frame linked to the source). This procedure was for instance used in [Ruyssen et al., 2017, Ruyssen, 2021] to simulate additive manufacturing phenomena

A fundamental advantage is that the need of projection information in order to express $u_{n-1}^f$ in the configuration

adopted by the local domain at time $t_n$ is not needed anymore. Then, the discrete formulation of the problem is given as:

$$\begin{bmatrix} \mathbb{M}^c + \theta\Delta t\mathbb{K}^c & 0 & \mathbb{B}^{c,T} \\ 0 & \mathbb{M}^f + \theta\Delta t(\mathbb{K}^f - \mathbb{A}^f) & \mathbb{B}^{f,T} \\ \mathbb{B}^c & \mathbb{B}^f & 0 \end{bmatrix} \begin{pmatrix} \mathbf{u}_n^c \\ \mathbf{u}_n^f \\ \boldsymbol{\lambda} \end{pmatrix} = \begin{pmatrix} \Delta t(\theta q_n^c + (1-\theta)q_{n-1}^c) + (\mathbb{M}^c - (1-\theta)\Delta t\mathbb{K}^c)u_{n-1}^c \\ \Delta t(\theta q_n^f + (1-\theta)q_{n-1}^f) + (\mathbb{M}^f + (1-\theta)\Delta t[\mathbb{A}^f - \mathbb{K}^f])u_{n-1}^f \\ 0 \end{pmatrix} \tag{C.6}$$

where $\mathbb{A}^f$ is the advection matrix. The problem in the local domain being given by a time-dependent advection-diffusion equation, a stabilization term has to be used for Péclet numbers larger than 1. However, the stabilization of the formulation is considered out of the scope as it is assumed that the local domain can be refined as much as needed in order to avoid large Péclet numbers.

The previous (direct) approach has limitations: (i) it is not possible to split the solution scheme on each of the two models; (ii) remeshing at each time step (for moving local domain) is necessary at interface. To circumvent this issue, we proceed as follows:

- Local analysis: computations performed on the local domain by considering as boundary conditions the global solution field (cf. Figure C.3 for an illustration on a 1D model);
- Computation of the residual: computation of unbalance of nodal forces between global and local domains
- Global correction: update of the global solution by considering the residual applied to the structure as an internal force.

At the local step, we compute the solution on the fixed local domain (saving in memory multiplier values on the interface). Residuals (that can be used as stopping criterion) are computed on each node of the local/global interface:

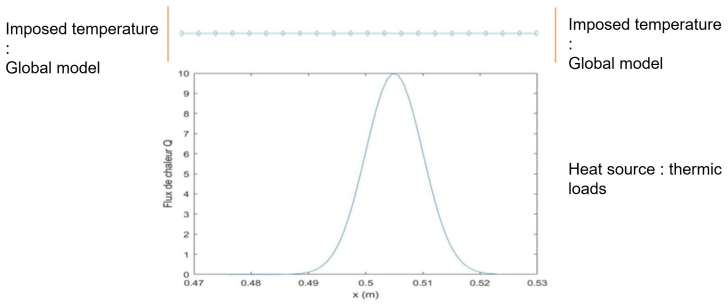


Figure C.3: Example of local model.

$$r(v^*) = -\int_\Gamma k[\nabla u^f \cdot n + \nabla u^c \cdot n].v^* \tag{C.7}$$

with $u = u^f$ on $\Omega_f$ and $u = u^c$ on $\hat{\Omega}_c = \Omega_c - \Omega_c \cap \Omega_f$.

For the global correction, we first compute a corrective term $\Delta u^c \in H_c^1$, from the global model and residual loading applied on the interface. It is such that:

$$m_c(\delta u^c, \Delta u^c) + k_c(\delta u^c, \Delta u^c) + c(\delta u^c, \lambda) = r(\delta u^c) \quad \forall \delta u^c \in H_c^1 \tag{C.8}$$

The global field is then updated as $u^c + \Delta u^c$.

In [Gupta et al., 2012], a buffer zone is introduced, which enlarges the local domain using layers of coarse elements in order to introduce smoother boundary conditions to the local problem.

In [Le Tallec and Tidriri, 1999], there is the study of convergence properties of a time marching algorithm solving advection-diffusion problems on two domains using incompatible discretizations (in the context of DD). The analysis is made at the continuous level (mesh independent). Here two subdomains are fully overlap and solutions are coupled through Neumann forces acting on the internal boundary of the domain. These forces are updated inside the time marching algorithm used for the solution of the initial advection-diffusion problem. The method is defined by imposing Neumann type boundary conditions on the internal boundary of the global domain and Dirichlet boundary conditions on the external boundary of the local domain; this enables to uncouple the global problem and the local one (they can thus be discretized by two independent approximation methods). Here the approach is shown in 1D, but practical applications of the method can be found in [Tidriri, 1995]. In this framework, the unconditional stability and linear convergence of the fully implicit algorithm are theoretically proved. When using the uncoupled semi-explicit algorithm, the algorithm is unstable for large values of $\Delta t$ and small overlapping, and it becomes linearly convergent when $\Delta t$ is small (conditional stability).

Fractional-step methods can also be used for time integration of advection-diffusion (reaction) problems. The idea is to fraction a complex problem into several simpler problems. In our case, the technique leads to a pure convection problem, and a diffusion-reaction problem. An interest is that independent and suited numerical techniques can be then used to solve each of the problems separately.
Assuming the semi-discretized problem reads $\dot{\mathbf{u}} + \mathcal{L}\mathbf{u} = \mathbf{F}$, with $\mathcal{L} = \mathcal{L}_1 + \mathcal{L}_2$ (algebraic fractioning), we may use:

$$\begin{aligned} &\frac{\mathbf{u}^{n+1/2} - \mathbf{u}^n}{\Delta t} + \mathcal{L}_1 \mathbf{u}^{n+1/2} = 0 \\ &\frac{\mathbf{u}^{n+1} - \mathbf{u}^{n+1/2}}{\Delta t} + \mathcal{L}_2 \mathbf{u}^{n+1} =^{\mathbf{n}} \end{aligned} \tag{C.9}$$

The fractioning can also be conducted on the convection-diffusion-reaction differential operator $\mathcal{L}$, under the form:

$$\mathcal{L} = \mathcal{L}_1 + \mathcal{L}_2 \quad ; \quad \mathcal{L}_1 = \mathbf{c} \cdot \nabla \quad ; \quad \mathcal{L}_2 = -\nabla \cdot (\mathcal{K}\nabla) + r \tag{C.10}$$

We then use the sequential algorithm:

$$\begin{aligned} v_{,t} + \mathcal{L}_1 v = 0 \quad \forall (x,t) \in \Omega \times [t_n, t_{n+1}[ \quad ; \quad v(t^n) = u^n \quad \text{(step 1)} \\ w_{,t} + \mathcal{L}_2 w = f \quad \forall (x,t) \in \Omega \times [t_n, t_{n+1}[ \quad ; \quad w(t^n) = v^{n+1} \quad \text{(step 2)} \\ u^{n+1} = w^{n+1} \quad \text{(updating)} \end{aligned} \tag{C.11}$$

The first step corresponds to a pure convection problem, and we can use methods for hyperbolic equations, such as the 3rd order Taylor-Galerkin explicit scheme:

$$(1 - \frac{\Delta t^2}{6}\mathcal{L}_1^2)\frac{v^{n+1} - v^n}{\Delta t} = -(\mathcal{L}_1 - \frac{\Delta t}{2}\mathcal{L}_1^2)v^n \tag{C.12}$$

The second step corresponds to a diffusion-reaction problem, and we can use the Crank-Nicolson scheme:

$$(1 + \frac{\Delta t}{2}\mathcal{L}_2)\frac{w^{n+1} - w^n}{\Delta t} = -\mathcal{L}_2 w^n + \frac{1}{2}(f^n + f^{n+1}) \tag{C.13}$$

When fractioning operators, boundary conditions should also be fractioned. For instance, for the convection phase, boundary conditions may be applied on the ingoing flux part.

## Treatment of non-geometrically conforming meshes

To address non-conforming solutions, we can introduce an auxiliary mesh as performed in [Gosselet et al., 2018] for non-intrusive global-local coupling algorithms between two non-overlapping subdomains: the zone of interest where a fine model is required for a reliable simulation (superscript F) and a complement zone (superscript C) where a simpler model is sufficient, with interface $\Gamma = \partial\Omega^C \cap \partial\Omega^F$. In practice, the complement model is not created. Out of the fine model, the zone of interest is equipped with an auxiliary representation (which shares the same features as the complement zone and which is thus coarser than the fine representation). The global problem is the assembly of the complement zone the auxiliary (coarse) representation of the zone of interest (cf. Figure C.4). We assume that the interface is on the boundary of the auxiliary domain $\Gamma \subset \partial\Omega^A$.

The reference problem reads:

$$a^R(u,v) = a^C(u,v) + a^F(u,v) = l^C(v) + l^F(v) = l^R(v) \quad \forall v \tag{C.14}$$

Using the auxiliary model, the global problem (solved by commercial software) ignores the fine model and reads:

$$a^G(u,v) = l^G(v) + (a^A(u,v) - l^A(v)) - (a^F(u,v) - l^F(v)) \quad \forall v \tag{C.15}$$

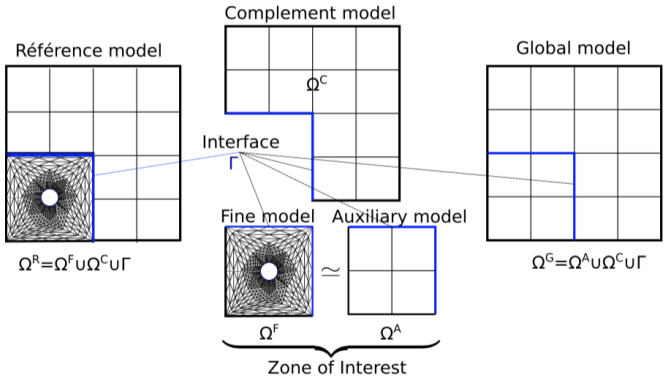


Figure C.4: Illustration of the models. The zone of interest has a fine and auxiliary representation (from [Gosselet et al., 2018]).

Using a fixed point approach (with initial loading $p_0 = 0$), the basic global/local iteration is thus recast as:

- Global problem (coarse problem with extra load $p_n$): find $u_n^G$ such that:

$$a^G(u_n^G, v) = l^G(v) + < p_n, v > \quad \forall v \tag{C.16}$$

- Fine problem (with imposed Dirichlet conditions): find $(u_n^F, \lambda_n^F)$ such that:

$$\begin{aligned} a^F(u_n^F, v) &= l^F(v) + < \lambda_n^F, v >_\Gamma \quad \forall v \\ < \mu, u_n^F - u_n^G >_\Gamma &= 0 \quad \forall \mu \end{aligned} \tag{C.17}$$

- Auxiliary problem (with imposed Dirichlet conditions): find $(u_n^A, \lambda_n^A)$ such that:

$$\begin{aligned} a^A(u_n^A, v) &= l^A(v) + < \lambda_n^A, v >_\Gamma \quad \forall v \\ < \mu, u_n^A - u_n^G >_\Gamma &= 0 \quad \forall \mu \end{aligned} \tag{C.18}$$

- Update

$$< p_{n+1}, v > = \left(a^A(u_n^A, v^A) - l^A(v^A)\right) - \left(a^F(u_n^F, v^F) - l^F(v^F)\right) \tag{C.19}$$

  with $v^A_{|\Gamma} = v^F_{|\Gamma} = v$.

We have the following properties:

- Assuming fine and auxiliary problems are solved exactly, we have $p_{n+1} = \lambda_n^A - \lambda_n^F$. The corrective load is then an immersed surface traction.

- Because the auxiliary problem corresponds to the restriction of the global problem on the zone of interest with global displacement imposed, we directly have $u_n^A = u^G_{n|\Omega^A}$. The introduction of the auxiliary problem is thus

not mandatory, it is just a workaround in case of software unable to compute the reaction in an immersed surface. The auxiliary problem can be solved in parallel with the fine problem.

- We can also define the reaction from the complement zone for a given $u_n^G$:

$$< \lambda_n^C, v >_\Gamma = a^C(u_n^G, v) - l^C(v) \quad \forall v \tag{C.20}$$

Then we see that $\lambda_n^C + \lambda_n^A = p_n$. The surface traction $p_n$ generates a discontinuity in the normal stress of the global problem.

- If we replace the auxiliary reaction by the complement one, we have $p_{n+1} = p_n + r_n$ with $r_n = -(\lambda_n^F + \lambda_n^C)$. In other words, the correction brought to $p_{n+1}$ corresponds to the lack of balance between the complement zone and the fine representation of the zone of interest. It is the residual $r$ of the algorithm. The algorithm converges when the two representations are in equilibrium ($r = 0$) in which case the extra load $p$ shall not evolve anymore.

- The algorithm makes use of domain integrals to communicate between subdomains; only interface data (on $\Gamma$) are exchanged, namely the displacement $u^G$ and the reactions $\lambda^F$ and $\lambda^A$ (or $\lambda^C$). As long as the interface $\Gamma$ is well represented in all models, it is not necessary to use the exact fine domain $\Omega^F$ in the auxiliary problem, any coarser representation is possible ($\Omega^A$). Typically micro-perforations or micro cracks need not be represented in the auxiliary problem. Of course modifying the representation of the zone of interest may have consequences on the convergence of the algorithm (but not on its limit which is the reference solution).

We now investigate a way to circumvent the constraint of coincidence between auxiliary and fine domains. This is important for our case where interface $\Gamma^F$ is moving while interface $\Gamma^A$ is fixed; only the separation between complementary and auxiliary models will evolve. We first focus on the overlap issue between fine and complementary models (similar to Schwarz decomposition with overlap).

Up to now, it was assumed that the interface was described as the boundary of elements for all models (so that a simple transfer matrix $T$ (an easy choice is the interpolation matrix of the coarse kinematics in the fine kinematics, or Mortar) is then sufficient to communicate between models on the interface). An alternative strategy is proposed which makes use of the possibility to have model overlap. In this case, there is no restriction of the definition of the meshes.

The starting point is the observation that the method can be formulated as the search for $p$ which is the stress discontinuity of the global mesh between the complement zone and the auxiliary description of the zone of interest. This discontinuity must be such that the complement zone is in equilibrium with the fine description of zone of interest loaded with Dirichlet conditions. Since $p$ is a discontinuity, for it to be well described in the coarse FE

model, it must be supported by the boundary of coarse elements. But there is no need for the support of $p$ to match the boundary of the zone of interest. The idea described in Figure C.6 can thus be followed. The fine subdomain $\Omega^F$ is positioned where needed in the zone of interest, its mesh is independent from the coarse mesh; we note $\Gamma^F = \partial\Omega^F$ its boundary. The auxiliary subdomain is the largest set of coarse elements fully contained in the zone of interest; we note $\Gamma^A = \partial\Omega^A$ its boundary. The two interfaces $\Gamma^F$ and $\Gamma^A$ thus do not coincide. $\Omega^C$ is defined as the complement of $\Omega^A$ in the global model ($\Omega^C = \Omega^G \backslash \Omega^A$). The fine and global model displacements are connected on $\Gamma^F$; $p$ is applied to the global model on $\Gamma^A$ with the aim to reach balance between the nodal reaction from complement model and the normal from the fine model projected on $\Gamma^A$. In the end, the coupled solution is $u^F$ in $\Omega^A$ and $u^G$ in $\Omega^G \backslash \Omega^F$. In the overlap, also called buffer zone $\Omega^B = \Omega^F \backslash \Omega^A$, the complement and fine models coexist.

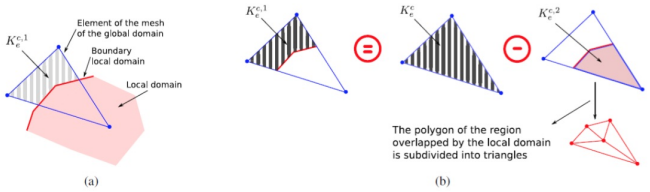


Figure C.5: Overlap case.

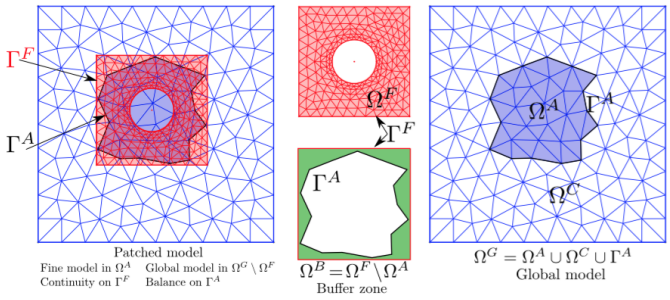


Figure C.6: Technique with overlap for non-conforming meshes (from [Gosselet et al., 2018].

The basic stationary iteration in the presence of overlap is:

- arbitrary initialization $p_0$
- compute $u_j^G$ from $p_j$ on $\Gamma^A$
- compute $\lambda_j^A$ from $u_j^G$ on $\Gamma^A$
- get $u^F_{\Gamma^F,i} = u^G(x_i)$ for $i$ a fine dof of $\Gamma^F$
- compute $u_j^F$ and $\sigma^F_{h,j}$ from $u^F_{\Gamma^F,i}$
- for $i$ spanning all global dofs on $\Gamma^A$, compute $\lambda^F_{j,i} = \int_{\Omega^A}(\sigma^F_{h,j} : \epsilon(\phi_i^G) - f.\phi_i^G) - \int_{\partial_n\Omega^A} g.\phi_i^G$

- compute residual $r_j = -(\lambda_j^F + p_j - \lambda_j^A)$

- update: $p_{j+1} = p_j + r_j$

The main practical difficulty is the computation of the fine reaction on $\Gamma^A$ with $\Omega^F$ not exactly represented on the coarse grid. This computation mixes the fine stress $\sigma_h^F$ and the coarse shape functions $\phi_i^G$. For each global dof $i$ over $\Gamma^A$, we consider iteration $j$ of the local-global algorithm:

$$\tilde{\lambda}_{j,i}^F = A^A(\phi_i^G, u_j^F) - l^A(\phi_i^G) \tag{C.21}$$

with $\phi_i^G$ the shape fonctions of the global model. The computation of this quantity can lead to numerical issues as the dual quantity to the unknown field is known only at Gauss points. Furthermore, micro quantities $u^F$ and macro quantities $\phi_i^G$ have to be mixed. The algorithm is similar to the previous one except that the updating phase now reads $p_{n+1,i} = \lambda_{n,i}^A - \tilde{\lambda}_{n,i}^F$. A technique which can be used to ciompute this quantity is using a Mortar coupling as describe in Figure C.5.

We develop the previous approach when coupling a diffusion-reaction problem (global model) with a convection-diffusion-reaction problem (local model). Figure C.7 shows the evolution of the local, global and auxiliary domain along with the time discretization of each models.

The fine model moves inside the global domain, and we distinguish two cases:

- when $\partial\Omega^G \cap \partial\Omega^F = 0$, the geometry of the fine model corresponds to the nominal geometry. In the following, we suppose we are always in this case;

- when $\partial\Omega^G \cap \partial\Omega^F = \Gamma_{GF}$, the geometry of the fine model evolves so that the velocity field of the mesh is not uniform. In the algorithm, we should split the boundaries of the fine and auxiliary domains in two entities: the one linked to the coupling and the one that copies boundary conditions of the global model.

Here, we assume that the time discretizations for each model are different. However, the time discretization of the fine local model can be seen as a subdivision of the global time discretization. We thus compute loading corrections to be applied to the global model at coexisting time points. Boundary conditions to be applied to the fine model are obtained by interpolation of the global solution between global time points.

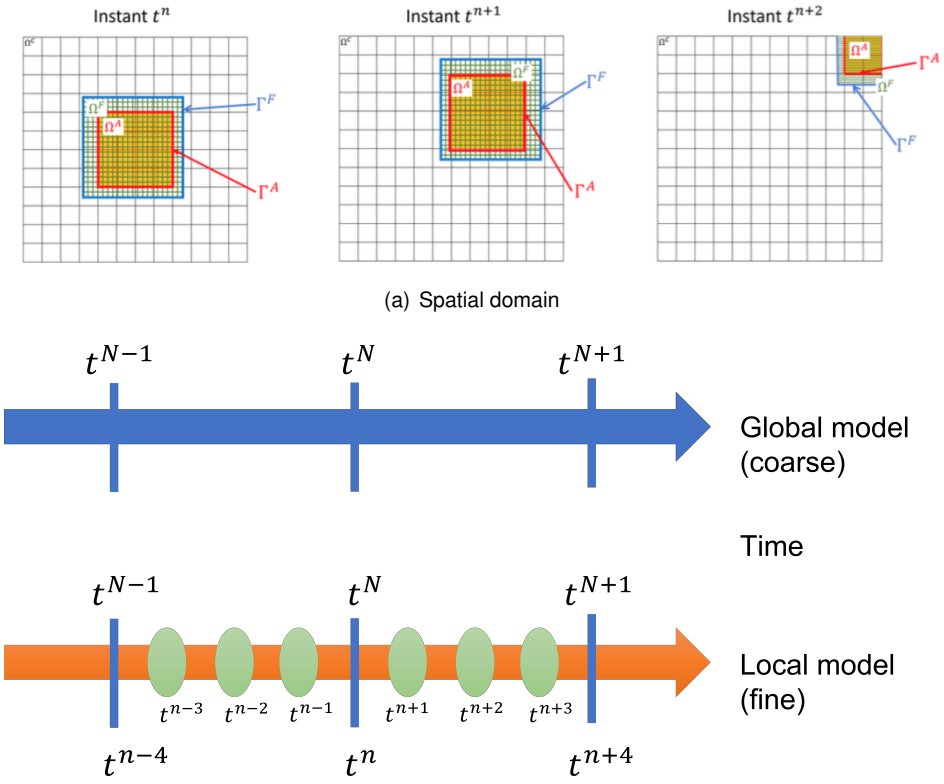


Figure C.7: Representation of the various models during the simulation.

The problem reads: find $\Delta u$ such that

$$
\begin{aligned}
&(\frac{\Delta u_G}{\Delta t_G}, v)_{\Omega^G} + \theta_G[a(\Delta u_G, v)_{\Omega^G} + (r\Delta u_G, v)_{\Omega^G}] \\
&+ (\frac{\Delta u_F}{\Delta t_F}, v)_{\Omega^F} + \theta_F[c(\mathbf{c}; \Delta u_F, v)_{\Omega^F} + a(\Delta u_F, v)_{\Omega^F} + (r\Delta u_F, v)_{\Omega^F}] \\
&- (\frac{\Delta u_G}{\Delta t_G}, v)_{\Omega^A(t^N)} + \theta_G[a(\Delta u_G, v)_{\Omega^A(t^N)} + (r\Delta u_G, v)_{\Omega^A(t^N)}] \\
&= -[a(u_G^{N-1}, v)_{\Omega^G} + (ru_G^{N-1}, v)_{\Omega^G}] + \theta_G(f_G^N, v)_{\Omega^G} + (1-\theta_G)(f_G^{N-1}, v)_{\Omega^G} \\
&- [c(\mathbf{c}; u_F^{N-1}, v)_{\Omega^F} + a(u_F^{N-1}, v)_{\Omega^F} + (ru_F^{N_1}, v)_{\Omega^F}] + \theta_F(f_F^N, v)_{\Omega^F} + (1-\theta_F)(f_F^{N-1}, v)_{\Omega^F} \\
&+ [a(u_G^{N-1}, v)_{\Omega^A(t^{N-1})} + (ru_G^{N-1}, v)_{\Omega^A(t^{N-1})}] - \theta_G(f_G^N, v)_{\Omega^A(t^N)} + (1-\theta_G)(f_G^{N-1}, v)_{\Omega^A(t^N-1)}
\end{aligned}
\tag{C.22}
$$

The problem involves $\Omega^A(t^{N-1})$ and $\Omega^A(t^N)$. As auxiliary and fine models do not coincide, we need to integrate the micro unknowns by macro shape functions. This implies $\Omega^A(t) \subset \Omega^F(t)$. We denote $\Omega_N^A$ the largest subset that respects this condition. We then restrict the auxiliary problem over this global time step to $\Omega_N^A$. The reference

problem thus reads: find $\Delta u$ such that

$$
\begin{aligned}
&(\frac{\Delta u_G}{\Delta t_G}, v)_{\Omega^G} + \theta_G[a(\Delta u_G, v)_{\Omega^G} + (r\Delta u_G, v)_{\Omega^G}] \\
&+ (\frac{\Delta u_F}{\Delta t_F}, v)_{\Omega^F} + \theta_F[c(\mathbf{c}; \Delta u_F, v)_{\Omega^F} + a(\Delta u_F, v)_{\Omega^F} + (r\Delta u_F, v)_{\Omega^F}] \\
&- (\frac{\Delta u_G}{\Delta t_G}, v)_{\Omega_N^A} + \theta_G[a(\Delta u_G, v)_{\Omega_N^A} + (r\Delta u_G, v)_{\Omega_N^A}] \\
&= -[a(u_G^{N-1}, v)_{\Omega^G} + (ru_G^{N-1}, v)_{\Omega^G}] + \theta_G(f_G^N, v)_{\Omega^G} + (1-\theta_G)(f_G^{N-1}, v)_{\Omega^G} \\
&- [c(\mathbf{c}; u_F^{N-1}, v)_{\Omega^F} + a(u_F^{N-1}, v)_{\Omega^F} + (ru_F^{N_1}, v)_{\Omega^F}] + \theta_F(f_F^N, v)_{\Omega^F} + (1-\theta_F)(f_F^{N-1}, v)_{\Omega^F} \\
&+ [a(u_G^{N-1}, v)_{\Omega_N^A} + (ru_G^{N-1}, v)_{\Omega_N^A}] - \theta_G(f_G^N, v)_{\Omega_N^A} + (1-\theta_G)(f_G^{N-1}, v)_{\Omega_N^A}
\end{aligned}
\tag{C.23}
$$

A priori, $\Omega_N^A$ changes at each interval $[t^{N-1}, t^N]$, but this should not induce numerical difficulties as the auxiliary problem is only a restriction of the global problem on which Dirichlet boundary conditions are imposed (on $\Gamma^A$).

The final algorithm is showed in Figure C.8.

**for** $N \leftarrow 2$ **to** $Nt_G$ **do**

Initialisation:

Compute $\Omega_N^A$

$n1 = (N-2) \times (Nt_L/Nt_G) + 1$ ; $n2 = (N-1) \times (Nt_L/Nt_G) + 1$ ;

**for** $n \leftarrow n1$ **to** $n2$ **do**

$\tilde{\Omega}_n^A = \arg \sup_{(\Omega \in \Omega^G) \subset \Omega_n^F} \Omega$

**end**

$\Omega_N^A = \bigcap_n \tilde{\Omega}_n^A$

**for** $m \leftarrow 1$ **to** $nbIter$ **do**

Global Problem:

Find $u_m^{N,G} = u_m^{N-1,G} + \Delta u_m^G \in \mathcal{V}(\Omega^G)$, $\forall w \in \mathcal{V}^0(\Omega^G)$

$$\left(w, \frac{\Delta u_m^G}{\Delta t_G}\right)_{\Omega^G} + \theta_G\left[a(w, \Delta u_m^G)_{\Omega^G} + (w, \sigma \Delta u_m^G)_{\Omega^G}\right] = -\left[a(w, u_m^{N-1,G})_{\Omega^G} + (w, \sigma u_m^{N-1,G})_{\Omega^G}\right]$$
$$+ \theta_G(w, s_G^N)_{\Omega^G} + (1-\theta_G)(w, s_G^{N-1})_{\Omega^G} + \langle p_m^N, w \rangle_{\Omega^G}$$

Local Problem:

**for** $n \leftarrow (n1+1)$ **to** $n2$ **do**

Find $u_m^{n,F} = u_m^{n-1,F} + \Delta u_m^F \in \mathcal{V}(\Omega^F)$ et $\lambda_m^{n,F} \in \mathcal{V}_{\Gamma^F}^*$, $\forall (w, \mu) \in \mathcal{V}^0(\Omega^F) \times \mathcal{V}_{\Gamma^F}^*$

$$\left(w, \frac{\Delta u_m^F}{\Delta t_F}\right)_{\Omega^F} + \theta_F\left[c(\boldsymbol{a}; w, \Delta u_m^F)_{\Omega^F} + a(w, \Delta u_m^F)_{\Omega^F} + (w, \sigma \Delta u_m^F)_{\Omega^F}\right] =$$
$$-\left[c(\boldsymbol{a}; w, u_m^{n-1,F})_{\Omega^F} + a(w, u_m^{n-1,F})_{\Omega^F} + (w, \sigma u_m^{n-1,F})_{\Omega^F}\right]$$
$$+ \theta_F(w, s_F^n)_{\Omega^F} + (1-\theta_F)(w, s_F^{n-1})_{\Omega^F} + \langle \lambda_m^{n,F}, w \rangle_{\Gamma^F}$$
$$\langle \mu, u_m^{n,F} - \tilde{u}_m^{n,G} \rangle_{\Gamma^F} = 0$$

$\tilde{u}_m^{n,G}$ is obtain by projection on the domain $\Omega^F$

the global solution $u_m^G$ is interpolated at local time steps $t^n$

**end**

Auxiliary Problem:

Find $u_m^{N,A} = u_m^{N-1,A} + \Delta u_m^A \in \mathcal{V}(\Omega^A)$ et $\lambda_m^{N,A} \in \mathcal{V}_{\Gamma^A}^*$, $\forall (w, \mu) \in \mathcal{V}^0(\Omega^A) \times \mathcal{V}_{\Gamma^A}^*$

$$\left(w, \frac{\Delta u_m^A}{\Delta t_G}\right)_{\Omega_N^A} + \theta_G\left[a(w, \Delta u_m^A)_{\Omega_N^A} + (w, \sigma \Delta u_m^A)_{\Omega_N^A}\right] = -\left[a(w, u_m^{N-1,A})_{\Omega_N^A} + (w, \sigma u_m^{N-1,A})_{\Omega_N^A}\right]$$
$$+ \theta_G(w, s_G^N)_{\Omega_N^A} + (1-\theta_G)(w, s_G^{N-1})_{\Omega_N^A} + \langle \lambda_m^{N,A}, w \rangle_{\Gamma^A}$$
$$\langle \mu, u_m^{N,A} - u_m^{N,G} \rangle_{\Gamma^A} = 0, \text{ Et } u_m^{N-1,A} = u_m^{N-1,G}$$

Update:

For all global degree of freedom $i$ on $\Gamma^A$

$$\tilde{\Delta} u_m^F = u_m^{n2,F} - u_m^{n1,F}$$
$$\tilde{\lambda}_{m,i}^{N,F} = \left(\phi_i^G, \frac{u_m^{n2,F}}{\Delta t_G}\right)_{\Omega_N^A} + \theta_G\left[a(\phi_i^G, u_m^{n2,F})_{\Omega_N^A} + (\phi_i^G, \sigma u_m^{n2,F})_{\Omega_N^A}\right]$$
$$- \left(\phi_i^G, \frac{u_m^{n1,F}}{\Delta t_G}\right)_{\Omega_N^A} + (1-\theta_G)\left[a(\phi_i^G, u_m^{n1,F})_{\Omega_N^A} + (\phi_i^G, \sigma u_m^{n1,F})_{\Omega_N^A}\right]$$
$$- \theta_G(w, s_G^N)_{\Omega_N^A} - (1-\theta_G)(w, s_G^{N-1})_{\Omega_N^A}$$
$$p_{m+1,i}^N = \left(\lambda_{m,i}^{N,A} - \tilde{\lambda}_{m,i}^{N,F}\right)$$

**end**

Projection:

For all degree of freedom of $\Omega_N^A$

$u_m^{N,G} = u_m^{n2,F}$

**end**

Figure C.8: Coupling algorithm.

## Local reduced order modeling

A ROM technique of interest for problems characterized by steep moving gradients has been introduced in [Cosimo et al., 2014, Cosimo et al., 2017]. In this work, considering parabolic problems with highly concentrated moving sources, a non-iterative global-local ROM is formulated, in which the local nature of the steep moving gradients is exploited by modeling the neighborhood of the heat source with a moving local domain (with fine mesh), which is coupled to the global domain (described by a coarse mesh). This way, there is no local mesh refinement, i.e. no change in the mesh topology, and the local solution is quasi-stationary. A POD-based ROM is then developed for the moving local domain (but a PGD-based ROM could also be applied). The proposed technique establishes a valid approach to tackle non-separability of space and time dimensions of these problems.
In order to address compatibility conditions between local and global domains, the mortar element approach on overlapping non-nested grids developed in [Christophe et al., 2015] was implemented. Also, several other aspects specific to transient problems with moving local domains were carefully studied, such as the projection of the information from the previous time step to the current time step.

Exploiting the local nature of the steep moving gradients was also performed in [Canales et al., 2016] within the vademecum-GFEM (V-GFEM) method. In this method, the FE space was locally enriched using GFEM [Melenk and Babuska, 1996] to capture sharp local features, with local parametric solution taking the solution field of the surrounding as boundary conditions. This local solution is precomputed offline using PGD and stored in the form of a computational vademecum so that it can be used online with negligible cost. It is then particularized to fit the approximation space in the enrichment region attached to a moving source at each time step, with no need of conformal meshes and within the GFEM framework applied to the global problem. This may be performed with an explicit scheme (using solution at the enrichment domain boundary at the previous time step) or with an implicit scheme using a fixed-point strategy to update the enrichment solution.
Extra-coordinates are not limited to technological parameters of the process, but also include essential boundary conditions at the border $\Gamma_e$ of the enriched region (after projection on a polynomial global basis).
However, the enrichment function was the solution of a steady-state problem (neglecting transient effects locally), solved in a fixed geometry after introducing a convective operator, which does not permit to describe correctly the non-stationary regime of the problem. An alternative would be the global-local GFEM [O'Hara et al., 2009] where a time-dependent enrichment function is used.

In [Gonzalez et al., 2013], efficient stabilizations are proposed when performing PGD on high dimensional advection-diffusion models which naturally lead to unstable oscillating solutions [Donea and Huerta, 2003]. They resort to classical stabilization methods in FEM including upwinding of convective terms [Heinrich et al., 1977], such

that the streamline upwind/Petrov-Galerkin (SUPG) method [Hughes and Brooks, 1979]. The focus is on the extension of standard SUPG or subgrid scale stabilizations to solutions expressed in a separated approximation format. The following steady-state convection-diffusion reaction equation is considered:

$$\begin{aligned} \mathbf{c}\cdot\nabla u - \nabla\cdot(k\nabla u) + ru = s \quad &\text{in } \Omega \subset \mathcal{R}^{n_d} \\ u = u_d \quad &\text{on } \Gamma_D \\ k\nabla u\cdot\mathbf{n} = t \quad &\text{on } \Gamma_N \end{aligned} \tag{C.24}$$

with $\mathbf{c}$ is the advective velocity, $k > 0$ the diffusivity, $r$ a reaction term and $s$ a volumetric source term. The weak form is to find $u$ such that:

$$a(u,w) + c(\mathbf{c};u,w) + (ru,w) = (s,w) + (t,w)_{\Gamma_N} \quad \forall w \tag{C.25}$$

with

$$a(u,w) = \int_\Omega k\nabla u\cdot\nabla w \quad ; \quad c(\mathbf{c};u,w) = \int_\Omega (\mathbf{c}\cdot\nabla u)w \quad ; \quad (u,w) = \int_\Omega uw \quad ; \quad (t,w)_{\Gamma_N} = \int_{\Gamma_N} tw \tag{C.26}$$

The general form of a consistent stabilization technique is [Donea and Huerta, 2003]:

$$a(u,w) + c(\mathbf{c};u,w) + (ru,w) + \sum_e \int_{\Omega^e} \mathbb{P}(w)\tau\mathbb{R}(u) = (s,w) + (t,w)_{\Gamma_N} \tag{C.27}$$

where $\mathbb{P}(w)$ is some operator applied to test functions, $\mathbb{R}(u) = \mathbf{c}\cdot\nabla u - \nabla\cdot(k\nabla u) + ru - s$ is the residual associated to the strong form, and $\tau$ is the stabilization parameter. In the SUPG method, $\mathbb{P}(w) = \mathbf{c}\cdot\nabla w$, whereas in SGS (subgrid scale) $\mathbb{P}(w) == -\mathbb{L}^*(w)$ (adjoint operator).

Two alternative approaches are developed to get a stabilized technique based on the use of PGD: the first one does the separation in infinite dimensional spaces, then when the FE discretization is needed the optimal stabilization parameter is chosen; the second one proceeds conversely, first the high-dimensional convection-diffusion equation is discretized taking into account that stabilization is needed, then separation following the PGD rationale is imposed. The PGD is applied to the weak form, the reaction term being neglected $r = 0$ for the sake of simplicity. The weak problem becomes to find $R$ and $S$ such that:

$$a(RS,w) + c(\mathbf{c};RS,w) = (s,w) + (t,w)_{\Gamma_N} - a(u^n,w) - c(\mathbf{c};u^n,w) \quad \forall w \tag{C.28}$$

The PGD proceeds by a sort of alternating direction strategy, assuming iteratively that either $R$ or $S$ is known.

Assuming for instance that $R$ is given, the weak form reads:

$$a(RS, RS^*) + c(\mathbf{c}; RS, RS^*) = (s, RS^*) + (t, RS^*)_{\Gamma_N} - a(u^n, RS^*) - c(\mathbf{c}; u^n, RS^*) \quad \forall w \tag{C.29}$$

which is a 1D convection-diffusion reaction problem ($\Omega = \Omega_x \otimes \Omega_y$). This weak form is stabilized as follows:

$$(\gamma_y S', (S^*)')_{\Omega_y} + (c_y S, S*)_{\Omega_y} + (k_y S, S*)_{\Omega_y} + \sum_e \int_{\Omega_y^e} \mathbb{P}_y(S^*)\tau_y(c_y S' - (\gamma_y S')' + k_y S) = (b_y, S^*)_{\Omega_y} + S^* p_{y|\Gamma_N^y y} + \sum_e \int_{\Omega_y^e} \mathbb{P}_y(S^*)\tau_y b_y \tag{C.30}$$

with $\mathbb{P}_y(w) = c_y w'$ in SUPG and $\mathbb{P}_y(w) = c_y w' + (\gamma_y w')' - k_y w$ in SGS. Optimal values of the stabilization parameter can be obtained if PGD results in 1D problems. For linear elements, the second derivatives in the stabilization terms are zero but recall that for high-order elements, consistent stabilization is important.

The other natural possibility is to perform a separated approximation of the already stabilized equation. The method proceeds in a very similar way but only one stabilization parameter is now needed.

*Remark. In [Badias et al., 2017], the construction of local PGD reduced order models is addressed in order to circumvent the difficulty of poor separability of the solution. Several strategies are introduced to estimate the size of the different patches in the solution manifold where PGD is applied. No gluing or special technique is needed to deal with the resulting set of local reduced order models. We also mention the possible use of space-time (non-separated) basis functions, as in [Gerbeau and Lombardi, 2012] where the concept of Lax pairs is employed to obtain a reduced model with a special application to wave and soliton problems, or in [Allier et al., 2015] where an analytic solution in an infinite medium is used as a lifting and complemented with a PGD solution.*

# Appendix D

# List of personal publications

## National & international conferences

[C1] A. Verwee, L. Chamoin, O. Allix, Certification and adaptive control of non-intrusive coupling methods for problems with highly concentrated moving sources, *14th World Congress in Computational Mechanics (WCCM 2020)*, Paris, France (2020)

[C2] A. Verwee, L. Chamoin, Certification, adaptivity, and reduction in non-intrusive model couplings, *10th International Conference on Adaptive Modeling and Simulation (ADMOS 2021)*, Göteborg, Suède (2021)

## Articles in international journals

[A1] A posteriori error estimation and adaptivity in non-intrusive model couplings using the Constitutive Relation Error framework, *in preparation* (2021)

[A2] Certified local reduced order modeling in non-intrusive model couplings, *in preparation* (2021)

# Bibliography

[Abdulle and Nonnenmacher, 2009] Abdulle, A. and Nonnenmacher, A. (2009). A posteriori error analysis of the heterogeneous multiscale method for homogenization problems. *Comptes Rendus Académie des Sciences Paris I*, 347:1081–1086.

[Ainsworth, 2001] Ainsworth, M. (2001). Essential boundary conditions and multi-point constraints in finite element analysis. *Computer Methods in Applied Mechanics and Engineering*, 190:6323–6339.

[Ainsworth and Oden, 2000] Ainsworth, M. and Oden, J. (2000). *A Posteriori Error Estimation in Finite Element Analysis*. John Wiley & Sons.

[Aitken, 1926] Aitken, A. (1926). On bernoulli's numerical solution of algebraic equations. *Proceedings of the Royal Society of Edinburgh*, 46:289–305.

[Alfaro et al., 2015] Alfaro, I., Gonz·lez, D., Zlotnik, S., DÌez, P., Cueto, E., and Chinesta, F. (2015). An error estimator for real-time simulators based on model order reduction. *Advanced Modeling & Simulation in Engineering Sciences*, 2(1):30.

[Allier et al., 2015] Allier, P.-E., Chamoin, L., and Ladevèze, P. (2015). Proper generalized decomposition computational methods on a benchmark problem: introducing a new strategy based on constitutive relation error minimization. *Advanced Modeling and Simulation in Engineering Sciences*, 2:17.

[Ammar et al., 2010] Ammar, A., Chinesta, F., Diez, P., and Huerta, A. (2010). An error estimator for separated representations of highly multidimensional models. *Computer Methods in Applied Mechanics and Engineering*, 199(25-28):1872–1880.

[Ammar et al., 2014] Ammar, A., Huerta, A., Leygue, A., Chinesta, F., and Cueto, E. (2014). Parametric solutions involving geometry: a step towards efficient shape optimization. *Computer Methods in Applied Mechanics and Engineering*, 268(1):178–193.

[Aubin and Bouchard, 1970] Aubin, J.-P. and Bouchard, H. (1970). Some aspects of the method of the hypercircle applied to elliptic variational problems. *in Numerical Solution of Partial Differential Equations, Academic Press*.

[Babuska et al., 2003] Babuska, I., Banerjee, U., and Osborn, J. (2003). Survey of meshless and generalized finite element methods. *Acta Numerica*, 12:1–125.

[Babuska et al., 1994] Babuska, I., Strouboulis, T., Upadhyay, C., Gangaraj, S., and Copps, K. (1994). Validation of a posteriori error estimators by numerical approach. *International Journal for Numerical Methods in Engineering*, 37(7):1073–1123.

[Badias et al., 2018] Badias, A., Alfaro, I., Gonzalez, D., Chinesta, F., and Cueto, E. (2018). Reduced order modeling for physically-based augmented reality. *Computer Methods in Applied Mechanics and Engineering*, 341:53–70.

[Badias et al., 2017] Badias, A., Gonzalez, D., Alfaro, I., Chinesta, F., and Cueto, E. (2017). Local proper generalized decomposition. *International Journal for Numerical Methods in Engineering*, 112(12):1715–1732.

[Barrault et al., 2004] Barrault, M., Maday, Y., Nguyen, N., and Patera, A. (2004). An 'empirical interpolation' method: application to efficient reduced-basis discretization of partial differential equations. *Comptes Rendus Mathématique*, 339(9):667–672.

[Bauman et al., 2009] Bauman, P., Oden, J., and Prudhomme, S. (2009). Adaptive multiscale modeling of polymeric materials: Arlequin coupling and goals algorithms. *Computer Methods in Applied Mechanics and Engineering*, 198:799–818.

[Becker and Rannacher, 1996] Becker, R. and Rannacher, R. (1996). A feed-back approach to error control in finite element methods: Basic analysis and examples. *East-West Journal of Numerical Mathematics*, 4:237–264.

[Becker and Rannacher, 2001] Becker, R. and Rannacher, R. (2001). An optimal control approach to a posteriori error estimation in finite element methods. *A. Isereles (Ed.), Acta Numerica, Cambridge University Press*, 10:1–120.

[Belgacem, 1999] Belgacem, F. (1999). The mortar finite element method with lagrange multipliers. *Numerische Mathematik*, 84(2):173–197.

[Ben Dhia, 1998] Ben Dhia, H. (1998). Problèmes mécaniques multi-échelles: la méthode arlequin. *Comptes Rendus Académie des Sciences II*, 326:899–904.

[Ben Dhia and Rateau, 2005] Ben Dhia, H. and Rateau, G. (2005). The arlequin method as a flexible engineering design tool. *International Journal for Numerical Methods in Engineering*, 62(11):1442–1462.

[Berger et al., 2016] Berger, J., Gasparin, S., Chhay, M., and Mendes, N. (2016). Estimation of temperature- dependent thermal conductivity using proper generalised decomposition for building energy management. *Journal of Building Physics*, 40(3):235–262.

[Berger et al., 2017] Berger, J., Orlande, H., and Mendes, N. (2017). Proper generalized decomposition model reduction in the bayesian framework for solving inverse heat transfer problems. *Inverse Problems in Science and Engineering*, 25(2):260–278.

[Beringhier and Gigliotti, 2015] Beringhier, M. and Gigliotti, M. (2015). A novel methodology for the rapid identification of the water diffusion coefficients of composite materials. *Composites: Part A*, 68:212–218.

[Bernardi et al., 2005] Bernardi, C., Maday, Y., and Rapetti, F. (2005). Basics and some applications of the mortar element method. *GAMM-Mitteilungen*, 28(2):97–123.

[Bettinotti et al., 2014] Bettinotti, O., Allix, O., Perego, U., Oancea, V., and Malherbe, B. (2014). A fast weakly intrusive multiscale method in explicit dynamics. *International Journal for Numerical Methods in Engineering*, 100(8):577–595.

[Bettinotti et al., 2017] Bettinotti, O., Allix, O., Perego, U., Oancea, V., and Malherbe, B. (2017). Simulation of delamination under impact using a global-local method in explicit dynamics. *Finite Elements in Analysis and Design*, 125:1–13.

[Blanchard et al., 2019] Blanchard, M., Allix, O., Gosselet, P., and Desmeure, G. (2019). Space/time global/local noninvasive coupling strategy: application to viscoplastic structures. *Finite Elements in Analysis and Design*, 156:1–12.

[Bognet et al., 2012] Bognet, B., Bordeu, F., Chinesta, F., Leygue, A., and Poitou, A. (2012). Advanced simulation of models defined in plate geometries: 3d solutions with 2d computational complexity. *Computer Methods in Applied Mechanics and Engineering*, 201-204:1–12.

[Bouclier and Passieux, 2018] Bouclier, R. and Passieux, J. (2018). A nitsche-based non-intrusive coupling strategy for global/local isogeometric structural analysis. *Computer Methods in Applied Mechanics and Engineering*, 340:253–277.

[Bouclier et al., 2016] Bouclier, R., Passieux, J., and Salaun, M. (2016). Local enrichment of nurbs patches using a non-intrusive coupling strategy: geometric details, local refinement, inclusion, fracture. *Computer Methods in Applied Mechanics and Engineering*, 300:1–26.

[Bouclier et al., 2017] Bouclier, R., Passieux, J., and Salaun, M. (2017). Development of a new, more regular, mortar method for the coupling of nurbs subdomains within a nurbs patch: Application to a non-intrusive local enrichment of nurbs patches. *Computer Methods in Applied Mechanics and Engineering*, 316(1):123–150.

[Brezinski, 2000] Brezinski, C. (2000). Convergence acceleration during the 20th century. *Journal of Computational and Applied Mathematics*, 122:1–21.

[Brezzi et al., 2001] Brezzi, F., Lions, J., and Pironneau, O. (2001). Analysis of a chimera method. *Comptes Rendus Académie des Scences I*, 332(7):655–660.

[Brivadis et al., 2015] Brivadis, E., Buffa, A., Wohlmuth, B., and Wunderlich, L. (2015). Isogeometric mortar methods. *Computer Methods in Applied Mechanics and Engineering*, 284:292–319.

[Broughton et al., 1999] Broughton, J., Abraham, F., Bernstein, N., and Kaxiras, E. (1999). Concurrent coupling of length scales: methodology and application. *Physical Review B*, 60(4):2391–2403.

[Cai and Keyes, 2002] Cai, X. and Keyes, D. (2002). Nonlinearly preconditioned inexact newton algorithms. *SIAM Journal on Scientific Computing*, 24(1):183–200.

[Canales et al., 2016] Canales, D., Leygue, A., Chinesta, F., Gonzalez, D., Cueto, E., Feulvarch, E., Bergheau, J., and Huerta, A. (2016). Vademecum-based gfem (v-gfem): optimal enrichment for transient problems. *International Journal for Numerical Methods in Engineering*, 108:971–989.

[Canuto and Kozubek, 2007] Canuto, C. and Kozubek, T. (2007). A fictitious domain approach to the numerical solution of pdes in stochastic domains. *Numerische Mathematik*, 107(2):257–293.

[Cao and Kelly, 2003] Cao, T. and Kelly, D. (2003). Pointwise and local error estimates for the quantities of interest in two-dimensional elasticity. *Computers and Mathematics with Applications*, 46(1):69–79.

[Carneiro and Antonio, 2019] Carneiro, G. and Antonio, C. (2019). Reliability-based robust design optimization with the reliability index approach applied to composite laminate structures. *Composite Structures*, 209:844–855.

[Chamoin and Desvillettes, 2013] Chamoin, L. and Desvillettes, L. (2013). Control of modeling errors in the coupling of linear transport and diffusion models. *Computer Methods in Applied Mechanics and Engineering*, 261-262:83–95.

[Chamoin and Díez, 2016] Chamoin, L. and Díez, P. (2016). *Verifying Calculations, Forty Years on: An Overview of Classical Verification Techniques for FEM Simulations*. SpringerBriefs.

[Chamoin et al., 2012] Chamoin, L., Florentin, E., Pavot, S., and Visseq, V. (2012). Robust goal-oriented error estimation based on the constitutive relation error for stochastic problems. *Computers and Structures*, 106-107:189–195.

[Chamoin and Ladevèze, 2007] Chamoin, L. and Ladevèze, P. (2007). Bounds on history-dependent or independent local quantities in viscoelasticity problems solved by approximate methods. *International Journal for Numerical Methods in Engineering*, 71(12):1387–1411.

[Chamoin and Ladevèze, 2008] Chamoin, L. and Ladevèze, P. (2008). A non-intrusive method for the calculation of strict and efficient bounds of calculated outputs of interest in linear viscoelasticity problems. *Computer Methods in Applied Mechanics and Engineering*, 197(9-12):994–1014.

[Chamoin and Ladevèze, 2012] Chamoin, L. and Ladevèze, P. (2012). Robust control of pgd-based numerical simulations. *European Journal of Computational Mechanics*, 21(3-6):195–207.

[Chamoin and Legoll, 2018] Chamoin, L. and Legoll, F. (2018). A posteriori error estimation and adaptive strategy for the control of msfem computations. *Computer Methods in Applied Mechanics and Engineering*, 336:1–38.

[Chamoin and Legoll, 2021] Chamoin, L. and Legoll, F. (2021). Goal-oriented error estimation and adaptivity in msfem computations. *Computational Mechanics*, 67:1201–1228.

[Chamoin et al., 2017] Chamoin, L., Pled, F., Allier, P.-E., and Ladevèze, P. (2017). A posteriori error estimation and adaptive strategy for pgd model reduction applied to parametrized linear parabolic problems. *Computer Methods in Applied Mechanics and Engineering*, 327:118–146.

[Chamoin and Thai, 2019] Chamoin, L. and Thai, H. (2019). Certified real-time shape optimization using isogeometric analysis, pgd model reduction, and a posteriori error estimation. *International Journal for Numerical Methods in Engineering*, 119:151–176.

[Chantrait et al., 2014] Chantrait, T., Rannou, J., and Gravouil, A. (2014). Low intrusive coupling of implicit and explicit time integration schemes for structural dynamics: application to low energy impacts on composite structures. *Finite Elements in Analysis and Design*, 86:23–33.

[Chatterjee, 2000] Chatterjee, A. (2000). An introduction to the proper orthogonal decomposition. *Current Science*, 78(7):808–817.

[Chen et al., 2017] Chen, P., Quarteroni, A., and Rozza, G. (2017). Reduced basis methods for uncertainty quantification. *SIAM/ASA Journal on Uncertainty Quantification*, 5(1):813–869.

[Chevreuil et al., 2013] Chevreuil, M., Nouy, A., and Safatly, E. (2013). A multiscale method with patch for the solution of stochastic partial differential equations with localized uncertainties. *Computer Methods in Applied Mechanics and Engineering*, 255:255–274.

[Chinesta et al., 2010] Chinesta, F., Ammar, A., and Cueto, E. (2010). Recent advances and new challenges in the use of the proper generalized decomposition for solving multidimensional models. *Archives of Computational Methods in Engineering*, 17(4):327–350.

[Chinesta and Cueto, 2014] Chinesta, F. and Cueto, E. (2014). *PGD-Based Modeling of Materials, Structures and Processes*. ESAFORM Bookseries on Material Forming.

[Chinesta et al., 2017] Chinesta, F., Huerta, A., Rozza, G., and Willcox, K. (2017). Model order reduction. *in Encyclopedia of Computational Mechanics*.

[Chinesta et al., 2014] Chinesta, F., Keunings, R., and Leygue, A. (2014). *The proper generalized decomposition for advanced numerical simulation*. Springer.

[Chinesta et al., 2011] Chinesta, F., Ladevèze, P., and Cueto, E. (2011). A short review on model reduction based on proper generalized decomposition. *Archives of Computational Methods in Engineering*, 18:395–404.

[Chinesta et al., 2013] Chinesta, F., Leygue, A., Bordeu, F., Aguado, J., Cueto, E., Gonzalez, D., Alfaro, I., Ammar, A., and Huerta, A. (2013). Pgd-based computational vademecum for efficient design, optimization and control. *Archives of Computational Methods in Engineering*, 20:31–59.

[Christophe et al., 2015] Christophe, A., Bihan, Y., and Rapetti, F. (2015). A mortar element approach on overlapping non-nested grids: Application to eddy current non- destructive testing. *Applied Mathematics and Computation*, 267:71–82.

[Chung et al., 2016] Chung, E., Leung, W., and Pollock, S. (2016). Goal-oriented adaptivity for gmsfem. *Journal of Computational and Applied Mathematics*, 296:625–637.

[Cirak and Ramm, 1998] Cirak, F. and Ramm, E. (1998). A posteriori error estimation and adaptivity for linear elasticity using the reciprocal theorem. *Computer Methods in Applied Mechanics and Engineering*, 156:351–362.

[Conn et al., 1991] Conn, A., Gould, N., and Toint, P. (1991). Convergence of quasi-newton matrices generated by the symmetric rank one update. *Mathematical Programming*, 50:177–195.

[Coorevits et al., 1992] Coorevits, P., Ladevèze, P., Pelle, J.-P., and Rougeot, P. (1992). Some new applications of a method for the control and optimization of fe computations. *New Advances in Computational Structural Mechanics*.

[Cormier et al., 1999] Cormier, N., Smallwood, B., Sinclair, G., and Meda, G. (1999). Aggressive submodelling of stress concentrations. *International Journal for Numerical Methods in Engineering*, 46(6):889–909.

[Cosimo et al., 2014] Cosimo, A., Cardona, A., and Idelsohn, S. (2014). Improving the k-compressibility of hyper reduced order models with moving sources: applications to welding and phase change problems. *Computer Methods in Applied Mechanics and Engineering*, 274:237–263.

[Cosimo et al., 2017] Cosimo, A., Cardona, A., and Idelsohn, S. (2017). Global-local rom for the solution of parabolic problems with highly concentrated moving sources. *Computer Methods in Applied Mechanics and Engineering*, 326:739–756.

[Cottereau et al., 2009] Cottereau, R., Díez, P., and Huerta, A. (2009). Strict error bounds for linear solid mechanics problems using a subdomain based flux-free method. *Computational Mechanics*, 44(4):533–547.

[Courard et al., 2016] Courard, A., Néron, D., Ladevèze, P., and Ballere, L. (2016). Integration of pgd- virtual charts into an engineering design process. *Computational Mechanics*, 57:637–651.

[Cresta et al., 2007] Cresta, P., Allix, O., Rey, C., and Guinard, S. (2007). Nonlinear localization strategies for domain decomposition methods: application to post-buckling analyses. *Computer Methods in Applied Mechanics and Engineering*, 196(8):1436–1446.

[Cui et al., 2015] Cui, T., Marzouk, Y., and Willcox, K. (2015). Data-driven model reduction for the bayesian solution of inverse problems. *International Journal for Numerical Methods in Engineering*, 102(5):966–990.

[Daghia and Ladevèze, 2012] Daghia, F. and Ladevèze, P. (2012). A micro-meso computational strategy for the prediction of the damage and failure of laminates. *Composites and Structures*, 94(12):3644–3653.

[Darema, 2004] Darema, F. (2004). Dynamic data driven applications systems: a new paradigm for application simulations and measurements. *In International Conference on Computational Science, Springer*, pages 662–669.

[Darema, 2015] Darema, F. (2015). Dddas, a key driver for large-scale-big-data and large-scale-big-computing. *In S. Koziel, L. Leifsson, M. Lees, V.V Krzhizhanovskaya, J. Dongarra, P.M.A Sloot editors, ICCS 2015, Procedia Computer Science*, 51:2463.

[Debongnie et al., 1995] Debongnie, J., Zhong, H., and Beckers, P. (1995). Dual analysis with general boundary conditions. *Computer Methods in Applied Mechanics and Engineering*, 122:183–192.

[Destuynder and Métivet, 1999] Destuynder, P. and Métivet, B. (1999). Explicit error bounds in a conforming finite element method. *Mathematics of Computation*, 68(228):1379–1396.

[Donea and Huerta, 2003] Donea, J. and Huerta, A. (2003). *Finite Element Methods for Flow Problems*. John Wiley & Sons.

[Donea et al., 2004] Donea, J., Huerta, A., Ponthot, J., and Rodriguez-Ferran, A. (2004). Arbitrary lagrangian-eulerian methods. *in Encyclopedia of Computational Mechanics*.

[Drohmann et al., 2012] Drohmann, M., Haasdonk, B., and Ohlberger, M. (2012). Reduced basis approximation for nonlinear parametrized evolution equations based on empirical operator interpolation. *SIAM Journal of Scientific Computing*, 34:937–969.

[Drucker, 1964] Drucker, D. (1964). On the postulate of stability of material in the mechanics of continua. *Journal of Mechanics*, 3(2):235–249.

[Duarte and Kim, 2008] Duarte, C. and Kim, D. (2008). Analysis and applications of a generalized finite element method with global-local enrichment functions. *Computer Methods in Applied Mechanics and Engineering*, 197(6-8):487–504.

[Dumon et al., 2011] Dumon, A., Allery, C., and Ammar, A. (2011). Proper generalized decomposition (pgd) for the resolution of navier stokes equations. *Journal of Computational Physics*, 230(4):1387–1407.

[Dureisseix and Bavestrello, 2006] Dureisseix, D. and Bavestrello, H. (2006). Information transfer between incompatible finite element meshes: application to coupled thermo-viscoelasticity. *Computer Methods in Applied Mechanics and Engineering*, 195(44-47):6523–6541.

[Duval et al., 2018] Duval, M., Lozinski, A., Passieux, J., and Salaun, M. (2018). Residual error based adaptive mesh refinement with the non-intrusive patch algorithm. *Computer Methods in Applied Mechanics and Engineering*, 329:118–143.

[Duval et al., 2016] Duval, M., Passieux, J., Salaun, M., and Guinard, S. (2016). Non-intrusive coupling: recent advances and scalable nonlinear domain decomposition. *Archives of Computational Methods in Engineering*, 23(1):17–38.

[Efendiev and Hou, 2009] Efendiev, Y. and Hou, T. (2009). *Multiscale Finite Element Methods: Theory and Applications*. Springer, New York.

[Ern et al., 2007] Ern, A., Nicaise, S., and Vohralik, M. (2007). An accurate h(div) flux reconstruction for discontinuous galerkin approximations of elliptic problems. *Comptes Rendus Académie des Sciences, Paris, Série I*, 345(12):709–712.

[Ern and Vohralik, 2010] Ern, A. and Vohralik, M. (2010). A posteriori error estimation based on potential and flux reconstruction for the heat equation. *SIAM Journal on Numerical Analysis*, 345(48):198–223.

[Ern and Vohralik, 2015] Ern, A. and Vohralik, M. (2015). Polynomial-degree-robust a posteriori estimates in a unified setting for conforming, nonconforming, discontinuous galerkin, and mixed discretizations. *SIAM Journal on Numerical Analysis*, 53(2):1058–1081.

[Falco et al., 2013] Falco, A., Hilario, L., Montes, N., and Mora, M. (2013). Numerical strategies for the galerkin-proper generalized decomposition method. *Mathematical and Computer Modelling*, 57(7):1694–1702.

[Farhat et al., 2001] Farhat, C., Lesoinne, M., Tallec, P. L., Pierson, K., and Rixen, D. (2001). Feti-dp: a dual-primal unified feti method - part i: A faster alternative to the two-level feti method. *International Journal for Numerical Methods in Engineering*, 50(7):1523–1544.

[Farhat and Roux, 1991] Farhat, C. and Roux, F. (1991). A method of finite element tearing and interconnecting and its parallel solution algorithm. *International Journal for Numerical Methods in Engineering*, 32:1205–1227.

[Favoretto et al., 2019] Favoretto, B., Hillerin, C., Bettinotti, O., Oancea, V., and Barbarulo, A. (2019). Reduced order modeling via pgd for highly transient thermal evolutions in additive manufacturing. *Computer Methods in Applied Mechanics and Engineering*, 349:405–430.

[Feyel, 2003] Feyel, F. (2003). A multilevel finite element method (fe2) to describe the response of highly non-linear structures using generalized continua. *Computer Methods in Applied Mechanics and Engineering*, 192:3233–3244.

[Florentin et al., 2002] Florentin, E., Gallimard, L., and Pelle, J.-P. (2002). Evaluation of the local quality of stresses in 3d finite element analysis. *Computer Methods in Applied Mechanics and Engineering*, 191:4441–4457.

[Fourment and Chenot, 1995] Fourment, L. and Chenot, J. (1995). Error estimators for viscoplastic materials: application to forming processes. *International Journal for Numerical Methods in Engineering*, 12(5):469–490.

[Fraeijs de Veubeke, 1965] Fraeijs de Veubeke, B. (1965). Displacement and equilibrium models in the finite element method. *Stress Analysis, Zienkiewicz and Holister editors, Wiley, London, Chap. 9*.

[Fraeijs de Veubeke, 2001] Fraeijs de Veubeke, B. (2001). Displacement and equilibrium models in the finite element method. *International Journal for Numerical Methods in Engineering*, 52(3):287–342.

[Fraeijs de Veubeke and Hogge, 1972] Fraeijs de Veubeke, B. and Hogge, M. (1972). Dual analysis for heat conduction problems by finite elements. *International Journal for Numerical Methods in Engineering*, 5:65–82.

[Gallimard, 2009] Gallimard, L. (2009). A constitutive relation error estimator based on traction-free recovery of the equilibrated stress. *International Journal for Numerical Methods in Engineering*, 78(4):460–482.

[Gallimard et al., 1996] Gallimard, L., Ladevèze, P., and Pelle, J.-P. (1996). Error estimation and adaptivity in elastoplasticity. *International Journal for Numerical Methods in Engineering*, 39:189–217.

[Gastebois, 2015] Gastebois, S. (2015). *Simulation numérique du soudage FSW à l'aide d'une formulation ALE*. PhD Mines ParisTech.

[Gendre et al., 2011] Gendre, L., Allix, O., and Gosselet, P. (2011). A two-scale approximation of the schur complement and its use for non-intrusive coupling. *International Journal for Numerical Methods in Engineering*, 87(9):889–905.

[Gendre et al., 2009] Gendre, L., Allix, O., Gosselet, P., and Comte, F. (2009). Non-intrusive and exact global/local techniques for structural problems with local plasticity. *Computational Mechanics*, 44(2):233–245.

[Gerasimov et al., 2018] Gerasimov, P., Noii, N., Allix, O., and Lorenzis, L. D. (2018). A non-intrusive global/local approach applied to phase-field modeling of brittle fracture. *Advanced Modeling and Simulation in Engineering Sciences*, 5:14.

[Gerbeau and Lombardi, 2012] Gerbeau, J.-F. and Lombardi, D. (2012). Reduced-order modeling based on approximated lax pairs. *RR-8137, INRIA*.

[Germain et al., 1983] Germain, P., Nguyen, Q., and Suquet, P. (1983). Continuum thermodynamics. *Journal of Applied Mechanics*, 50(4):1010–1020.

[Ghnatios et al., 2012] Ghnatios, C., Masson, F., Huerta, A., Leygue, A., Cueto, E., and Chinesta, F. (2012). Proper generalized decomposition based dynamic data-driven control of thermal processes. *Computer Methods in Applied Mechanics and Engineering*, 213-216:29–41.

[Giles and Suli, 2002] Giles, M. and Suli, E. (2002). Adjoint methods for pdes: a posteriori error analysis and postprocessing by duality. *Acta Numerica, Cambridge University Press*, pages 145–236.

[Glowinski et al., 2005] Glowinski, R., He, J., Lozinski, A., Rappaz, J., and Wagner, J. (2005). Finite element approximation of multi-scale elliptic problems using patches of elements. *Numerische Mathematik*, 101(4):663–687.

[Gonzalez et al., 2013] Gonzalez, D., Cueto, E., Chinesta, F., Diez, P., and Huerta, A. (2013). Streamline upwind/petrov-galerkin-based stabilization of proper generalized decompositions for high-dimensional advection-diffusion equations. *International Journal for Numerical Methods in Engineering*, 94:1216–1232.

[Gonzalez et al., 2012] Gonzalez, D., Masson, F., Poulhaon, F., Leygue, A., Cueto, E., and Chinesta, F. (2012). Proper generalized decomposition based dynamic data-driven inverse identification. *Mathematics and Computers in Simulation*, 82:1677–1695.

[Gosselet et al., 2018] Gosselet, P., Blanchard, M., Allix, O., and Guguin, G. (2018). Non-invasive global-local coupling as a schwarz domain decomposition method: acceleration and generalization. *Advanced Modeling and Simulation in Engineering Sciences*, 5:4.

[Gosselet and Rey, 2006] Gosselet, P. and Rey, C. (2006). Non-overlapping domain decomposition methods in structural mechanics. *Archives of Computational Methods in Engineering*, 13:515–572.

[Grepl et al., 2007] Grepl, M., Nguyen, N., Veroy, K., Patera, A., and Liu, G. (2007). Certified rapid solution of partial differential equations for real-time parameter estimation and optimization. *In Real-time PDE-constrained optimization*.

[Guedri et al., 2012] Guedri, M., Cogan, S., and Bouhaddi, N. (2012). Robustness of structural reliability analyses to epistemic uncertainties. *Mechanical Systems and Signal Processing*, 28:458–469.

[Guguin et al., 2014] Guguin, G., Allix, O., Gosselet, P., and Guinard, S. (2014). Non-intrusive coupling of 3d and 2d laminated composite models based on finite element 3d recovery. *International Journal for Numerical Methods in Engineering*, 98:324–343.

[Guguin et al., 2016] Guguin, G., Allix, O., Gosselet, P., and Guinard, S. (2016). On the computation of plate assemblies using realistic 3d joint model: a non-intrusive approach. *Advanced Modeling and Simulation in Engineering Sciences*, 3:16.

[Guinard et al., 2018] Guinard, S., Bouclier, R., Toniolli, M., and Passieux, J. (2018). Multiscale analysis of complex aeronautical structures using robust non-intrusive coupling. *Advanced Modeling and Simulation in Engineering Sciences*, 5:1–27.

[Gunzburger et al., 2007] Gunzburger, M., Peterson, J., and Shadid, J. (2007). Reduced-order modeling of time-dependent pdes with multiple parameters in the boundary data. *Computer Methods in Applied Mechanics and Engineering*, 196(4-6):1030–1047.

[Gupta et al., 2012] Gupta, P., Pereira, J., Kim, D., Duarte, C., and Eason, T. (2012). Analysis of three-dimensional fracture mechanics problems: A non-intrusive approach using a generalized finite element method. *Engineering Fracture Mechanics*, 90:41–64.

[Halphen and Nguyen, 1975] Halphen, B. and Nguyen, Q. (1975). On generalized standard materials (in french). *Journal de Mécanique*, 14:39–62.

[Hansbo and Hansbo, 2002] Hansbo, A. and Hansbo, P. (2002). An unfitted finite element method, based on nitsche's method, for elliptic interface problems. *Computer Methods in Applied Mechanics and Engineering*, 191(47-48):5537–5552.

[Hansbo et al., 2005] Hansbo, P., Lovadina, C., Perugia, I., and Sangalli, G. (2005). A lagrangian multiplier method for the fe solution of elliptic interface problems using non-matching grids. *Numerische Mathematik*, 100(1):91–115.

[Haslinger and Makinen, 2003] Haslinger, J. and Makinen, R. (2003). *Introduction to shape optimization: theory, approximation, and computation*. SIAM.

[Heinrich et al., 1977] Heinrich, J., Huyakorn, P., Zienkiewicz, O., and Mitchell, A. (1977). An 'upwind' finite element scheme for two-dimensional convective transport equation. *International Journal for Numerical Methods in Engineering*, 11(1):131–143.

[Henning et al., 2014] Henning, P., Ohlberger, M., and Schweizer, B. (2014). An adaptive multiscale finite element method. *SIAM Multiscale Modeling and Simulation*, 12(3):1078–1107.

[Hirai et al., 1984] Hirai, I., Wang, B., and Pilkey, W. (1984). An efficient zooming method for finite element analysis. *International Journal for Numerical Methods in Engineering*, 20(9):1671–1683.

[Hou and Wu, 1997] Hou, T. and Wu, X. (1997). A multiscale finite element method for elliptic problems in composite materials and porous media. *Journal of Computational Physics*, 134:169–189.

[Huerta and Diez, 2000] Huerta, A. and Diez, P. (2000). Error estimation including pollution assessment for nonlinear finite element analysis. *Computer Methods in Applied Mechanics and Engineering*, 181:21–41.

[Hughes and Brooks, 1979] Hughes, T. and Brooks, A. (1979). A multidimensional upwind scheme with no crosswind diffusion. *Finite Element Methods for Convection Dominated Flows, AMD*, 34.

[Hughes et al., 1998] Hughes, T., Feijoo, G., Mazzei, L., and Quincy, J. (1998). The variational multiscale method - a paradigm for computational mechanics. *Computer Methods in Applied Mechanics and Engineering*, 166(1-2):3–24.

[Irons and Tuck, 1969] Irons, B. and Tuck, R. (1969). A version of the aitken accelerator for computer iteration. *International Journal for Numerical Methods in Engineering*, 1(3):275–277.

[Jara-Almonte and Knight, 1988] Jara-Almonte, C. and Knight, C. (1988). The specified boundary stiffness/force sbsf method for finite element subregion analysis. *International Journal for Numerical Methods in Engineering*, 26(7):1567–1578.

[Jhurani and Demkowicz, 2012] Jhurani, C. and Demkowicz, L. (2012). Multiscale modeling using goal-oriented adaptivity and numerical homogenization. part 1: mathematical formulation and numerical results. *Computer Methods in Applied Mechanics and Engineering*, 213-216:399–417.

[Johnson and Hansbo, 1992] Johnson, C. and Hansbo, P. (1992). Adaptative finite element methods in computational mechanics. *Computer Methods in Applied Mechanics and Engineering*, 101:143–181.

[Kang and Luo, 2010] Kang, Z. and Luo, Y. (2010). Reliability-based structural optimization with probability and convex set hybrid models. *Structural and Multidisciplinary Optimization*, 42:89–102.

[Karcher et al., 2018] Karcher, M., Boyaval, S., Grepl, M., and Veroy, K. (2018). Reduced basis approximation and a posteriori error bounds for 4d-var data assimilation. *Optimization and Engineering*, 19:663–95.

[Kempeneers et al., 2009] Kempeneers, M., Debongnie, J., and Beckers, P. (2009). Pure equilibrium tetrahedral finite ele- ments for global error estimation by dual analysis. *International Journal for Numerical Methods in Engineering*, 81(4):513–536.

[Kergrene et al., 2017] Kergrene, K., Prudhomme, S., Chamoin, L., and Laforest, M. (2017). Approximation of constrained problems using the pgd method with application to pure neumann problems. *Computer Methods in Applied Mechanics and Engineering*, 317:507–525.

[Klawonn et al., 2014] Klawonn, A., Lanser, M., and Rheinbach, O. (2014). Nonlinear feti-dp and bddc methods. *SIAM Journal on Scientific Computing*, 36(2):A737–A765.

[Kunisch and Volkwein, 2001] Kunisch, K. and Volkwein, S. (2001). Galerkin proper orthogonal decomposition methods for parabolic problems. *Numerische Mathematik*, 90(1):117–148.

[Ladevèze, 1975] Ladevèze, P. (1975). *Comparaison de modèles de milieux continus*. PhD thesis.

[Ladevèze, 1989] Ladevèze, P. (1989). La méthode à grand incrément de temps pour l'analyse des structures à comportement non linéaire décrit par variables internes. *Comptes-Rendus de l'Académie des Sciences*, 309:1095–1099.

[Ladevèze, 1998] Ladevèze, P. (1998). A modelling error estimator for dynamical structural model updating. In Elsevier, editor, *Advances in Adaptive Computational Methods in Mechanics*. P. Ladevèze, J.T. Oden eds.

[Ladevèze, 1999] Ladevèze, P. (1999). *Nonlinear computational structural mechanics: new approaches and non-incremental methods of calculation*. Springer-Verlag.

[Ladevèze, 2001] Ladevèze, P. (2001). Constitutive relation error estimations for finite element analyses considering (visco)-plasticity and damage. *International Journal for Numerical Methods in Engineering*, 52(5-6):527–542.

[Ladevèze, 2008] Ladevèze, P. (2008). Strict upper error bounds on computed outputs of interest in computational structural mechanics. *Computational Mechanics*, 42:271–286.

[Ladevèze, 2016] Ladevèze, P. (2016). On reduced models in nonlinear solid mechanics. *European Journal of Mechanics A/Solids*, 60:227–237.

[Ladevèze et al., 2012] Ladevèze, P., Blaysat, B., and Florentin, E. (2012). Strict upper bounds of the error in calculated outputs of interest for plasticity problems. *Computer Methods in Applied Mechanics and Engineering*, 245-246:194–205.

[Ladevèze and Chamoin, 2010] Ladevèze, P. and Chamoin, L. (2010). Calculation of strict error bounds for finite element approximations of nonlinear pointwise quantities of interest. *International Journal for Numerical Methods in Engineering*, 84:1638–1664.

[Ladevèze and Chamoin, 2011] Ladevèze, P. and Chamoin, L. (2011). On the verification of model reduction methods based on the proper generalized decomposition. *Computer Methods in Applied Mechanics and Engineering*, 200:2032–2047.

[Ladevèze and Chamoin, 2012] Ladevèze, P. and Chamoin, L. (2012). Toward guaranteed pgd-reduced models. *Bytes and Science, G. Zavarise & D.P. Boso (Eds.), CIMNE*.

[Ladevèze and Chamoin, 2015] Ladevèze, P. and Chamoin, L. (2015). The constitutive relation error method: a general verification tool. *Verifying calculations, forty years on: an overview of classical verification techniques for FEM simulations, L. Chamoin & P. Diez (Eds.), SpringerBriefs*.

[Ladevèze et al., 2010a] Ladevèze, P., Chamoin, L., and Florentin, E. (2010a). A new non-intrusive technique for the construction of admissible stress fields in model verification. *Computer Methods in Applied Mechanics and Engineering*, 199(9-12):766–777.

[Ladevèze and Leguillon, 1983] Ladevèze, P. and Leguillon, D. (1983). Error estimate procedure in the finite element method and application. *SIAM Journal of Numerical Analysis*, 20(3):485–509.

[Ladevèze et al., 2001] Ladevèze, P., Loiseau, O., and Dureisseix, D. (2001). A micro-macro and parallel computational strategy for highly heterogeneous structures. *International Journal for Numerical Methods in Engineering*, 52(1-2):121–138.

[Ladevèze and Maunder, 1996] Ladevèze, P. and Maunder, E. (1996). A general method for recovering equilibrating element tractions. *Computer Methods in Applied Mechanics and Engineering*, 137:111–151.

[Ladevèze and Moës, 1997] Ladevèze, P. and Moës, N. (1997). A new a posteriori error estimation for nonlinear time-dependent finite element analysis. *Computer Methods in Applied Mechanics and Engineering*, 157:45–68.

[Ladevèze and Moës, 1999] Ladevèze, P. and Moës, N. (1999). Adaptive control for finite element analysis in plasticity. *Computers and Structures*, 73:45–60.

[Ladevèze et al., 1999] Ladevèze, P., Moës, N., and Douchin, B. (1999). Constitutive relation error estimations for (visco) plasticity finite element analysis with softening. *Computer Methods in Applied Mechanics and Engineering*, 176:247–264.

[Ladevèze et al., 2010b] Ladevèze, P., Passieux, J.-C., and Néron, D. (2010b). The latin multiscale computational method and the proper generalized decomposition. *Computer Methods in Applied Mechanics and Engineering*, 199:1287–1296.

[Ladevèze and Pelle, 2005] Ladevèze, P. and Pelle, J. (2005). *Mastering Calculations in Linear and Nonlinear Mechanics*. Springer NY.

[Ladevèze et al., 2013] Ladevèze, P., Pled, F., and Chamoin, L. (2013). New bounding techniques for goal-oriented error estimation applied to linear problems. *International Journal for Numerical Methods in Engineering*, 93:1345–1380.

[Ladevèze and Rougeot, 1997] Ladevèze, P. and Rougeot, P. (1997). New advances on a posteriori error on constitutive relation in finite element analysis. *Computer Methods in Applied Mechanics and Engineering*, 150:239–249.

[Larson and Malqvist, 2007] Larson, M. and Malqvist, A. (2007). Adaptive variational multiscale methods based on a posteriori error estimation: energy norm estimates for elliptic problems. *Computer Methods in Applied Mechanics and Engineering*, 196(21-24):2313–2324.

[Larsson et al., 2002] Larsson, F., Hansbo, P., and Runesson, K. (2002). Strategies for computing goal-oriented a posteriori error measures in nonlinear elasticity. *International Journal for Numerical Methods in Engineering*, 55:879–894.

[Larsson and Runesson, 2011] Larsson, F. and Runesson, K. (2011). On two-scale adaptive fe analysis of micro-heterogeneous media with seamless scale-bridging. *Computer Methods in Applied Mechanics and Engineering*, 200:2662–2674.

[Larsson et al., 2003] Larsson, F., Runesson, K., and Hansbo, P. (2003). Time finite elements and error computation for (visco) plasticity with hardening or softening. *International Journal for Numerical Methods in Engineering*, 56:2213–2231.

[Le Tallec, 1994] Le Tallec, P. (1994). Domain decomposition methods in computational mechanics. *Computational Mechanics Advances*, 1(2):121–220.

[Le Tallec and Tidriri, 1999] Le Tallec, P. and Tidriri, M. (1999). Convergence analysis of domain decomposition algorithms with full overlapping for the advection-diffusion problems. *Mathematics of Computation*, 68(226):585–606.

[Leygue and Verron, 2010] Leygue, A. and Verron, E. (2010). A first step towards the use of proper general decomposition method for structural optimization. *Archives of Computational Methods in Engineering*, 17(4):465–472.

[Lions, 1987] Lions, P. (1987). On the schwarz method. *in: R. Glowinski, G.H. Golub, G.A. Meurant, J. Périaux (Eds.), Domain Decomposition Methods for Partial Differential Equations*.

[Liu et al., 2014] Liu, Y., Sun, Q., and Fan, X. (2014). A non-intrusive global/local algorithm with non-matching interface: derivation and numerical validation. *Computer Methods in Applied Mechanics and Engineering*, 277:81–103.

[Louf and Champaney, 2013] Louf, F. and Champaney, L. (2013). Fast validation of stochastic structural models using a pgd reduction scheme. *Finite Elements in Analysis and Design*, 70-71:44–56.

[Lozinski and Pironneau, 2011] Lozinski, A. and Pironneau, O. (2011). Numerical zoom for advection diffusion problems with localized multiscales. *Numerical Methods for Partial Differential Equations*, 27(1):197–207.

[Maday and Mula, 2013] Maday, Y. and Mula, O. (2013). A generalized empirical interpolation method: application of reduced basis techniques to data assimilation. *In Analysis and numerics of partial differential equations, Springer*, pages 221–235.

[Maday et al., 2015] Maday, Y., Patera, A., Penn, J., and Yano, M. (2015). A parameterized background data- weak approach to variational data assimilation: formulation, analysis, and application to acoustics. *International Journal for Numerical Methods in Engineering*, 102(5):933–965.

[Maday and Ronquist, 2002] Maday, Y. and Ronquist, E. (2002). A reduced-basis element method. *Comptes-Rendus de l'Académie des Sciences, I, Paris*, 335:195–200.

[Maier and Rannacher, 2018] Maier, M. and Rannacher, R. (2018). A duality-based optimization approach for model adaptivity in heterogeneous multiscale problems. *Multiscale Modeling & Simulation*, 16(1):412–428.

[Mandel, 1993] Mandel, J. (1993). Balancing domain decomposition. *Communications in Applied Numerical Methods*, 9:233–241.

[Manzoni et al., 2016] Manzoni, A., Pagani, S., and Lassila, T. (2016). Accurate solution of bayesian inverse uncertainty quantification problems combining reduced basis methods and reduction error models. *SIAM/ASA Journal on Uncertainty Quantification*, 4(1):380–412.

[Mao and Sun, 1991] Mao, K. and Sun, C. (1991). A refined global-local finite element analysis method. *International Journal for Numerical Methods in Engineering*, 32(1):29–43.

[Marchand et al., 2016] Marchand, B., Chamoin, L., and Rey, C. (2016). Real-time updating of structural mechanics models using kalman filtering, modified constitutive relation error and proper generalized decomposition. *International Journal for Numerical Methods in Engineering*, 107(9):786–810.

[Melenk and Babuska, 1996] Melenk, J. and Babuska, I. (1996). The partition of unity finite element method: basic theory and applications. *Computer Methods in Applied Mechanics and Engineering*, 39:289–314.

[Modesto et al., 2015] Modesto, D., Zlotnik, S., and Huerta, A. (2015). Proper generalized decomposition for parameterized helmholtz problems in heterogeneous and unbounded domains: Application to harbor agitation. *Computer Methods in Applied Mechanics and Engineering*, 295:127–149.

[Moitinho de Almeida and Almeida Pereira, 2006] Moitinho de Almeida, J. and Almeida Pereira, O. (2006). Upper bounds of the error in local quantities using equilibrated and compatible finite element solutions for linear elastic problems. *Computer Methods in Applied Mechanics and Engineering*, 195:279–296.

[Moitinho de Almeida and Maunder, 2017] Moitinho de Almeida, J. and Maunder, E. (2017). *Equilibrium Finite Element Formulations*. John Wiley & Sons.

[Moitinho de Almeida, 2013] Moitinho de Almeida, J.-P. (2013). A basis for bounding the errors of proper generalised decomposition solutions in solid mechanics. *International Journal for Numerical Methods in Engineering*, 94(10):961–984.

[Moreau, 1966] Moreau, J.-J. (1966). *Fonctionnelles convexes*. Cours du collège de France, Paris.

[Morton, 1996] Morton, K. (1996). *Numerical solution of convection-diffusion problems*.

[Moës and andT. Belytschko, 1999] Moës, N. and andT. Belytschko, J. D. (1999). A finite element method for crack growth without remeshing. *International Journal for Numerical Methods in Engineering*, 46:131–150.

[Nadal et al., 2015] Nadal, E., Chinesta, F., Diez, P., Fuenmayor, F., and Denia, F. (2015). Real time parameter identification and solution reconstruction from experimental data using the proper generalized decomposition. *Computer Methods in Applied Mechanics and Engineering*, 296:113–128.

[Nayroles, 1973] Nayroles, B. (1973). Point de vue algébrique - convexité et intégrales convexes en mécanique des solides. *in New Variational Techniques in Mathematical Physics, CISME*, pages 324–404.

[Néron et al., 2016] Néron, D., Ben Dhia, H., and Cottereau, R. (2016). A decoupled strategy to solve reduced-order multimodel problems in the pgd and arlequin frameworks. *Computational Mechanics*, 57(4):509–521.

[Neron et al., 2015] Neron, D., Boucard, P.-A., and Relun, N. (2015). Time-space pgd for the rapid solution of 3d nonlinear parametrized problems in the many-query context. *International Journal for Numerical Methods in Engineering*, 103:275–292.

[Néron and Ladevèze, 2010] Néron, D. and Ladevèze, P. (2010). Proper generalized decomposition for multiscale and multiphysics problems. *Archives of Computational Methods in Engineering*, 17(4):351–372.

[Nguyen et al., 2010] Nguyen, N., Rozza, G., Huynh, D., and Patera, A. (2010). Reduced basis approximation and a posteriori error estimation for parametrized parabolic pdes: application to real-time bayesian parameter estimation. *Large-Scale Inverse Problems and Quantification of Uncertainty, chap. 8*.

[Nouy, 2008] Nouy, A. (2008). Generalized spectral decomposition method for solving stochastic finite element equations: invariant subspace problem and dedicated algorithms. *Computer Methods in Applied Mechanics and Engineering*, 197(51):4718–4736.

[Nouy, 2010a] Nouy, A. (2010a). A priori model reduction through proper generalized decomposition for solving time dependent partial differential equations. *Computer Methods in Applied Mechanics and Engineering*, 199:1603–1626.

[Nouy, 2010b] Nouy, A. (2010b). Proper generalized decompositions and separated representations for the numerical solution of high dimensional stochastic problems. *Archives of Computational Methods in Engineering*, 17(4):403–434.

[Nouy et al., 2011] Nouy, A., Chevreuil, M., and Safatly, E. (2011). Fictitious domain method and separated representations for the solution of boundary value problems on uncertain parameterized domains. *Computer Methods in Applied Mechanics and Engineering*, 200(45):3066–3082.

[Nouy and Pled, 2018] Nouy, A. and Pled, F. (2018). A multiscale method for semi-linear elliptic equations with localized uncertainties and non-linearities. *ESAIM Mathematical Modelling and Numerical Analysis*, 52(5):1763–1802.

[Oberkampf et al., 2003] Oberkampf, W., Trucano, T., and Hirsh, C. (2003). *Verification, Validation and Predictive Capability in Computational Engineering and Physics*. Technical report, Sandia 2003-3769.

[Oden et al., 2005] Oden, J., Babuška, I., Nobile, F., Feng, Y., and Tempone, R. (2005). Theory and methodology for estimation and control of error due to modeling, approximation, and uncertainty. *Computer Methods in Applied Mechanics and Engineering*, 194(2-5):195–204.

[Oden et al., 2006a] Oden, J., Belytschko, T., Fish, J., Hughes, T., Johnson, C., Keyes, D., Laub, A., Petzold, L., Srolovitz, D., and Yip, S. (2006a). *Simulation Based Engineering Science - Revolutionizing Engineering Science through Simulation*. Report of the National Science Foundation Blue Ribbon Panel on SBES, USA.

[Oden and Prudhomme, 2001] Oden, J. and Prudhomme, S. (2001). Goal-oriented error estimation and adaptivity for the finite element method. *Computers & Mathematics with Applications*, 41(5):735–756.

[Oden and Prudhomme, 2002] Oden, J. and Prudhomme, S. (2002). Estimation of modeling error in computational mechanics. *Journal of Computational Physics*, 182:496–515.

[Oden et al., 2006b] Oden, J., Prudhomme, S., Romkes, A., and Bauman, P. (2006b). Multi-scale modeling of physical phenomena: Adaptive control of models. *SIAM Journal on Scientific Computing*, 28:2359–2389.

[Oden and Vemaganti, 2000] Oden, J. and Vemaganti, K. (2000). Estimation of local modeling error and goal-oriented modeling of heterogeneous materials. part i: Error estimates and adaptive algorithms. *Journal of Computational Physics*, 164:22–47.

[Oden et al., 1999] Oden, J., Vemaganti, K., and Moes, N. (1999). Hierarchical modeling of heterogeneous solids. *Computer Methods in Applied Mechanics and Engineering*, 172(1-4):3–25.

[Oden and Zohdi, 1997] Oden, J. and Zohdi, T. (1997). Analysis and adaptive modeling of highly heterogeneous elastic structures. *Computer Methods in Applied Mechanics and Engineering*, 148(3-4):367–391.

[O'Hara et al., 2009] O'Hara, P., Duarte, C., Eason, T., and Kim, D. (2009). Generalized finite element analysis of three-dimensional heat transfer problems exhibiting sharp thermal gradients. *Computer Methods in Applied Mechanics and Engineering*, 198(21-26):1857–1871.

[Ohnimus et al., 2001] Ohnimus, S., Stein, E., and Walhorm, E. (2001). Local error estimates of fem for displacements and stresses in linear elasticity by solving local neumann problems. *International Journal for Numerical Methods in Engineering*, 52:727–746.

[Oumaziz et al., 2018] Oumaziz, P., Gosselet, P., Boucard, P.-A., and Abbas, M. (2018). A parallel non-invasive multiscale strategy for a mixed domain decomposition method with frictional contact. *International Journal for Numerical Methods in Engineering*, 115(8):893–912.

[Oumaziz et al., 2017] Oumaziz, P., Gosselet, P., Boucard, P.-A., and Guinard, S. (2017). A non-invasive implementation of a mixed domain decomposition method for frictional contact problems. *Computational Mechanics*, 60(5):797–812.

[Paladim et al., 2017] Paladim, D., Moitinho de Almeida, J., Bordas, S., and Kerfriden, P. (2017). Guaranteed error bounds in homogenization: an optimum stochastic approach to preserve the numerical separation of scales. *International Journal for Numerical Methods in Engineering*, 110(2):103–132.

[Panetier et al., 2010] Panetier, J., Ladevèze, P., and Chamoin, L. (2010). Strict and effective bounds in goal-oriented error estimation applied to fracture mechanics problems solved with the xfem. *International Journal for Numerical Methods in Engineering*, 81(6):671–700.

[Paraschivoiu et al., 1997] Paraschivoiu, M., Peraire, J., and Patera, A. (1997). A posteriori finite element bounds for linear functional outputs of elliptic partial differential equations. *Computer Methods in Applied Mechanics and Engineering*, 150:289–312.

[Pares et al., 2006] Pares, N., Diez, P., and Huerta, A. (2006). Subdomain-based flux-free a posteriori error estimators. *Computer Methods in Applied Mechanics and Engineering*, 195:297–323.

[Pares et al., 2013] Pares, N., Diez, P., and Huerta, A. (2013). Computable exact bounds for linear outputs from linear outputs from stabilized solutions of the advection-diffusion-reaction equation. *International Journal for Numerical Methods in Engineering*, 93:483–509.

[Pares et al., 2009] Pares, N., Santos, H., and Diez, P. (2009). Guaranteed energy error bounds for the poisson equation using a flux-free approach: solving the local problems in subdomains. *International Journal for Numerical Methods in Engineering*, 79:1203–1244.

[Parret-Fréaud et al., 2010] Parret-Fréaud, A., Rey, C., Gosselet, P., and Feyel, F. (2010). Fast estimation of discretization error for fe problems solved by domain decomposition. *Computer Methods in Applied Mechanics and Engineering*, 199:3315–3323.

[Parsons and Hall, 1990] Parsons, I. and Hall, J. (1990). The multigrid method in solid mechanics - part i: Algorithm description and behaviour. *International Journal for Numerical Methods in Engineering*, 29(4):719–737.

[Passieux et al., 2013] Passieux, J., Rééthoréé, J., Gravouil, A., and Baietto, M. (2013). Local/global non-intrusive crack propagation simulation using a multigrid x-fem solver. *Computational Mechanics*, 52(6):1381–1393.

[Pelle and Ryckelynck, 2000] Pelle, J.-P. and Ryckelynck, D. (2000). An efficient adaptive strategy to master the global quality of viscoplastic analysis. *Computers and Structures*, 78:169–183.

[Peraire and Patera, 1998] Peraire, J. and Patera, A. (1998). Bounds for linear-functional outputs of coercive partial differential equations; local indicators and adaptive refinements. *Advances in Adaptive Computational Methods in Mechanics, Ladevèze and Oden Editors, Elsevier*, pages 199–216.

[Picasso et al., 2008] Picasso, M., Rappaz, J., and Rezzonico, V. (2008). Multiscale algorithm with patches of finite elements. *Communications in Numerical Methods in Engineering*, 24(6):477–491.

[Pled et al., 2011] Pled, F., Chamoin, L., and Ladevèze, P. (2011). On the techniques for constructing admissible stress fields in model verification: performances on engineering examples. *International Journal for Numerical Methods in Engineering*, 88(5):409–441.

[Pled et al., 2012] Pled, F., Chamoin, L., and Ladevèze, P. (2012). An enhanced method with local energy minimization for the robust a posteriori construction of equilibrated stress fields in finite element analyses. *Computational Mechanics*, 49(3):357–378.

[Plews et al., 2012] Plews, J., Duarte, C., and Eason, T. (2012). An improved nonintrusive global-local approach for sharp thermal gradients in a standard fea platform. *International Journal for Numerical Methods in Engineering*, 91(4):426–449.

[Prager and Synge, 1947] Prager, W. and Synge, J. (1947). Approximation in elasticity based on the concept of functions spaces. *Quarterly of Applied Mathematics*, 5:261–269.

[Prudhomme et al., 2012] Prudhomme, S., Bouclier, R., Chamoin, L., Dhia, H. B., and Oden, J. (2012). Analysis of an averaging operator for atomic-to-continuum coupling methods by the arlequin approach. *Numerical Analysis of Multiscale Computations, Lecture Notes in Computational Science and Engineering*, 82:369–400.

[Prudhomme and Bryant, 2015] Prudhomme, S. and Bryant, C. (2015). Adaptive surrogate modeling for response surface approximations with application to bayesian inference. *Advanced Modeling and Simulation in Engineering Sciences*, 2(1):22.

[Prudhomme et al., 2009] Prudhomme, S., Chamoin, L., Dhia, H. B., and Bauman, P. (2009). An adaptive strategy for the control of modeling error in two-dimensional atomic-to-continuum coupling simulations. *Computer Methods in Applied Mechanics and Engineering*, 198(21-26):1887–1901.

[Prudhomme and Oden, 1999] Prudhomme, S. and Oden, J. (1999). On goal-oriented error estimation for elliptic problems: application to the control of pointwise errors. *Computer Methods in Applied Mechanics and Engineering*, 176:313–331.

[Quarteroni and Valli, 1994] Quarteroni, A. and Valli, A. (1994). *Numerical approximation of partial differential equations*. Springer.

[Radermacher and Reese, 2016] Radermacher, A. and Reese, S. (2016). Pod-based model reduction with empirical interpolation applied to nonlinear elasticity. *International Journal for Numerical Methods in Engineering*, 107(6):477–495.

[Radovitzky and Ortiz, 1999] Radovitzky, R. and Ortiz, M. (1999). Error estimation and adaptive meshing in strongly nonlinear dynamics problems. *Computer Methods in Applied Mechanics and Engineering*, 172:203–240.

[Rannacher and Suttmeier, 1997] Rannacher, R. and Suttmeier, F. (1997). A feedback approach to error control in finite element methods: application to linear elasticity. *Computational Mechanics*, 19:434–446.

[Rannacher and Suttmeier, 1999] Rannacher, R. and Suttmeier, F. (1999). A posteriori error estimation and mesh adaptation for finite element models in elasto-plasticity. *Computer Methods in Applied Mechanics and Engineering*, 176:333–361.

[Rannou et al., 2009] Rannou, J., Gravouil, A., and Baietto, M. (2009). A local multigrid xfem strategy for 3d crack propagation. *International Journal for Numerical Methods in Engineering*, 77(4):581–600.

[Reis et al., 2020] Reis, J., Moitinho de Almeida, J.-P., Diez, P., and Zlotnik, S. (2020). Error estimation for pgd solutions: A dual approach. *International Journal for Numerical Methods in Engineering*, 121(23):5275–5294.

[Repin, 1999] Repin, S. (1999). A posteriori error estimates for approximate solutions to variational problems with strongly convex functionals. *Journal of Mathematical Sciences*, 97:4311–4328.

[Rey et al., 2014a] Rey, V., Gosselet, P., and Rey, C. (2014a). Study of the strong prolongation equation for the construction of statically admissible stress fields: implementation and optimization. *Computer Methods in Applied Mechanics and Engineering*, 268:82–104.

[Rey et al., 2015] Rey, V., Gosselet, P., and Rey, C. (2015). Strict bounding of quantities of interest in computations based on domain decomposition. *Computer Methods in Applied Mechanics and Engineering*, 287:212–228.

[Rey et al., 2016] Rey, V., Gosselet, P., and Rey, C. (2016). Strict lower bounds with separation of sources of error in non-overlapping domain decomposition methods. *International Journal for Numerical Methods in Engineering*, 108(9):1007–1029.

[Rey et al., 2014b] Rey, V., Rey, C., and Gosselet, P. (2014b). A strict error bound with separated contributions of the discretization and of the iterative solver in non-overlapping domain decomposition methods. *Computer Methods in Applied Mechanics and Engineering*, 270:293–303.

[Roache, 1998] Roache, P. (1998). *Verification and Validation in Computational Science and Engineering*. Hermosa publishers.

[Romkes et al., 2006] Romkes, A., Oden, J., and Vemaganti, K. (2006). Multi-scale goal-oriented adaptive modeling of random heterogeneous materials. *Mechanics of Materials*, 38:859–872.

[Rozza et al., 2008] Rozza, G., Huynh, D., and Patera, A. (2008). Reduced basis approximation and a posteriori error estimation for affinely parametrized elliptic coercive partial differential equations: application to transport and continuum mechanics. *Archives of Computational Methods in Engineering*, 15(3):229–275.

[Rubio et al., 2019a] Rubio, P.-B., Chamoin, L., and Louf, F. (2019a). Real-time bayesian data assimilation with data selection, correction of model bias, and on-the-fly uncertainty propagation. *Comptes Rendus de l?Académie des Sciences, Mécanique*, 347:762–779.

[Rubio et al., 2018] Rubio, P.-B., Louf, F., and Chamoin, L. (2018). Fast model updating coupling bayesian inference and pgd model reduction. *Computational Mechanics*, 62(6):1485–1509.

[Rubio et al., 2019b] Rubio, P.-B., Louf, F., and Chamoin, L. (2019b). Transport map sampling with pgd model reduction for fast dynamical bayesian data assimilation. *International Journal for Numerical Methods in Engineering*, 120(4):447–472.

[Ruess et al., 2014] Ruess, M., Schillinger, D., Ozcanand, A., and Rank, E. (2014). Weak coupling for isogeometric analysis of non-matching and trimmed multi-patch geometries. *Computer Methods in Applied Mechanics and Engineering*, 269:46–71.

[Ruyssen, 2021] Ruyssen, R. (2021). Contribution à la modélisation et simulation multi-échelle de problèmes en lien avec la fabrication additive par fusion laser sur lit de poudre. *PhD Thesis, Univ. Paris-Saclay*.

[Ruyssen et al., 2017] Ruyssen, R., Barbarulo, A., and Dhia, H. B. (2017). Contribution à la modélisation du procédé de fabrication additive: fusion laser sur lit de poudre. *Proceedings of 13e colloque national en calcul de structures*.

[Ryckelynck, 2009] Ryckelynck, D. (2009). Hyper-reduction of mechanical models involving internal variables. *International Journal for Numerical Methods in Engineering*, 77(1):75–89.

[Samareh, 2001] Samareh, J. (2001). Survey of shape parameterization techniques for high-fidelity multidisciplinary shape optimization. *AIAA Journal*, pages 877–884.

[Scarabosio et al., 2019] Scarabosio, L., Faghihi, D., Wohlmuth, B., and Oden, J. (2019). Goal-oriented adaptive modeling of random heterogeneous media and model-based multilevel monte-carlo methods. *Computers & Mathematics with Applications*, 78(8):2700–2718.

[Sevilla et al., 2020] Sevilla, R., Zlotnik, S., and Huerta, A. (2020). Solution of geometrically parametrised problems within a cad environment via model order reduction. *Computer Methods in Applied Mechanics and Engineering*, 358:112631.

[Signorini et al., 2017] Signorini, M., Zlotnik, S., and Diez, P. (2017). Proper generalized decomposition solution of the parameterized helmholtz problem: application to inverse geophysical problems. *International Journal for Numerical Methods in Engineering*, 109(8):1085–1102.

[Strouboulis et al., 2000a] Strouboulis, T., Babuska, I., and Copps, K. (2000a). The design and analysis of the generalized finite element method. *Computer Methods in Applied Mechanics and Engineering*, 181(1-3):43–69.

[Strouboulis et al., 2000b] Strouboulis, T., Babuska, I., Datta, D., Copps, K., and Gangaraj, S. (2000b). A posteriori estimation and adaptive control of the error in the quantity of interest – part i: a posteriori estimation of the error in the von mises stress and the stress intensity factor. *Computer Methods in Applied Mechanics and Engineering*, 181(1-3):261–294.

[Strouboulis and Haque, 1992] Strouboulis, T. and Haque, K. (1992). Recent experiences with error estimation and adaptivity, part i: review of error estimators for scalar elliptic problems. *Computer Methods in Applied Mechanics and Engineering*, 97(3):399–436.

[Strouboulis et al., 2006] Strouboulis, T., Zhang, L., Wang, D., and Babuska, I. (2006). A posteriori error estimation for generalized finite element methods. *Computer Methods in Applied Mechanics and Engineering*, 195:852–879.

[Thai et al., 2019] Thai, H., Chamoin, L., and Minh, C. H. (2019). A posteriori error estimation for isogeometric analysis using the concept of constitutive relation error. *Computer Methods in Applied Mechanics and Engineering*, 355:1062–1096.

[Tidriri, 1995] Tidriri, M. (1995). Domain decomposition for compressible navier-stokes equations with different discretizations and formulations. *Journal of Computational Physics*, 119:271–282.

[Tirvaudey et al., 2020a] Tirvaudey, M., Bouclier, R., Passieux, J., and Chamoin, L. (2020a). Non-invasive implementation of nonlinear isogeometric analysis in an industrial fe code. *Engineering Computations*, 37(1):237–261.

[Tirvaudey et al., 2020b] Tirvaudey, M., Chamoin, L., Bouclier, R., and Passieux, J. (2020b). A posteriori error estimation and adaptivity in non-intrusive couplings between concurrent models. *Computer Methods in Applied Mechanics and Engineering*, 367:113104.

[Tottenham, 1970] Tottenham, H. (1970). Basic principles. *in Finite Element Techniques in Structural Mechanics, Southampton University Press*.

[Uzawa, 1958] Uzawa, H. (1958). Iterative methods for concave programming. *Stud. Linear Nonlinear Program*, 6.

[Vemaganti and Oden, 2001] Vemaganti, K. and Oden, J. (2001). Estimation of local modeling error and goal-oriented modeling of heterogeneous materials; part 2: A computational environment for adaptive modeling of heterogeneous elastic solids. *Computer Methods in Applied Mechanics and Engineering*, 190:6089–6124.

[Verfürth, 1996] Verfürth, R. (1996). *A Review of A Posteriori Error Estimation and Adaptive Mesh-refinement Techniques*. Wiley-Teubner, Stuttgart.

[Vitse et al., 2014] Vitse, M., Néron, D., and Boucard, P.-A. (2014). Virtual charts of solutions for parametrized nonlinear equations. *Computational Mechanics*, 54(6):1529–1539.

[Vitse et al., 2019] Vitse, M., Néron, D., and Boucard, P.-A. (2019). Dealing with a nonlinear material behavior and its variability through pgd models: application to reinforced concrete structures. *Finite Elements in Analysis and Design*, 153:22–37.

[Vohralik, 2007] Vohralik, M. (2007). A posteriori error estimates for lowest-order mixed finite element discretizations of convection-diffusion-reaction equations. *SIAM Journal on Numerical Analysis*, 45:1570–1599.

[Vohralik, 2008] Vohralik, M. (2008). A posteriori error estimation in the conforming finite element method based on its local conservativity and using local minimization. *Comptes Rendus Mathématique*, 346(11-12):687–690.

[Vohralik, 2011] Vohralik, M. (2011). Guaranteed and fully robust a posteriori error estimates for conforming discretizations of diffusion problems with discontinuous coefficients. *Journal of Scientific Computing*, 46:397–438.

[Voleti et al., 1996] Voleti, S., Chandra, N., and Miller, J. (1996). Global-local analysis of large-scale composite structures using finite element methods. *Computers & Structures*, 58(3):453–464.

[Waeytens et al., 2012] Waeytens, J., Chamoin, L., and Ladevèze, P. (2012). Guaranteed error bounds on pointwise quantities of interest for transient viscodynamics problems. *Computational Mechanics*, 49(3):291–307.

[Wagner and Liu, 2003] Wagner, G. and Liu, W. (2003). Coupling of atomistic and continuum simulations using a bridging scale decomposition. *Journal of Computational Physics*, 190(1):249–274.

[Wang et al., 2016] Wang, L., Chamoin, L., Ladevèze, P., and Zhong, H. (2016). Computable upper and lower bounds on eigenfrequencies. *Computer Methods in Applied Mechanics and Engineering*, 302:27–43.

[W.E et al., 2003] W.E, Engquist, B., and Huang, Z. (2003). Heterogeneous multiscale method: a general methodology for multiscale modeling. *Physical Review B*, 67(9):092101.

[Whitcomb, 1991] Whitcomb, J. (1991). Iterative global-local finite element analysis. *Computers & Structures*, 40(4):1027–1031.

[Wohlmuth, 1999] Wohlmuth, B. (1999). A residual based error estimator for mortar finite element discretizations. *Numerische Mathematik*, 84(1):143–171.

[Xiao and Belytschko, 2004] Xiao, S. and Belytschko, T. (2004). A bridging domain method for coupling continua with molecular dynamics. *Computer Methods in Applied Mechanics and Engineering*, 193:1645–1669.

[Yu and Chakravorty, 2015] Yu, D. and Chakravorty, S. (2015). An iterative proper orthogonal decomposition (i-pod) technique with application to the filtering of partial differential equations. *Journal of Astronautical Sciences*, 60:468–493.

[Yu et al., 2018] Yu, W., Gu, Y., and Li, Y. (2018). Efficient randomized algorithms for the fixed-precision low-rank matrix approximation. *SIAM Journal on Matrix Analysis and Applications*, 39(3):1339–1359.

[Zaccardi et al., 2013] Zaccardi, C., Chamoin, L., Cottereau, R., and Dhia, H. B. (2013). Error estimation and model adaptation for a stochastic-deterministic coupling method based on the arlequin framework. *International Journal for Numerical Methods in Engineering*, 96(2):87–109.

[Zang et al., 2005] Zang, C., Friswell, M., and Mottershead, J. (2005). A review of robust optimal design and its application in dynamics. *Computers and Structures*, 83:315–326.

[Zlotnik et al., 2015] Zlotnik, S., Diez, P., Modesto, D., and Huerta, A. (2015). Proper generalized decomposition of a geometrically parametrized heat problem with geophysical applications. *International Journal for Numerical Methods in Engineering*, 103(10):737–758.

université PARIS-SACLAY
ÉCOLE DOCTORALE
Sciences mécaniques et énergétiques, matériaux et géosciences (SMEMAG)

**Titre:** Adaptation et réduction de modèle dans les couplages local-global non-intrusifs: application à la conception robuste

**Mots clés:** Couplage non-intrusif de modèles, Estimation d'erreur a posteriori, Erreur de modèle, Réduction de modèle, Techniques adaptatives, Conception robuste

**Résumé:** Ce travail de recherche porte sur la méthode de couplage local-global non-intrusive qui a été développée et largement analysée et appliquée en mécanique des structures durant la derniére décennie. Cette méthode constitue un outil de simulation à la fois flexible et performant pour l'analyse de phénomènes localisés avec un effort de mise eu oeuvre réduit. Dans ce contexte, le travail propose une technique spécifique de vérification, construite à partir du concept d'erreur en relation de comportement, qui permet de certifier la qualité des solutions approchées obtenues par une telle méthode de couplage. Elle fournit des estimateurs et indicateurs d'erreur *a posteriori* fiables afin de rendre compte quantitativement du niveau global d'erreur et de ses diverses sources. Elle permet notamment le contrôle d'erreur sur des quantités d'intérêt utiles pour le dimensionnement. Un algorithme adaptatif est alors construit afin de piloter efficacement et automatiquement la procédure de couplage, et ajuster de façon optimale les paramètres associés (position de l'interface de couplage, taille du maillage local, nombre d'itérations) pour atteindre une tolérance cible avec un coût numérique minimal. L'approche est analysée pour différents scénarios de couplage impliquant par exemple des modèles non-linéaires ou l'utilisation locale de modèle réduit par PGD. Ses performances sont illustrées via plusieurs exemples numériques, et son intérêt pour l'analyse de tolérance est aussi montrée avec le calcul rapide et certifié de quantités pour la conception optimale ou robuste.

**Title:** Adaptive and reduced order modeling in non-intrusive local-global couplings: application to robust design

**Keywords:** Non-intrusive model coupling, A posteriori error estimation, Modeling error, Model reduction, Adaptive techniques, Robust design

**Abstract:** This research work focuses on the so-called non-intrusive local-global model coupling procedure which has been proposed and widely analyzed and applied in structural mechanics during the last decade, and which constitutes a flexible and effective engineering simulation tool for the analysis of localized phenomena with low implementation effort. In this context, we propose a specific verification technique, constructed from the Constitutive Relation Error concept, that enables to certify the quality of approximate solutions obtained from such a non-intrusive model coupling. It consists in computable and reliable *a posteriori* error estimator and indicators in order to quantitatively assess the overall error level and its various sources. It particularly permits the practical control of the error on outputs of interest which are used for design purposes. An adaptive algorithm is then defined in order to effectively and automatically drive the coupling process, and optimally adjust the coupling parameters (location of the coupling interface, local mesh size, number of iterations) so that a given error tolerance is reached with minimal computing resources. The approach is analyzed for various coupling scenarios, including nonlinear local models or local use of PGD reduced order modeling. Its performance is shown on several numerical experiments involving various quantities of interest. It is also applied in the context of tolerance analysis in order to conduct fast and certified computations for optimal or robust design.

**Université Paris-Saclay**
Espace Technologique / Immeuble Discovery
Route de l'Orme aux Merisiers RD 128 / 91190 Saint-Aubin, France